

NACA RM L55D26



RESEARCH MEMORANDUM

AN INVESTIGATION AT SUPERSONIC SPEEDS OF THE EFFECT OF
VARYING THE MAXIMUM-THICKNESS POSITION UPON THE
AERODYNAMIC CHARACTERISTICS OF A SERIES
OF $3\frac{1}{2}$ -PERCENT-THICK DELTA WINGS

By James N. Mueller

Langley Aeronautical Laboratory
Langley Field, Va.

UNCLASSIFIED

To _____

By authority of *NASA TPA 8* Effective Date *7-22-59*

NB 9-14-59

CLASSIFIED DOCUMENT

This material contains information affecting the National Defense of the United States within the meaning of the espionage laws, Title 18, U.S.C., Secs. 793 and 794, the transmission or revelation of which in any manner to an unauthorized person is prohibited by law.

NATIONAL ADVISORY COMMITTEE FOR AERONAUTICS

WASHINGTON
August 9, 1955

LANGLEY AERONAUTICAL LABORATORY
LIBRARY, NACA
LANGLEY FIELD, VIRGINIA
AUG 10 1955

CONFIDENTIAL
UNCLASSIFIED

UNCLASSIFIED

NACA RM L55D26

~~CONFIDENTIAL~~

NATIONAL ADVISORY COMMITTEE FOR AERONAUTICS

RESEARCH MEMORANDUM

AN INVESTIGATION AT SUPERSONIC SPEEDS OF THE EFFECT OF
VARYING THE MAXIMUM-THICKNESS POSITION UPON THE
AERODYNAMIC CHARACTERISTICS OF A SERIES
OF $3\frac{1}{2}$ - PERCENT-THICK DELTA WINGS

By James N. Mueller

SUMMARY

A wind-tunnel investigation of a family of $3\frac{1}{2}$ -percent-thick symmetrical double-wedge delta wings was made to determine the effects of thickness distribution on lift, drag, and pitching moment. Six maximum-thickness positions (18, 30, 40, 50, 60, and 70 percent chord) were tested on each of three basic wings which had semiapex angles of 30° , 35° , and 40° . The tests were made at Mach numbers of 1.62, 1.94, and 2.41 and Reynolds numbers of 1.96×10^6 to 2.75×10^6 in the Langley 9-inch supersonic tunnel. The experimental data are compared with linear theory throughout.

The results indicated that the wing drag calculated by the linearized theory was in qualitative agreement with the test results in indicating the effects of varying the maximum-thickness position. The decrease in minimum drag coefficient as a result of moving the wing maximum-thickness position from 18 to 70 percent chord was as much as 50 percent, whereas the gain achieved in lift-curve slope was about 22 percent. The optimum maximum-thickness position appeared to be near 60 to 70 percent chord. Lift-curve slope was accurately predicted by linear theory for the condition of shock-wave attachment to the leading edge of the wings. The maximum lift-drag ratio obtained was 10.8. The predictions of the drag-due-to-lift factor based on the method of linear theory is adequate only for those wings which approach closely the restrictions of the theory. The chordwise center of pressure of all wings coincided approximately with the wing center of area and remained essentially invariant with maximum-thickness location, Mach number, and the ratio of the tangent of the wing semiapex angle to the tangent of the Mach angle ($\tan \epsilon / \tan m$).

~~CONFIDENTIAL~~

UNCLASSIFIED

INTRODUCTION

The effects of chordwise thickness distribution on the theoretical pressure-drag characteristics of delta wings with symmetrical double-wedge profiles have been determined on the basis of linear theory by Puckett (ref. 1) and by Puckett and Stewart (ref. 2) for the complete range of sweepback angles of both the leading edge and the ridge line. The results of these analyses showed that for any given value of the tangent ratio $\tan \epsilon / \tan m$ (where ϵ is defined as the wing semiapex angle and m is the Mach angle of the free-stream flow) the wing pressure drag could be held to a relatively low value, dependent on the choice of the chordwise position of maximum thickness. The results of a limited investigation of the effect of thickness distribution at a Mach number M of 1.53 conducted on 5-percent-thick symmetrical double-wedge delta wings mounted on slender bodies and which had maximum-thickness locations at 20 and 50 percent chord (reported in refs. 3, 4, 5, and 6), have tended to support the theoretical prediction of references 1 and 2 after due consideration had been given the friction drag. More recently, data obtained by Eugene S. Love and Richard E. Lovett in an investigation conducted in the Langley 9-inch supersonic tunnel (these data are included herein) for Mach numbers of 1.62, 1.93, and 2.40 on 8-percent-thick delta wings with the maximum-thickness location at 50 percent chord showed significant wing-drag reductions as compared to previous tests by Love (ref. 7) on wings which had the maximum thickness located at 18 percent chord. Ulmann and Dunning (ref. 8) have also shown, in tests at $M = 4.04$ on 8-percent-thick delta wings with maximum thicknesses at 18 and 60 percent chord, significant wing-drag reductions with a rearward shift in the location of maximum thickness. Welsh, as a result of rocket-model tests conducted on 6-percent-thick symmetrical double-wedge delta wings having maximum-thickness locations of 20, 50, and 80 percent chord (ref. 9), concluded that the wing drag calculated by the linearized theory was in qualitative agreement with test results in indicating the effects of varying the position of maximum thickness.

Although the linearized theory does not consider maximum-thickness location in the lift calculations, a comparison of the experimental data of Love and Lovett on 8-percent-thick delta wings having maximum thicknesses at 50 percent chord with the results obtained in reference 7 on wings of the same thickness but with the maximum-thickness location at 18 percent chord, shows a significant increase in lift-curve slope as a result of the rearward movement of the maximum-thickness position. The results of the investigation of Ulmann and Dunning (ref. 8) at $M = 4.04$ on geometrically similar wings indicate similar behavior upon relocation of the maximum-thickness position from 18 to 60 percent chord.

A review of the available literature on experimental investigations of delta-wing thickness-distribution effects (as discussed in the preceding paragraphs) has shown that, to date, all the investigations have been of a limited nature with regard to the variation in the maximum-thickness position. Moreover, these tests have been concerned with relatively thick wings which are, aerodynamically speaking, less efficient than thin wings at supersonic speeds. Therefore, on the basis of the foregoing findings and in an effort to further the knowledge of thickness-distribution effects on the aerodynamic characteristics of delta wings, a systematic wind-tunnel investigation has been made of a series of thin, symmetrical, double-wedge delta wings having thickness ratios of $\frac{1}{2}$ percent. The selection of the thickness ratio was based upon considerations of structural feasibility and the fact that thin wings and control surfaces are an aerodynamic necessity at supersonic speeds if high lift-drag ratios are to be realized. A secondary, though important, purpose of the investigation was the assessment of the usefulness of linear theory for wings which approach closely the restrictions of the theory.

The scope of the investigation included the measurement of the lift, drag, and pitching moment on a family of 18 delta wings having semiapex angles of 30° , 35° , and 40° . For each semiapex angle there were six wings with the maximum-thickness positions at 18, 30, 40, 50, 60, and 70 percent chord. The wings were sting mounted and were tested in the Langley 9-inch supersonic tunnel at Mach numbers of 1.62, 1.94, and 2.41. The Reynolds number range of the tests was from 1.96×10^6 to 2.75×10^6 based on mean aerodynamic chord.

SYMBOLS

A	aspect ratio
b	wing span
c	wing root chord
\bar{c}	wing mean aerodynamic chord, $\frac{2}{3} c$
C_L	lift coefficient, $\frac{\text{Lift}}{qS}$
C_m	pitching-moment coefficient, $\frac{\text{Pitching moment about wing center of area}}{qS\bar{c}}$

C_D	drag coefficient, $\frac{\text{Drag}}{qS}$
$C_{D_{\min}}$	drag coefficient at zero lift
C_{D_p}	pressure-drag coefficient, $C_{D_{\min}} - C_{D_f}$
C_{D_f}	skin-friction-drag coefficient
ΔC_D	rise in drag coefficient above minimum, $C_D - C_{D_{\min}}$
$C_{L_{\alpha}}$	rate of change of lift coefficient with angle of attack at zero lift
$C_{L_{\alpha_{2D}}}$	two-dimensional value of rate of change of lift coefficient with angle of attack
E	elliptic integral of second kind with modulus $\sqrt{1 - w^2}$
L/D	lift-drag ratio
$(L/D)_{\max}$	maximum lift-drag ratio
m	Mach angle, $\sin^{-1} \frac{1}{M}$
M	Mach number
P	pressure coefficient, $\frac{P_{\text{local}} - P}{q}$
p	static pressure
q	dynamic pressure, $\frac{\gamma}{2} M^2 p$
R	Reynolds number based on \bar{c}
r	distance of ridge-line apex from trailing edge, percent root chord
S	wing area
t	wing maximum thickness

$$w = \frac{\tan \epsilon}{\tan m}$$

α angle of attack

$$\beta = \sqrt{M^2 - 1}$$

ϵ wing semiapex angle

γ ratio of specific heats, 1.4 for air

τ airfoil thickness ratio, t/c

APPARATUS AND TESTS

Wind Tunnel, Balance, and Model Support

Wind tunnel.- The investigation was conducted in the Langley 9-inch supersonic tunnel, which is a continuous-operation closed-return type of tunnel with provisions for the control of the humidity, temperature, and pressure of the enclosed air. The test Mach number is varied by means of interchangeable nozzle blocks forming test sections approximately 9 inches square. Eleven fine-mesh screens in the relatively large settling chamber ahead of the nozzle aid in keeping the turbulence in the tunnel test section at a low level. During the tests, the quantity of water vapor in the tunnel air was kept sufficiently low so that the effects of water condensation in the supersonic nozzle were negligible.

Balance and model support.- Figure 1(a) is a sketch which shows the salient features of the three-component strain-gage balance used in the investigation to measure lift, drag, and pitching moment. The method of model support is shown in figure 1(b). As can be seen, the wings were mounted on support stings whose shanks passed through the opening of the movable-windshield nose with small clearance and were attached to the floating-frame section of the balance through insertion in the angle-of-attack spindle. The streamwise gap between the nose of the movable windshield and the base of the support sting was 0.020 inch or less, and the nose of the movable windshield had the same shape (but slightly smaller dimensions) as the perimeter of the base of the sting.

Models

The geometric characteristics of the wings are given in table I. The wings were machined from heat-treated steel and the surfaces were

ground and polished to a smooth finish. The thickness of the leading and trailing edges was from 0.001 to 0.002 inch. All the wings were made to the same nominal area. For structural reasons wing support stings of two sizes (see figs. 2 and 3) were used. The larger wing support stings, designated "sting A," were used on those wings which had the maximum-thickness position at or forward of the midchord point and the smaller wing-support stings ("sting B") were employed on the remainder of the wings. (See fig. 4.) In all cases, the nose of the wing support stings was behind the wing ridge lines in order to minimize sting tare-interference effects. The stings were made of sufficient width to minimize the danger of wing failure in the regions of extreme thinness where the stings are attached to the wings. Mirrors approximately 1/16 inch in diameter were flush-mounted in the sting shoulder (as shown in fig. 1(b)) as a part of the optical angle-of-attack system.

In order to evaluate the effects of the presence of the stings on the lift, drag, and pitching moment of the test configurations, two pressure-distribution models were constructed as shown in figure 5. (For a detailed description of these models, see appendix A.)

Test Procedure

Measurements of the lift, drag, and pitching moment were made at Mach numbers of 1.62, 1.94, and 2.41 through an angle-of-attack range of -2° to 6° in increments of 1° , except near $\alpha = 0^{\circ}$ where $1/2^{\circ}$ increments were obtained. With the optical system for indicating angle of attack, the indicated angle may be taken as the true value since the load deflection of the wings ahead of the mirrors is negligible. All the wings were tested consecutively (numbers 1 to 18) at $M = 1.62$, $M = 1.94$, and $M = 2.41$. (The test procedure used on the two pressure-distribution models is discussed in detail in appendix A.) The Reynolds number range of the tests was from 1.96×10^6 to 2.75×10^6 based on mean aerodynamic chord.

Corrections to Experimental Data

The wing support stings used in the tests were of necessity large as a result of wing-load considerations; hence it was considered mandatory to obtain an accurate estimate of the magnitude of the sting tare-interference effects, particularly in regard to drag at zero lift. Test models used for this purpose are shown in figure 5 and a detailed description of the sting tare-interference tests can be found in appendix A. The change in pressure drag of the wing-sting configurations due to the presence of the stings (A and B) was applied to the measured drag data of the force tests. Figure 6 shows the magnitude and variation of these changes in pressure-drag coefficient with angle of attack (up to 6°) and

at all test Mach numbers. Lift and pitching-moment changes due to the presence of the stings were found to be negligible.

Additional corrections, which have been standardized and considered routine for wing-sting tests in the Langley 9-inch supersonic tunnel, were applied to the drag of the wing-sting configurations to account for the difference between free-stream pressure and (1) the measured pressure on the base of the support-sting shoulders and (2) the pressure in the fixed-windshield—shield—balance-box enclosure.

Precision of Data

Stream surveys obtained with the empty test section have indicated that the mean values of the Mach numbers in the region occupied by the test models in the test nozzles were 1.62, 1.94, and 2.41 and that the variation about these means was ± 0.01 or less. The estimated probable errors in the aerodynamic quantities are included in the following table:

C_L	± 0.002
C_D	± 0.0002
C_m	± 0.0018
α , deg	
Initial	± 0.05
Relative	± 0.01
R	$\pm 0.05 \times 10^6$

The value of $\pm 0.05^\circ$ given for angle of attack is a result of the error in initial referencing of each wing with respect to stream direction. The value of $\pm 0.01^\circ$ is the error that might be incurred in relative angle-of-attack readings for a given test.

Reynolds Number

The Reynolds numbers of the wings based on mean aerodynamic chord (see table I) varied as shown in the following table:

Wings	Reynolds number		
	M = 1.62	M = 1.94	M = 2.41
1 to 6	2.75×10^6	2.70×10^6	2.36×10^6
7 to 12	2.50	2.46	2.14
13 to 18	2.28	2.25	1.96

The small variations in Reynolds number shown are believed to be negligible insofar as the aerodynamic forces and moments are affected, as is indicated in the results of references 10, 11, and 12.

RESULTS AND DISCUSSION

The variation of lift, drag, pitching moment, and lift-drag ratios for an angle-of-attack range of -2° to 6° are given in figures 7 to 15 for all the wings of the investigation at Mach numbers of 1.62, 1.94, and 2.41. Table II presents a summary of the results of the investigation.

Lift

For the individual wings, the lift varies linearly with angle of attack. For this reason, the lift results can be discussed and compared with theory on the basis of lift-curve slope. The analyses of references 13, 14, 15, and 16 using linear theory indicate that the tangent ratio $\tan \epsilon / \tan m$ is a basic parameter in sweptback-wing or triangular-wing theory. Values of $\tan \epsilon / \tan m$ greater than 1 represent a wing whose leading edge is ahead of the Mach cone originating at the wing apex (supersonic leading edge); values of $\tan \epsilon / \tan m$ less than 1 represent a wing with a subsonic leading edge. References 1, 2, 14, and 15 have shown that, for thin triangular wings with leading edges ahead of the Mach cone, the lift-curve slope has Ackeret's (ref. 17) theoretical two-dimensional value of

$$C_{L\alpha_{\infty}} = \frac{4}{\sqrt{M^2 - 1}} \quad (1)$$

and that, for triangular wings with leading edges behind the Mach cone, this value becomes

$$C_{L\alpha} = \frac{2\pi \frac{\tan \epsilon}{\tan m}}{E\sqrt{M^2 - 1}} \quad (2)$$

The lift-curve slopes of the wings at all test Mach numbers are shown in figure 16 as a function of maximum-thickness position. Also included in the figure are the test values of the tangent ratio $\tan \epsilon / \tan m$, along with the lift-curve slopes predicted by linear theory. A cursory examination of the data for the condition in which the shock wave is detached from the leading edge of the wing shows an increase in lift-curve slope as the maximum-thickness position is moved rearward. This result is believed to be directly attributable

to the fact that significant transonic-flow effects occur on triangular wings at supersonic speeds for detached-shock conditions as conclusively shown by Boyd and Phelps in reference 18. Also, as shown in reference 19, airfoil thickness distribution has a pronounced effect on the flow characteristics over the wings (and thus force characteristics) when the flow over the wing is transonic in nature. Rearward movement of the wing maximum-thickness position, with the consequent reduction in the leading-edge wedge angle, would tend to favor shock attachment and thereby minimize the severity of the transonic flow phenomena (characterized by shock waves and flow separation) on the wing. Thus, an improvement in wing lifting ability and consequently better agreement with theory could reasonably be expected. A maximum increase in lift-curve slope of about 22 percent was realized (at $\tan \epsilon / \tan m = 1.070$ test condition) when the maximum-thickness position was moved from 18 percent to 70 percent chord. This percentage increase in the lift-curve slope with rearward movement of the wing maximum-thickness position agrees well with the value of 19 percent obtained on geometrically similar 8-percent-thick delta wings with maximum-thickness positions at 18 and 50 percent chord (ref. 7 and unpublished data of Love and Lovett, respectively) at comparable Mach numbers.

The lift-curve-slope data for attached-shock conditions (figs. 16(b) and (c)) show no appreciable change in slope with rearward movement of the wing maximum-thickness position and there is excellent agreement between experiment and theory. (Shock attachment has occurred on all wings when $\tan \epsilon / \tan m = 1.584$.)

The importance of shock attachment to the aerodynamic characteristics of delta wings has long been recognized, having been discussed by Clinton E. Brown of the Langley Laboratory before a technical group as early as 1948. Love also discussed this subject in reference 7. More recently, Ulmann and Bertram took cognizance of this phenomenon and presented (ref. 20) some simple methods for modifying the predictions of linear theory to account for shock detachment.

The lift-curve slopes have been replotted in figure 17 as a ratio to the theoretical two-dimensional slope, as given by equation (1), against the tangent ratio $\tan \epsilon / \tan m$ for the six maximum-thickness positions. (Because the test points shown in this figure represent data obtained at different Mach numbers, and because displacements occur in the data with Mach number for a given maximum-thickness position, it was not considered feasible to show faired curves.) It is at once apparent from an inspection of the figure that the maximum-thickness position is extremely critical insofar as the lift-curve-slope value is concerned when the flow over the wing is of a transonic nature. At the highest test value of the tangent ratio, the test points at all thickness locations tend to merge, a condition directly attributable to shock attachment to the leading edges of the wings.

At the lowest values of the tangent ratio (abscissa of plot) for which tests were made, the maximum-thickness position appears, again, to be tending toward secondary importance, as might be expected. In reference 20, it was pointed out that the analysis of delta-wing data for Mach numbers below 2.5, plotted to the variables of figure 17, has led to the conclusion that the linear theory gives a fairly accurate prediction of the lift of thin delta wings at low values of the tangent ratio but overestimates the lift at tangent ratios from about 0.7 to 1.5. Figure 17, however, shows that if the leading-edge wedge angle is relatively small, thereby approaching closely the restrictions of linear theory, the lift-curve slope of the wing is predicted closely by linear theory. For example, the lift-curve slopes of the wing with the location of maximum thickness at $0.70c$ are predicted within ± 3.5 percent throughout the tangent-ratio range of the tests (0.736 to 1.840).

Figure 18 has been prepared by using the results of the present investigation and published (refs. 3, 4, 5, 7, 8, 10, and 21 to 26) and unpublished delta-wing test data to show, primarily, some effects of thickness ratio on the variation of the lift-curve-slope ratio against the parameter $\tan \epsilon / \tan m$. Figure 18(a) is for wings with the maximum-thickness position relatively far forward (0.18c to 0.20c). Shown in the figure are wings having thicknesses of $3\frac{1}{2}$, 5, 6, and 8 percent. At the lower end of the tangent-ratio scale (around $\tan \epsilon / \tan m = 0.5$ and lower) the data points for all the wings tested at Mach numbers of 2.41 and below exhibit a tendency to cluster, which would indicate that the wing thickness has very little effect on the lift-curve slope when the flow over the wing is basically subsonic in nature. Hall (ref. 27) obtained similar results on triangular wing-body combinations. As one moves further along the tangent-ratio scale (an increase in $\tan \epsilon / \tan m$), the advent of transonic-flow phenomena on the wings is manifested by the divergence of the test data for the wings of different thickness ratios. Further increase in the tangent ratio results in the flow over the wings becoming predominantly supersonic, and when leading-edge shock attachment occurs the importance of the thickness on lift-curve slope is once again minimized, as evidenced by the fact that the thin- and thick-wing data appear to merge in the vicinity of $\tan \epsilon / \tan m = 2.2$. Except at those localities where the test points for all thickness ratios merged, the data exhibit systematic variation with thickness ratio with the wings of least thickness following the trend of the theoretical curve most closely. The agreement and the magnitude of disagreement between theory and experiment may be attributed to leading-edge wedge angle and shock attachment in the manner described in the discussion of figure 17.

The displacement of the hypersonic Mach number ($M = 6.9$) data relative to the data obtained at the lower Mach numbers (particularly those data obtained in ref. 7 for geometrically similar models) is to be expected, because, for these relatively thick wings, the correlating

parameters based on linear theory are not applicable at high supersonic Mach numbers, that is, Mach numbers above about 3 (ref. 22). The same reasoning would be expected to apply to the $M = 4.04$ data. Predictions of high Mach number results can be more accurately determined through use of a method based on shock-expansion theory presented in reference 20 by Ulmann and Bertram.

Figure 18(b) shows the compiled data for wings of various thickness ratios having their maximum-thickness positions near midchord (0.50c to 0.62c). Basically, the data of this compilation show results similar to those for the wings with maximum thickness well forward for the low and high tangent-ratio values. However, in the intermediate tangent-ratio range (where the transonic-flow phenomena were so prevalent for the wings with maximum thickness at 0.18c to 0.20c) the effects of thickness are considerably reduced. This is due, of course, to the fact that the leading-edge wedge angle becomes less with rearward movement of the maximum-thickness position. The better agreement with theory for these wings as compared with the wings of figure 18(a) may also be attributed for the most part to the reduction in leading-edge wedge angle. Again as expected (see ref. 20) the data at $M = 4.04$ and 6.9 are considerably higher than the data at the lower supersonic Mach numbers.

Drag

Minimum drag.- The minimum drag coefficients for the $3\frac{1}{2}$ -percent-thick delta wings of the investigation are presented in figure 19 as a function of the wing maximum-thickness position for the three test Mach numbers. Included in the figure is the theoretical pressure-drag coefficient computed by the method of reference 1, the equations of which are given in appendix B. Also shown in the figure, for illustrative purposes only, are the theoretical total-drag-coefficient curves (pressure drag plus friction drag) computed on the basis of the skin-friction coefficients corresponding to completely laminar and completely turbulent flow in the boundary layer. Laminar skin-friction coefficients were estimated from the Blasius flat-plate incompressible theory (ref. 28), since differences are negligible at the test Mach numbers (1.62, 1.94, and 2.41) between this theory and the more accurate theories which account for compressibility (refs. 29, 30, and 31). Turbulent skin-friction coefficients, on the other hand, were obtained from reference 32 (extended Frankl and Voishel results). The Reynolds number used in the selection of the skin-friction coefficients was based on the mean aerodynamic chord ($\frac{2}{3}c$) of the wings. The peaks on the theoretical curves (fig. 19(a), $\epsilon = 30^\circ$) represent the condition whereby the Mach line and wing ridge line are coincident and are characteristic of the linear theory, although unrealistic. (See refs. 7, 20, and 22.)

As can be seen in the figure, all the test points fall generally within the boundaries of the theoretical total-drag-coefficient curves. It is seen also that the data, in most cases, exhibit a smooth variation with maximum-thickness position, going from an initial value near the theoretically all-turbulent drag curve to a final value near the theoretically all-laminar drag curve. (This observation is most evident at $M = 1.94$ and 2.41 .) This variation of the experimental test points strongly suggests that the wing ridge lines are instrumental in "triggering" boundary-layer transition as observed in reference 7. Actually, the locations of the boundary-layer transition lines are determined by the presence of shock waves on the wing surface and the steep adverse pressure gradients that are predicted to occur just downstream of the ridge line and which are accentuated by these surface shock waves (see refs. 3, 7, and 18). The beneficial effect on wing drag of moving the maximum-thickness position rearward from 18 percent chord to 70 percent chord is reflected in a maximum decrease of around 50 percent in the minimum drag coefficient. These findings are comparable to results obtained on 8-percent-thick delta wings (for rearward shifts in the maximum-thickness position, from 18 to 50 and 60 percent chord) by other investigators, for example, Love (ref. 7) and Love and Lovett (data presented herein) at Mach numbers 1.62, 1.93, and 2.40 and Ulmann and Dunning (ref. 8) at $M = 4.04$.

The variation of the minimum drag with Mach number is shown in figure 20 for wings with common maximum-thickness positions. (For the sake of clarity the designation of individual test points has been omitted.) For those wings having the location of the maximum thickness from 18 to 50 percent chord, the variation of minimum drag with Mach number is generally linear and the rate of decrease with increase in Mach number is found to be comparable to similar wings of 8-percent thickness tested through the same Mach number range (ref. 7 and data of Love and Lovett). The minimum-drag variations of wings with more rearward maximum-thickness positions (60 to 70 percent chord) show an initial decline through half of the Mach number range (to about $M = 2$) similar to the forward-thickness-location wings; however, the curves have a tendency to level out with further increase in Mach number. This result is probably due to more favorable flow conditions over the wing incurred with the advent, or near advent, of shock-wave attachment to the wing leading edge. The lowest value of minimum drag coefficient (0.0049) occurred at $M = 2.41$ on the aspect ratio 3.36 wing ($\epsilon = 40^\circ$) with the maximum-thickness position at the 70-percent-chord station (wing 18).

The linear theory for delta wings, as derived by Puckett (ref. 1), indicates that all delta wings with double-wedge airfoil sections having a given maximum-thickness location and the same value of the tangent ratio will have the same value of $C_{D_p} \beta / \tau^2$ (where C_{D_p} is the minimum pressure-drag coefficient) within the restrictions of linear theory.

Thus, the theoretical predictions of the minimum pressure drag for wings of the same maximum-thickness position appear as single curves when plotted in the form $C_{D_p}\beta/\tau^2$ against $\tan \epsilon/\tan m.$

In order to compare the experimental drag data of the present investigation on the basis of the linear theory, it was necessary to deduct a calculated friction-drag coefficient from the experimental values of measured minimum drag coefficients. For the purpose of these calculations, therefore, boundary-layer transition was assumed to occur at the wing ridge line and laminar and turbulent friction-drag coefficients were calculated by using the methods described previously. The variations of the theoretically derived and the experimentally adjusted wave-drag parameter $C_{D_p}\beta/\tau^2$ with tangent ratio are shown in figure 21 for all maximum-thickness locations. A cursory inspection of the figure reveals fair agreement of the test points with theory, with the exception of the wings with maximum thickness relatively far forward (0.18c). However, correlation of the experimental data along a single curve appears to be best for the wings with the maximum thickness at this forward chordwise wing station. In general, as the maximum-thickness position is moved rearward, the scatter of the data increases; thus the correlation as predicted by linear theory appears to become progressively worse. The key to a true comparison of this nature, however, lies in the accurate assessment of the skin-friction-drag coefficients. With this in mind, on the basis of the comparison shown in figure 21 (based on approximated values of skin-friction-drag coefficients), the quantitative and qualitative predictions of the linear theory can be considered good, at least for nonblunt wings.

To illustrate the effects of thickness ratio on the variation of the drag parameters $C_{D_{min}}\beta/\tau^2$ and $C_{D_p}\beta/\tau^2$ with tangent ratio of double-wedge delta wings, results obtained in other facilities (refs. 3, 4, 5, 7, 8, 9, 21 to 26, 33, 34, and unpublished data) on delta wings of various thicknesses and those of the present tests are compiled in figures 22 and 23. The plots of the minimum-drag parameter $C_{D_{min}}\beta/\tau^2$ (figs. 22(a) and 23(a)) are intended solely for the discretionary use of the reader and to afford a comparison of the pressure drag ($C_{D_p}\beta/\tau^2$) values with the minimum-drag ($C_{D_{min}}\beta/\tau^2$) values from which they were obtained by subtraction of a skin-friction-drag coefficient ($C_{D_p} = C_{D_{min}} - C_{D_f}$). (The minimum drag coefficients $C_{D_{min}}$ of the tests of refs. 3, 4, and 5 include the forces on the mounting body; for the rocket-model tests of ref. 9, $C_{D_{min}}$ represents wing drag plus wing-body interference drag.) For those data from tests up to and including $M = 2.41$, the skin-friction-drag coefficients were determined as described in the previous paragraph. At $M = 4.04$, skin-friction-drag coefficients have been determined for those wings with the maximum thickness near midchord (0.50c to 0.60c) by means of fluorescent-lacquer

tests (ref. 24) and references 30 and 35; therefore, these values have been used in computing the pressure drag for this series of wings. For those wings with the maximum thickness at $0.18c$, an experimental value of friction-drag coefficient was obtained by plotting the drag coefficients of wings having the same plan form and section against the square of the wing thickness ratio and making a straight-line extrapolation through the experimental points to the zero-thickness ordinate. The skin-friction-drag coefficients for those wings at the hypersonic Mach number ($M = 6.9$) have been determined as outlined in reference 23.

In figure 22(b) are shown those drag data for wings with the maximum-thickness positions at or near the 20-percent-chord location ($0.18c \leq 1 - r \leq 0.20c$). It is at once apparent that the difference between the experimentally derived and the theoretically predicted wing drag is quite large. Thus, the conclusion that linear theory is inadequate for predicting drag characteristics for wings with relatively blunt leading edges previously determined by Love (ref. 7) and others appears to be valid even for the thin ($3\frac{1}{2}$ -percent-thick) wings of the present investigation. The overall correlation of the data cannot be considered good. For those data obtained at the relatively low Mach numbers (up to and including $M = 2.41$), it would be expected that a better degree of correlation could be obtained if the accuracy of assessment of the skin-friction-drag coefficients was improved. As regard the high Mach number data ($M = 4.04$ and 6.9), Ulmann and Bertram (ref. 20) have pointed out that, for wings with maximum thickness at locations other than midchord, higher order terms become important and the two-dimensional shock-expansion theory indicates Mach number effects in the shock-attached region which cannot be correlated by these parameters. (See fig. 22(b).)

In figure 23(b) are shown the drag data for wings which have maximum-thickness positions near or at the midchord station $0.50c \leq 1 - r \leq 0.62c$. Again, the overall correlation of the data cannot be considered good. However, a better degree of correlation of all the experimental data would probably be realized with a more accurate assessment of friction drag.

Drag due to lift.- In delta-wing theory (ref. 13), a subsonic leading edge is characterized by an infinite pressure peak at the nose of the airfoil which, in the drag-due-to-lift calculations, must be accounted for by a leading-edge-suction term. The following equation (extracted from ref. 7) gives the theoretical drag due to lift with leading-edge suction as

$$\frac{\Delta C_D}{C_L^2} = \frac{1}{\frac{dC_L}{d\alpha}} - \frac{\beta\sqrt{1-w^2}}{4\pi w} \quad (3)$$

where α is in radians. Although the theory shows a forward thrust on the thin plate with a sharp edge, it is not to be expected that this characteristic will be realized in practice because very thin delta wings produce a laminar separation at the leading edge which tends to reduce the very high suction pressures that produce the drag relief (ref. 36).

When the leading edge is supersonic; that is, when $\tan \epsilon / \tan m \geq 1.0$, no leading-edge suction force exists theoretically and the drag due to the lift is given by the expression

$$\frac{\Delta C_D}{C_L^2} = \frac{1}{\frac{dC_L}{d\alpha}} \quad (4)$$

For this condition the pressure at the nose is finite and the theoretical stagnation point is at the leading edge; therefore, no flow can occur between the upper and lower surfaces.

Figure 24 shows some effects of maximum-thickness position on the variation of the drag-due-to-lift factor $\Delta C_D / C_L^2$ for the wings of the investigation at the three test Mach numbers. Included in the figure are the theoretical drag-due-to-lift curves with and without leading-edge suction and the test points representing the reciprocal of the experimental lift-curve slopes obtained on the wings. The experimental values of $\Delta C_D / C_L^2$ were obtained by evaluating the slopes of the straight lines faired through the experimental points on plots of ΔC_D against C_L^2 . At all Mach numbers and tangent ratios of the tests, the wings with the maximum-thickness position at 18 percent chord indicate, according to the concepts of inviscid theory, leading-edge suction (the difference between the $\Delta C_D / C_L^2$ values and the reciprocals of the experimental lift-curve slopes). For the other wings, the indicated leading-edge suction is either less or nonexistent, depending on maximum-thickness location and tangent ratio.

The fact that substantial leading-edge suction is indicated is surprising in view of the sharpness of the wing leading edges and is believed to be misleading, because the method of indicating leading-edge suction based on equation (3) is obviously inadequate for those wings which fail to approach closely the restrictions of the linear theory. Although theory based on a wing of zero thickness predicts the drag-due-to-lift factor $\Delta C_D / C_L^2$ to be equivalent to the reciprocal of the lift-curve slope $1 / C_{L\alpha}$ when $\tan \epsilon / \tan m \geq 1$, experimentally with wings of finite thickness it appears that leading-edge wedge angle and therefore shock attachment or the approach thereto is the criterion rather than tangent ratio. Thus, for wings which approach closely the restrictions of the theory, good predictions can be expected.

Lift-Drag Ratio

Experimental and theoretical lift-drag ratios of the test wings are presented in figure 25 plotted against wing lift coefficient, and in figure 26 the maximum lift-drag ratios are compiled and shown as a function of the wing maximum-thickness position. In the calculations of the theoretical lift-drag ratios it was assumed that the flow over the wing was laminar to the ridge line, at which point transition occurred, with turbulent flow existing over the wing behind this line. Friction-drag coefficients (see table II) based on this type of boundary-layer flow were added to the previously calculated wave-drag values in determining the theoretical lift-drag ratios. In the calculation of the theoretical values of $(L/D)_{\max}$, the following equation, obtained from reference 13, was used:

$$(L/D)_{\max} = \frac{1}{2} \sqrt{\frac{1}{C_{D_{\min}} \frac{\Delta C_D}{C_L^2}}} \quad (5)$$

A cursory examination of figure 25 shows the trends of the experimental and theoretical L/D curves to be clearly allied; however, as shown in figure 26, the calculated values of $(L/D)_{\max}$ depart markedly from the experimental values in the low ($\tan \epsilon / \tan m = 0.736$ and 0.894) and high ($\tan \epsilon / \tan m = 1.535$ and 1.840) operating range of the investigation. The cause of this large discrepancy can possibly be attributed to the inaccurate theoretical assessment of the drag-due-to-lift factor $\Delta C_D / C_L^2$ (see table II), which enters into the equation for $(L/D)_{\max}$ (see eq. (5)). At intermediate $\tan \epsilon / \tan m$ values the agreement between the calculated and the experimental values is considerably improved, although in all probability the agreement is fortuitous.

As shown in figure 26, the trends of the experimental curves, which show an increase in $(L/D)_{\max}$ with rearward movement of the maximum-thickness position, are predicted rather closely by the theory in most cases. Both the calculated and experimental curves show a tendency to reach a maximum near the 60- to 70-percent-chord station. The highest lift-drag ratio (10.8) was obtained at $M = 2.41$ on the $\epsilon = 40^\circ$ wing of highest aspect ratio ($A = 3.36$) and with the position of maximum thickness at the most rearward station tested (70 percent chord). This wing also had the least minimum drag of all the wings. With minor exceptions the experimental values of $(L/D)_{\max}$ increased with Mach number; this is in opposition to the theoretical prediction.

Center of Pressure

The chordwise center-of-pressure location of the wings are shown in figure 27. The experimental center of pressure was determined from the change in pitching-moment-curve slope with lift-curve slope near zero lift. The chordwise center-of-pressure position is shown by linear theory to be fixed at the wing center of area (midpoint of the mean aerodynamic chord) and is shown in the figure. The experimental centers of pressure are approximately 3 percent ahead of the theoretical position and essentially independent of maximum-thickness location, Mach number, semiapex angle, and, therefore, tangent ratio $\tan \epsilon / \tan m$. Semispan tests of a 2.9-percent-thick double-wedge delta ($\epsilon = 30^\circ$) wing with the maximum thickness at 62 percent chord (ref. 33) showed a similar center-of-pressure location (between 47 and 48 percent of the mean aerodynamic chord) at Mach numbers of 1.50 and 2.00.

In contrast to the negligible variation of center of pressure with tangent ratio $\tan \epsilon / \tan m$ indicated by the present results, results for thicker wings (8 percent, ref. 7) have shown a forward movement of the center of pressure of about 10 percent with increase in tangent ratio.

CONCLUSIONS

An investigation of the effects of thickness distribution on the aerodynamic characteristics of eighteen $3\frac{1}{2}$ -percent-thick delta wings was made at Mach numbers of 1.62, 1.94, and 2.41 in the Reynolds number range from 1.96×10^6 to 2.75×10^6 . An analysis of the results has indicated the following conclusions:

1. The wing drag at zero lift calculated by the linearized theory was in qualitative agreement and fair quantitative agreement with the test results in indicating the effects of varying the maximum-thickness position.

2. The decrease in minimum drag coefficient $C_{D_{min}}$ as a result of moving the wing maximum-thickness position from 18 to 70 percent chord was, for some cases, as much as 50 percent. The optimum maximum-thickness position, from the standpoint of minimum drag, appeared to be near 60 to 70 percent chord.

3. The lift-curve slope was accurately predicted by linear theory for the condition of shock-wave attachment to the leading edge of the wings. In addition, equally good agreement between theory and experiment was obtained for the condition of shock-wave detachment for those wings with the location of the maximum thickness at 60 to 70 percent

chord; however, as the maximum-thickness position was moved forward on the wing, the agreement between theory and experiment deteriorated.

4. The gain in lift-curve slope achieved by shifting the maximum-thickness position from 18 to 70 percent chord was as much as 22 percent.

5. The maximum lift-drag ratios increased with rearward movement of the wing maximum-thickness position and appeared to reach a maximum at all Mach numbers and wing semiapex angles when the maximum thickness was located at the 60- to 70-percent-chord station. The maximum lift-drag ratio obtained in the tests was 10.8 and occurred at a Mach number of 2.41 on the wing which had the least minimum drag of the series. The experimental variation of the maximum lift-drag ratio with Mach number was in opposition to the theoretical prediction of decreasing maximum lift-drag ratio with increasing Mach number.

6. The prediction of the drag-due-to-lift factor based on the method of linear theory is adequate for wings which approach closely the restrictions of the theory.

7. The locations of the chordwise centers of pressure of the wings were at the 47- to 48-percent-mean-aerodynamic-chord stations and remained essentially invariant with maximum-thickness location, Mach number, semiapex angle (therefore, aspect ratio), and ratio of the tangent of the wing semiapex angle to the tangent of the Mach angle ($\tan \epsilon / \tan m$).

Langley Aeronautical Laboratory,
National Advisory Committee for Aeronautics,
Langley Field, Va., April 6, 1955.

APPENDIX A

EVALUATION OF SUPPORT-STING TARE-INTERFERENCE EFFECTS

It was considered necessary in this investigation to evaluate the sting tare forces and interference effects if a correct analysis of the drag results was to be made, particularly for the minimum drag. Tests were therefore undertaken on two configurations considered representative of the test models of the primary investigation.

Description of Models

The models used in the tests are shown in figure 5. As previously described in the body of this report, two stings of different sizes were employed to support the wings used in the primary investigation. (See figs. 2, 3, and 4.) Therefore, in the tests of sting tare-interference effects it was necessary to obtain data on wings equipped with the stings of different sizes. The wings chosen for the tests were geometrically similar to wings 10 and 11 of the primary investigation (wings 10 and 11 were supported by sting A (large) and sting B (small), respectively, in the primary investigation) and were considered to be representative of the wings of the investigation.

As shown in figure 5, the wings were mounted on sweptback struts which attached to an angle-of-attack bar (not shown in sketch). Mirrors approximately 1/16 inch in diameter (not visible in sketch) were flush-mounted in the struts as part of the optical angle-of-attack system. Sting replicas (or dummy stings) were attached to the wings as shown to simulate the actual support stings. These dummy stings were detachable. Measurements of the pressure distributions over the portions of the wings influenced by the disturbances created by the stings and over the faces of the stings were accomplished by means of pressure orifices located on the surfaces of the models at the positions shown in figure 28. A complete set of orifices was placed in the strut-free side of the models only.

The models were made from hardened steel, similar to those used in the main investigation, with comparable tolerances.

Test Procedure

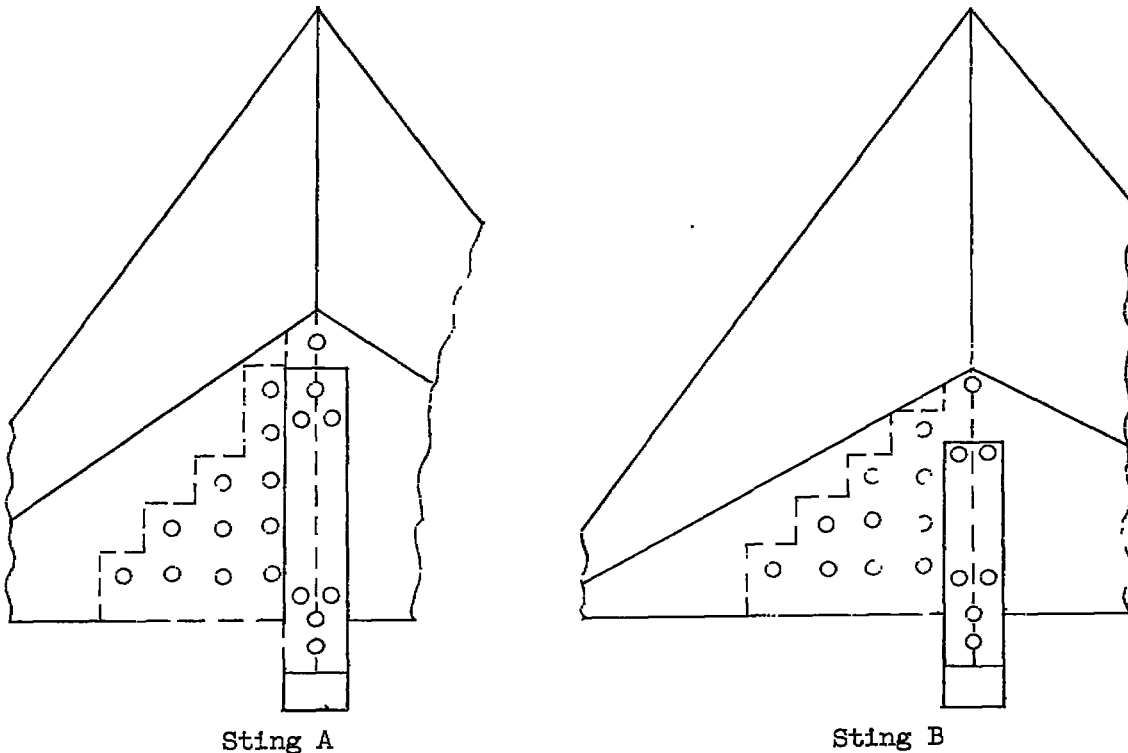
The procedure followed in conducting the tests was to obtain pressure data on both models at all Mach numbers (1.62, 1.94, and 2.41) and the desired angles of attack with the dummy stings attached and

then repeat the tests with the stings removed. The angle of attack was usually varied from 0° to 6° in increments of 2° . Since a complete set of orifices was present in only one surface, tests were made at both positive and negative angles of attack in order that complete data might be obtained. For purposes of calculation, it was necessary to assume that the pressures existing on the bottom surface at a given positive angle of attack were identical to those measured on the top surface at the same negative angle of attack.

Pressure Measurements and Reduction of Data

The pressures on the wing and sting surfaces and the total pressure in the tunnel settling chamber were recorded manually from a multiple-tube manometer.

Inasmuch as the tests of sting tare-interference effects were for the determination of the change in force and moment coefficients of the wing-sting configurations due to the presence of the support stings on the wings, integrations of the measured pressures recorded on the models were made for the conditions with and without the dummy stings attached to the wings and over an area on each model as shown in outline in the following sketches:



Precision of Data

The estimated probable errors in the aerodynamic quantities for $M = 1.62, 1.94, \text{ and } 2.41$ are included in the following table:

P	± 0.005
α , deg	
Initial	± 0.075
Relative	± 0.01
C_{D_p}	± 0.0001

The value of ± 0.075 given for angle of attack is a result of the error incurred in the initial referencing of each wing with respect to stream direction. The value of $\pm 0.01^\circ$ is the error that might be incurred in relative angle-of-attack readings for a given test.

Results

The principal results are shown in figure 6 as the change in pressure-drag coefficients due to the presence of the stings. No plots of change in lift and pitching-moment coefficients due to sting presence are shown, because these changes were negligible.

Figures 29 and 30 show the pressure changes which occurred on the test configurations due to the presence of sting A and sting B, respectively. With the aid of the pressure diagrams (figs. 29 and 30) and figure 28, the extent and magnitude of the sting interference regions are easily visualized. The largest changes in pressure occurred at the wing stations occupied by the stings, and, as expected, a rapid decrease in pressure change occurred with rearward movement along the faces of the stings. Since the areas under the curves are indicative of the pressure drag, the reduction in pressure change is indeed favorable as regards the tare drag of the stings. It is also seen that the pressure change at the sting station (station I) is smaller for sting A than for sting B, because, of course, of the smaller wedge angle of sting A. On the other hand, it is seen that the area of influence of sting A is considerably more than that of sting B. This fact and the moderate pressures over the face of sting A combine advantageously to produce a relatively small tare-interference drag force (and, at some angles of attack, a thrust) as shown in figure 6(a). On the contrary, the area of influence of sting B on the wing pressures is relatively small; consequently, most of the tare-interference drag is due to the pressures on the face of the sting.

APPENDIX B

CALCULATION OF PRESSURE DRAG

The equations for computation of the pressure drag of triangular wings are as follows:

For the Mach line behind both the leading edge and the ridge line,

$$C_{Dp} = \frac{2r^2}{\beta\pi(1-r^2)} \left[\frac{1}{\sqrt{1-n^2}} \cos^{-1} n + \frac{1}{r\sqrt{1-r^2n^2}} \left(\frac{\pi}{2} + \sin^{-1} rn \right) \right] \quad (B1)$$

For the Mach line ahead of the leading edge but behind the ridge line,

$$C_{Dp} = \frac{2r^2}{\beta\pi} \left[\frac{G_2(n,r)}{r(1-r)^2} + \frac{1}{r(1-r)} \left(\frac{\pi}{2} - \frac{\log n}{\sqrt{n^2-1}} - \sin^{-1} \frac{1}{n} \right) \right] \quad (B2)$$

where

$$G_2(n,r) = \frac{1-r}{1+r} \left[\frac{\log n}{\sqrt{n^2-1}} + \frac{r \cos^{-1} n}{\sqrt{n^2-1}} + \frac{2}{\sqrt{1-r^2n^2}} \tan^{-1} \left(\frac{\sqrt{1-r^2n^2}}{n-rn+\sqrt{n^2-1}} \right) \right] \quad (B3)$$

For the Mach line ahead of both leading edge and ridge line,

$$C_{Dp} = \frac{2r^2}{\beta\pi} \left[\frac{G_2'}{r(1-r)^2} \frac{F'}{(1-r)^2} \frac{1}{r(1-r)} \left(\frac{\log nr}{\sqrt{r^2n^2-1}} - \frac{\log n}{\sqrt{n^2-1}} + \sin^{-1} \frac{1}{rn} - \sin^{-1} \frac{1}{n} \right) \right] \quad (B4)$$

where

$$G_2' = \frac{1-r}{1+r} \left\{ \frac{\log n}{\sqrt{n^2-1}} + \frac{r \cos^{-1} n}{\sqrt{n^2-1}} + \frac{1}{\sqrt{r^2 n^2-1}} \log \left[1 + \frac{2\sqrt{r^2 n^2-1}}{n(1-r) + \sqrt{n^2-1} - \sqrt{r^2 n^2-1}} \right] \right\} \quad (B5)$$

and

$$F' = \frac{1-r}{1+r} \left\{ \frac{\log rn}{\sqrt{r^2 n^2-1}} + \frac{1}{\sqrt{n^2-1}} \log \left[\frac{rn^2-1 + \sqrt{(r^2 n^2-1)(n^2-1)}}{n(1-r)} \right] \right\} \quad (B6)$$

In these equations,

$$\beta = \sqrt{M^2 - 1}$$

τ thickness ratio at root

r distance of ridge-line apex from trailing edge, percent root chord

$$n = \frac{\tan m}{\tan \epsilon}$$

REFERENCES

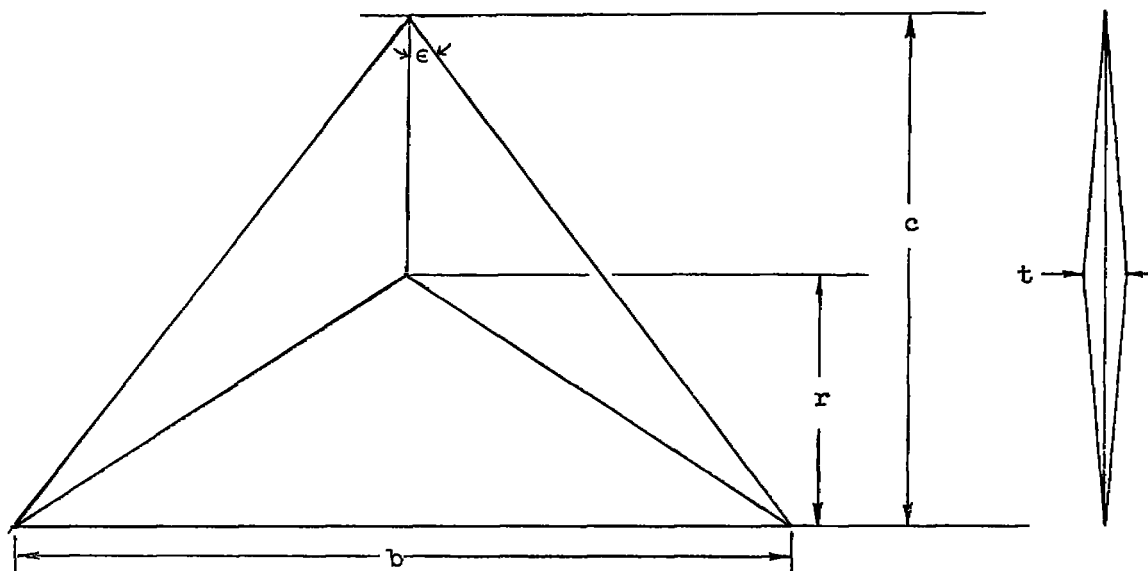
1. Puckett, Allen E.: Supersonic Wave Drag of Thin Airfoils. Jour. Aero. Sci., vol. 13, no. 9, Sept. 1946, pp. 475-484.
2. Puckett, A. E., and Stewart, H. J.: Aerodynamic Performance of Delta Wings at Supersonic Speeds. Jour. Aero. Sci., vol. 14, no. 10, Oct. 1947, pp. 567-578.
3. Vincenti, Walter G., Nielsen, Jack N., and Matteson, Frederick H.: Investigation of Wing Characteristics at a Mach Number of 1.53. I - Triangular Wings of Aspect Ratio 2. NACA RM A7110, 1947.
4. Berggren, Robert E., and Summers, James L.: Aerodynamic Characteristics at Subsonic and Supersonic Mach Numbers of a Thin Triangular Wing of Aspect Ratio 2. I - Maximum Thickness at 20 Percent of the Chord. NACA RM A8116, 1948.
5. Walker, Harold J., and Berggren, Robert E.: Aerodynamic Characteristics at Subsonic and Supersonic Mach Numbers of a Thin Triangular Wing of Aspect Ratio 2. II - Maximum Thickness at Midchord. NACA RM A8120, 1948.
6. Vincenti, Walter G.: Comparison Between Theory and Experiment for Wings at Supersonic Speeds. NACA Rep. 1033, 1951. (Supersedes NACA TN 2100.)
7. Love, Eugene S.: Investigation at Supersonic Speeds of 22 Triangular Wings Representing Two Airfoil Sections for Each of 11 Apex Angles. NACA RM L9D07, 1949.
8. Ulmann, Edward F., and Dunning, Robert W.: Aerodynamic Characteristics of Two Delta Wings at Mach Number 4.04 and Correlations of Lift and Minimum-Drag Data for Delta Wings at Mach Numbers From 1.62 to 6.9. NACA RM L52K19, 1952.
9. Welsh, Clement J.: Results of Flight Tests To Determine the Zero-Lift Drag Characteristics of a 60° Delta Wing With NACA 65-006 Airfoil Section and Various Double-Wedge Sections at Mach Numbers From 0.7 to 1.6. NACA RM L50F01, 1950.
10. Goldbaum, G. C., Delameter, H. D., and Stamper, J. C.: Analysis of Force and Moment Characteristics From Supersonic Wind-Tunnel Tests of a 45-Percent-Scale Model of the Sparrow 13-D Wing. Rep. No. SM-13627 (Bur. Aero. Contract NOa(s)-9392), Douglas Aircraft Co., Inc., Feb. 20, 1950.

11. Hatch, John E., Jr., and Gallagher, James J.: Aerodynamic Characteristics of a 68.4° Delta Wing at Mach Numbers of 1.6 and 1.9 Over a Wide Reynolds Number Range. NACA RM L53I08, 1953.
12. Hatch, John E., Jr., and Hargrave, L. Keith: Effects of Reynolds Number on the Aerodynamic Characteristics of a Delta Wing at a Mach Number of 2.41. NACA RM L51H06, 1951.
13. Jones, Robert T.: Estimated Lift-Drag Ratios at Supersonic Speed. NACA TN 1350, 1947.
14. Brown, Clinton E.: Theoretical Lift and Drag of Thin Triangular Wings at Supersonic Speeds. NACA Rep. 839, 1946. (Supersedes NACA TN 1183.)
15. Stewart, H. J.: The Lift of a Delta Wing at Supersonic Speeds. Quarterly Appl. Math., vol. IV, no. 3, Oct. 1946, pp. 246-254.
16. Robinson, A.: Lift and Drag of a Flat Delta Wing at Supersonic Speeds. Tech. Note No. Aero. 1791, British R.A.E., June 1946.
17. Ackeret, J.: Air Forces on Airfoils Moving Faster Than Sound. NACA TM 317, 1925.
18. Boyd, John W., and Phelps, E. Ray: A Comparison of the Experimental and Theoretical Loading Over Triangular Wings at Supersonic Speeds. NACA RM A50J17, 1951.
19. Lindsey, W. F., Daley, Bernard N., and Humphreys, Milton D.: The Flow and Force Characteristics of Supersonic Airfoils at High Subsonic Speeds. NACA TN 1211, 1947.
20. Ulmann, Edward F., and Bertram, Mitchel H.: Aerodynamic Characteristics of Low-Aspect-Ratio Wings at High Supersonic Mach Numbers. NACA RM L53I23, 1953.
21. Henderson, Arthur, Jr.: Experimental Investigation of the Zero-Lift Wave Drag of Seven Pairs of Delta Wings With Constant and Varying Thickness Ratios at Mach Numbers of 1.62, 1.93, and 2.41. NACA RM L55D13, 1955.
22. Bertram, Mitchel H., and McCauley, William D.: Investigation of the Aerodynamic Characteristics at High Supersonic Mach Numbers of a Family of Delta Wings Having Double-Wedge Sections With the Maximum Thickness at 0.18 Chord. NACA RM L54G28, 1954.
23. Bertram, Mitchel H., and McCauley, William D.: An Investigation of the Aerodynamic Characteristics of Thin Delta Wings With a Symmetrical Double-Wedge Section at a Mach Number of 6.9. NACA RM L55B14, 1955.

24. Dunning, Robert W., and Ulmann, Edward F.: Effects of Sweep and Angle of Attack on Boundary-Layer Transition on Wings at Mach Number 4.04. NACA TN 3473, 1955.
25. Shevell, R. S.: Project Nike - Second Aberdeen Wind Tunnel Test - Mach Number = 1.28. Rep. No. SM-11900, Douglas Aircraft Co., Inc., July 8, 1946.
26. Michel, L. R., and Shef, A. L.: Project Nike - Third Aberdeen Wind Tunnel Test - Mach Number = 1.72. Rep. No. SM-12041, Douglas Aircraft Co., Inc., Aug. 27, 1948.
27. Hall, Charles F.: Lift, Drag, and Pitching Moment of Low-Aspect-Ratio Wings at Subsonic and Supersonic Speeds. NACA RM A53A30, 1953.
28. Blasius, H.: The Boundary Layers in Fluids With Little Friction. NACA TM 1256, 1950.
29. O'Donnell, Robert M.: Experimental Investigation at a Mach Number of 2.41 of Average Skin-Friction Coefficients and Velocity Profiles for Laminar and Turbulent Boundary Layers and an Assessment of Probe Effects. NACA TN 3122, 1954.
30. Van Driest, E. R.: Investigation of Laminar Boundary Layer in Compressible Fluids Using the Crocco Method. NACA TN 2597, 1952.
31. Chapman, Dean R., and Rubesin, Morris W.: Temperature and Velocity Profiles in the Compressible Laminar Boundary Layer With Arbitrary Distribution of Surface Temperature. Jour. Aero. Sci., vol. 16, no. 9, Sept. 1946, pp. 547-565.
32. Rubesin, Morris W., Maydew, Randall C., and Varga, Steven A.: An Analytical and Experimental Investigation of the Skin Friction of the Turbulent Boundary Layer on a Flat Plate at Supersonic Speeds. NACA TN 2305, 1951.
33. Johnson, M. C.: Analysis of Force and Moment Characteristics from Wind Tunnel Tests at Mach Numbers of 1.50 and 2.00 of a 45-Percent-Scale Semi-Span Model of the Sparrow 13-D Wing. Rep. No. SM-14060 (Bur. Aero. Contract NOa(s)-10872), Douglas Aircraft Co., Inc., Nov. 30, 1951.
34. Delameter, H. D., Stamper, J. C., and Solvason, J. C.: Model XAAM-N-2. Preliminary Analysis of Force and Moment Characteristics From Supersonic Wind Tunnel Tests of a 45% Scale Semi-Span Model. Mach No. = 1.72. Rep. No. SM-13469, Douglas Aircraft Co., Inc., Aug. 10, 1949.

35. Van Driest, E. R.: The Turbulent Boundary Layer for Compressible Fluids on a Flat Plate With Heat Transfer. Rep. No. AL-997, North American Aviation, Inc., Jan. 27, 1950.
36. Brown, Clinton E., and Hargrave, L. K.: Investigation of Minimum Drag and Maximum Lift-Drag Ratios of Several Wing-Body Combinations Including a Cambered Triangular Wing at Low Reynolds Numbers and at Supersonic Speeds. NACA RM L51E11, 1951.

TABLE I

GEOMETRIC CHARACTERISTICS OF $3\frac{1}{2}$ - PERCENT-THICK DELTA WINGS

(a) Dimensions of wings

Wings	ϵ , deg	b , in.	c , in.	\bar{c} , $\frac{2}{3} c$, in.	S , sq in.	A	t , in.
1 to 6	30	4.298	3.722	2.481	8.00	2.31	0.130
7 to 12	35	4.734	3.380	2.253	8.00	2.80	.118
13 to 18	40	5.180	3.087	2.058	8.00	3.36	.108

(b) Maximum-thickness locations

Wing	ϵ , deg	$1 - r$, percent c	Wing	ϵ , deg	$1 - r$, percent c	Wing	ϵ , deg	$1 - r$, percent c
1	30	18	7	35	18	13	40	18
2	30	30	8	35	30	14	40	30
3	30	40	9	35	40	15	40	40
4	30	50	10	35	50	16	40	50
5	30	60	11	35	60	17	40	60
6	30	70	12	35	70	18	40	70

TABLE II
SUMMARY OF RESULTS

(a) $M = 1.62$

Wing	ϵ , deg	l - r, percent chord	Lift		Drag						Pitching moment		Lift-drag ratio		Center of pressure		Optimum lift coefficient			
			$C_{L\alpha}$		C_{Dp}		C_{Df}		C_{Dmin}		$\Delta C_D/C_L^2$		$C_{m\alpha}$		$(L/D)_{max}$		$C_{m\alpha}/C_{L\alpha}$, percent M.A.C.		C_{Lopt}	
			Theor.	Exp.	Theor.	Exp.	Theor.	Exp.	Theor.	Exp.	Theor.	Exp.	Theor.	Exp.	Theor.	Exp.	Theor.	Exp.	Theor.	Exp.
1	30	18	0.0465	0.0420	0.00411	-----	0.00549	-----	0.00960	0.0114	0.2856	0.3250	0	0.0005	9.566	8.4	50	49.29	0.1857	0.1775
2	30	30	.0465	.0424	.00538	-----	.00495	-----	.01051	.0105	.2856	.3360	0	.00004	9.256	8.5	50	48.02	.1905	.1775
3	30	40	.0465	.0435	.00451	-----	.00445	-----	.00896	.0102	.2856	.3715	0	.0013	9.902	8.45	50	47.25	.1774	.1774
4	30	50	.0465	.0440	.00419	-----	.00398	-----	.00817	.0084	.2856	.3880	0	.0008	10.370	8.85	50	48.18	.1694	.1589
5	30	60	.0465	.0481	.00426	-----	.00351	-----	.00777	.0090	.2856	.3600	0	.0013	10.654	9.00	50	46.89	.1652	.1550
6	30	70	.0465	.0475	.00478	-----	.00265	-----	.00745	.0092	.2856	.3624	0	.0012	10.872	8.8	50	47.47	.1616	.1625
7	35	18	0.0519	0.0429	0.00918	-----	0.00561	-----	0.01479	0.0128	0.2863	0.3160	0	0.00104	7.685	7.95	50	47.67	0.2273	0.1925
8	35	30	.0519	.0450	.00576	-----	.00505	-----	.01079	.0113	.2863	.3280	0	.00167	8.998	8.5	50	46.29	.1942	.1750
9	35	40	.0519	.0467	.00474	-----	.00456	-----	.00950	.0088	.2863	.3250	0	.0014	9.691	9.29	50	47.01	.1723	.1690
10	35	50	.0519	.0475	.00435	-----	.00408	-----	.00843	.0105	.2863	.3270	0	.0016	10.179	9.05	50	48.32	.1716	.1750
11	35	60	.0519	.0505	.00438	-----	.00360	-----	.00798	.0092	.2863	.3350	0	.0017	10.462	9.19	50	46.65	.1670	.1670
12	35	70	.0519	.0509	.00486	-----	.00313	-----	.00799	.0083	.2863	.3340	0	.0021	10.452	9.85	50	45.87	.1671	.1590
13	40	18	0.0548	0.0438	0.01059	-----	0.00570	-----	0.01598	0.0140	0.319	0.2850	0	0.0018	7.005	8.00	50	45.89	.2238	.2075
14	40	30	.0548	.0458	.00643	-----	.00512	-----	.01155	.0117	.319	.2846	0	.0015	8.258	8.70	50	46.72	.1905	.1954
15	40	40	.0548	.0485	.00515	-----	.00465	-----	.00980	.0098	.319	.3026	0	.0021	8.943	9.25	50	45.65	.1753	.1700
16	40	50	.0548	.0488	.00462	-----	.00417	-----	.00879	.0085	.319	.3124	0	.0020	9.443	9.9	50	45.90	.1660	.1625
17	40	60	.0548	.0517	.00458	-----	.00369	-----	.00827	.0078	.319	.3280	0	.0020	9.755	10.08	50	46.14	.1610	.1500
18	40	70	.0548	.0536	.00502	-----	.00322	-----	.00824	.0099	.319	.3304	0	.0020	9.752	9.95	50	46.27	.1607	.1570

TABLE II.- Continued

SUMMARY OF RESULTS

(b) $M = 1.94$

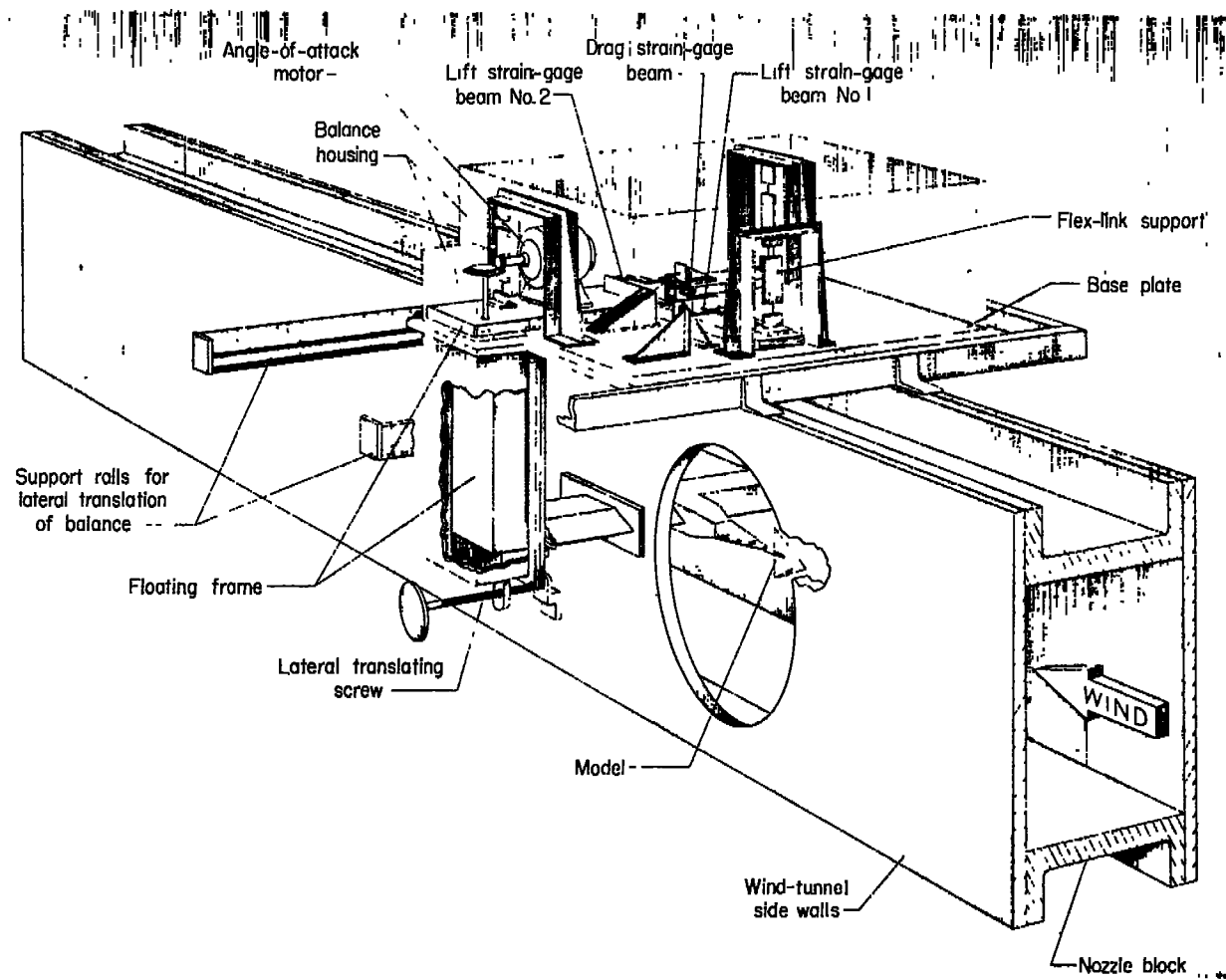
Wing	ϵ , deg	l - r, percent chord	Lift		Drag						Pitching moment		Lift-drag ratio		Center of pressure		Optimum lift coefficient			
			$C_{L\alpha}$		C_{Dp}		C_{Df}		C_{Dmin}		$\Delta C_D/C_L^2$		$C_{m\alpha}$		$(L/D)_{max}$		$C_{m\alpha}/C_{L\alpha}$, percent M.A.C.		C_{Lopt}	
			Theor.	Exp.	Theor.	Exp.	Theor.	Exp.	Theor.	Exp.	Theor.	Exp.	Theor.	Exp.	Theor.	Exp.	Theor.	Exp.	Theor.	Exp.
1	30	18	0.0412	0.0348	0.00757	-----	0.00520	-----	0.01277	0.0107	0.5802	0.4290	0	0.00083	7.195	7.60	50	47.61	0.1857	0.1500
2	30	30	.0412	.0363	.00463	-----	.00468	-----	.00951	.0089	.3802	.4174	0	.0010	8.424	8.21	50	47.25	.1568	.1475
3	30	40	.0412	.0373	.00376	-----	.00425	-----	.00801	.0083	.3802	.4304	0	.0010	9.022	8.79	50	47.32	.1455	.1440
4	30	50	.0412	.0382	.00343	-----	.00381	-----	.00724	.0068	.3802	.4490	0	.00067	9.552	8.80	50	48.25	.1385	.1325
5	30	60	.0412	.0403	.00342	-----	.00337	-----	.00679	.0069	.3802	.4300	0	.0014	9.865	9.21	50	46.53	.1339	.1350
6	30	70	.0412	.0400	.00377	-----	.00294	-----	.00671	.00671	.3802	.4410	0	.0013	9.925	9.15	50	47.75	.1332	.1320
7	35	18	0.0420	0.0359	0.00733	-----	0.00528	-----	0.01261	0.0120	0.413	0.3924	0	0.0010	6.928	7.40	50	47.21	0.1747	0.1800
8	35	30	.0420	.0385	.00463	-----	.00475	-----	.00938	.0095	.413	.4150	0	.0010	8.032	8.35	50	47.40	.1507	.1400
9	35	40	.0420	.0392	.00379	-----	.00432	-----	.00811	.0080	.413	.4200	0	.0007	8.639	8.85	50	48.21	.1401	.1375
10	35	50	.0420	.0399	.00345	-----	.00388	-----	.00733	.0084	.413	.4160	0	.00071	9.087	9.05	50	48.12	.1332	.1470
11	35	60	.0420	.0415	.00345	-----	.00344	-----	.00689	.0069	.413	.4276	0	.0012	9.375	9.22	50	47.11	.1292	.1300
12	35	70	.0420	.0430	.00380	-----	.00301	-----	.00681	.0058	.413	.4770	0	.0012	9.427	9.20	50	47.21	.1284	.1000
13	40	18	0.0420	0.0378	0.00634	-----	0.00537	-----	0.01271	0.0128	0.413	0.3840	0	0.0015	6.900	7.40	50	46.05	0.1754	0.1725
14	40	30	.0420	.0388	.00422	-----	.00484	-----	.00906	.0095	.413	.3850	0	.00164	8.173	8.70	50	45.61	.1481	.1450
15	40	40	.0420	.0397	.00355	-----	.00441	-----	.00796	.0078	.413	.3990	0	.0017	8.720	9.21	50	45.61	.1388	.1375
16	40	50	.0420	.0416	.00329	-----	.00397	-----	.00726	.0071	.413	.4015	0	.0012	9.130	9.55	50	47.09	.1326	.1325
17	40	60	.0420	.0423	.00333	-----	.00333	-----	.00686	.0065	.413	.4254	0	.0014	9.395	10.30	50	46.70	.1289	.1175
18	40	70	.0420	.0430	.00372	-----	.00310	-----	.00682	.0060	.413	.4040	0	.0016	9.421	10.00	50	46.28	.1285	.1100

TABLE II. - Concluded

SUMMARY OF RESULTS

(c) $M = 2.41$

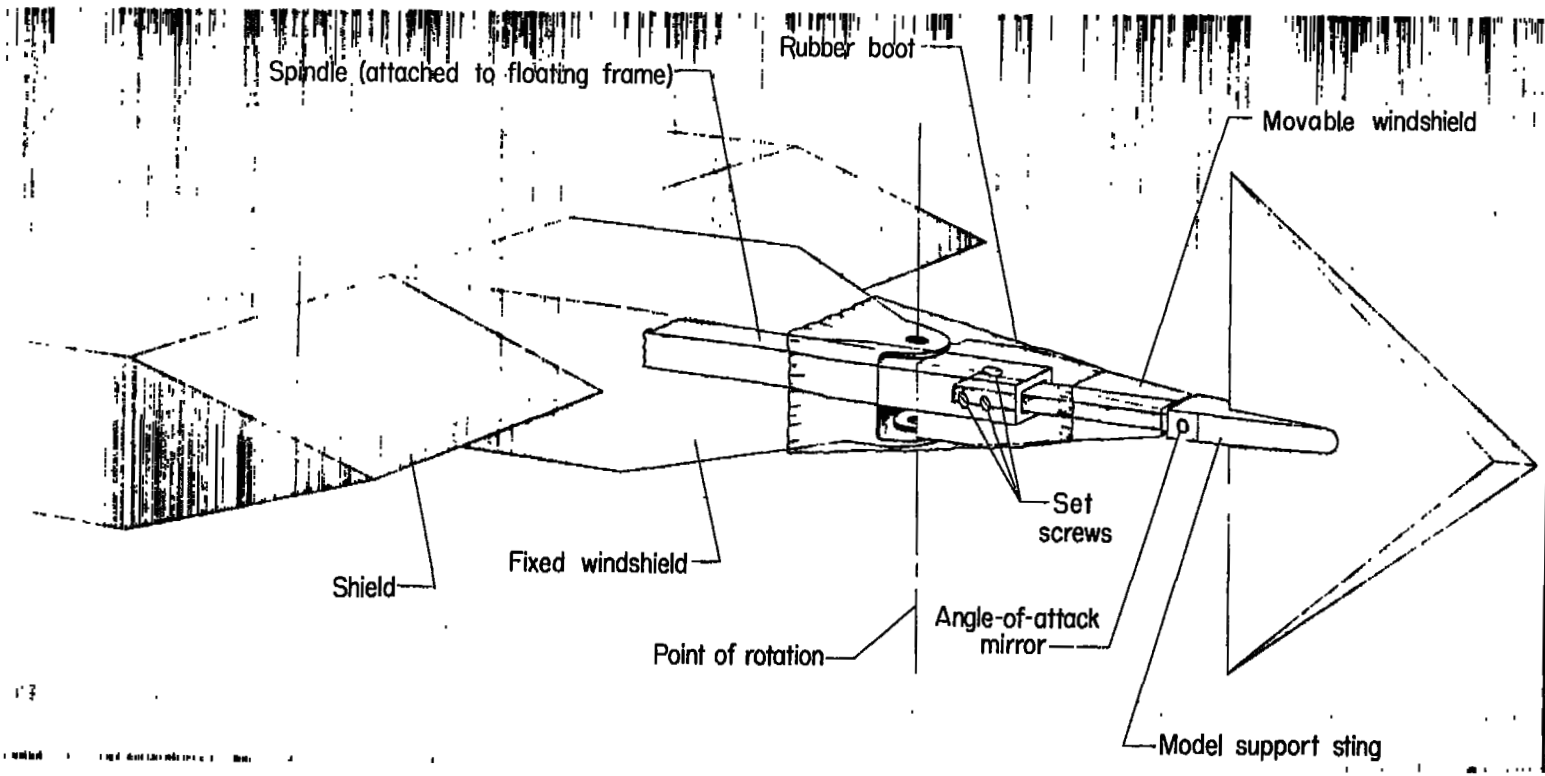
Wing	c, deg	l - r, percent chord	Lift		Drag								Pitching moment		Lift-drag ratio		Center of pressure		Optimum lift coefficient	
			$C_{L\alpha}$		C_{Dp}		C_{Dr}		C_{Dmin}		$\Delta C_D/C_L^2$		$C_{m\alpha}$		(L/D) _{max}		$C_{m\alpha}/C_{L\alpha}$, percent M.A.C.		C_{Lopt}	
			Theor.	Exp.	Theor.	Exp.	Theor.	Exp.	Theor.	Exp.	Theor.	Exp.	Theor.	Exp.	Theor.	Exp.	Theor.	Exp.	Theor.	Exp.
1	30	18	0.03184	0.0292	0.00510	----	0.00485	----	0.00995	0.0097	0.550	0.5343	0	0.00075	6.766	7.12	50	47.43	0.1346	0.1300
2	30	30	.03184	.0307	.00533	----	.00440	----	.00773	.0081	.550	.5483	0	.00075	7.677	8.08	50	47.56	.1187	.1150
3	30	40	.03184	.0314	.00277	----	.00401	----	.00678	.0065	.550	.5550	0	.0009	8.197	8.70	50	47.13	.1111	.1145
4	30	50	.03184	.0316	.00255	----	.00363	----	.00618	.0062	.550	.5667	0	.0008	8.585	9.00	50	47.47	.1061	.0925
5	30	60	.03184	.0326	.00257	----	.00325	----	.00582	.0062	.550	.5520	0	.0008	8.847	9.38	50	47.55	.1050	.0950
6	30	70	.03184	.0320	.00285	----	.00286	----	.00571	.0061	.550	.5460	0	.0007	8.932	9.40	50	47.81	.1020	.0870
7	35	18	0.03184	0.0302	0.00456	----	0.00495	----	0.00951	0.0104	0.550	0.5170	0	0.00103	6.921	7.20	50	46.69	0.1316	0.1325
8	35	30	.03184	.0315	.00308	----	.00450	----	.00758	.0074	.550	.5270	0	.0010	7.752	8.30	50	46.83	.1175	.1200
9	35	40	.03184	.0319	.00261	----	.00411	----	.00672	.0062	.550	.5337	0	.0012	8.234	9.30	50	46.24	.1106	.1050
10	35	50	.03184	.0320	.00245	----	.00373	----	.00618	.0059	.550	.5297	0	.0012	8.585	9.78	50	46.25	.1061	.0962
11	35	60	.03184	.0327	.00249	----	.00333	----	.00584	.0054	.550	.5400	0	.0008	8.832	10.05	50	47.55	.1032	.0962
12	35	70	.03184	.0330	.00280	----	.00296	----	.00576	.0057	.550	.5310	0	.0010	8.894	9.99	50	46.97	.1025	.1000
13	40	18	0.03184	0.0312	0.00428	----	0.00503	----	0.00931	0.0101	0.550	0.5000	0	0.00098	6.995	7.29	50	46.86	0.1302	0.1375
14	40	30	.03184	.0313	.00294	----	.00456	----	.00750	.0071	.550	.5283	0	.0010	7.794	8.55	50	46.81	.1169	.1190
15	40	40	.03184	.0321	.00252	----	.00418	----	.00670	.0059	.550	.5400	0	.0012	8.246	9.45	50	46.26	.1105	.0975
16	40	50	.03184	.0328	.00239	----	.00380	----	.00619	.0054	.550	.5317	0	.00025	8.579	9.75	50	49.24	.1062	.0950
17	40	60	.03184	.0323	.00245	----	.00342	----	.00587	.0050	.550	.5233	0	.00117	8.810	10.55	50	46.38	.1034	.0958
18	40	70	.03184	.0320	.00276	----	.00304	----	.00580	.0049	.550	.5333	0	.0012	8.863	10.80	50	46.25	.1028	.0925



(a) Strain-gage balance.

L-87926

Figure 1.- Sketch of strain-gage balance used to measure model forces, and method of model support.



(b) Method of model support.

L-87927

Figure 1.- Concluded.

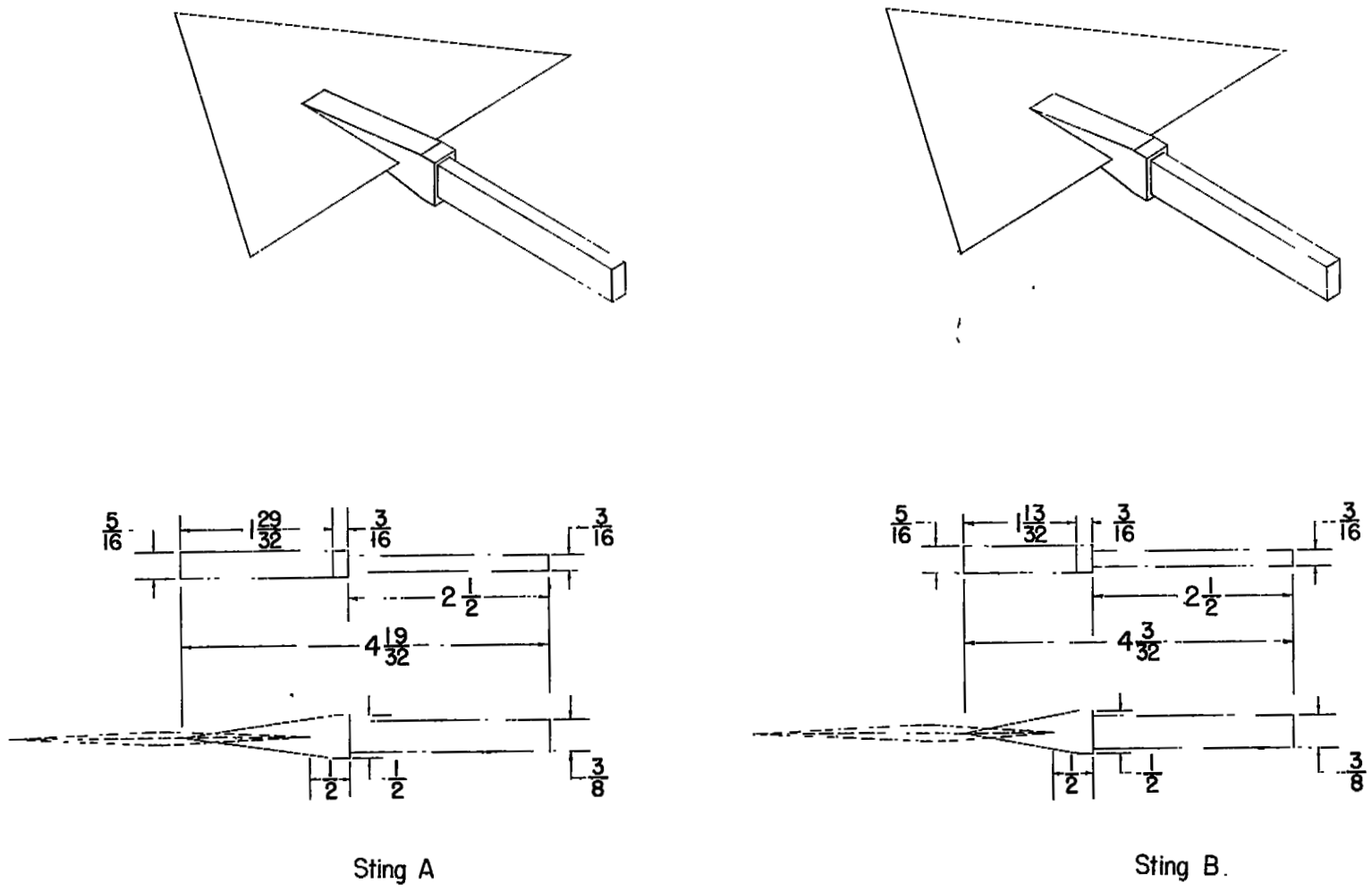
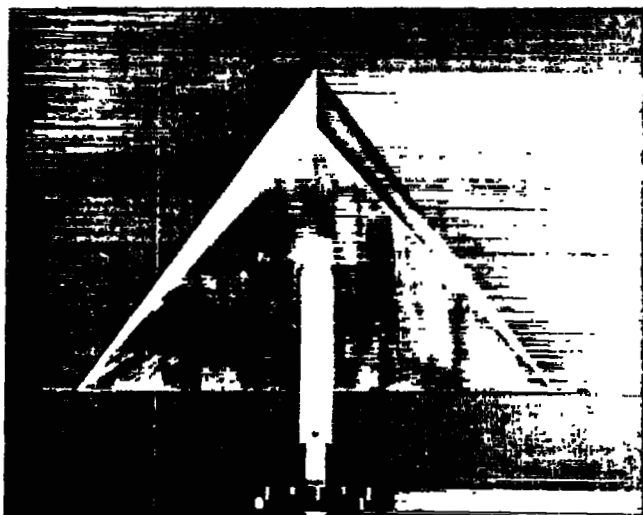
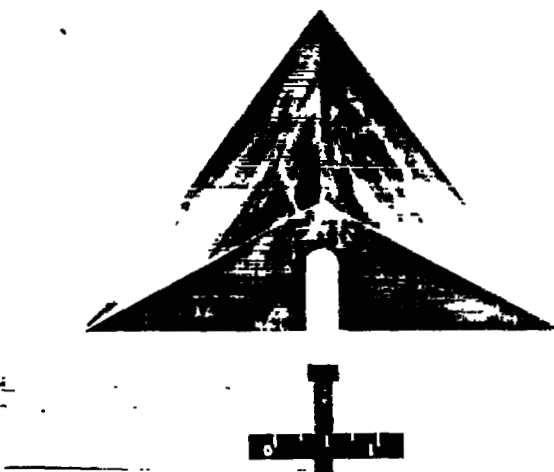


Figure 2.- Dimensional details of wing support stings used in investigation. All dimensions are in inches.



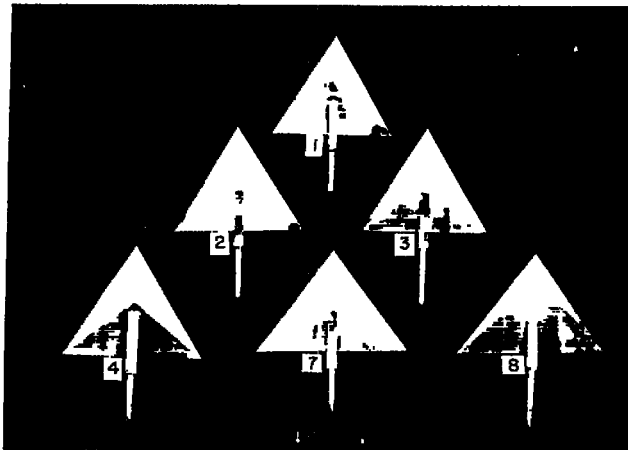
(a) Sting A on wing 7.



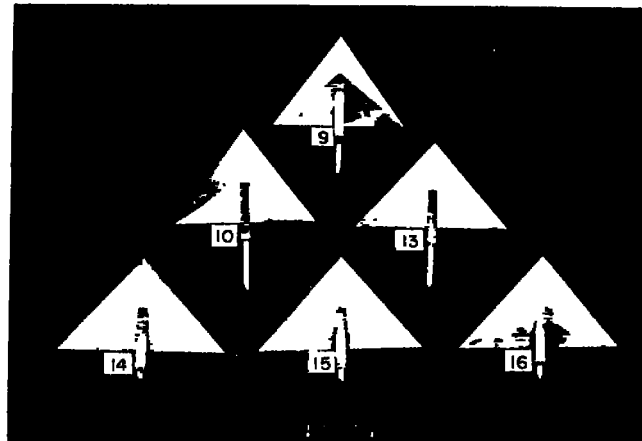
(b) Sting B on wing 11.

L-87947

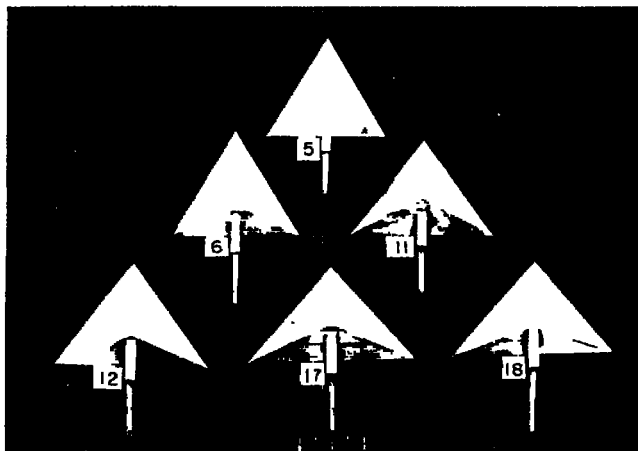
Figure 3.- Typical wings equipped with support stings A and B.



Test wings with sting A



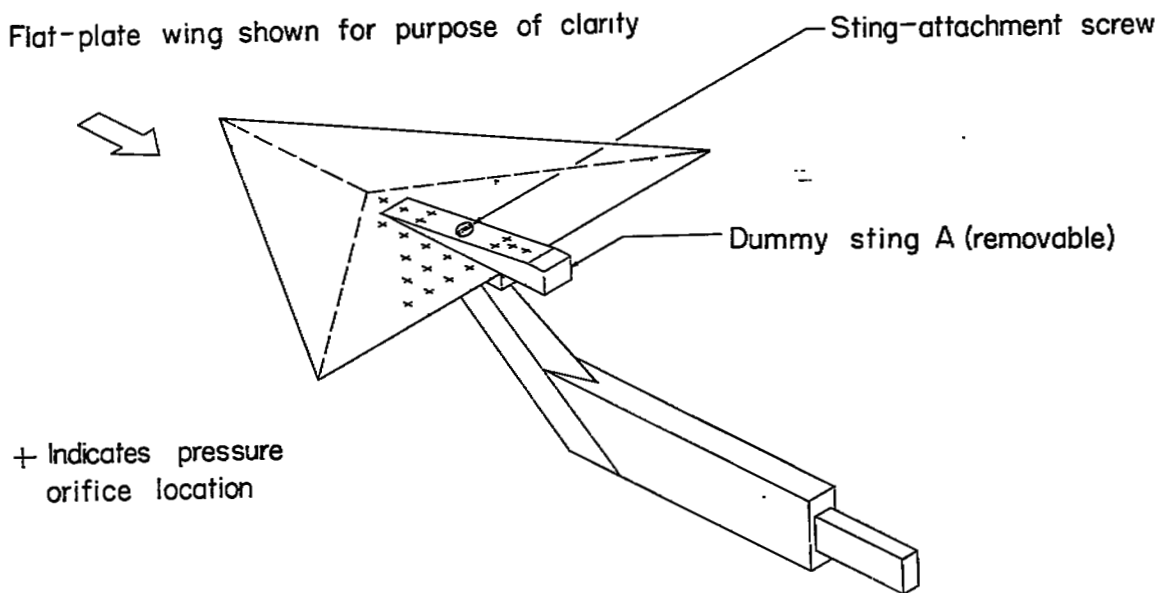
Test wings with sting A



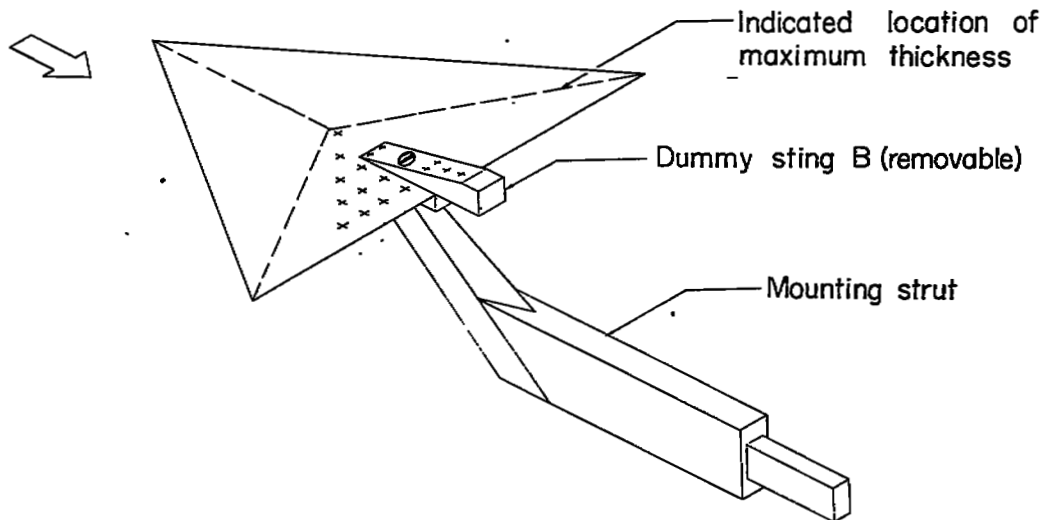
Test wings with sting B

L-87948

Figure 4.- Photographs of wing models used in investigation. (The apparent difference in wing areas is due to depth distortion.)

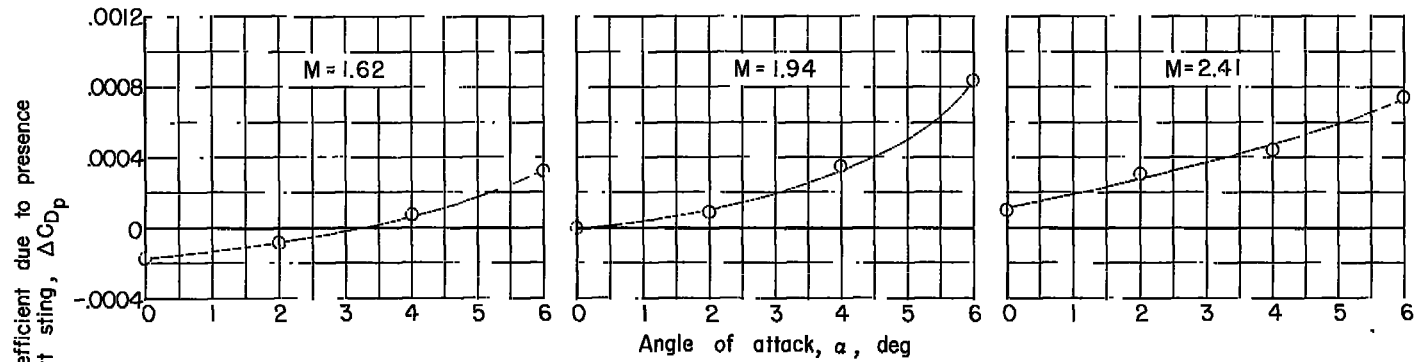


(a) Sting A on wing 10.

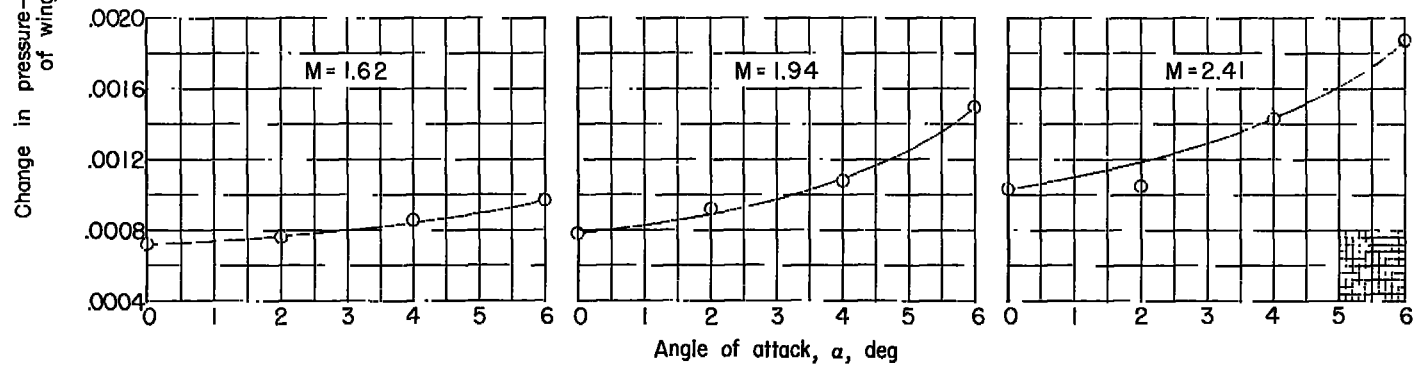


(b) Sting B on wing 11.

Figure 5.- Pressure-distribution models used for assessment of support-sting tare-interference effects.

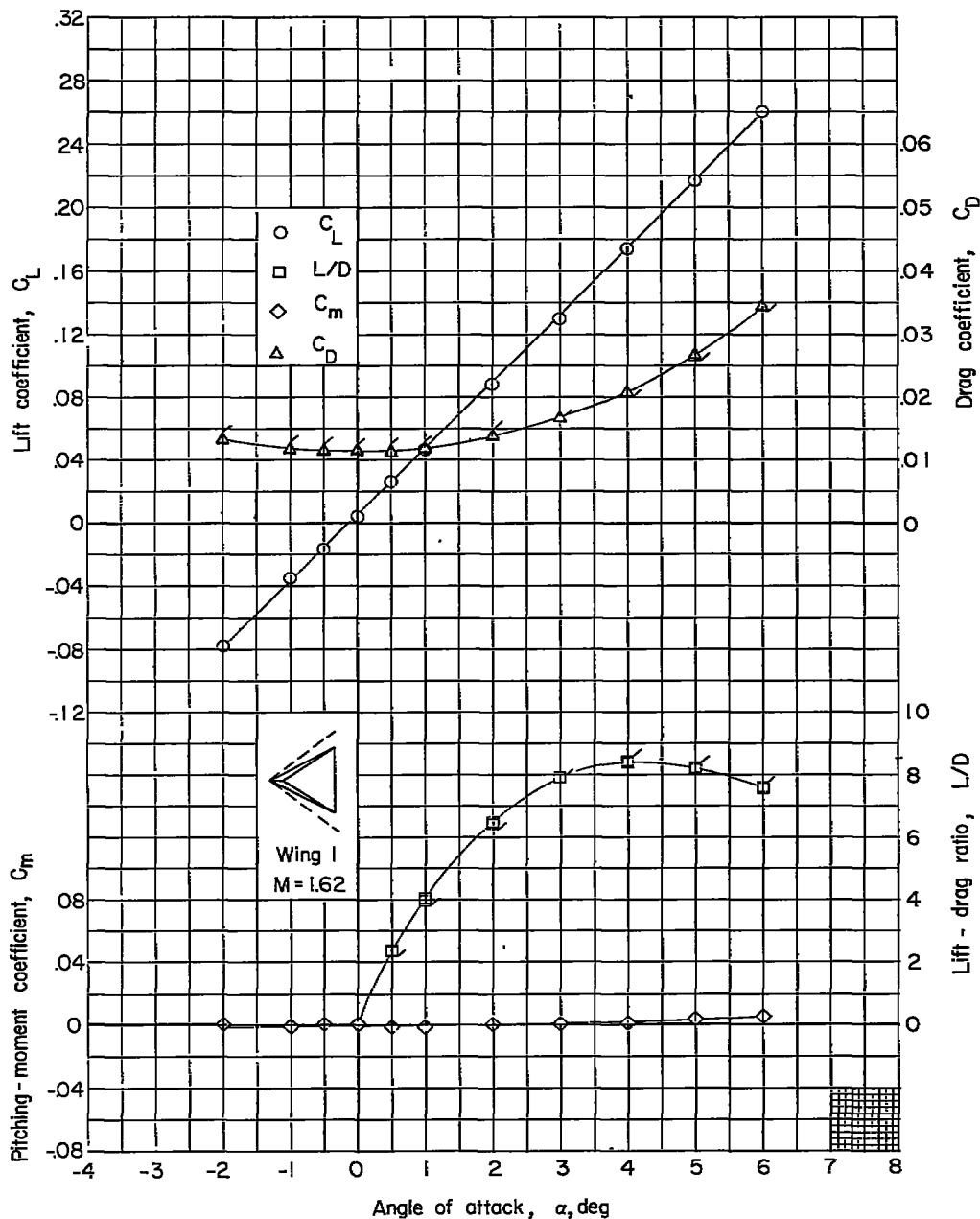


(a) Configurations equipped with sting A.



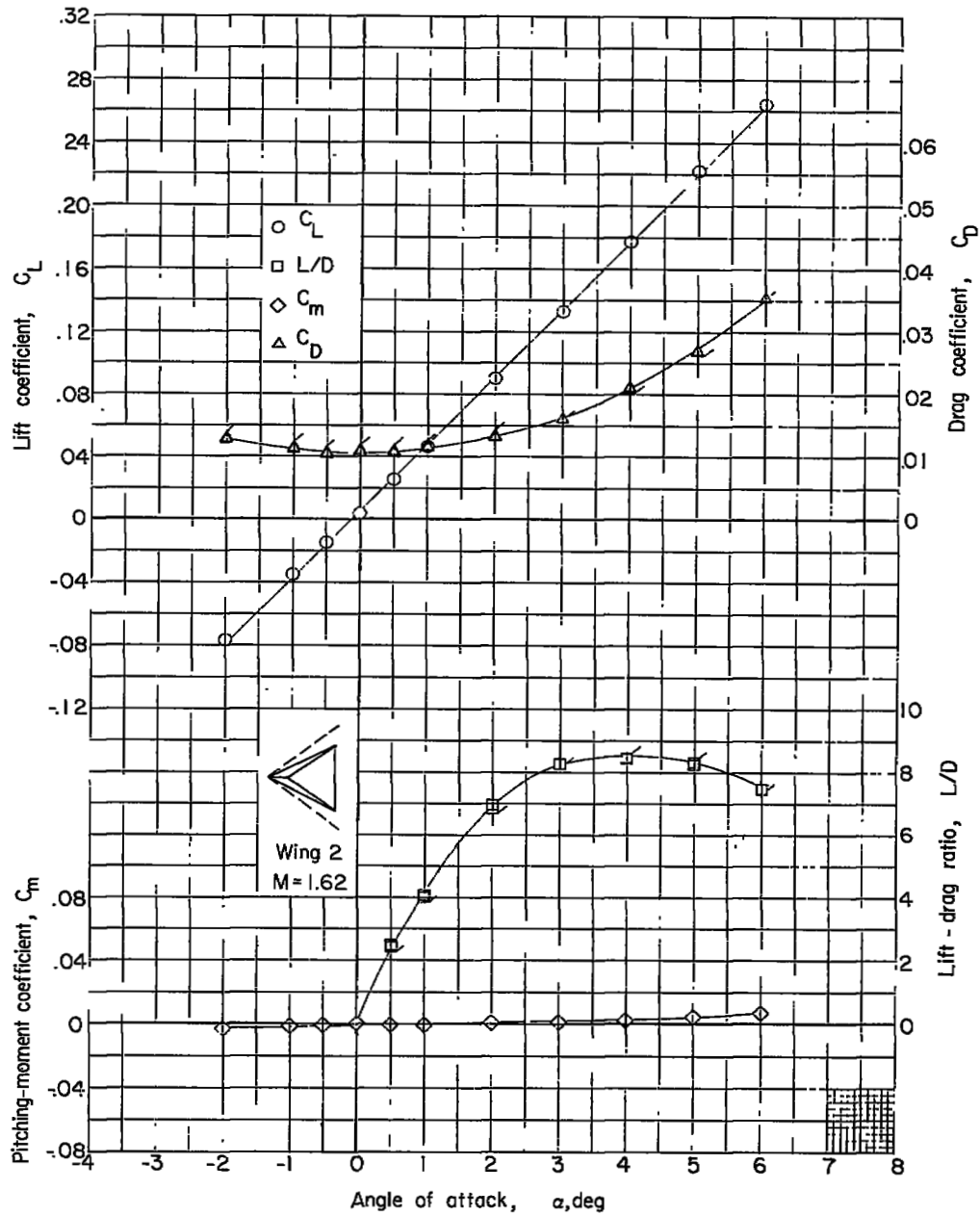
(b) Configurations equipped with sting B.

Figure 6.- Change in pressure-drag coefficient due to presence of wing support stings.



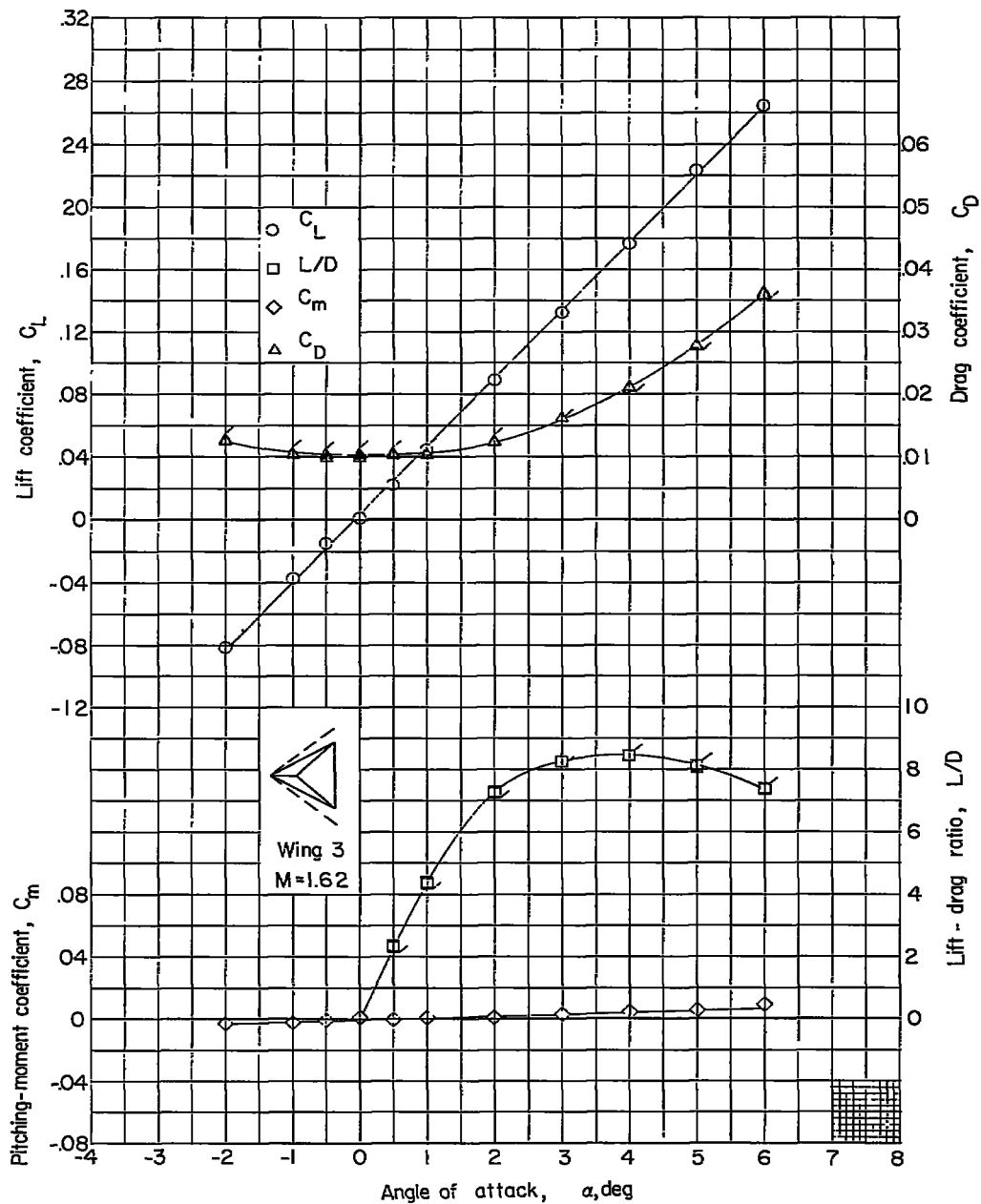
(a) $1 - r = 0.18c$.

Figure 7.- Aerodynamic characteristics of $3\frac{1}{2}$ -percent-thick delta wings. $M = 1.62$; semiapex angle ϵ , 30° . Flagged symbols denote correction applied to drag data to account for support-sting tare-interference effects.



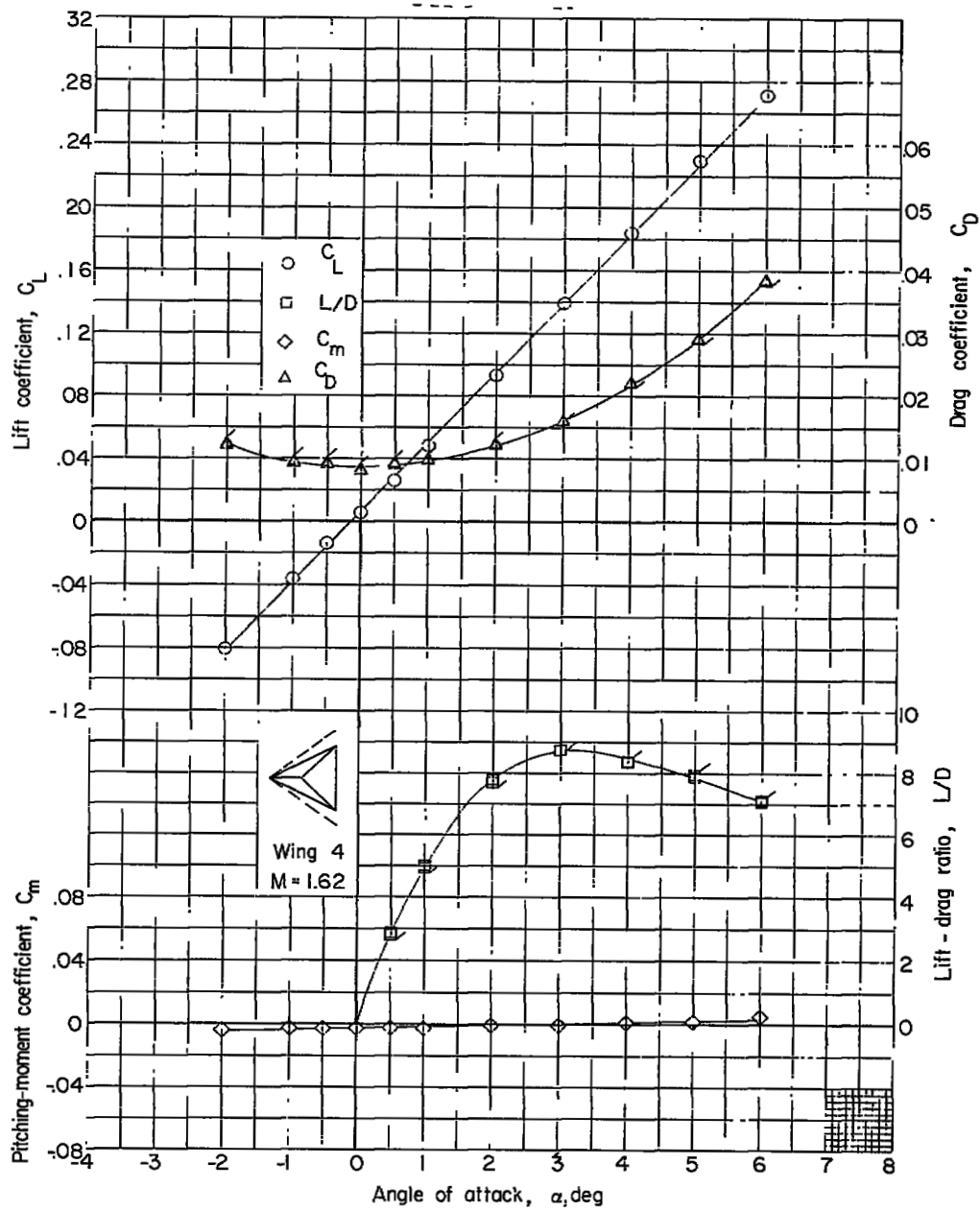
(b) $1 - r = 0.30c$.

Figure 7.- Continued.



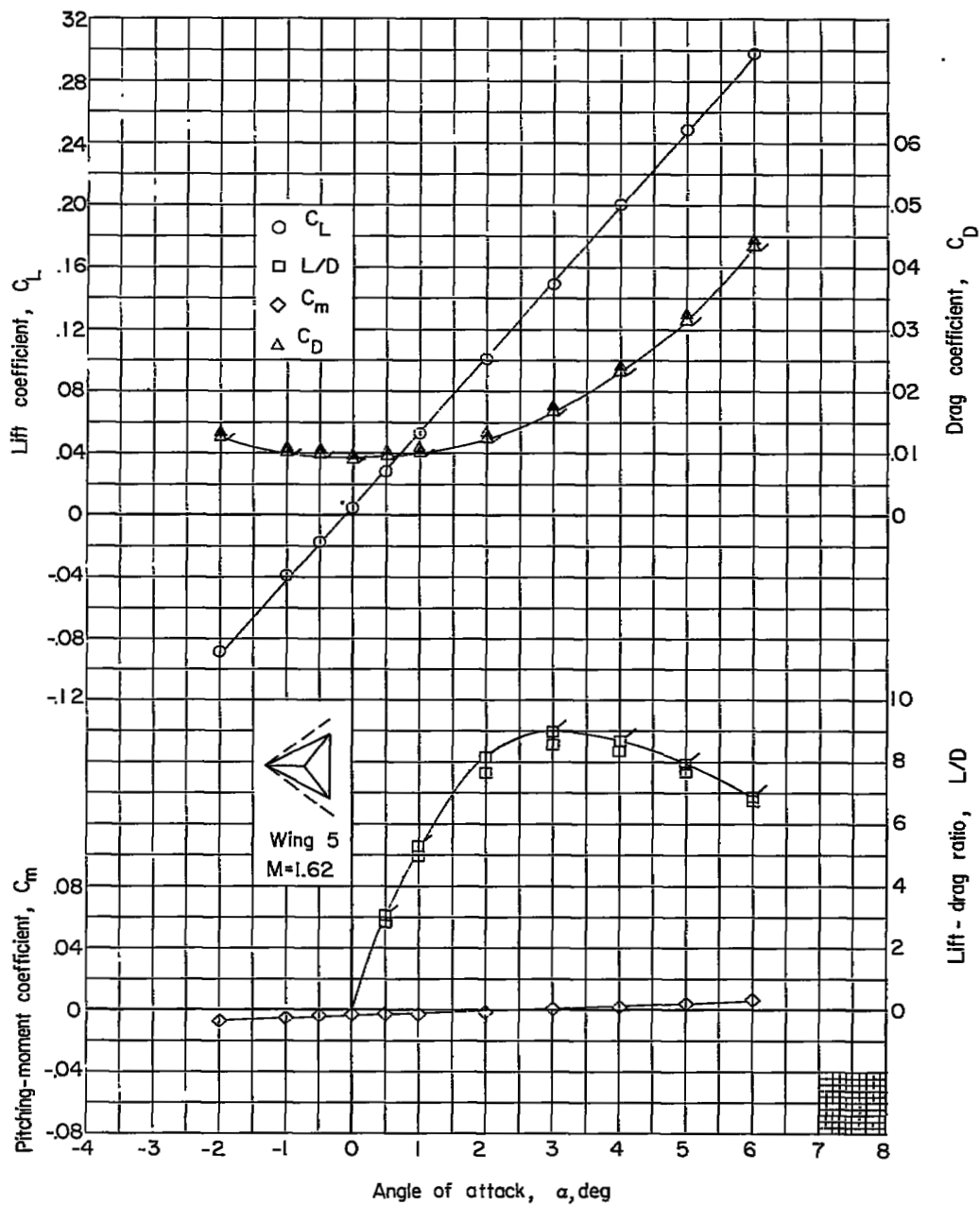
(c) $1 - r = 0.40c.$

Figure 7.- Continued.



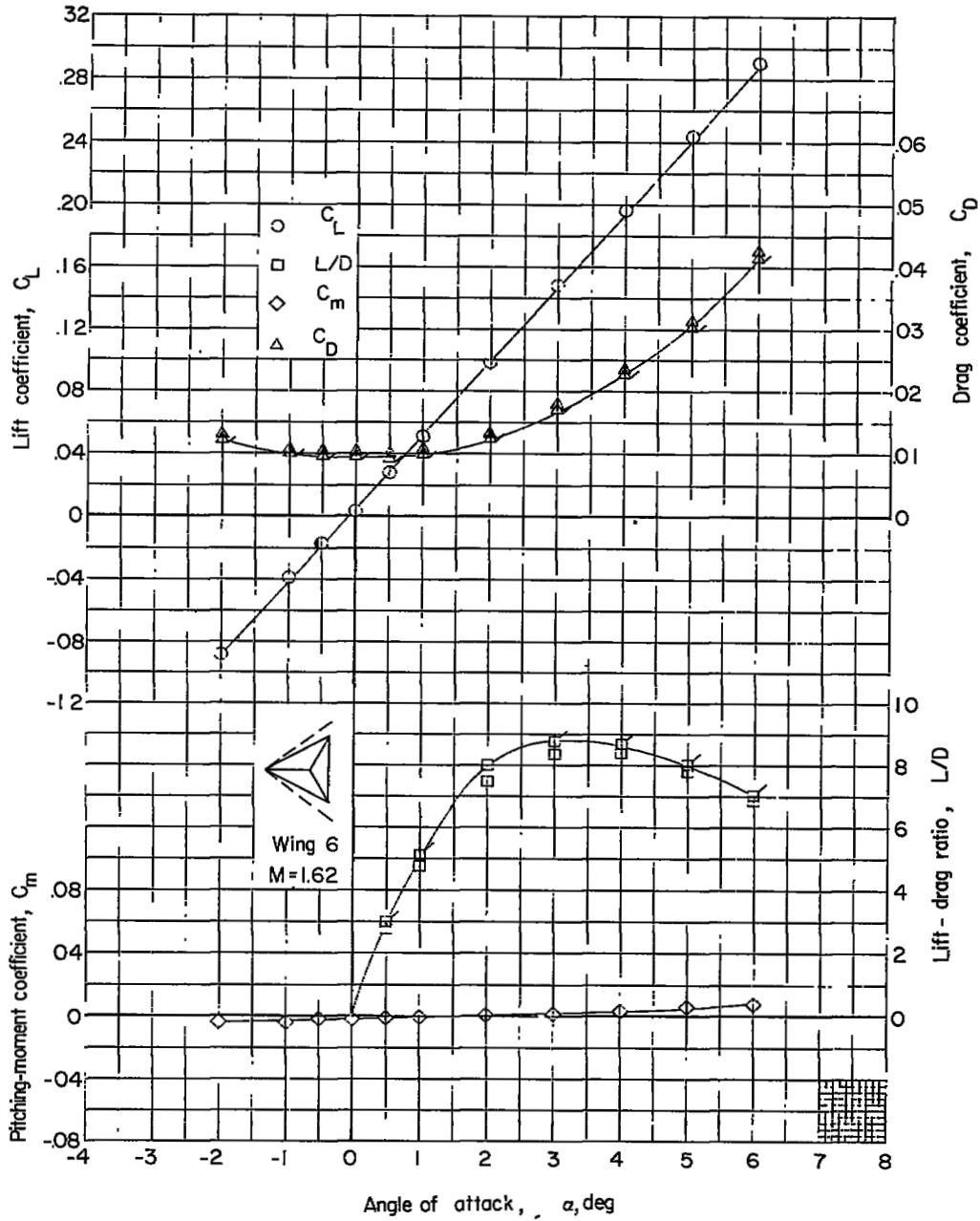
(d) $1 - r = 0.50c$.

Figure 7.- Continued.



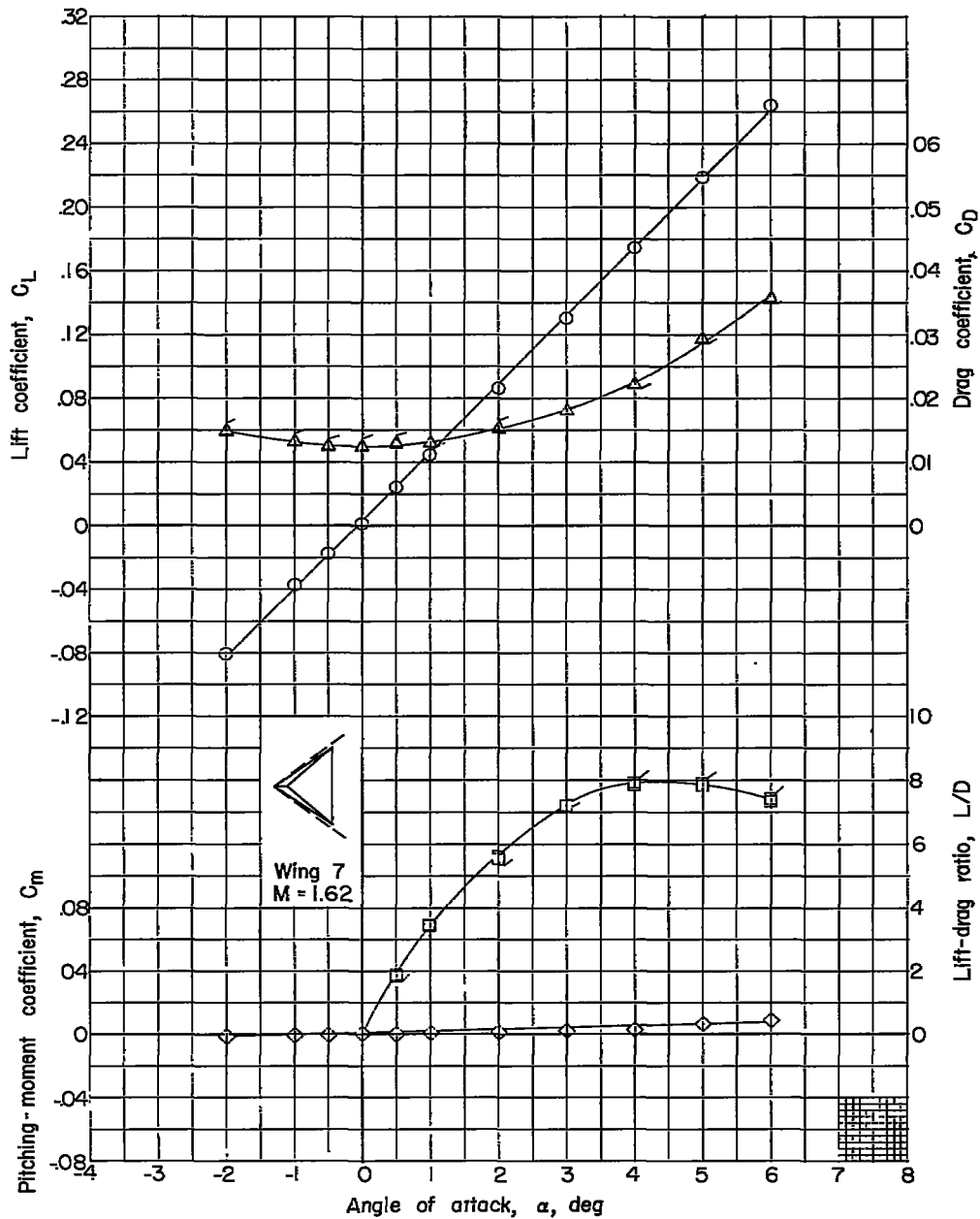
(e) $1 - r = 0.60c$.

Figure 7.- Continued.



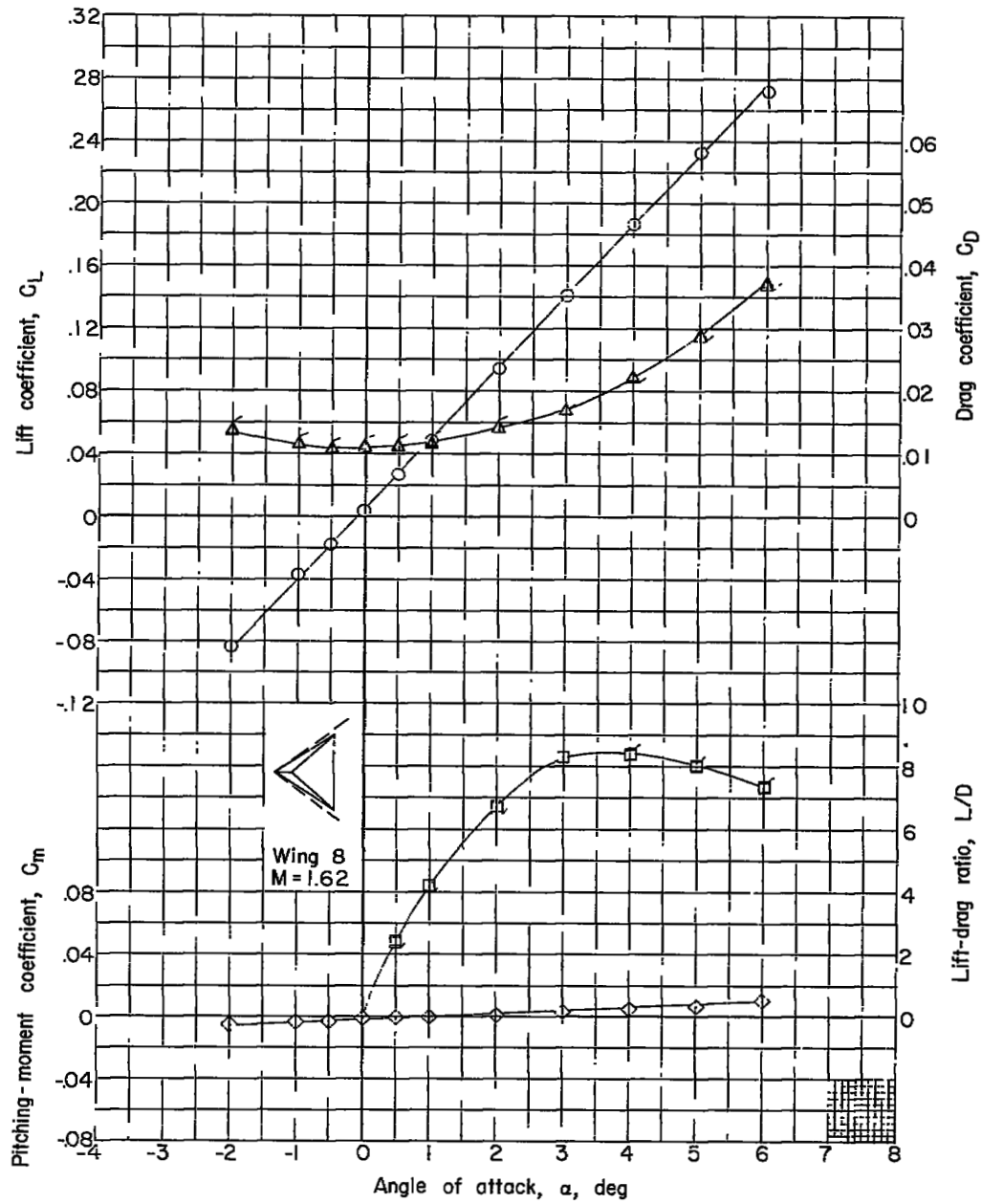
(f) $1 - r = 0.70c$.

Figure 7.- Concluded.



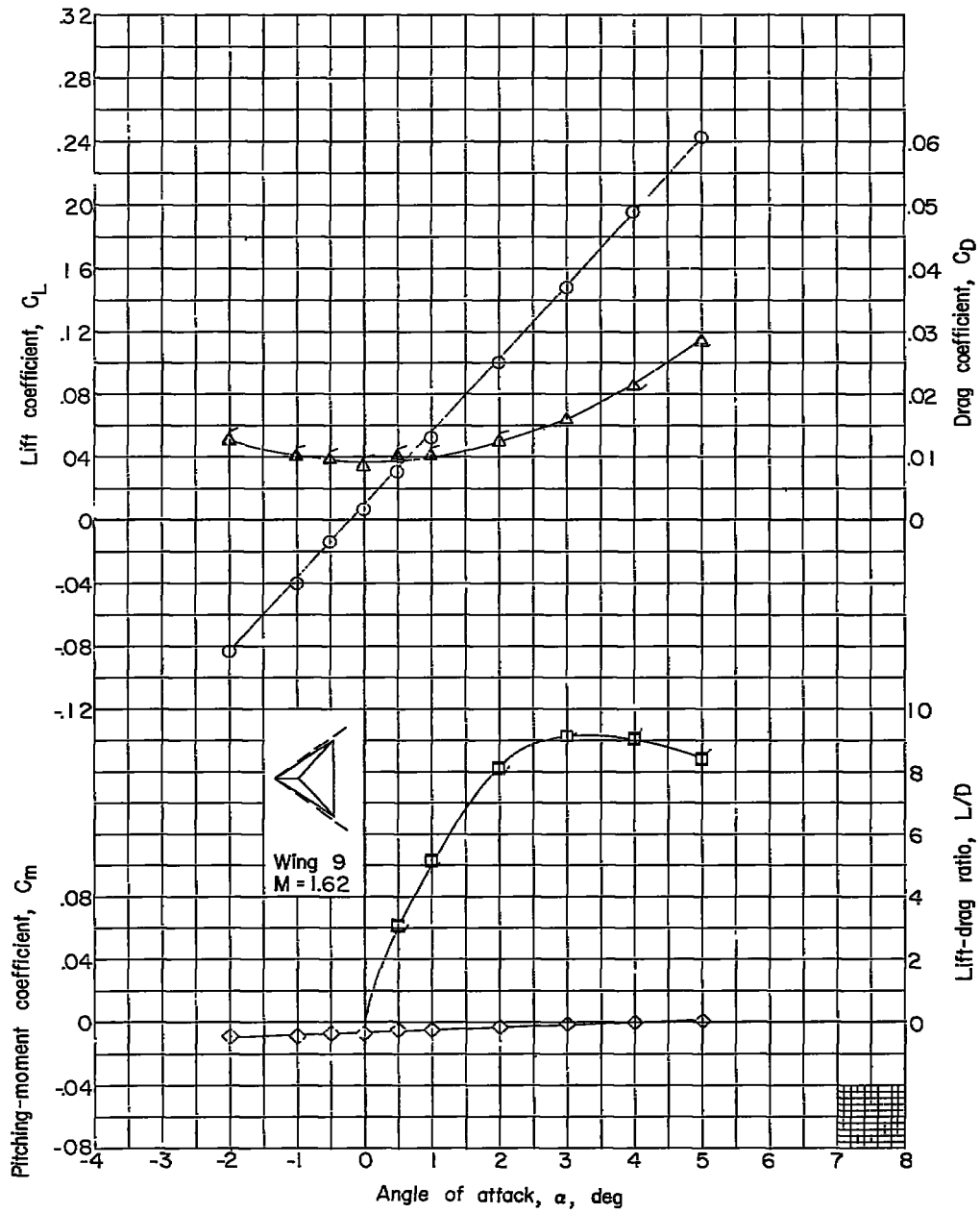
(a) $1 - r = 0.18c$.

Figure 8.- Aerodynamic characteristics of $\frac{1}{2}$ -percent-thick delta wings. $M = 1.62$; semiapex angle ϵ , 35° . Flagged symbols denote correction applied to drag data to account for support-sting tare-interference effects.



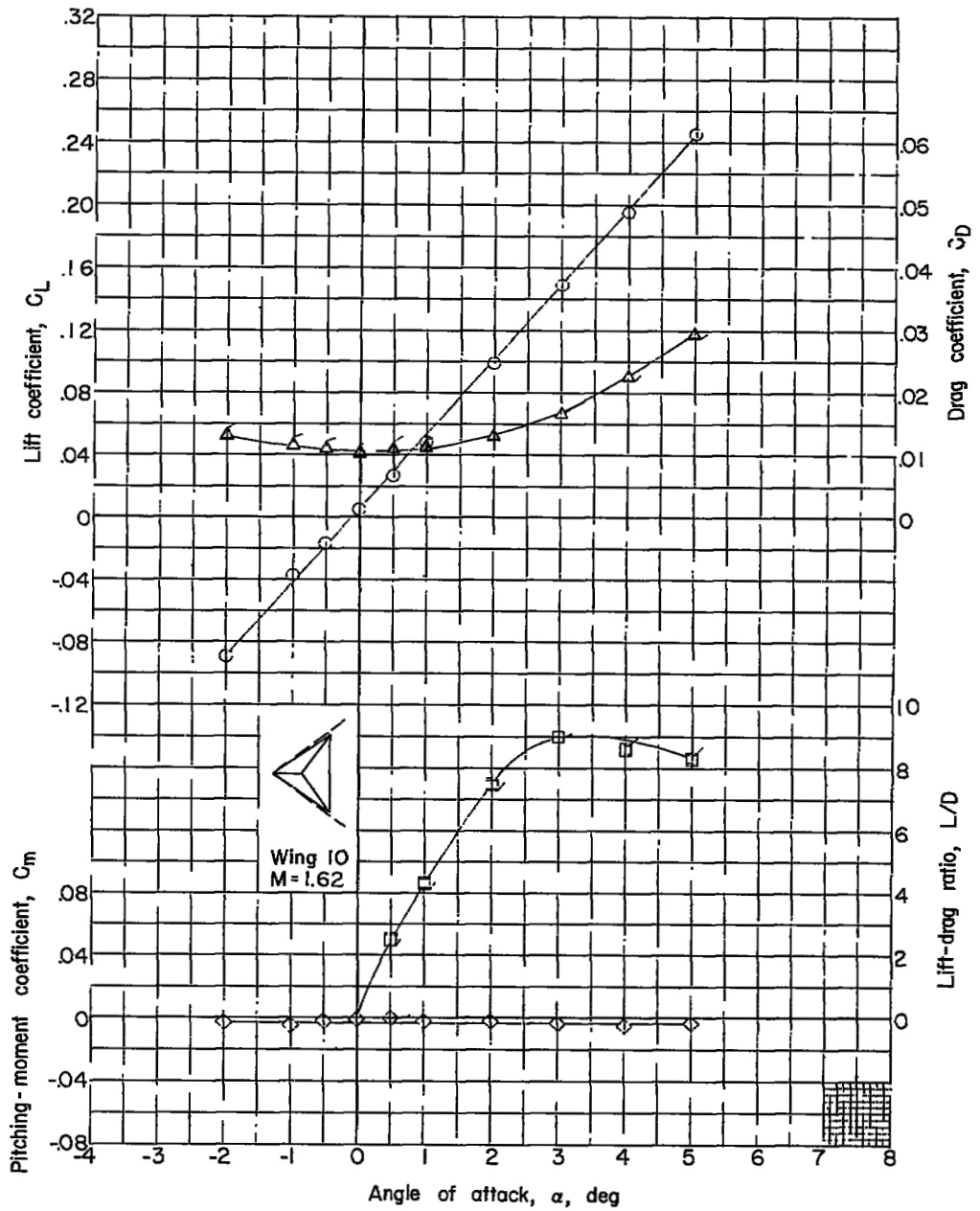
(b) $l - r = 0.30c$.

Figure 8.- Continued.



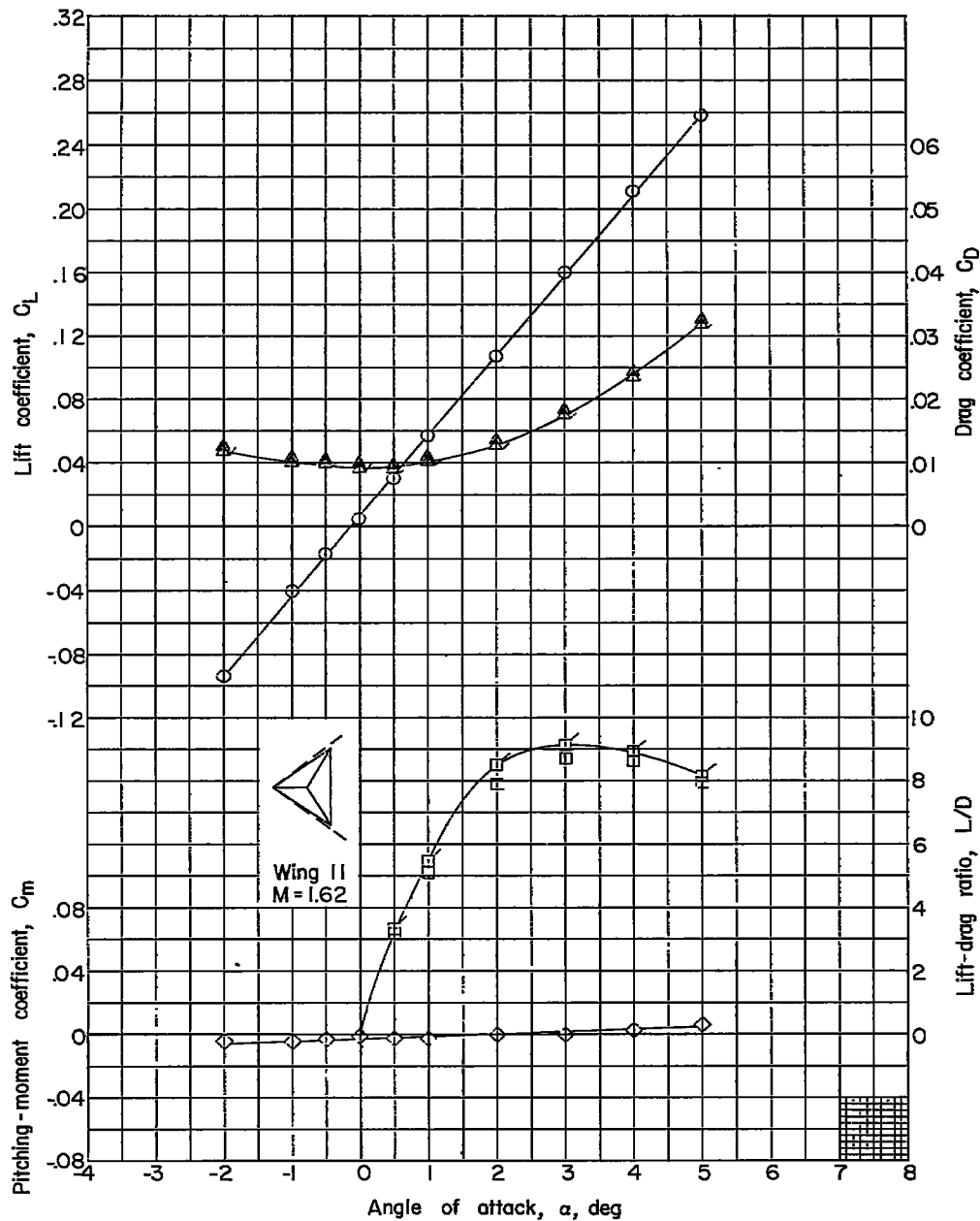
(c) $1 - r = 0.40c$.

Figure 8.- Continued.



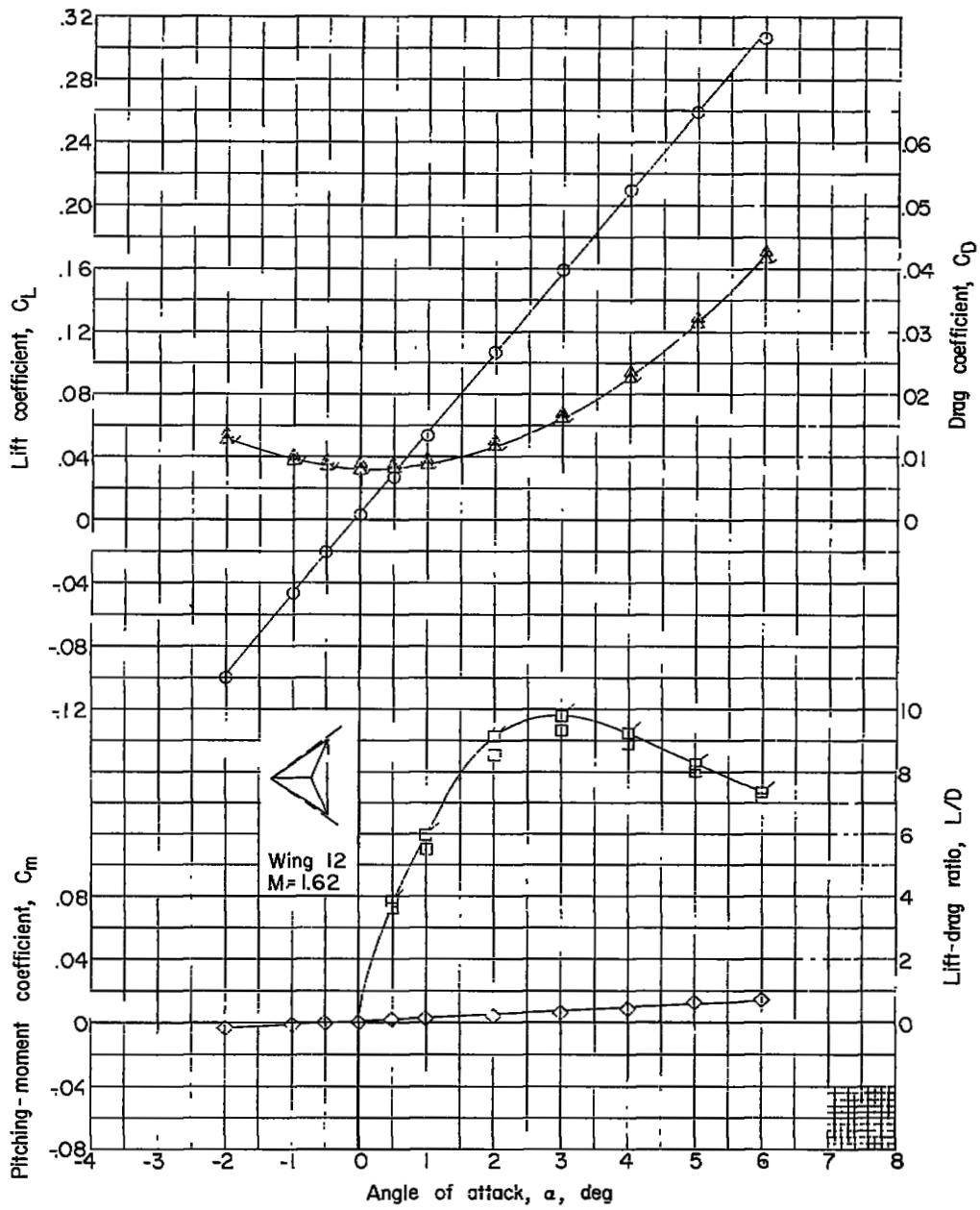
(d) $1 - r = 0.50c$.

Figure 8.- Continued.



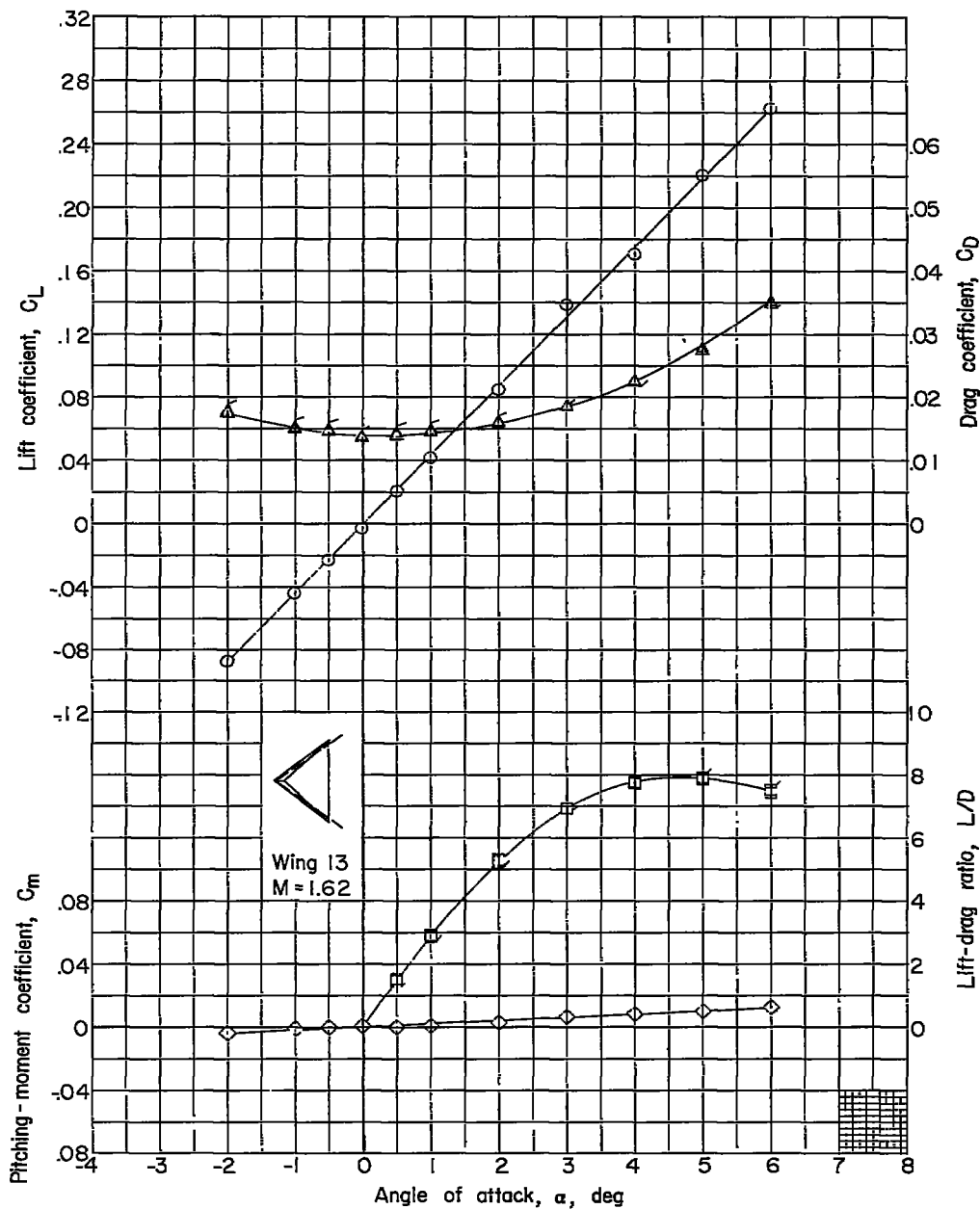
(e) $1 - r = 0.60c$.

Figure 8.- Continued.



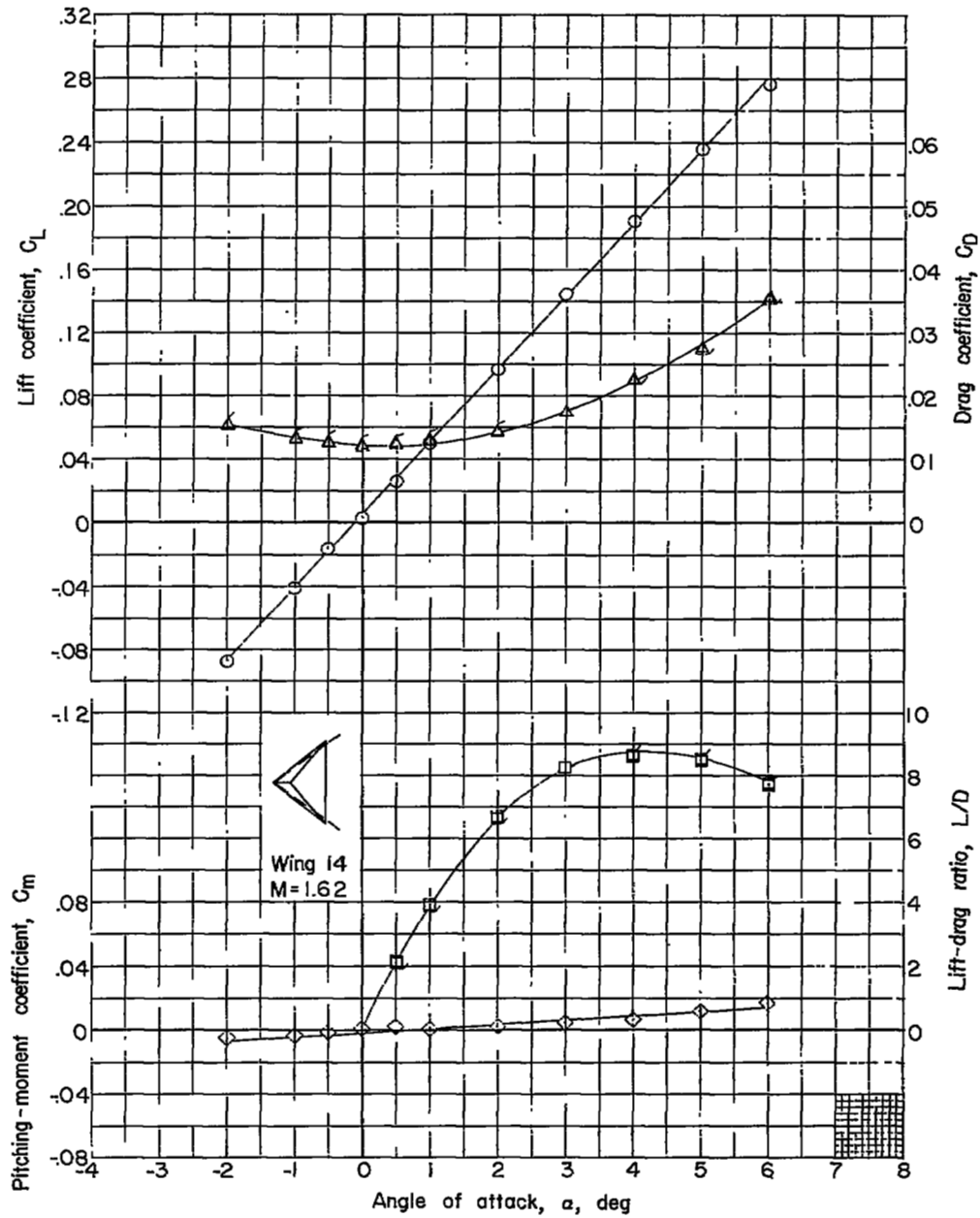
(f) $1 - r = 0.70c$.

Figure 8.- Concluded.



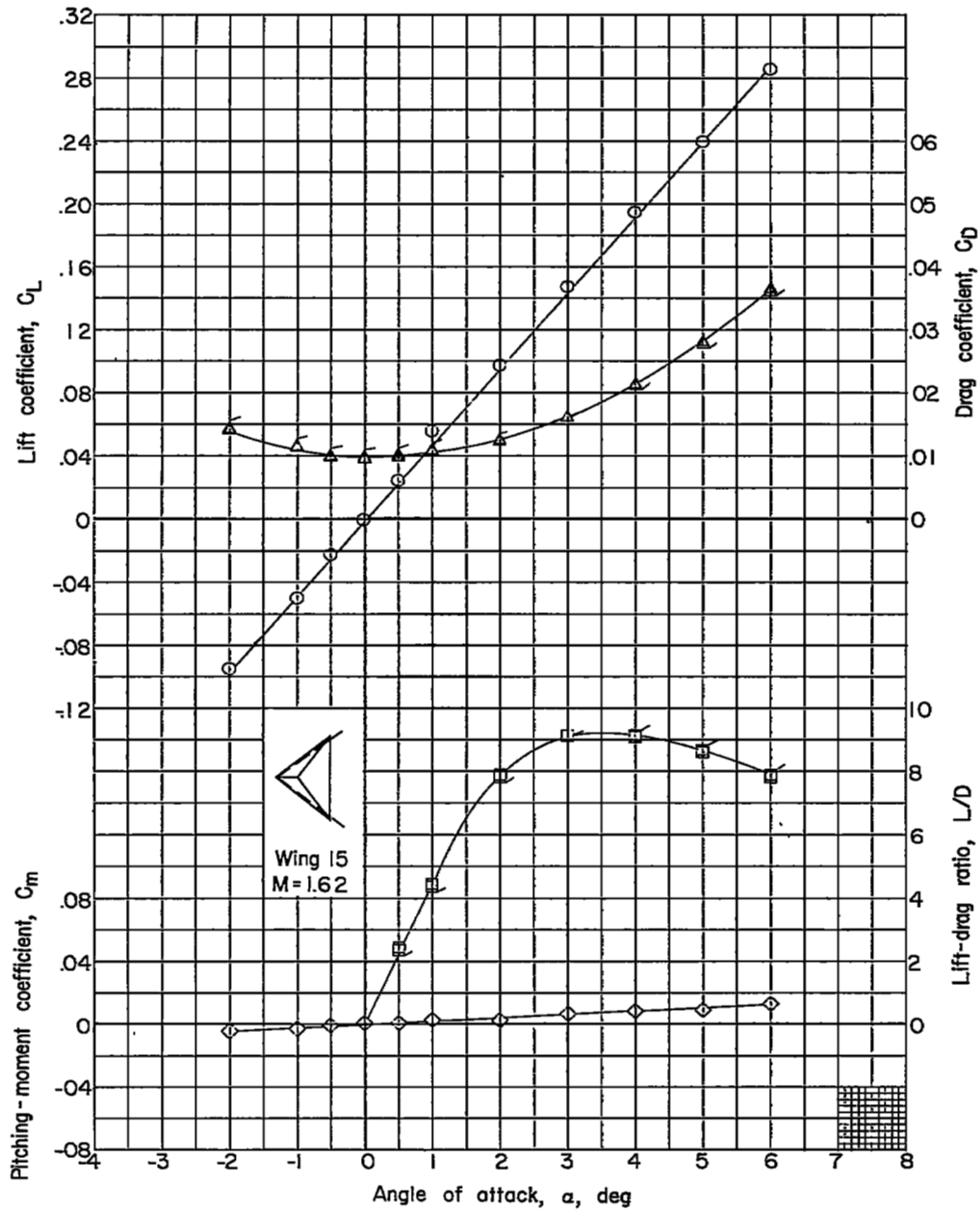
(a) $1 - r = 0.18c$.

Figure 9.- Aerodynamic characteristics of $3\frac{1}{2}$ -percent-thick delta wings. $M = 1.62$; semiapex angle ϵ , 40° . Flagged symbols denote correction applied to drag data to account for support-sting tare-interference effects.



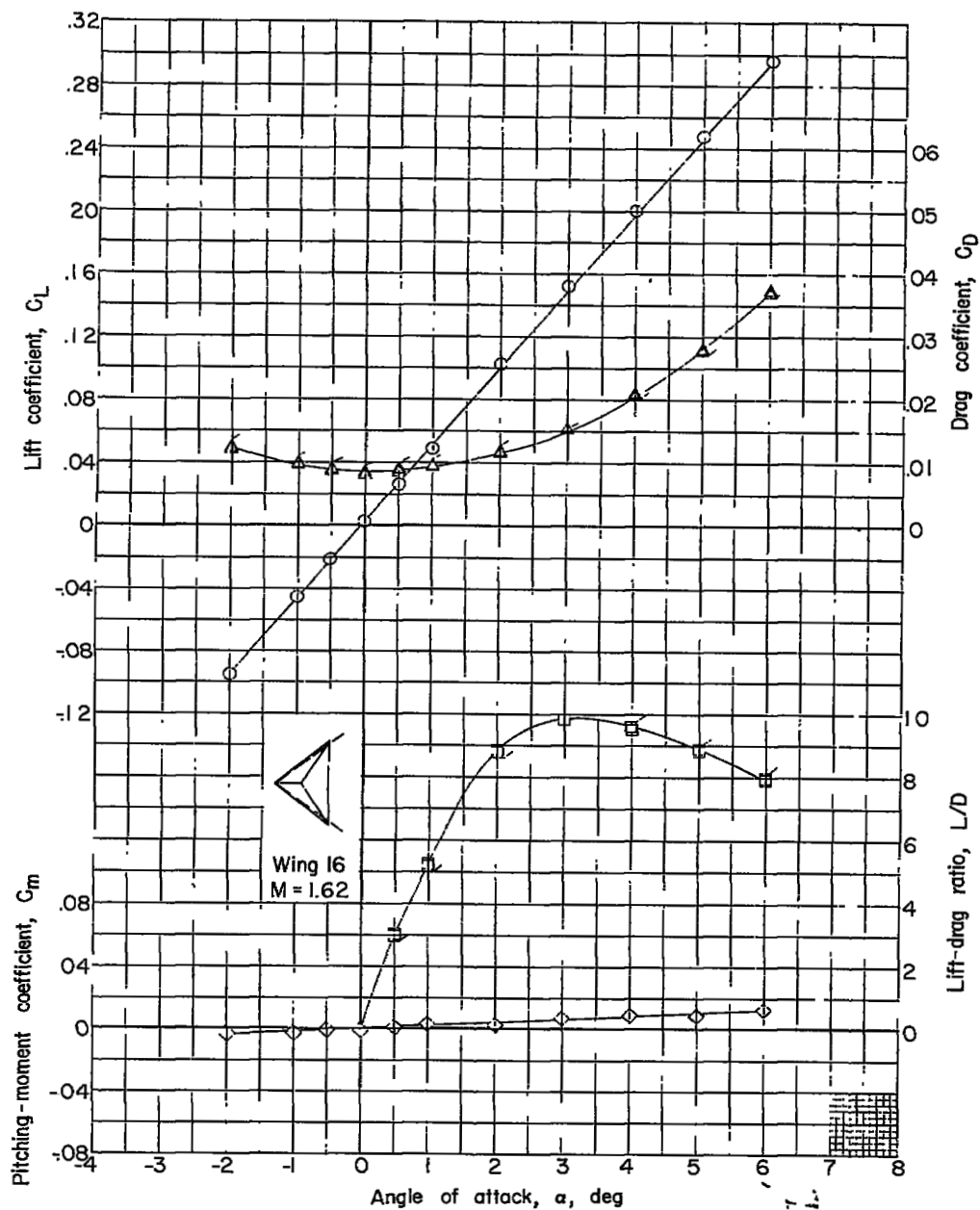
(b) $1 - r = 0.30c$.

Figure 9.- Continued.



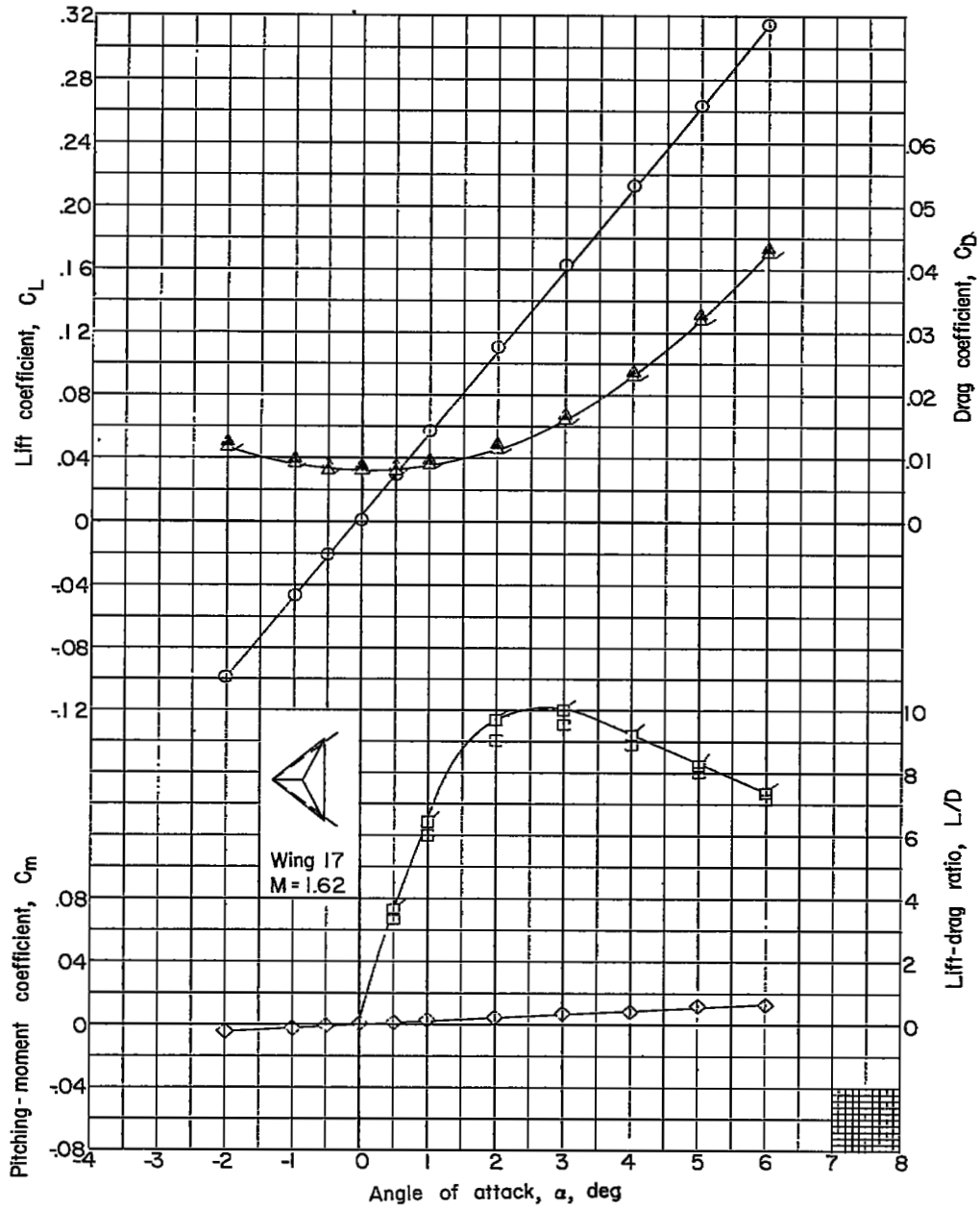
(c) $1 - r = 0.40c$.

Figure 9.- Continued.



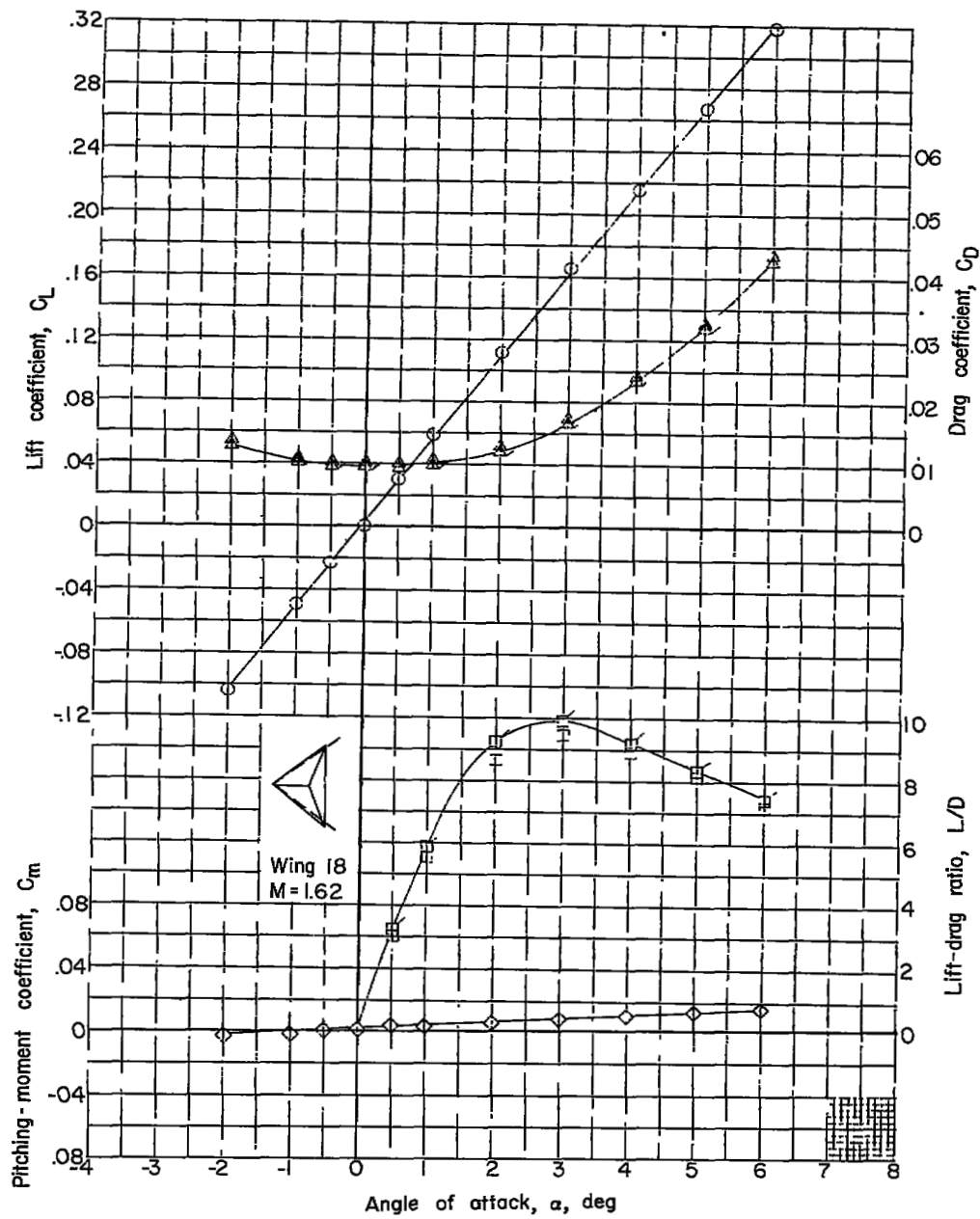
(d) $1 - r = 0.50c$.

Figure 9.- Continued.



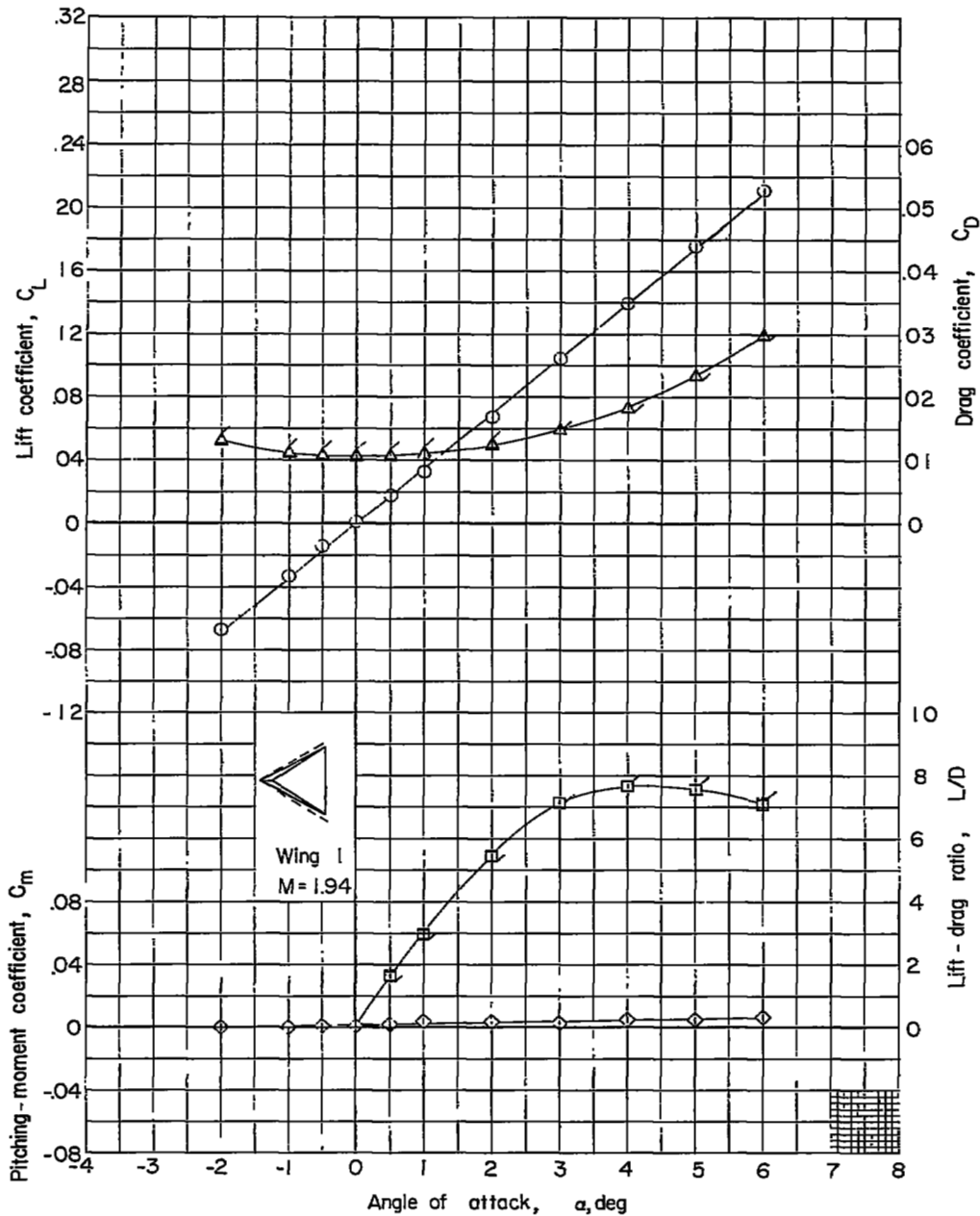
(e) $1 - r = 0.60c$.

Figure 9.- Continued.



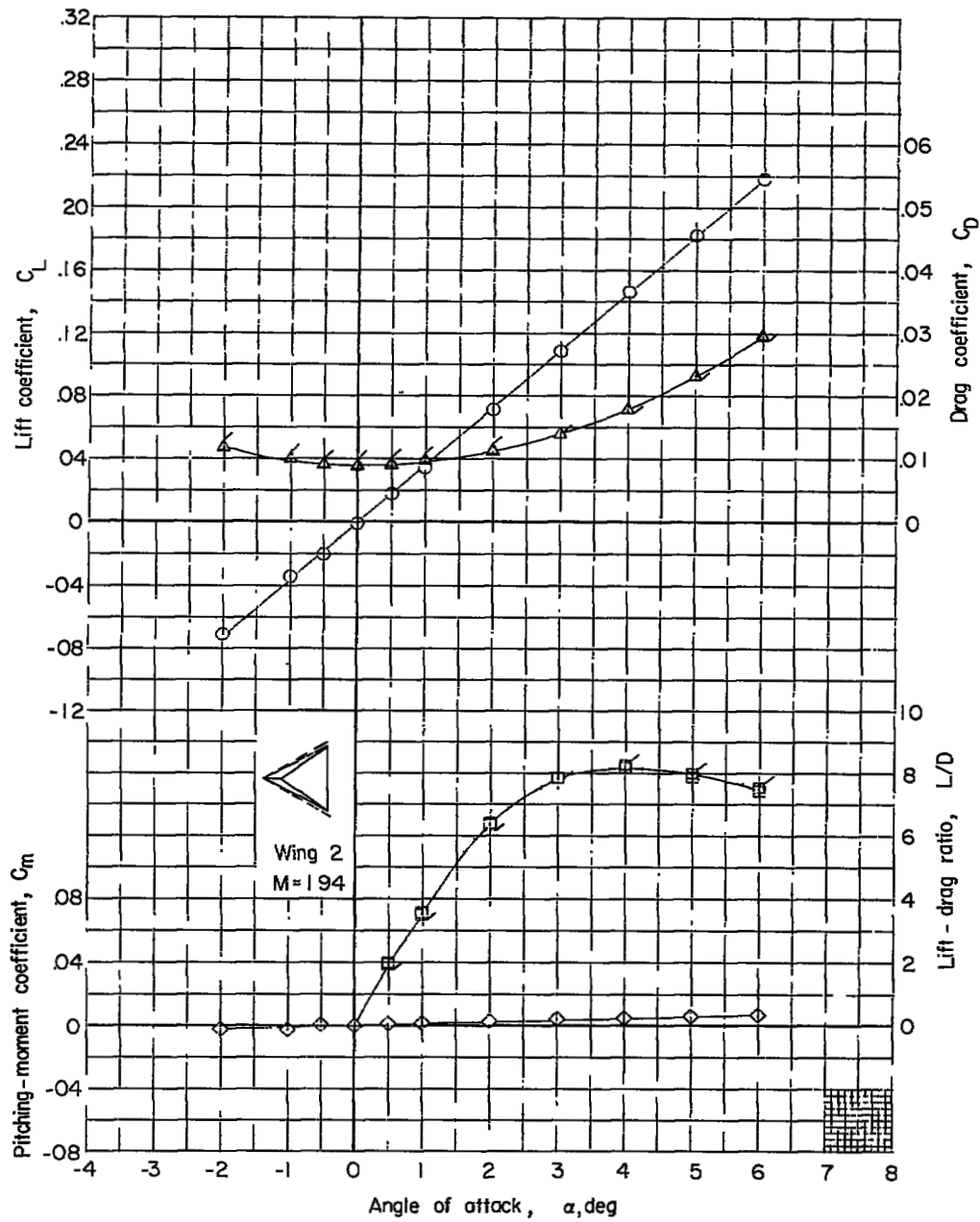
(f) $1 - r = 0.70c$.

Figure 9.- Concluded.



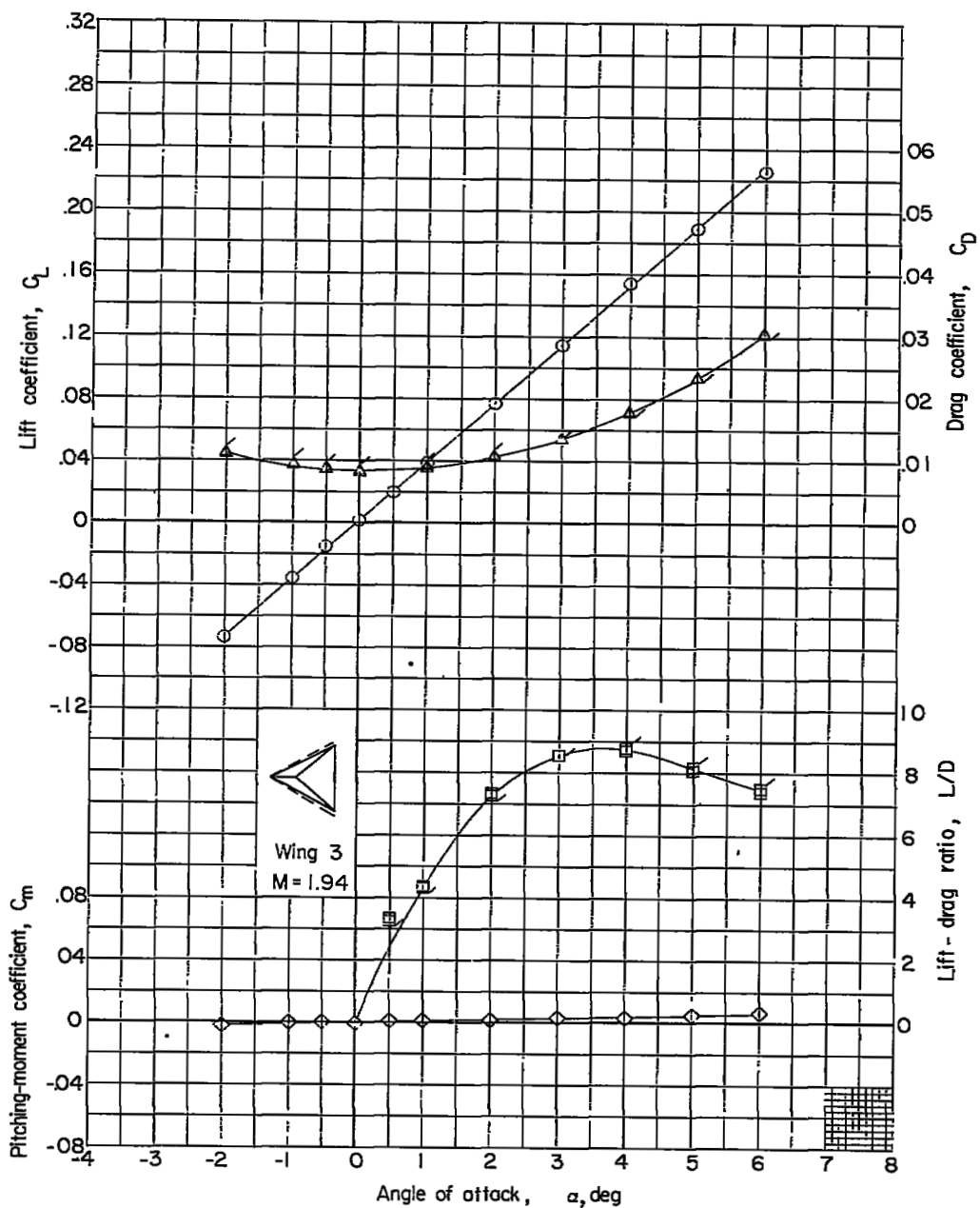
(a) $1 - r = 0.18c$.

Figure 10.- Aerodynamic characteristics of $3\frac{1}{2}$ -percent-thick delta wings. $M = 1.94$; semiapex angle ϵ , 30° . Flagged symbols denote correction applied to drag data to account for support-sting tare-interference effects.



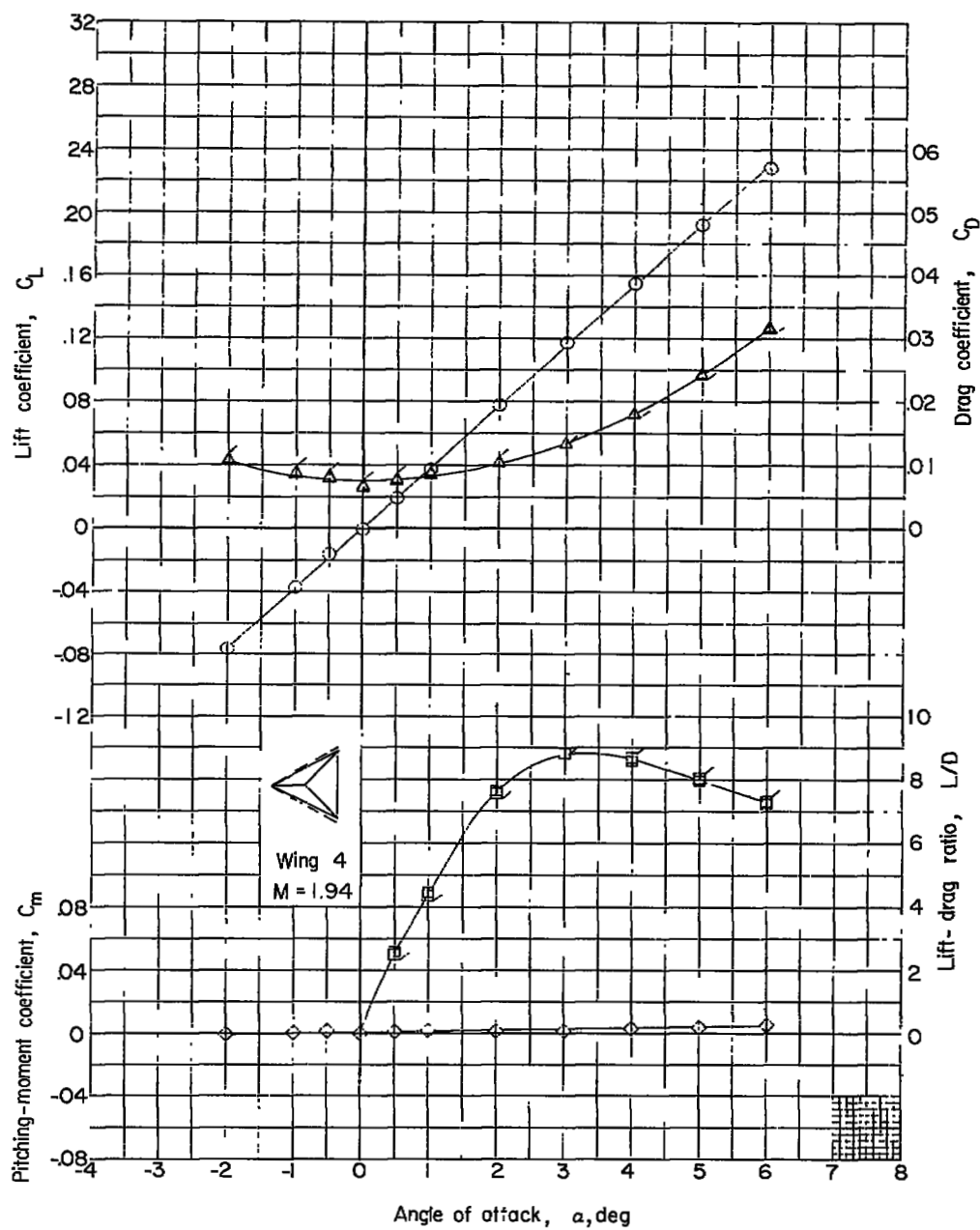
(b) $l - r = 0.30c$.

Figure 10.- Continued.



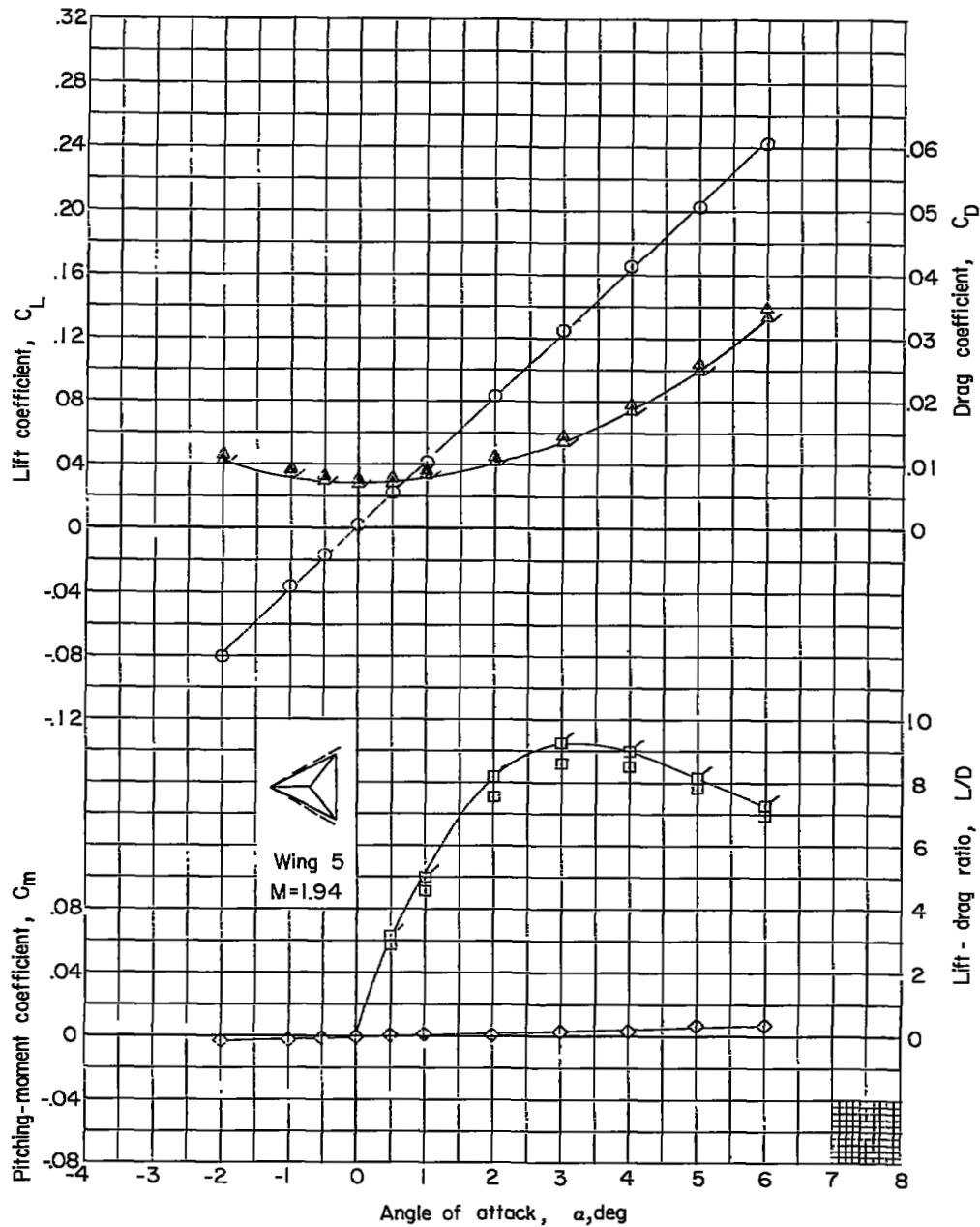
(c) $1 - r = 0.40c$.

Figure 10.- Continued.



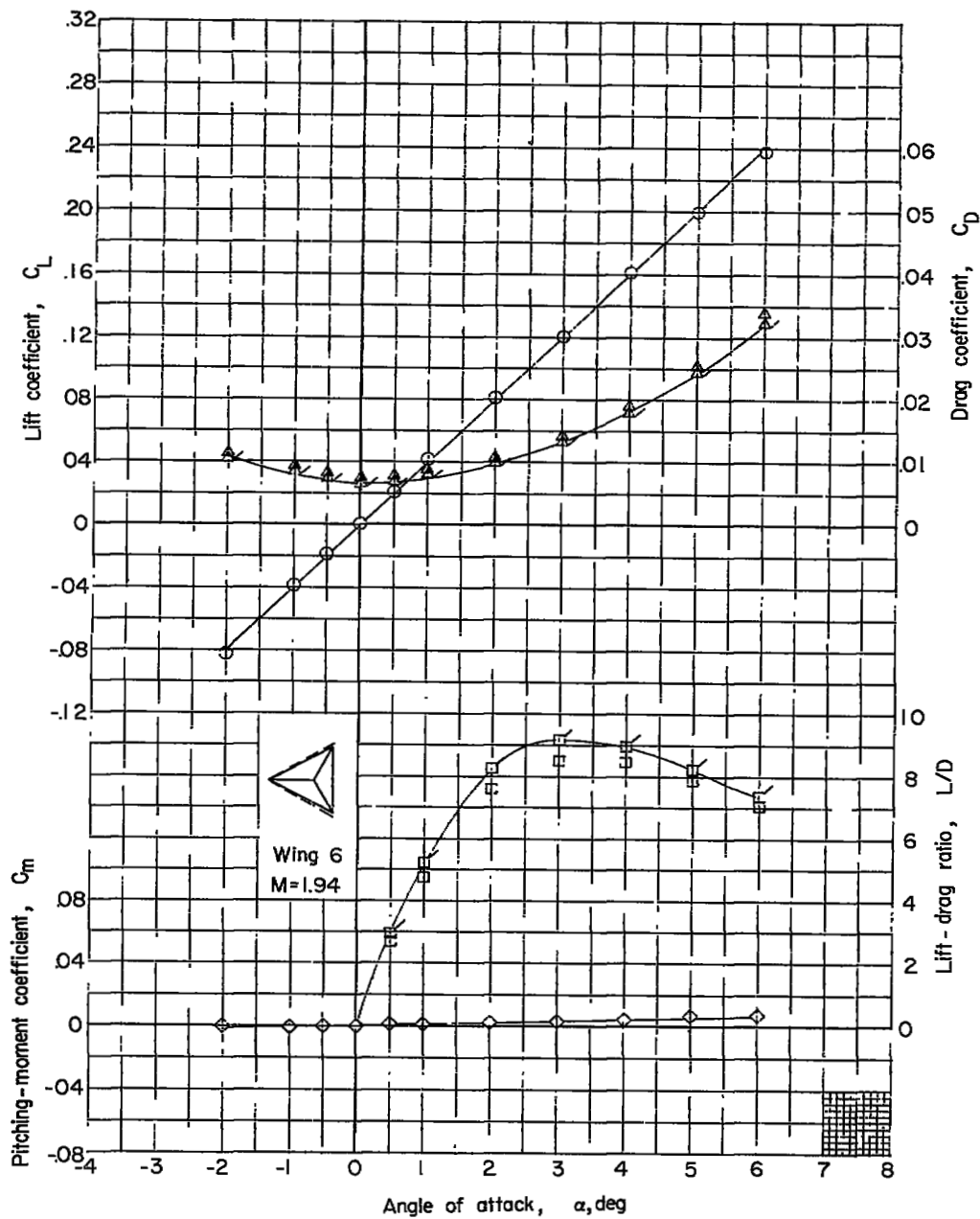
(d) $l - r = 0.50c$.

Figure 10.- Continued.



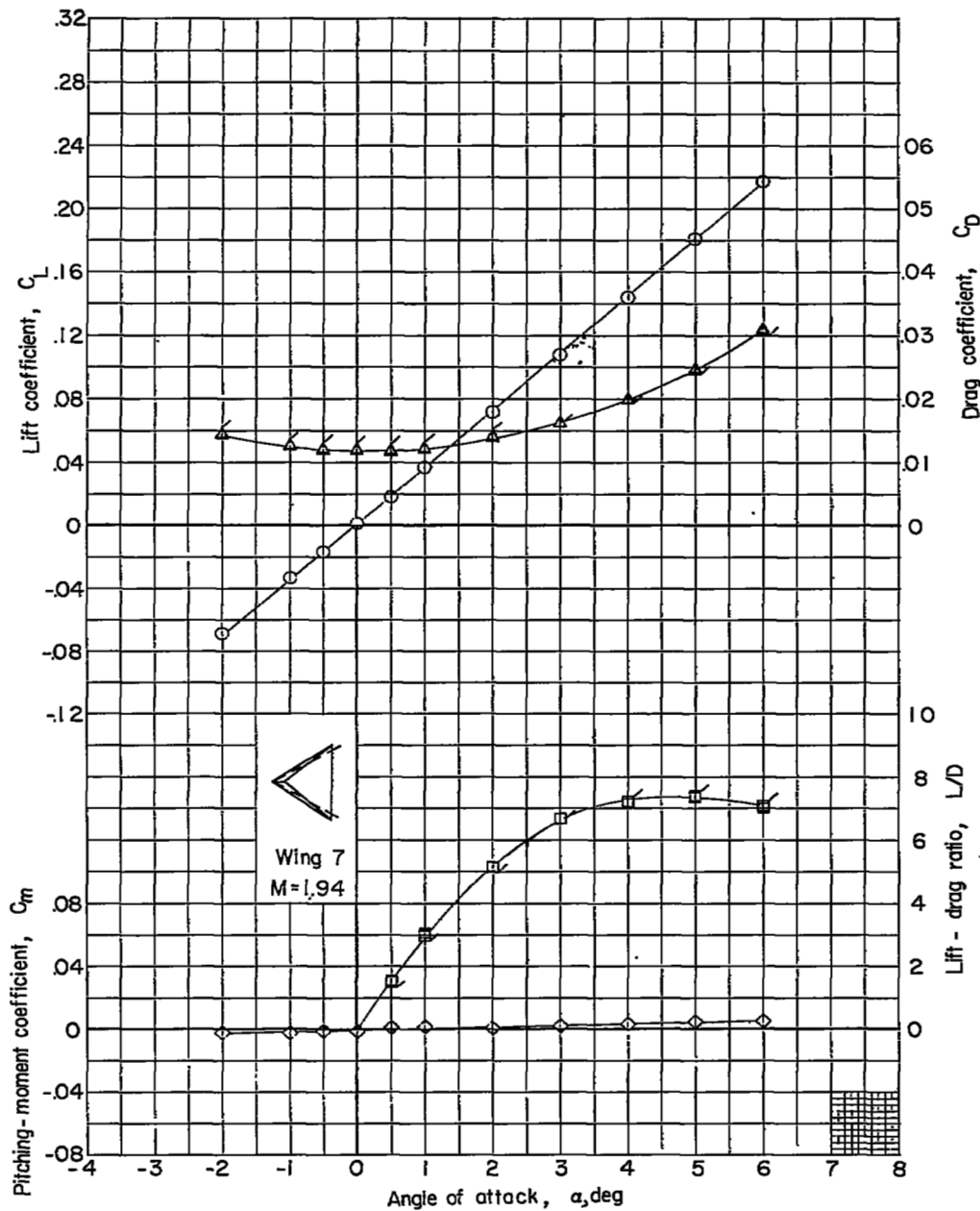
(e) $1 - r = 0.60c$.

Figure 10.- Continued.



(f) $l - r = 0.70c$.

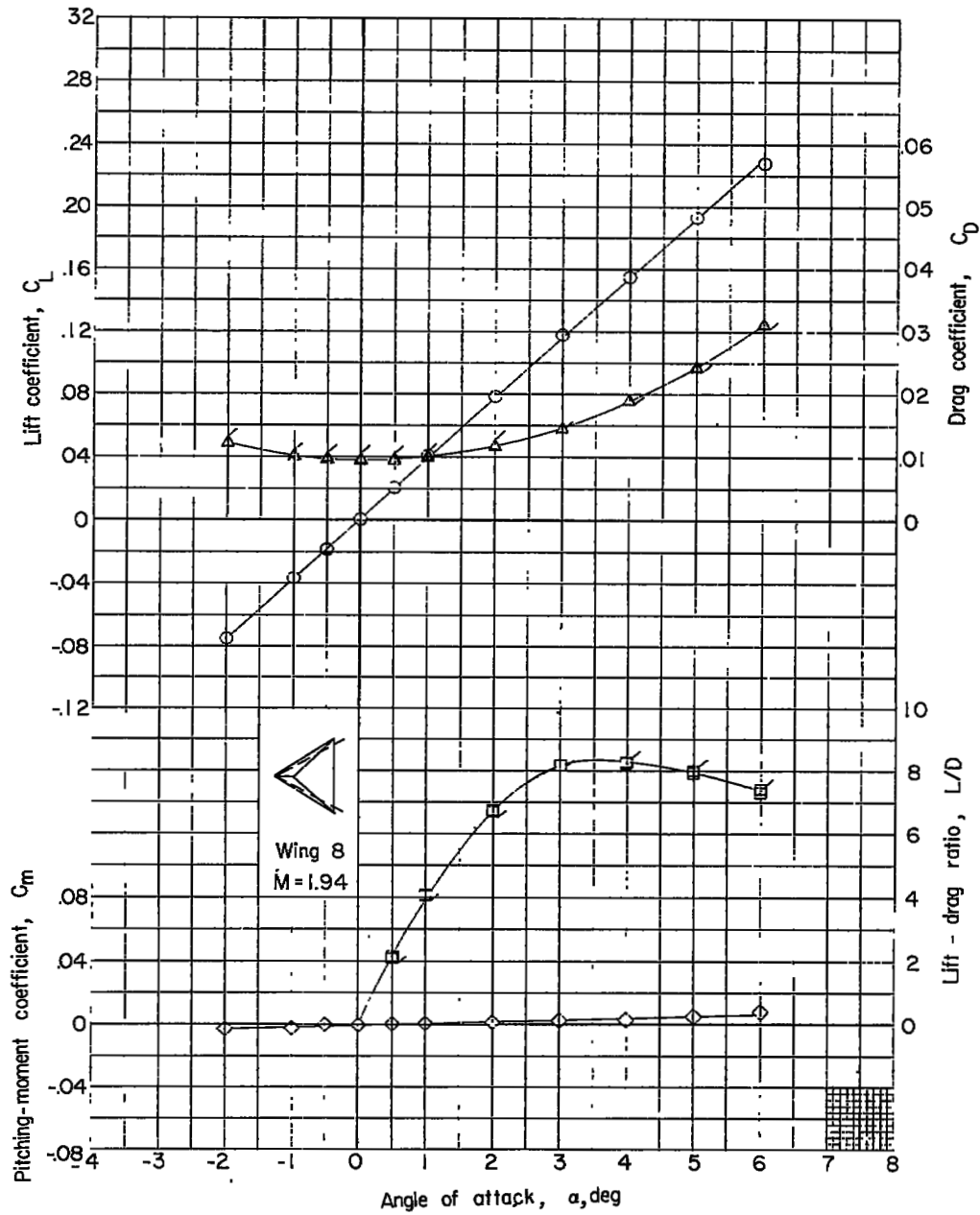
Figure 10.- Concluded.



(a) $1 - r = 0.18c$.

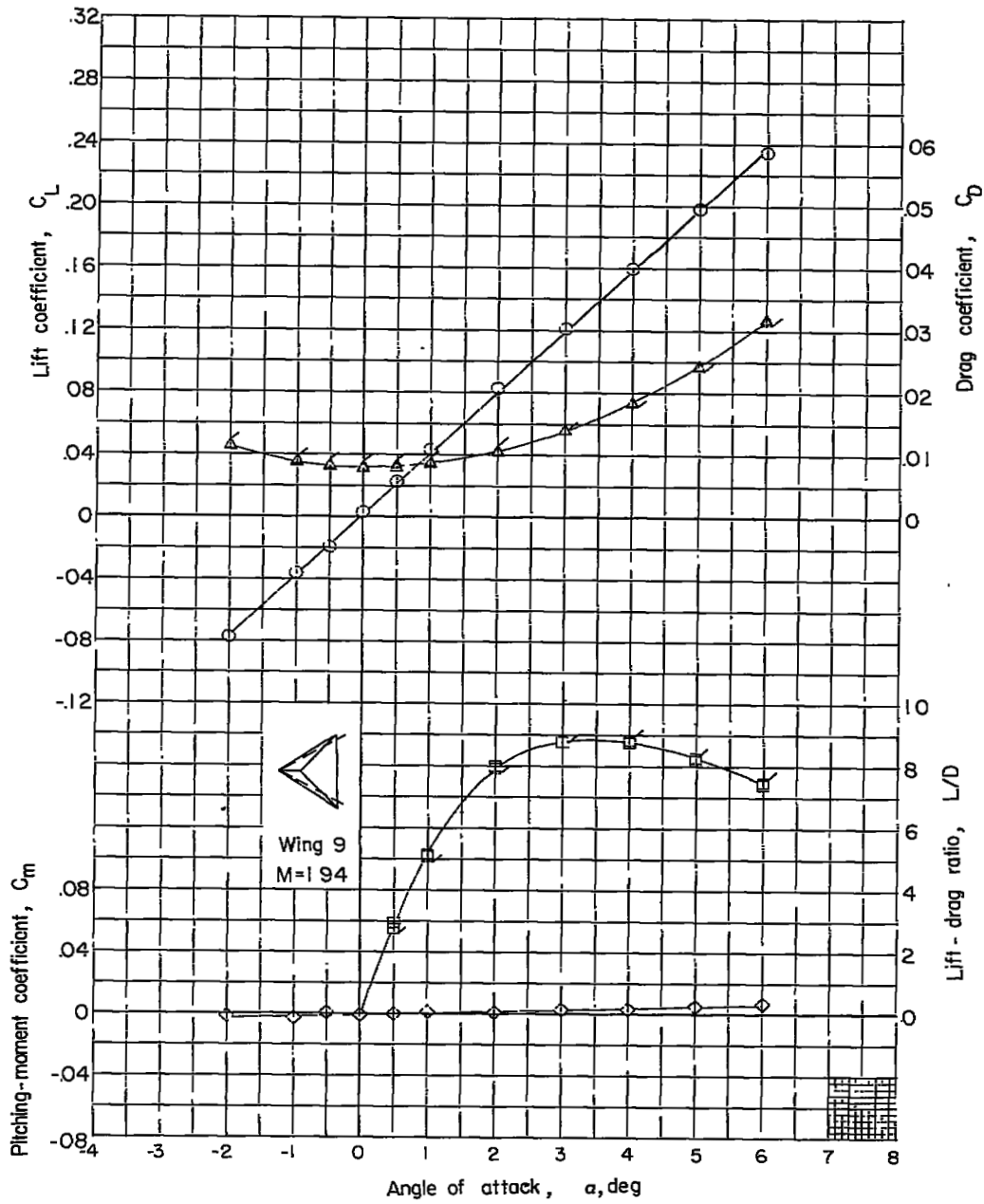
Figure 11.- Aerodynamic characteristics of $\frac{1}{2}$ -percent-thick delta wings.

$M = 1.94$; semiapex angle ϵ , 35° . Flagged symbols denote correction applied to drag data to account for support-sting tare-interference effects.



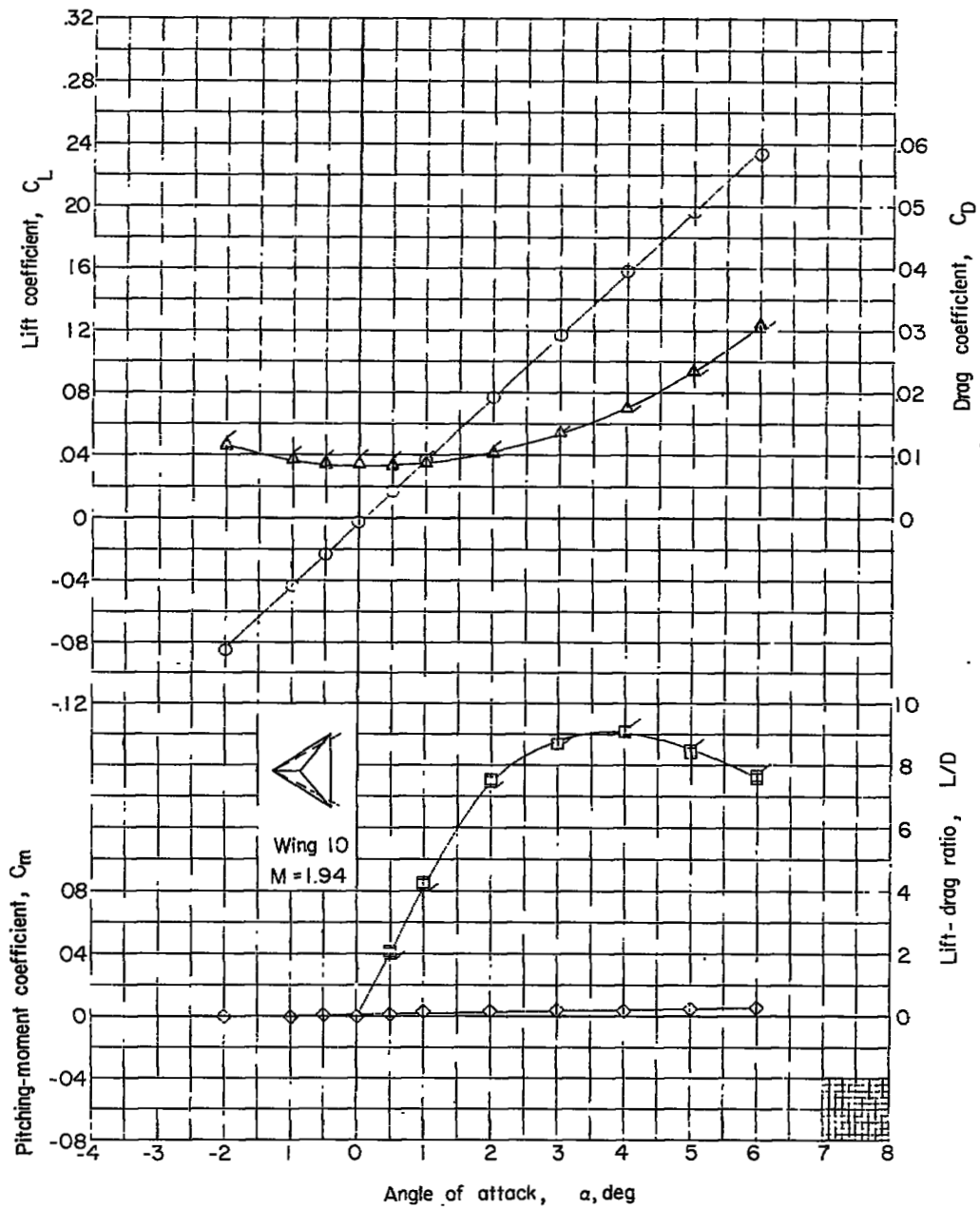
(b) $1 - r = 0.30c$.

Figure 11.- Continued.



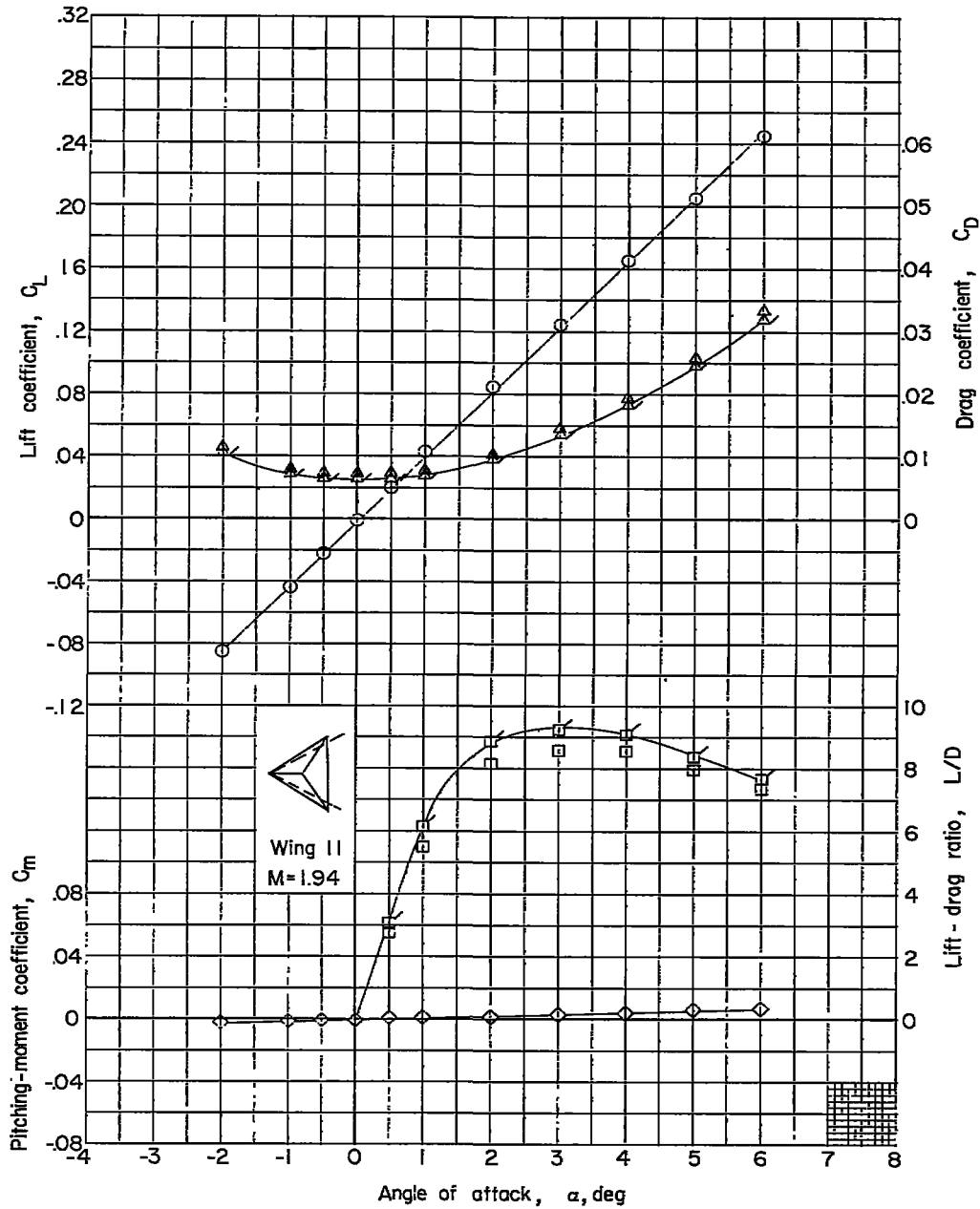
(c) $l - r = 0.40c$.

Figure 11.- Continued.



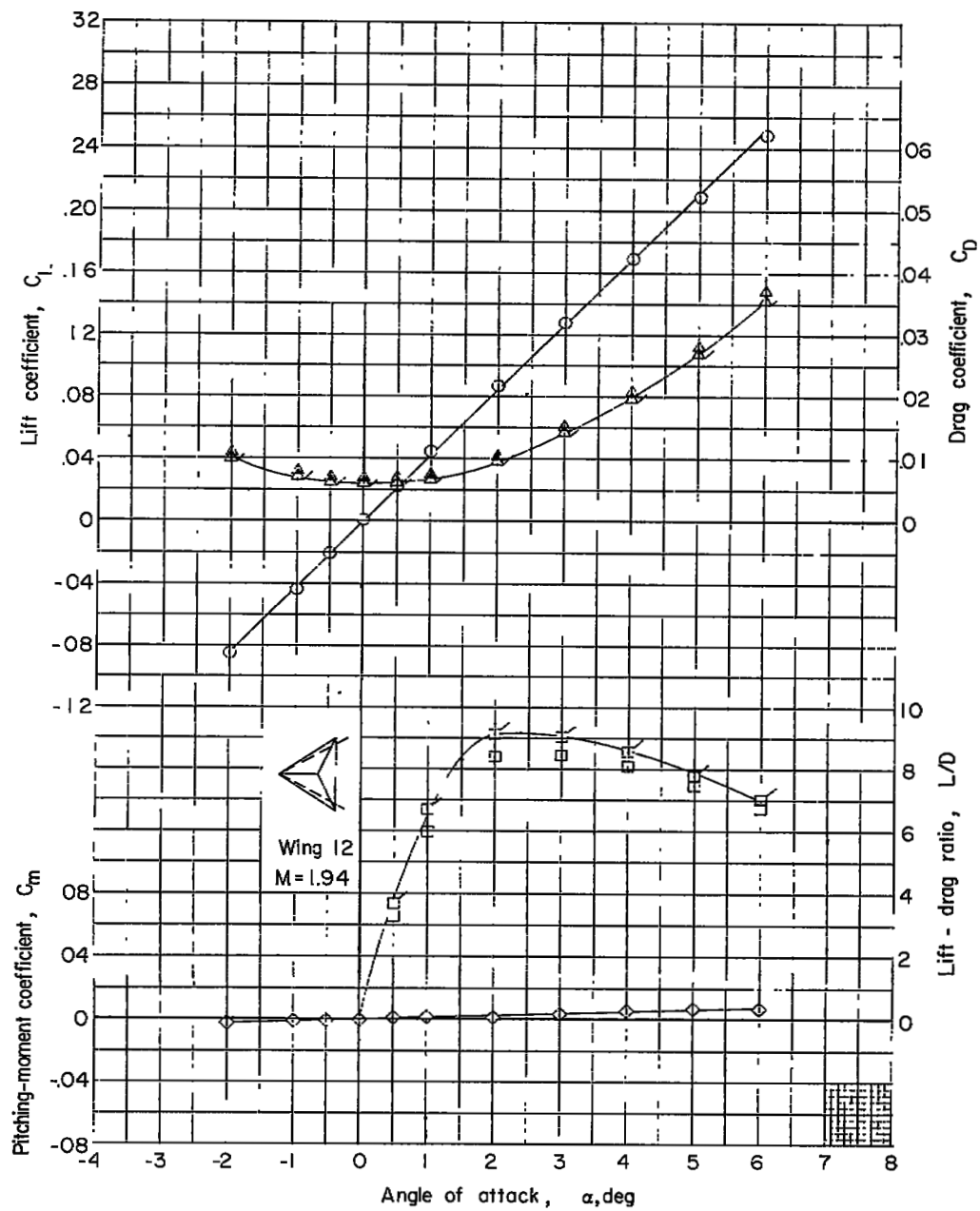
(d) $l - r = 0.50c$.

Figure 11.- Continued.



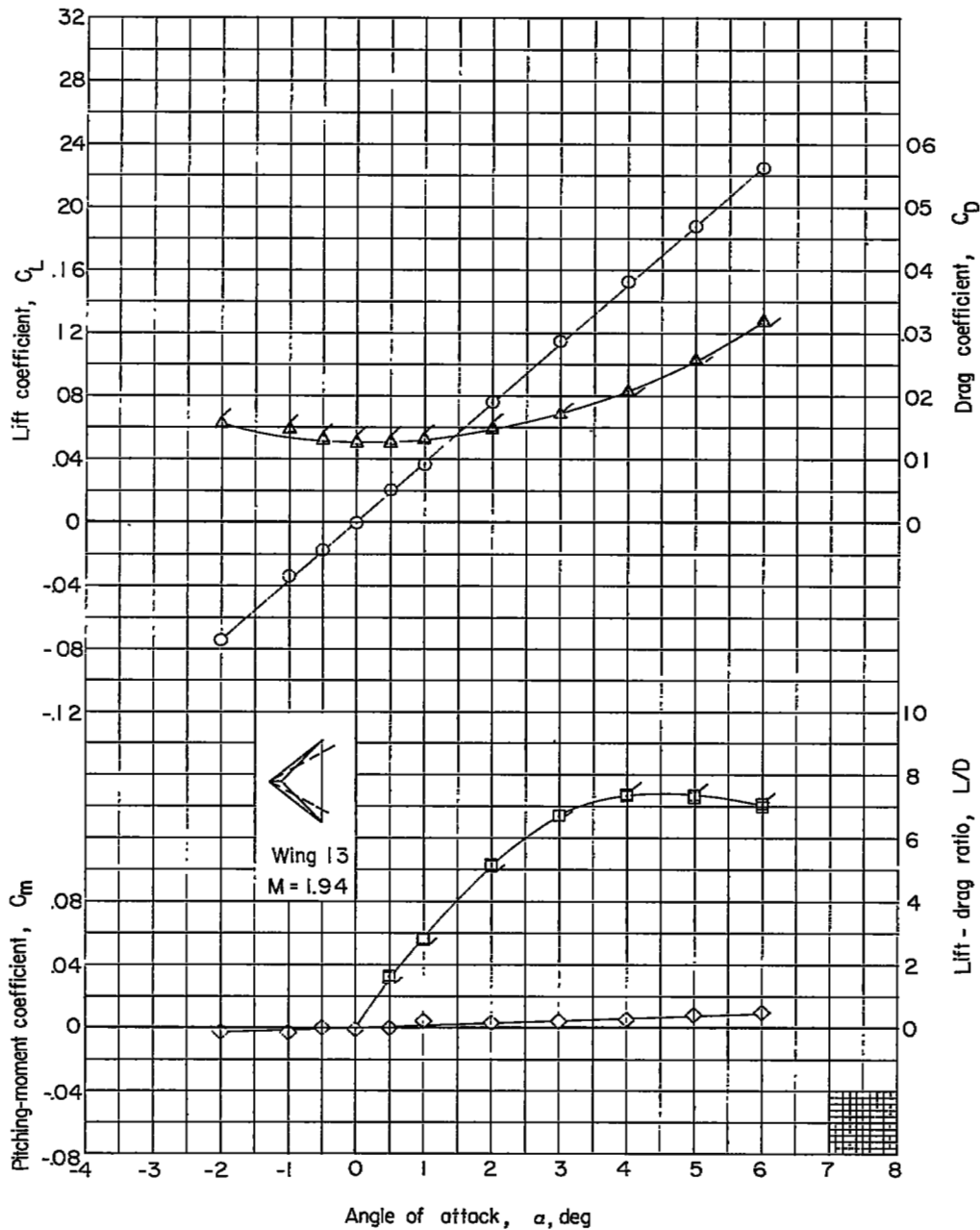
(e) $1 - r = 0.60c$.

Figure 11.- Continued.



(f) $1 - r = 0.70c$.

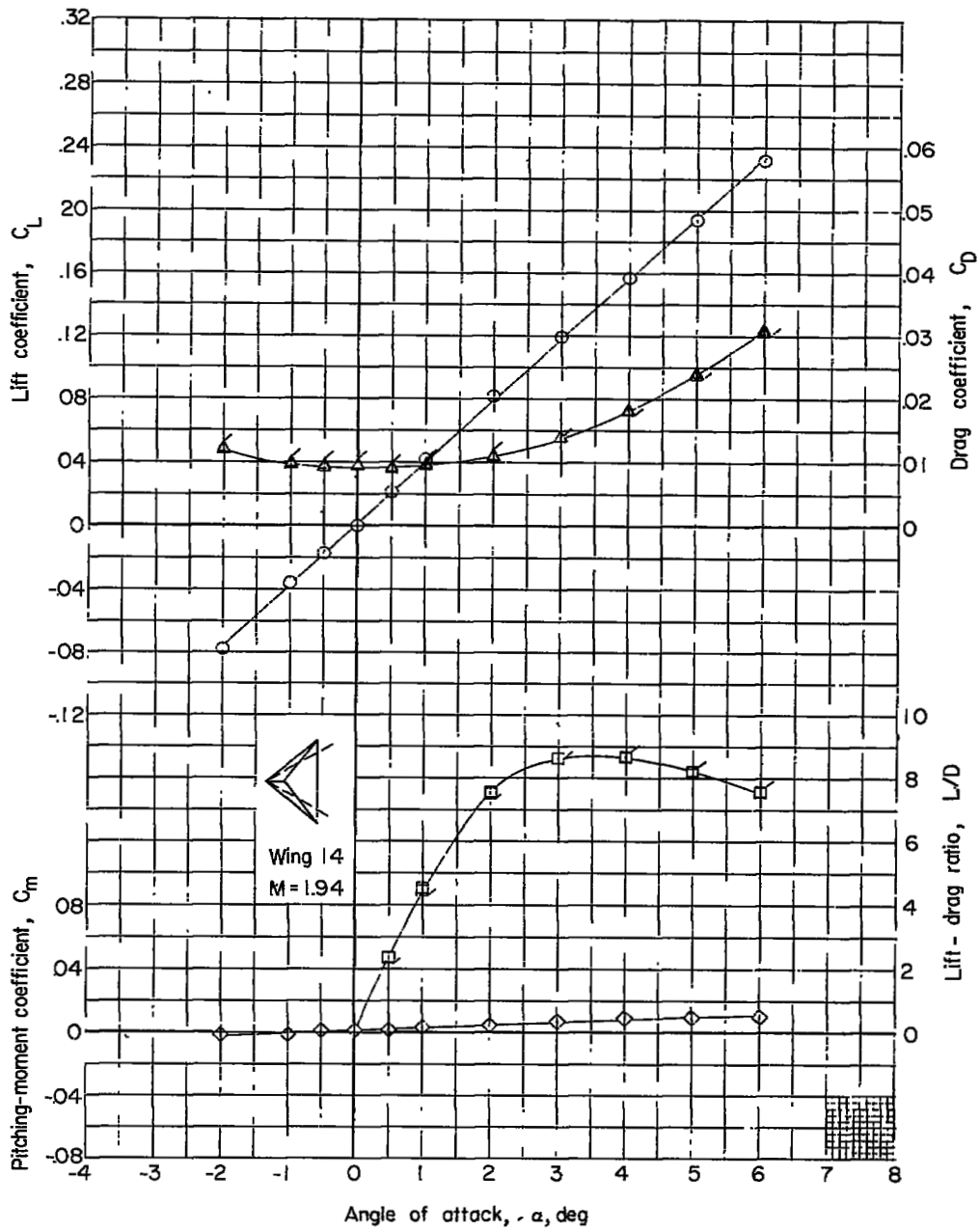
Figure 11.- Concluded.



(a) $1 - r = 0.18c$.

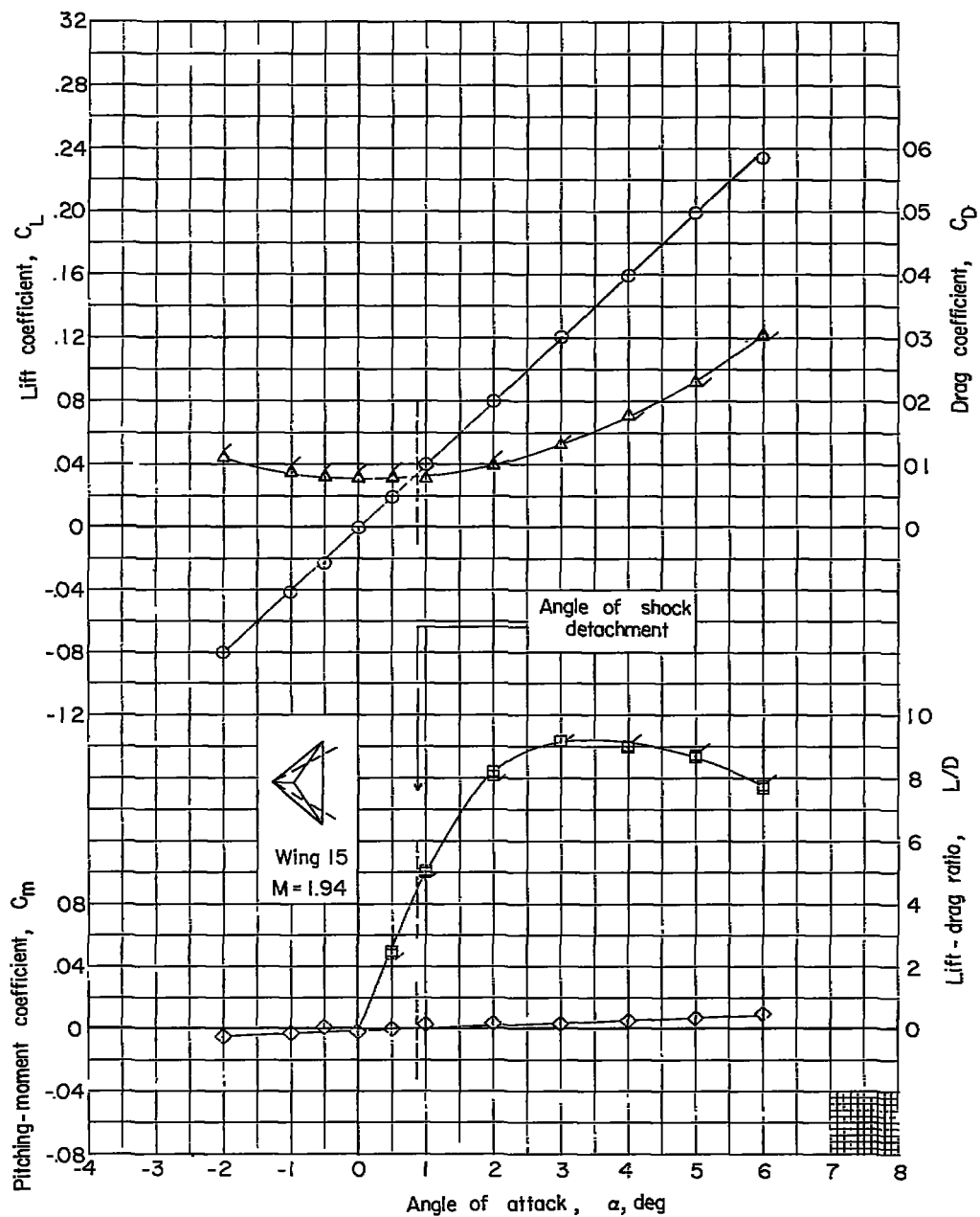
Figure 12.- Aerodynamic characteristics of $3\frac{1}{2}$ -percent-thick delta wings.

M = 1.94; semiapex angle ϵ , 35° . Flagged symbols denote correction applied to drag data to account for support-sting tare-interference effects.



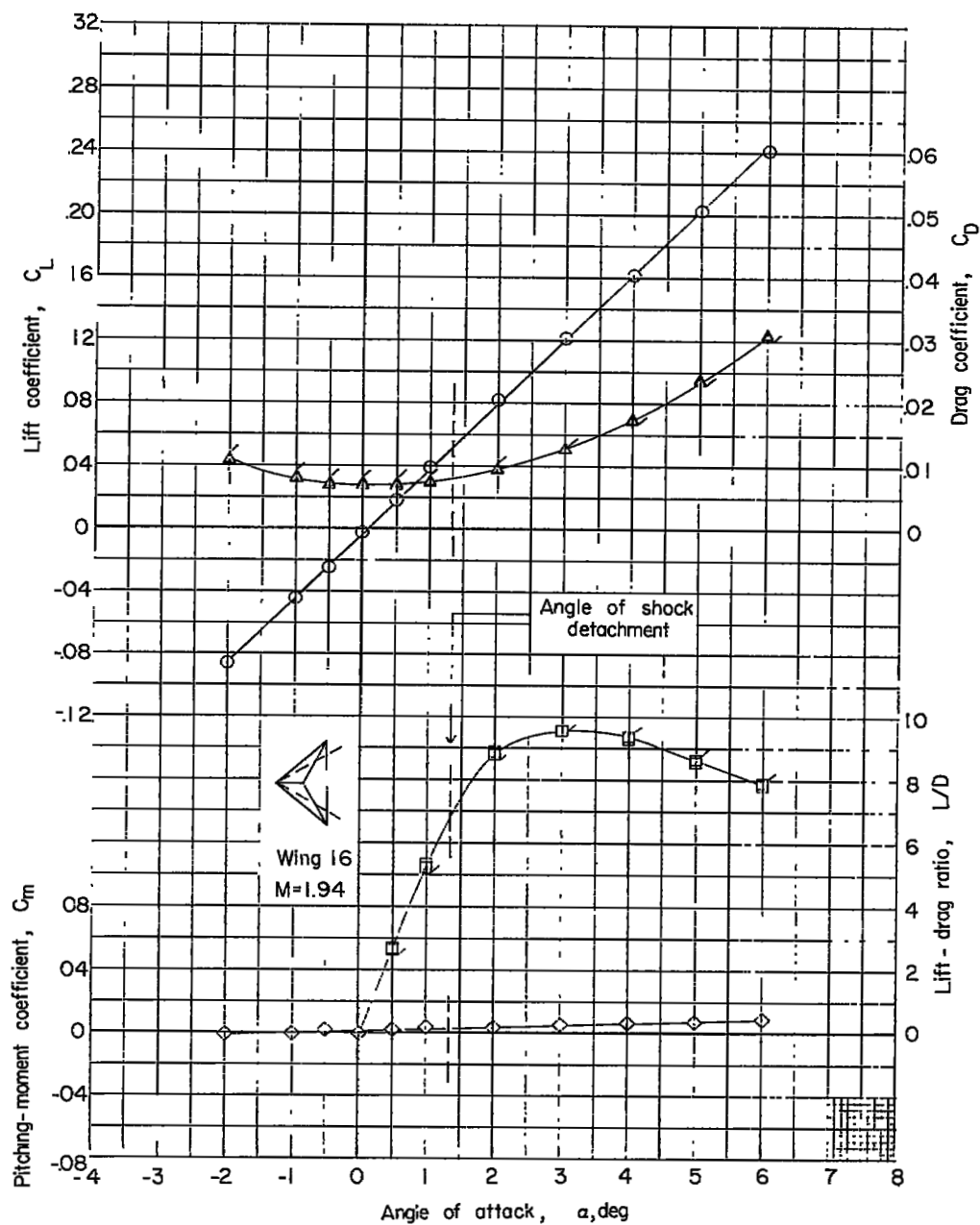
(b) $1 - r = 0.30c$.

Figure 12.- Continued.



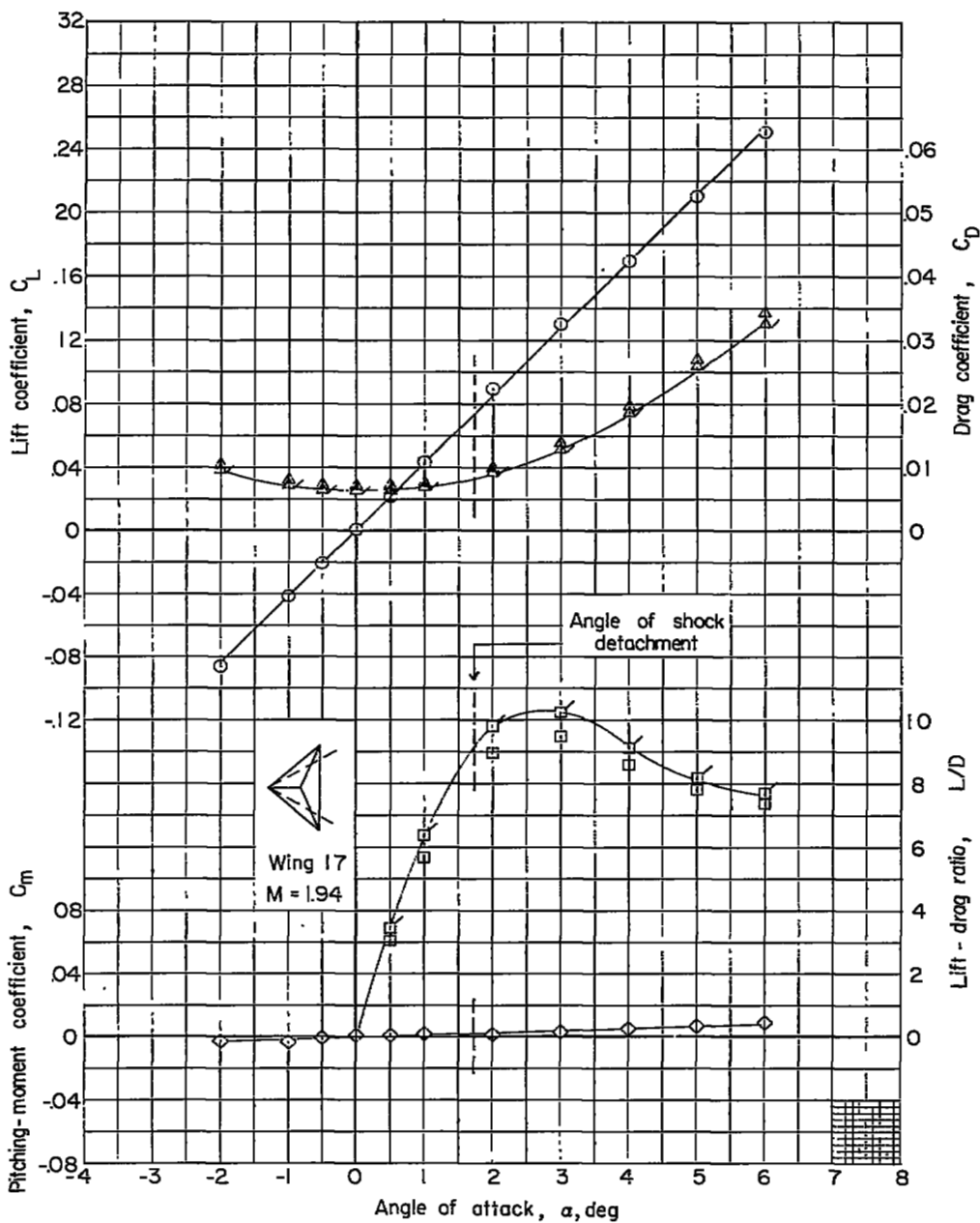
(c) $1 - r = 0.40c$.

Figure 12.- Continued.



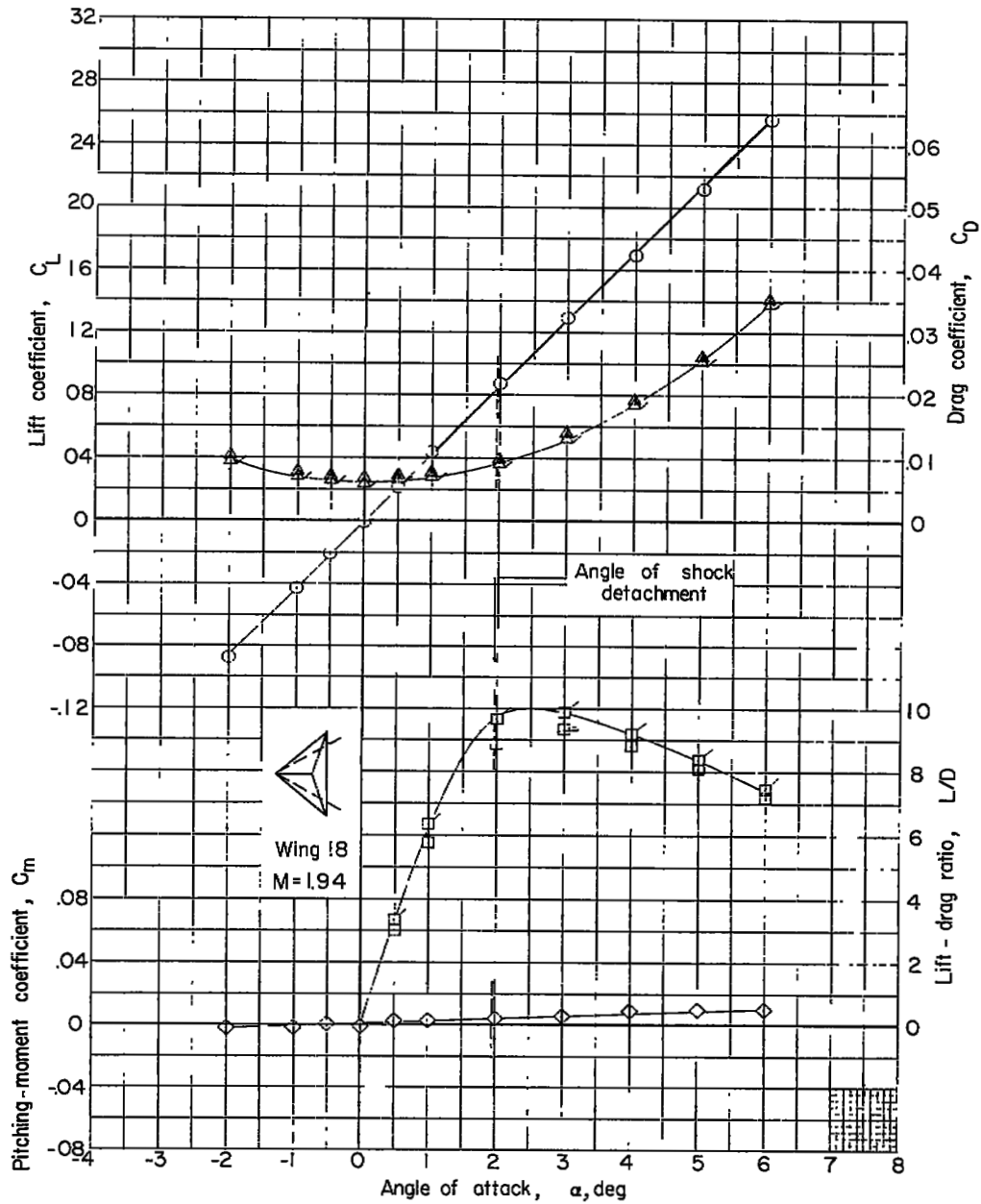
(d) $1 - r = 0.50c$.

Figure 12.- Continued.



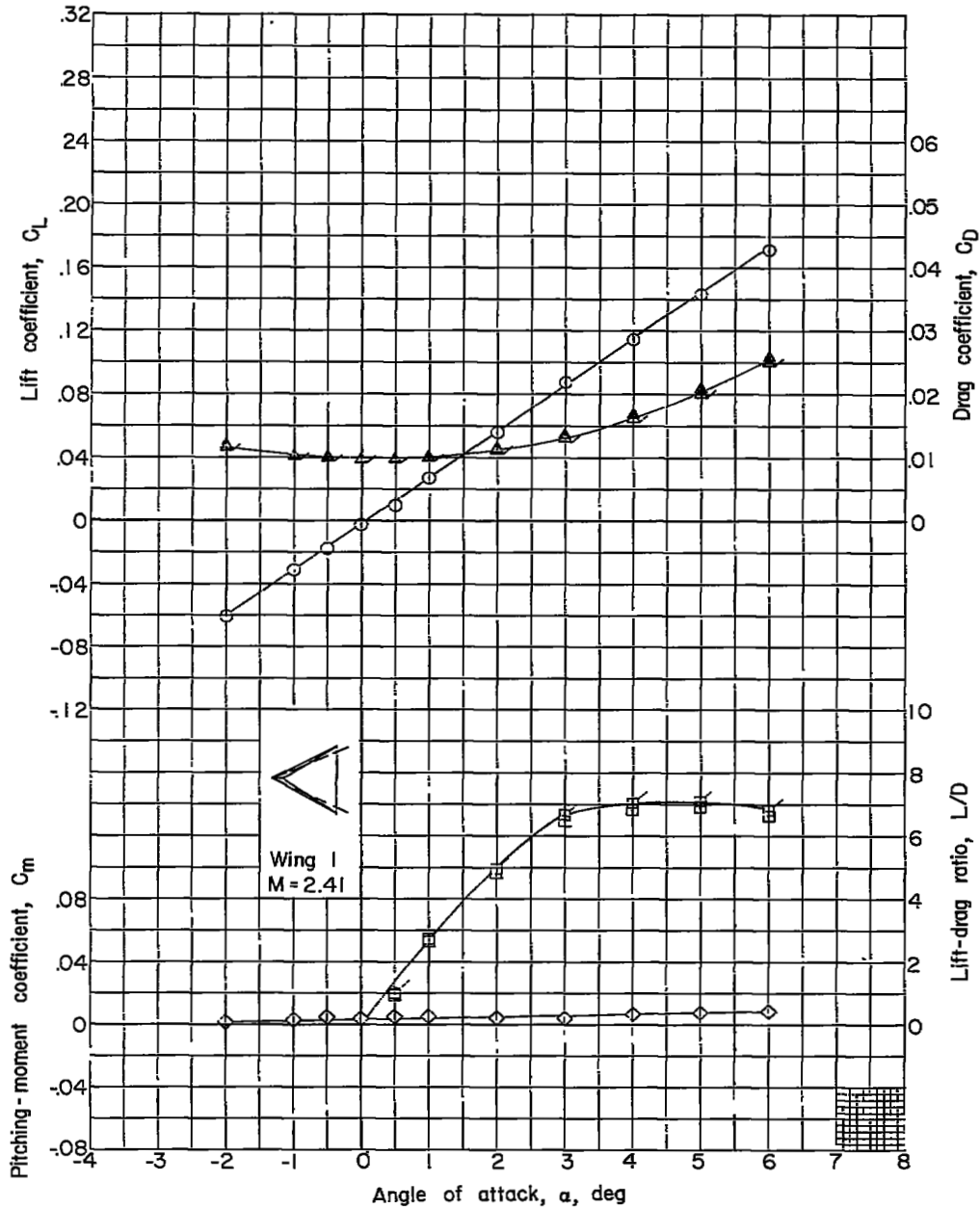
(e) $1 - r = 0.60c$.

Figure 12.- Continued.



(f) $\xi - r = 0.70c$.

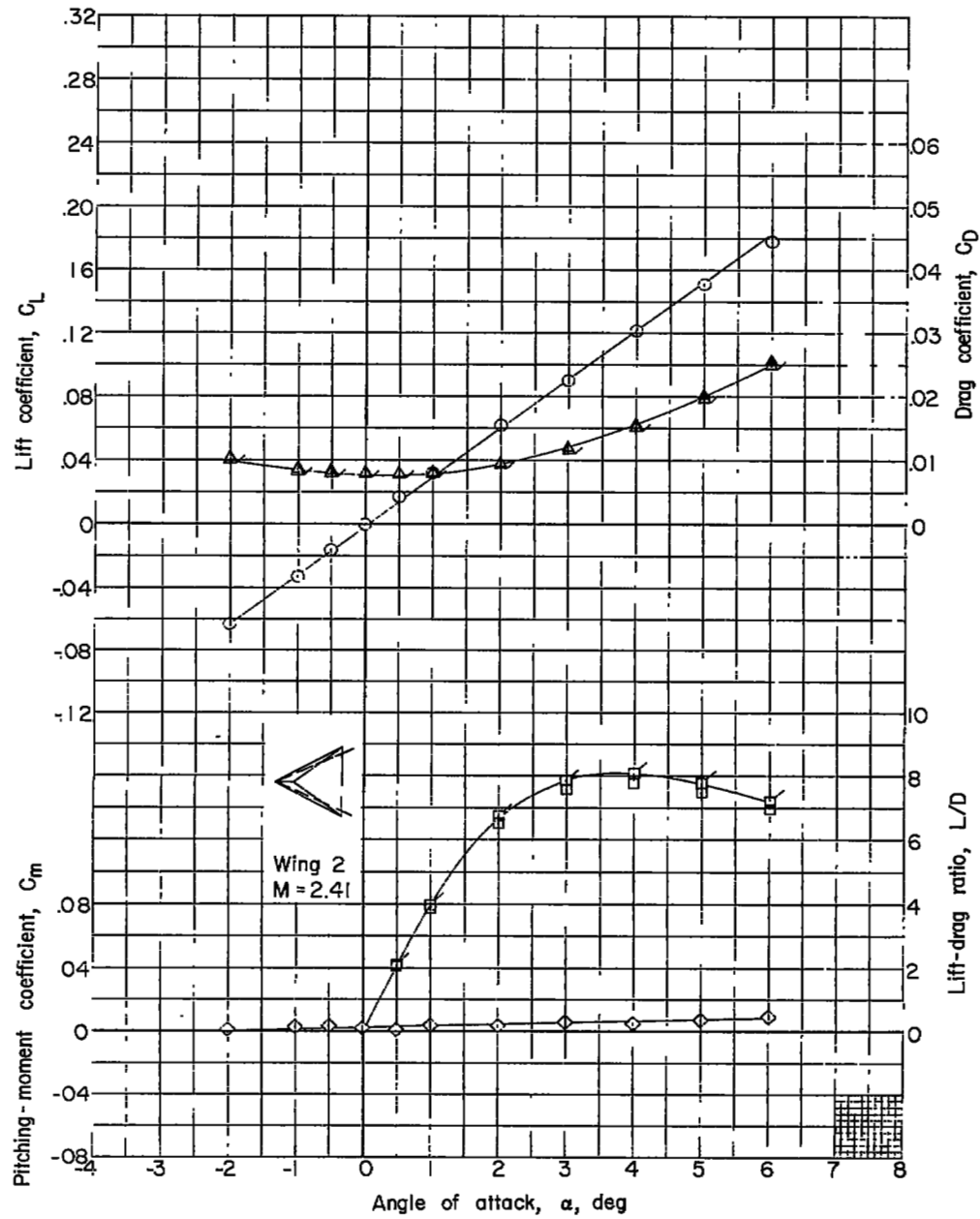
Figure 12.- Concluded.



(a) $1 - r = 0.18c$.

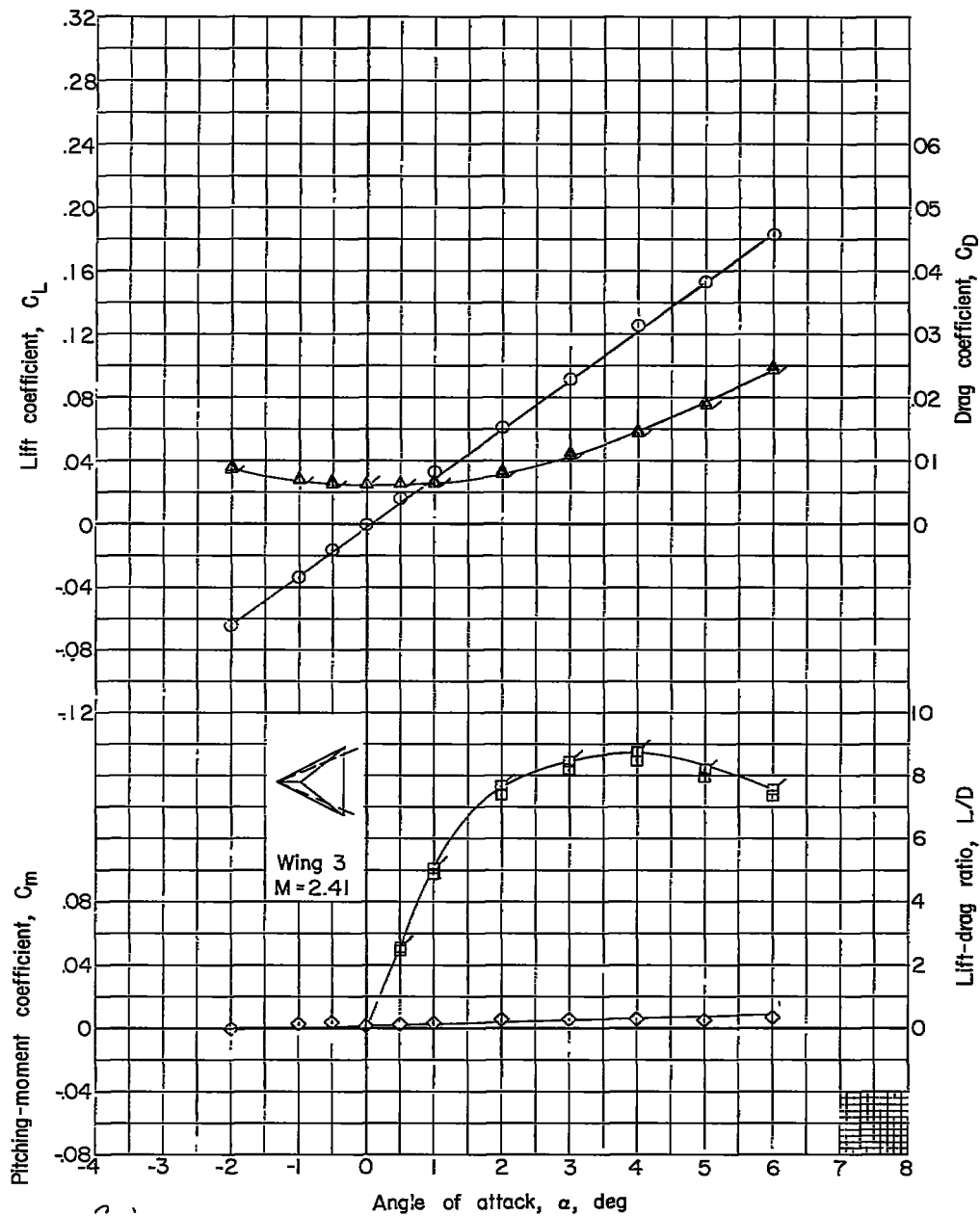
Figure 13.- Aerodynamic characteristics of $\frac{3}{2}$ -percent-thick delta wings.

$M = 2.41$; semiapex angle ϵ , 30° . Flagged symbols denote correction applied to drag data to account for support-sting tare-interference effects.



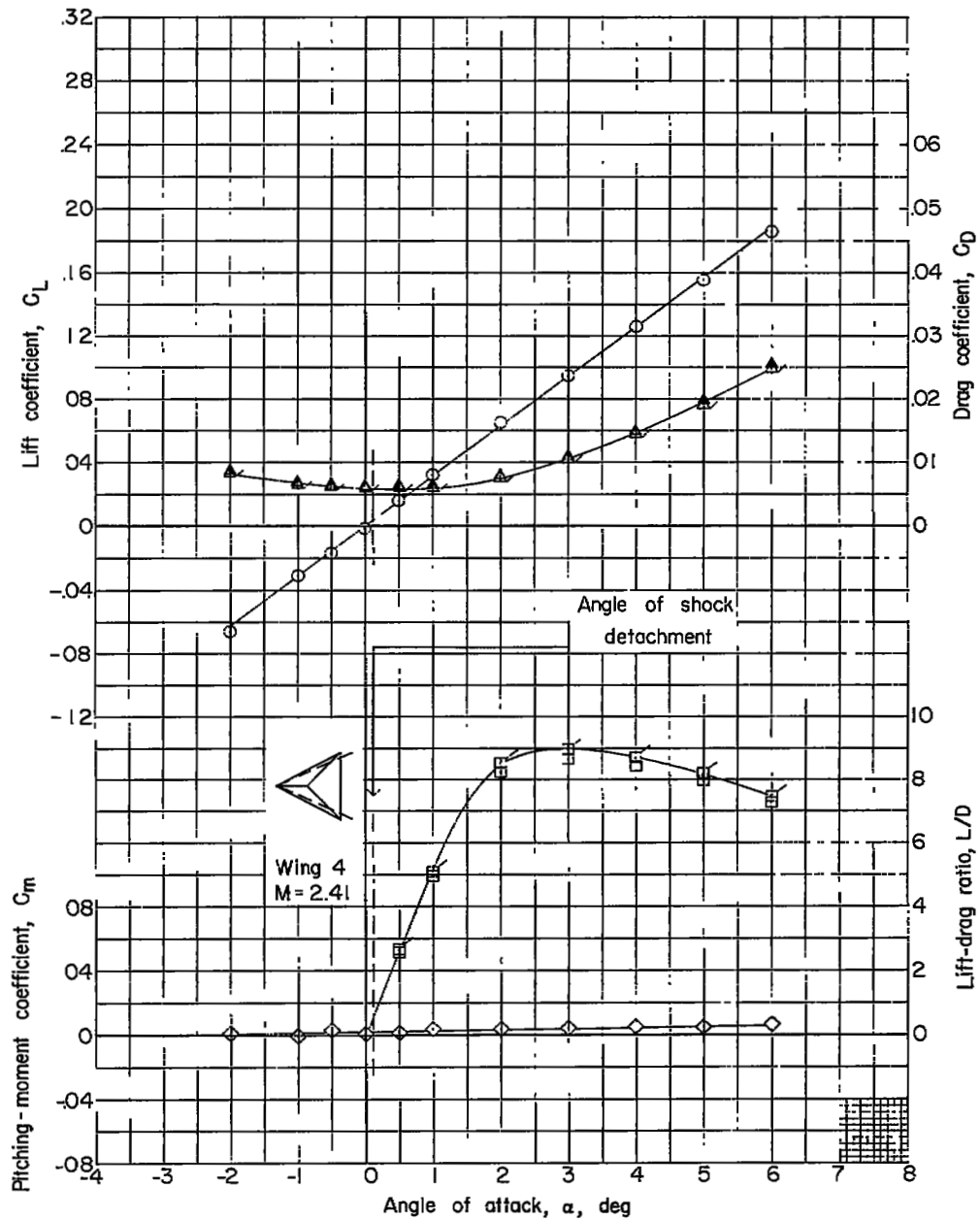
(b) $1 - r = 0.30c$.

Figure 13.- Continued.



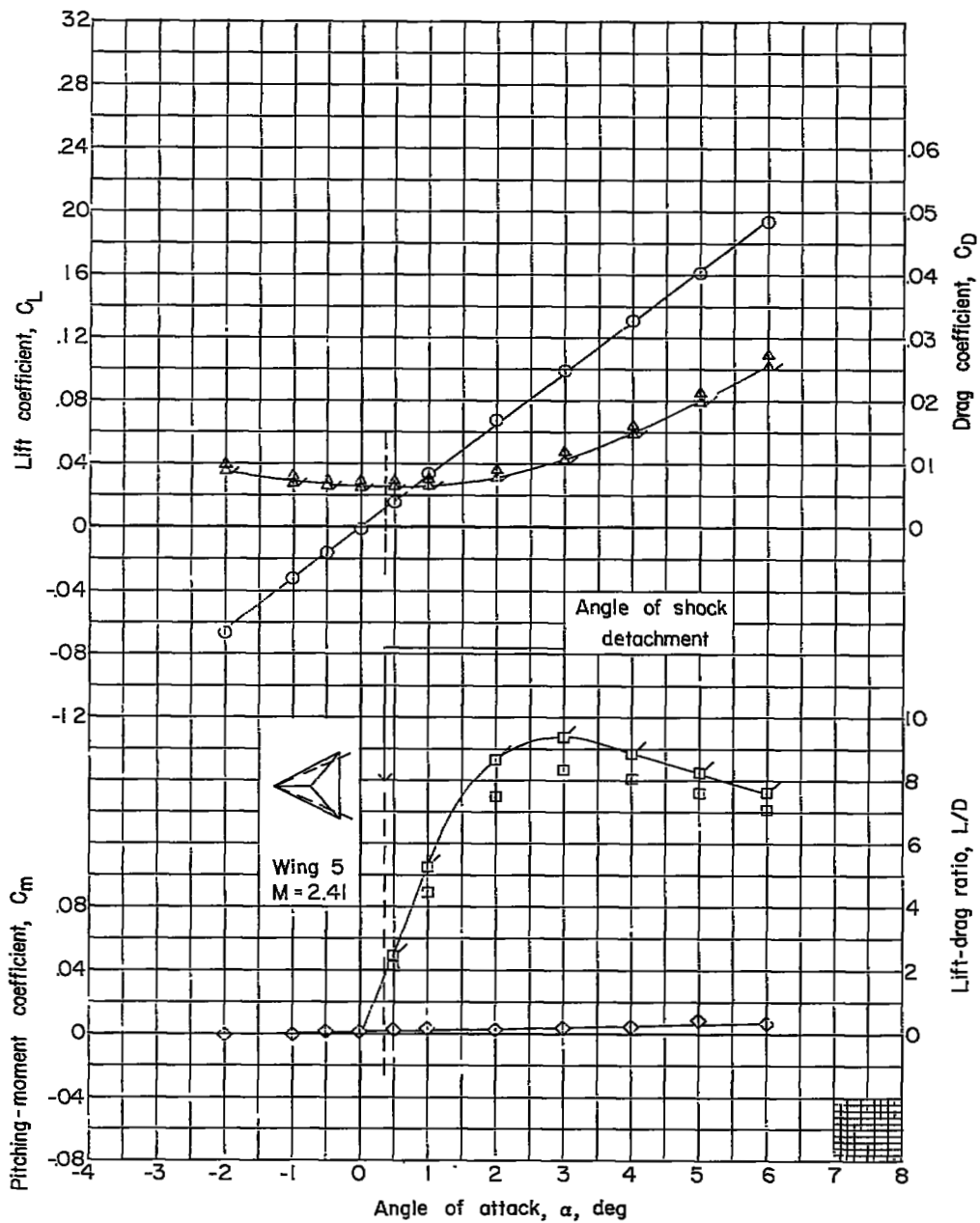
(c) $1 - r = 0.40c$.

Figure 13.- Continued.



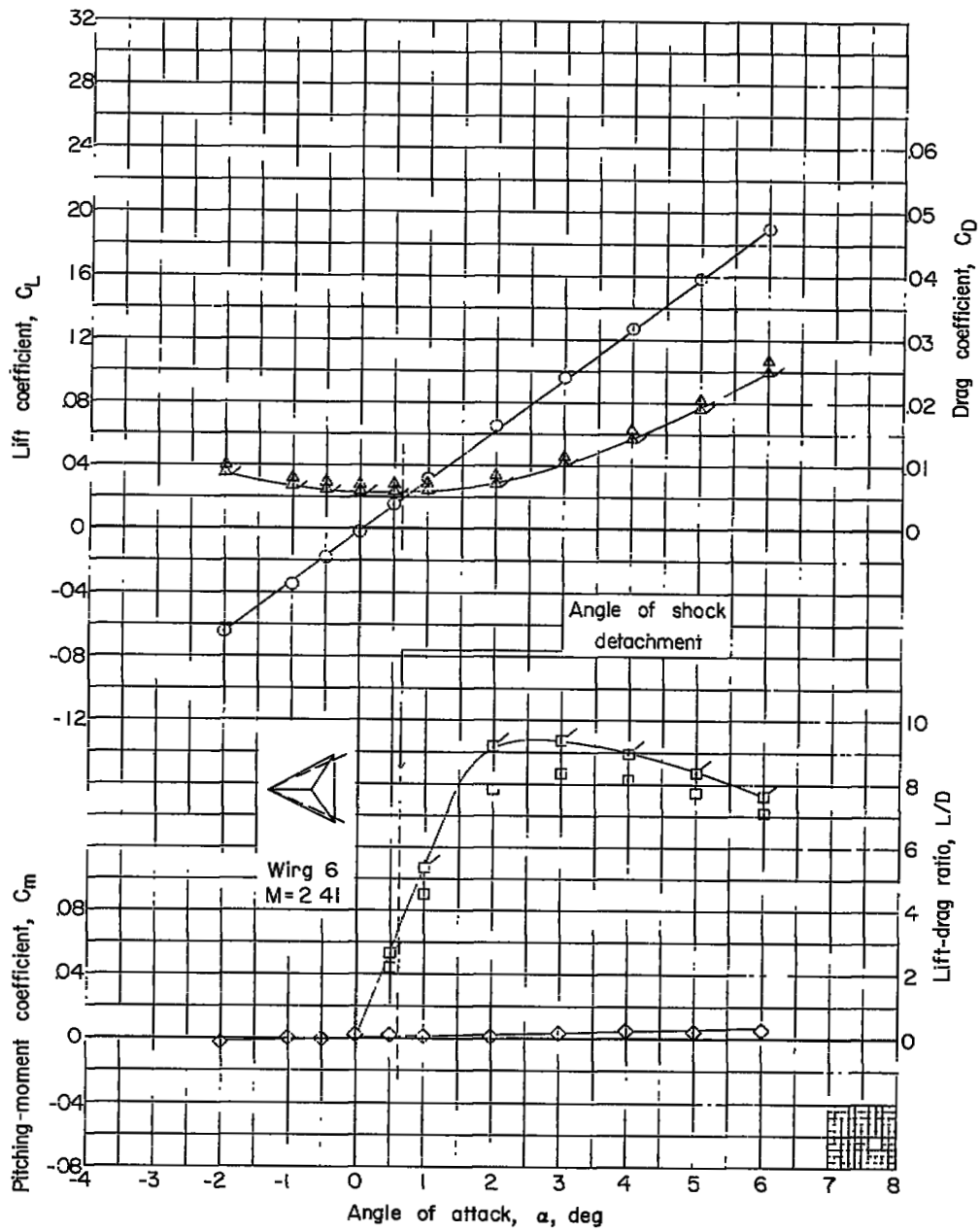
(d) $1 - r = 0.50c$.

Figure 13.- Continued.



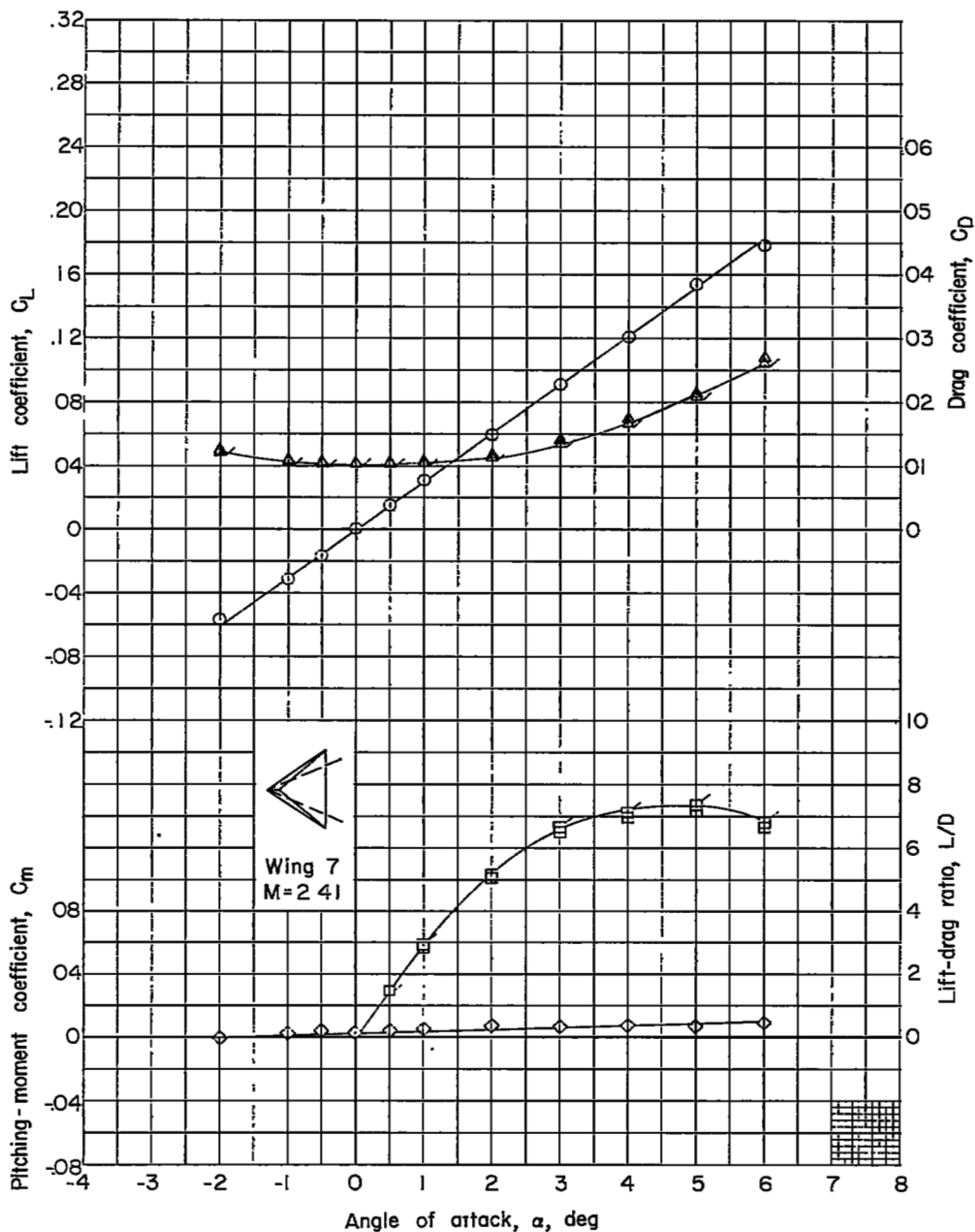
(e) $1 - r = 0.60c$.

Figure 13.- Continued.



(f) $1 - r = 0.70c$.

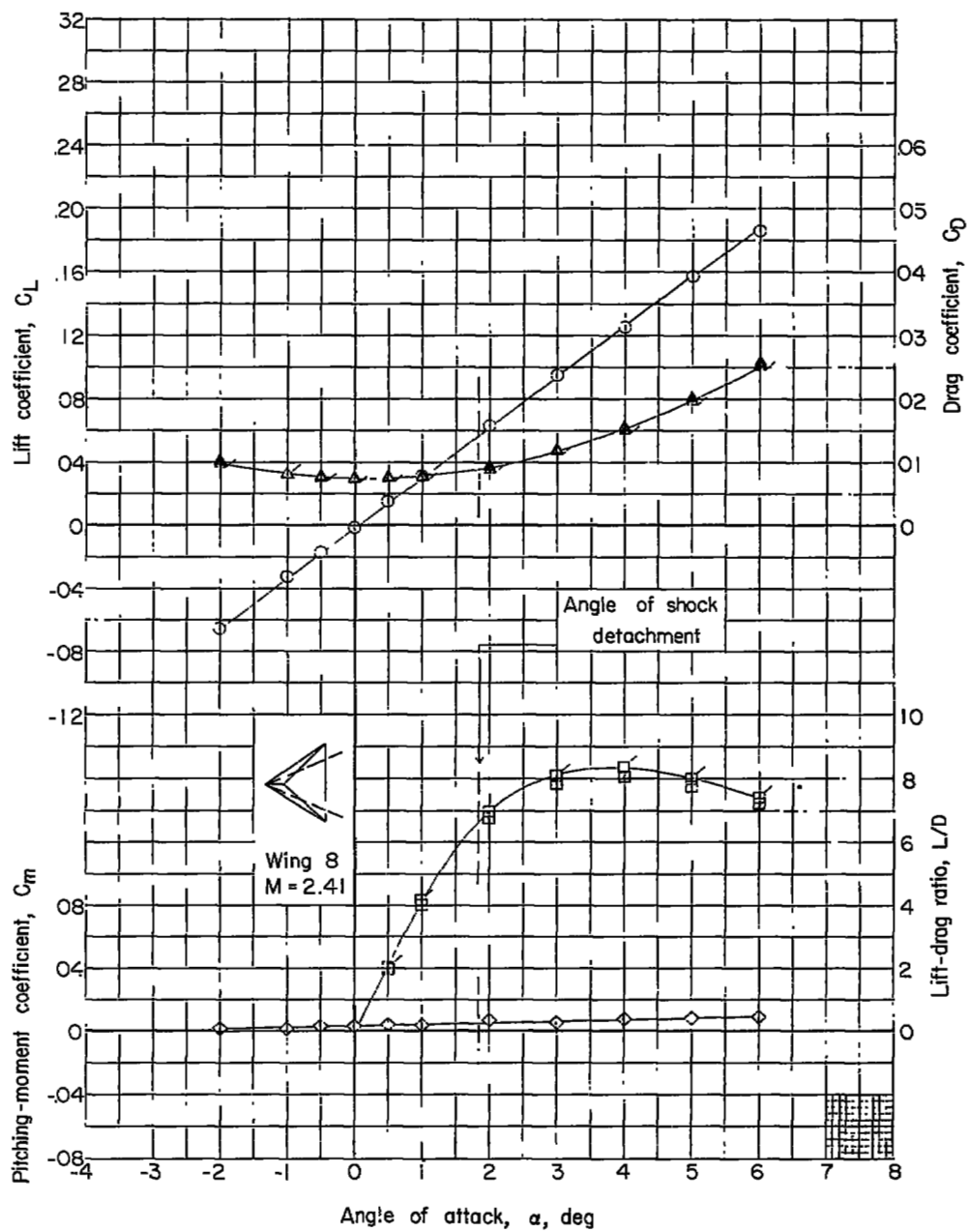
Figure 13.- Concluded.



(a) $1 - r = 0.18c$.

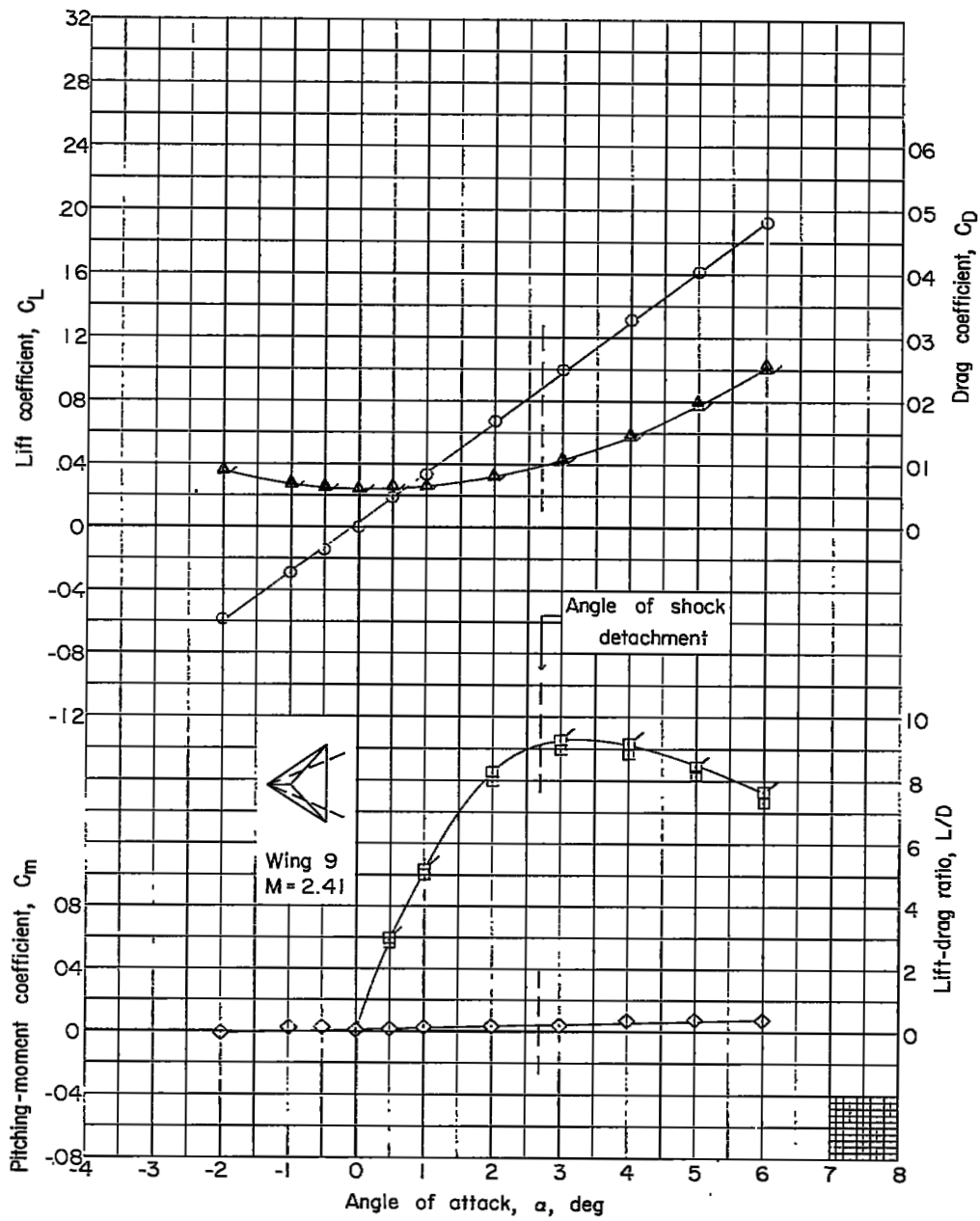
Figure 14.- Aerodynamic characteristics of $3\frac{1}{2}$ -percent-thick delta wings.

$M = 2.41$; semiapex angle ϵ , 35° . Flagged symbols denote correction applied to drag data to account for support-sting tare-interference effects.



(b) $l - r = 0.30c$.

Figure 14.- Continued.



(c) $1 - r = 0.40c.$

Figure 14.- Continued.

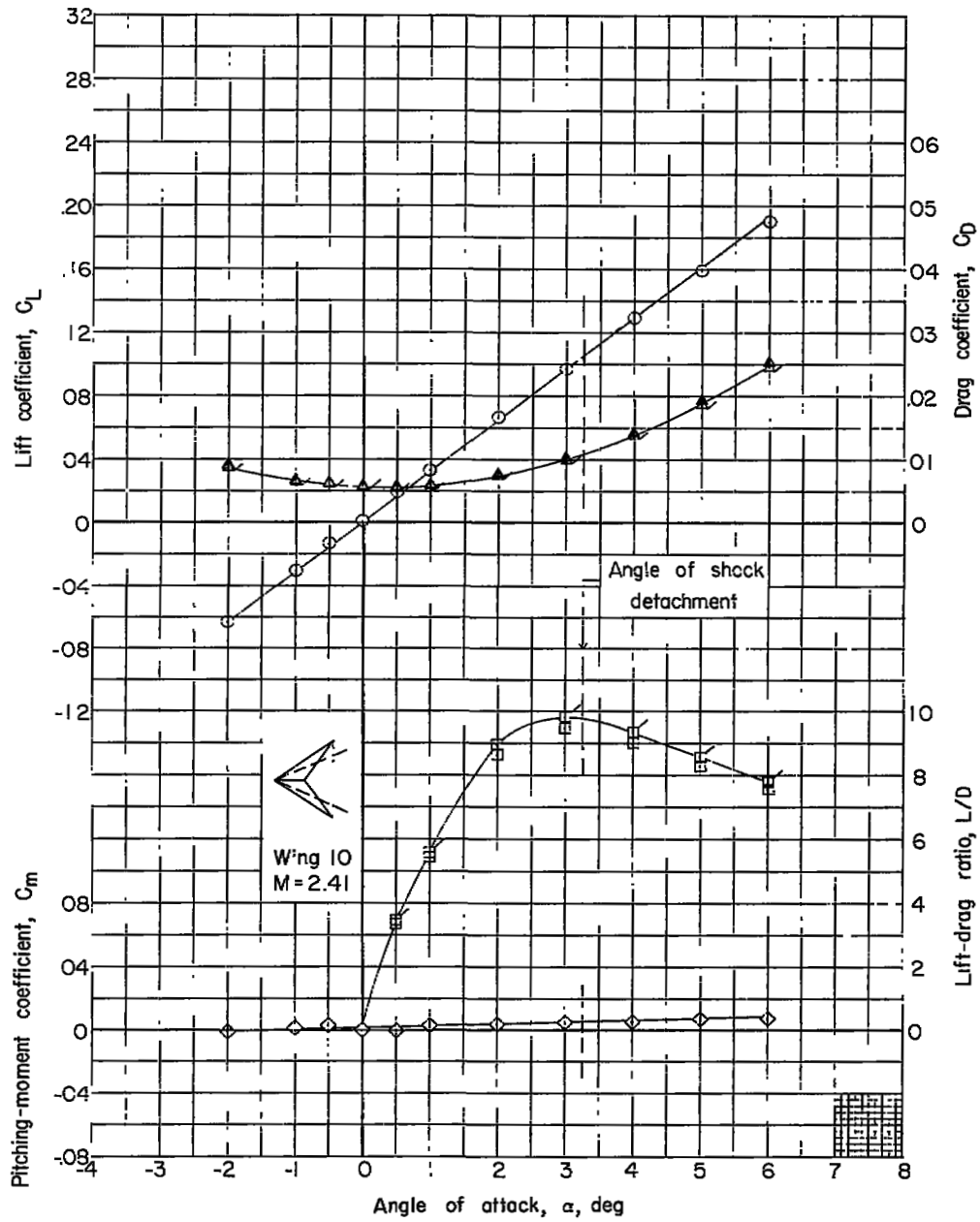
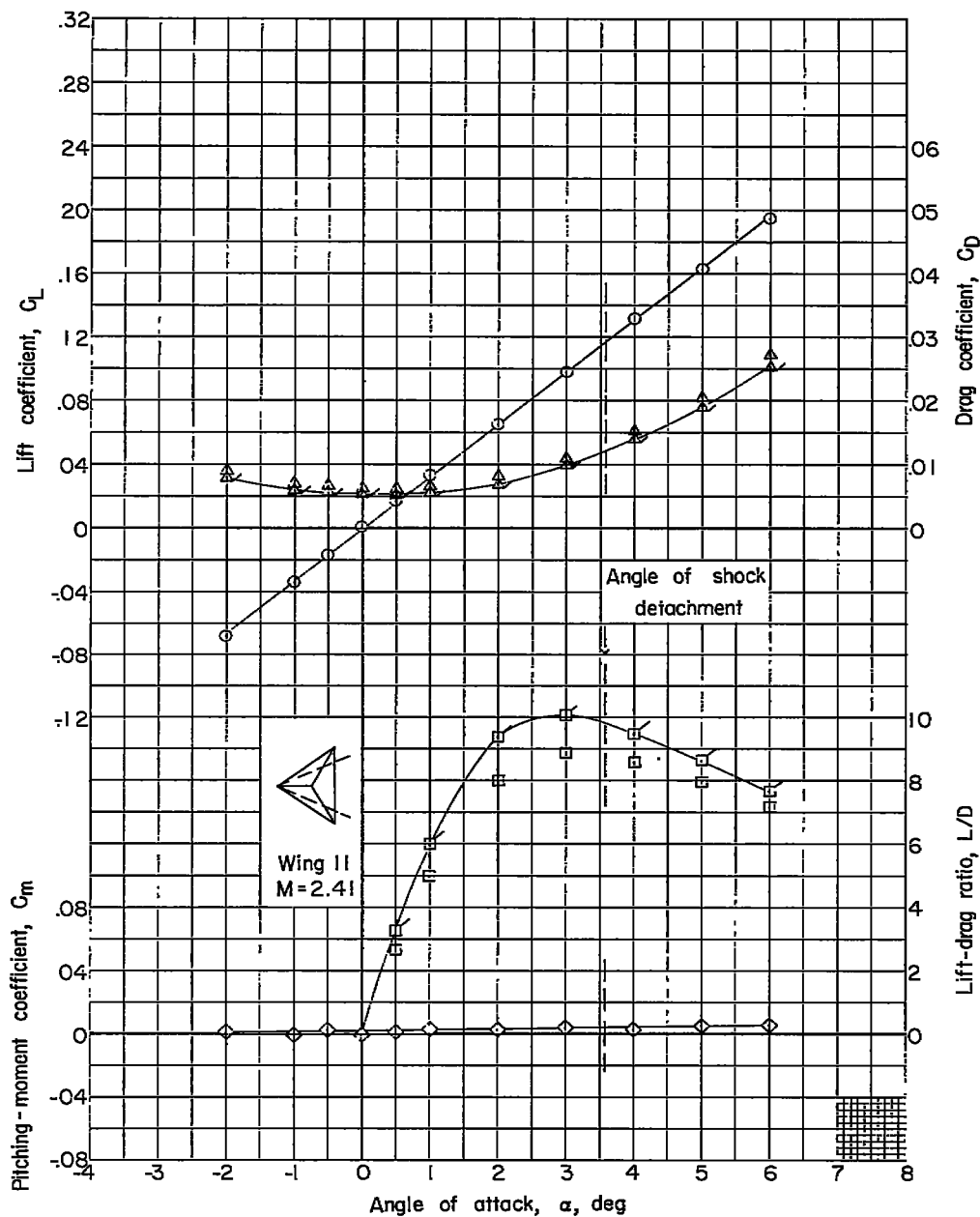
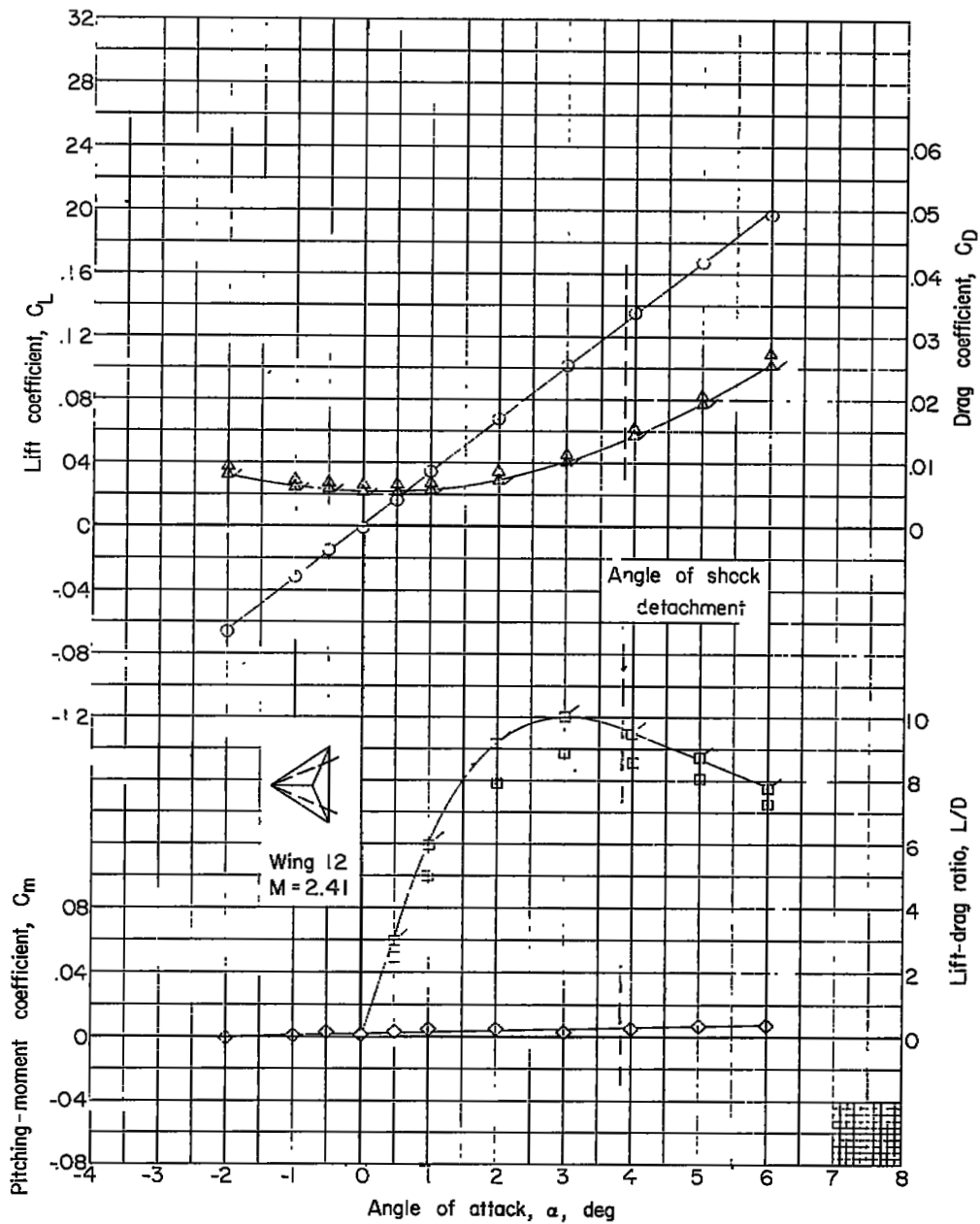
(d) $1 - r = 0.50c$.

Figure 14.- Continued.



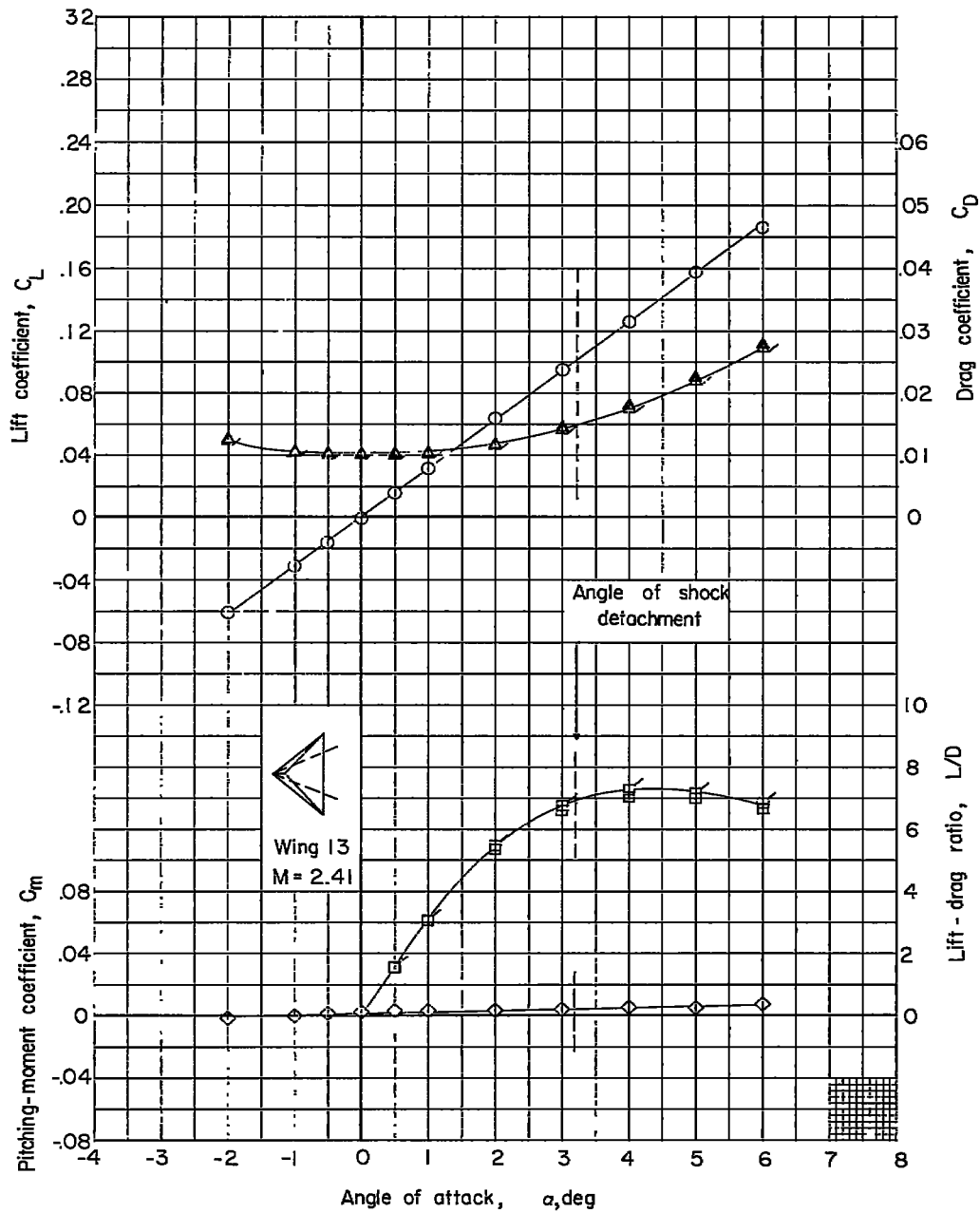
(e) $1 - r = 0.60c$.

Figure 14.- Continued.



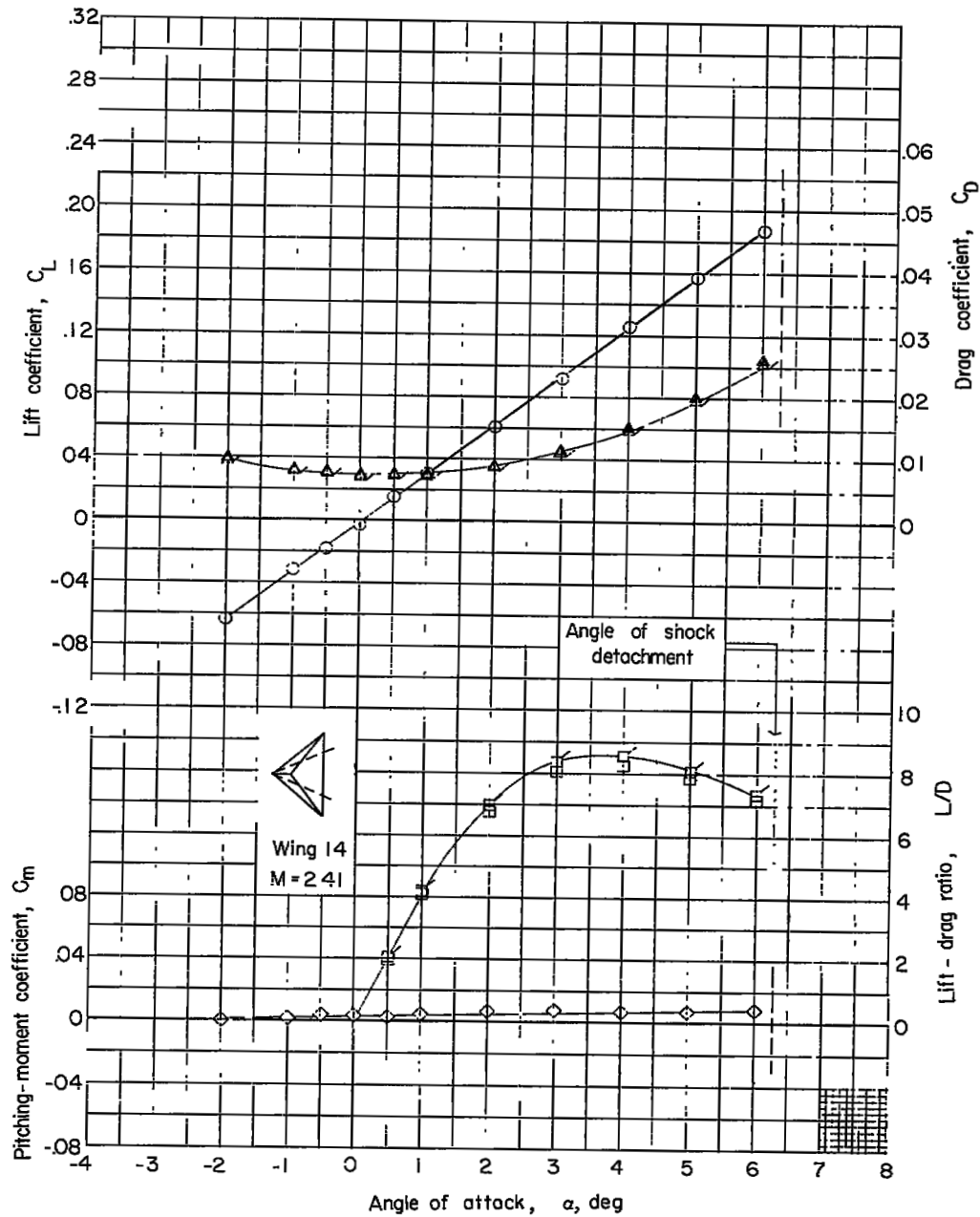
(f) $1 - r = 0.70c$.

Figure 14.- Concluded.



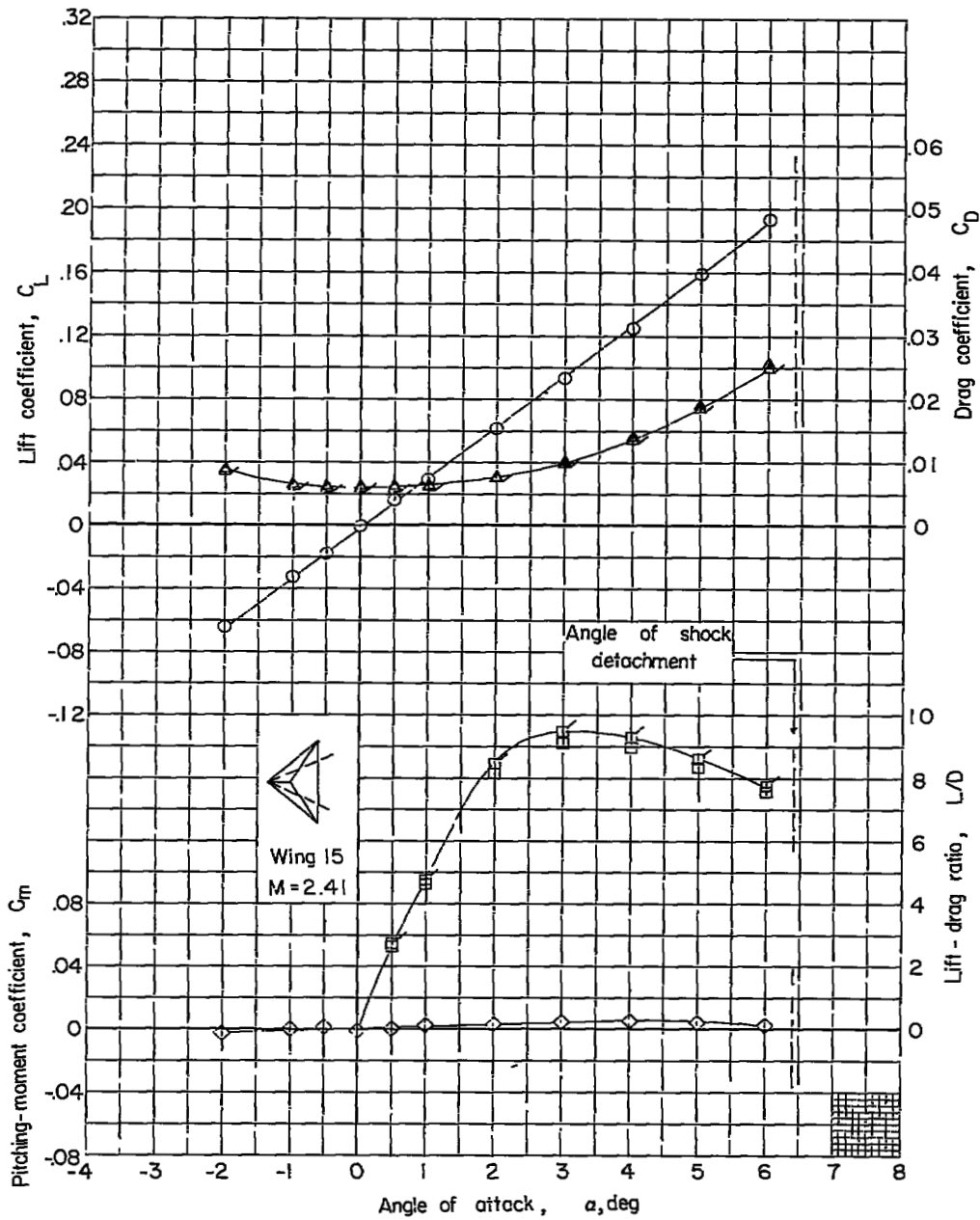
(a) $1 - r = 0.18c$.

Figure 15.- Aerodynamic characteristics of $\frac{3}{2}$ -percent-thick delta wings. $M = 2.41$; semiapex angle ϵ , 40° . Flagged symbols denote correction applied to drag data to account for support-sting tare-interference effects.



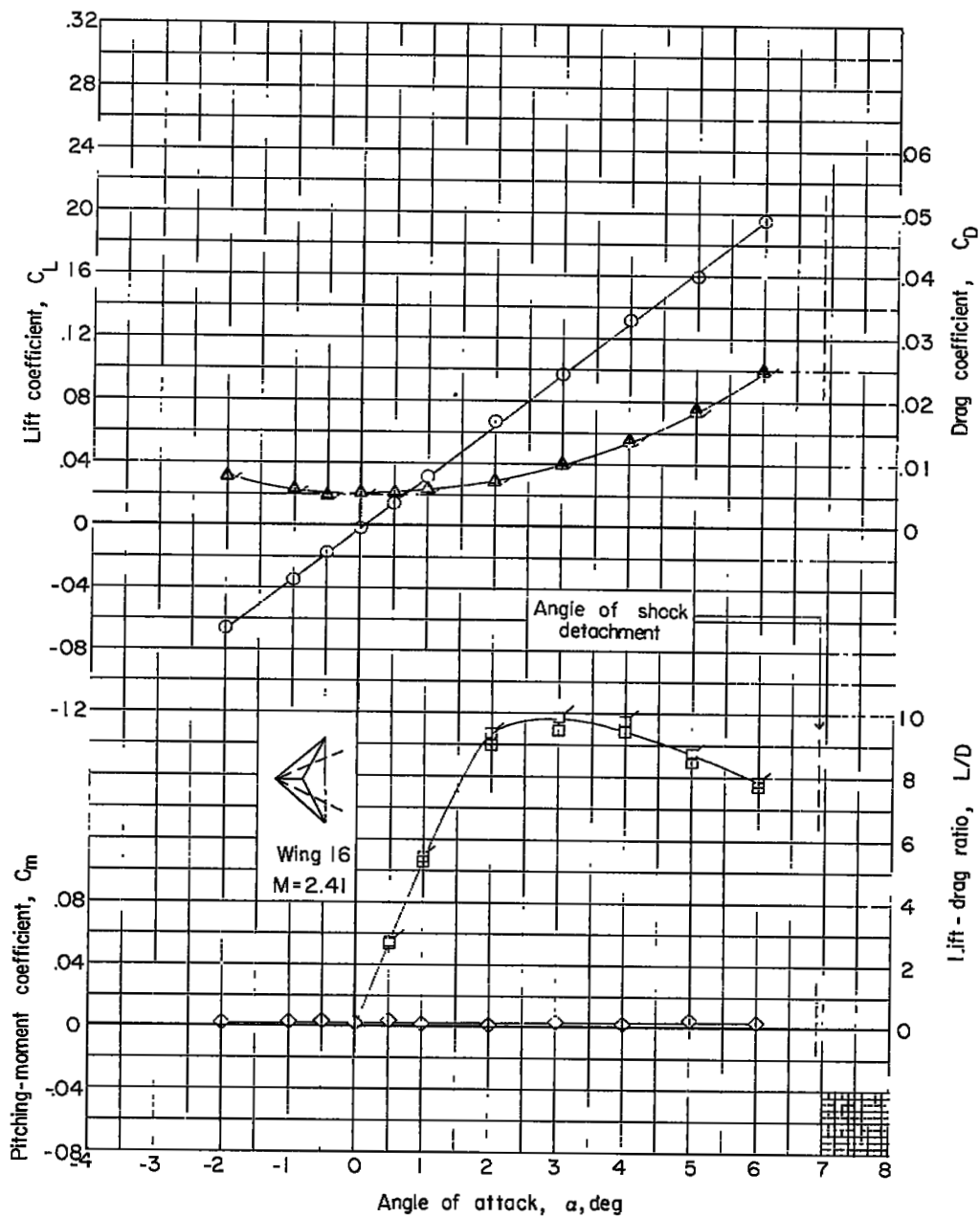
(b) $1 - r = 0.30c$.

Figure 15.- Continued.



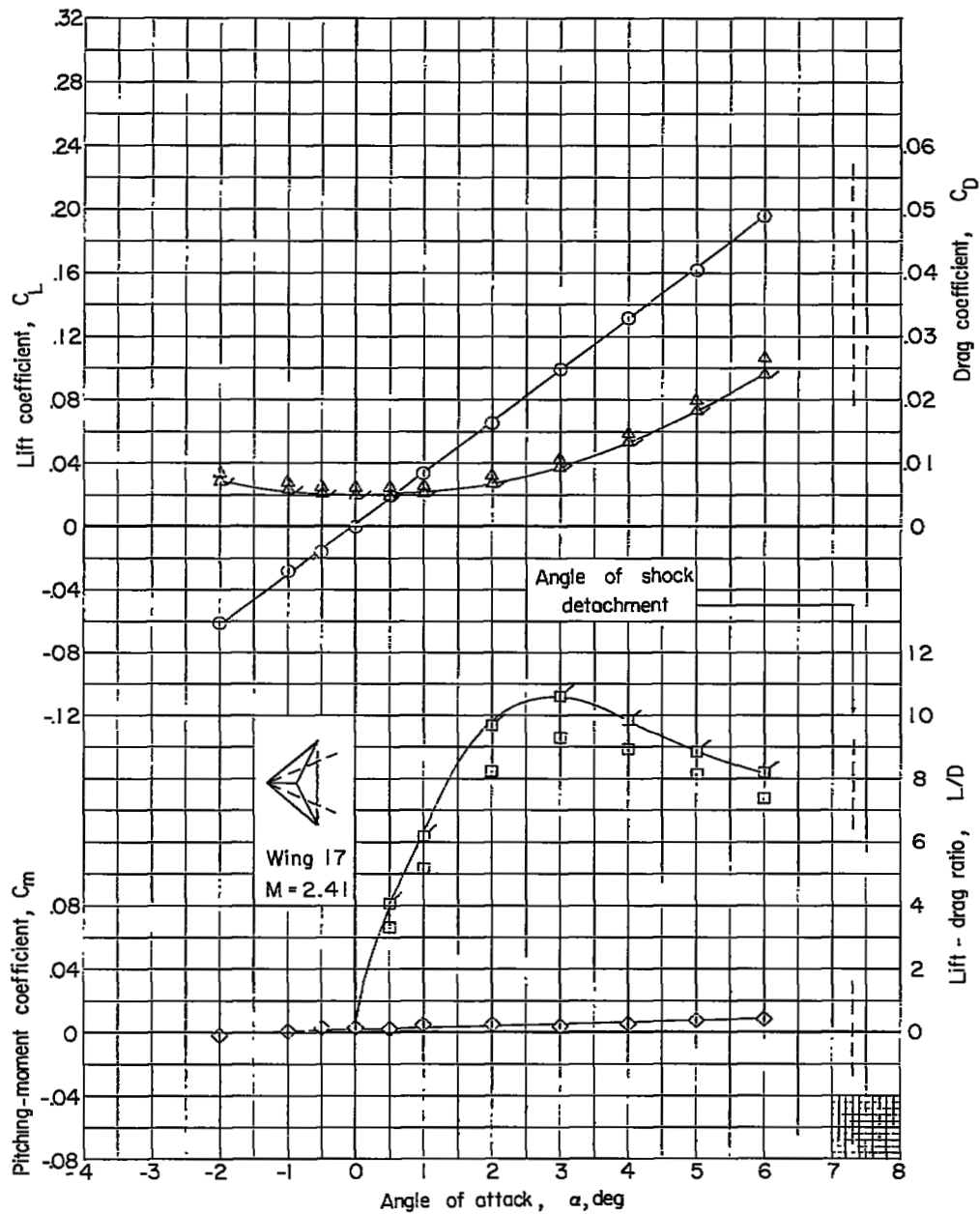
(c) $1 - r = 0.40c$.

Figure 15.- Continued.



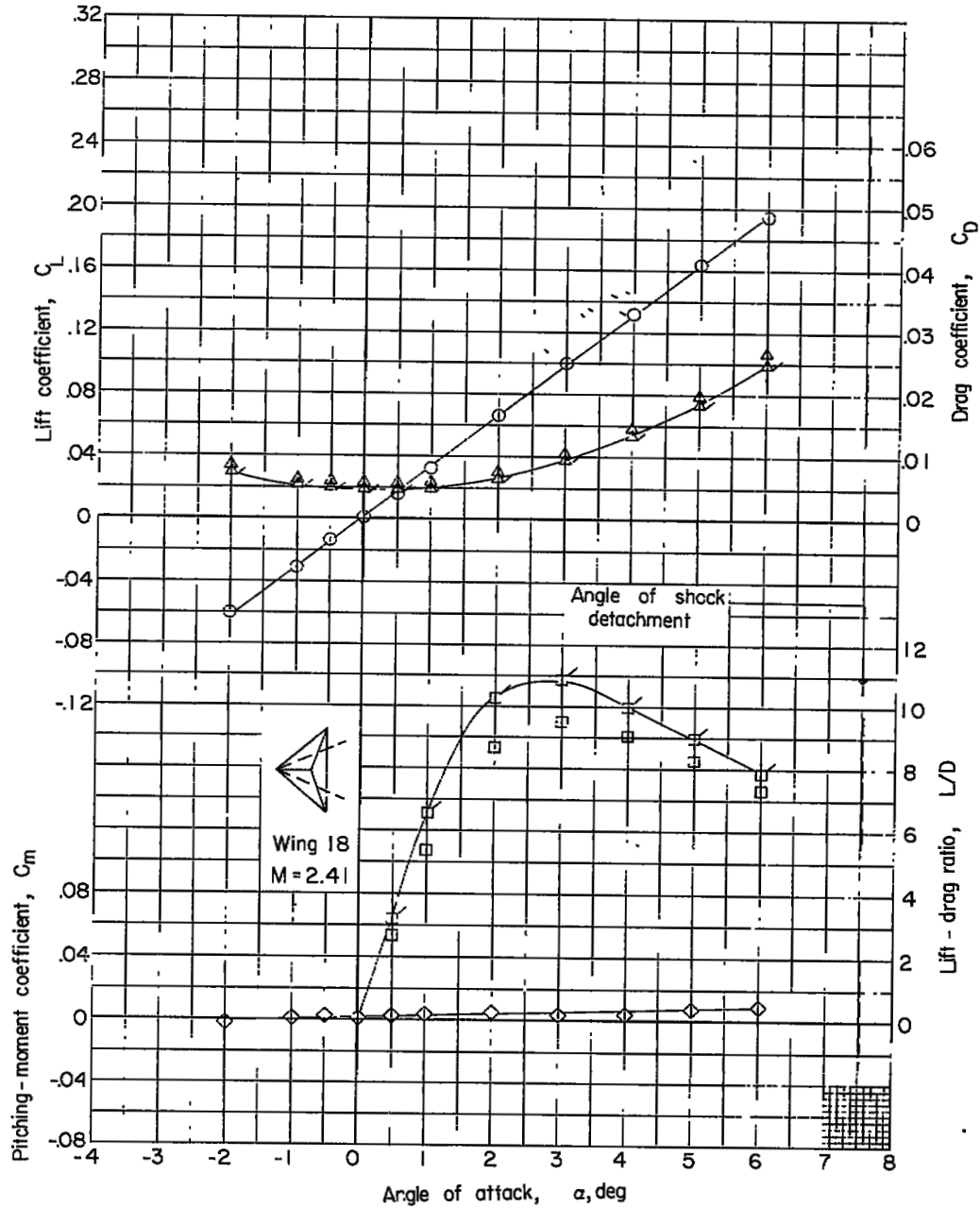
(d) $1 - r = 0.50c$.

Figure 15.- Continued.



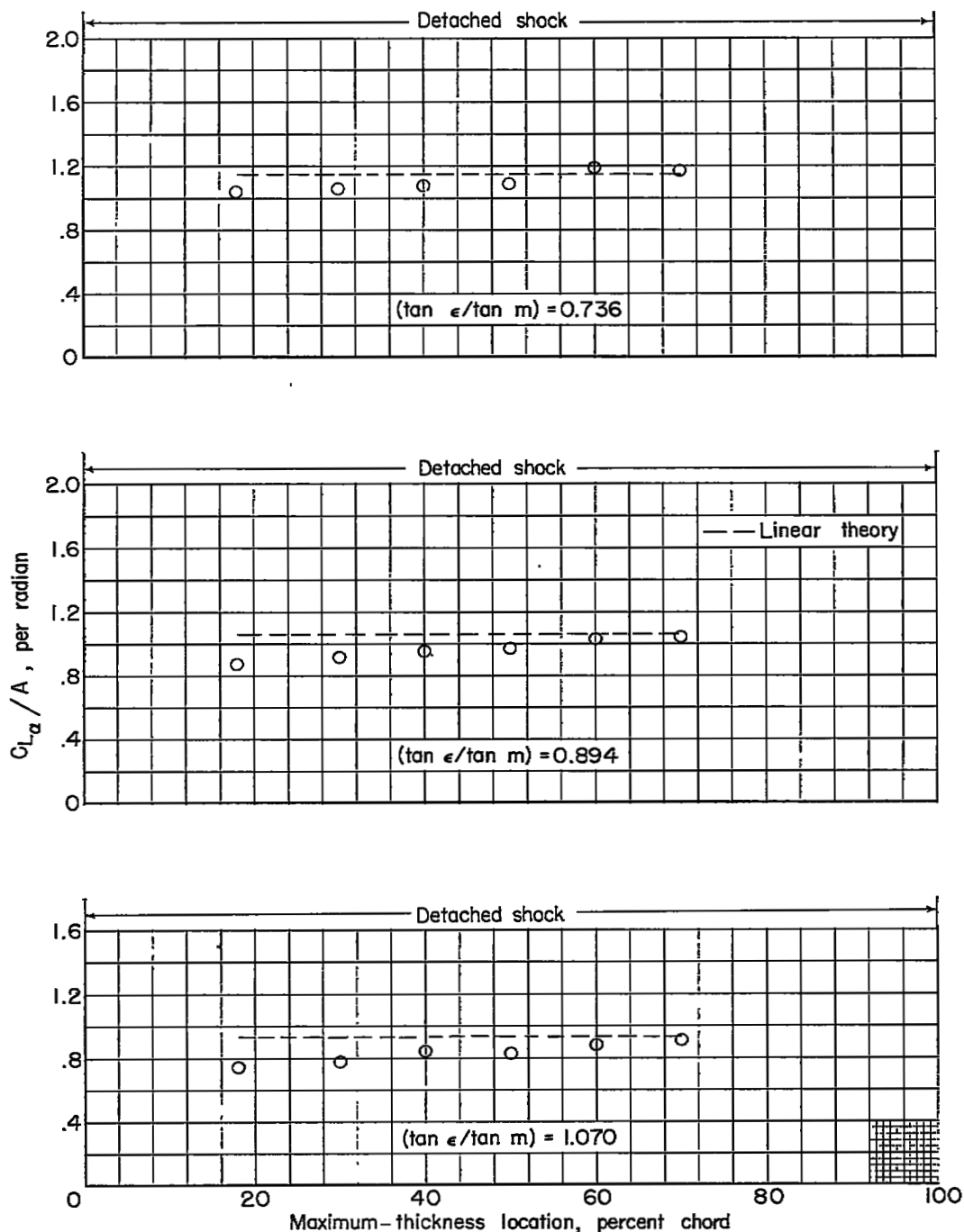
(e) $1 - r = 0.60c$.

Figure 15.- Continued.



(f) $1 - r = 0.70c$.

Figure 15.- Concluded.



(a) $M = 1.62$.

Figure 16.- Variation of the lift-curve slope with maximum-thickness location at several tangent-ratio ($\tan \epsilon / \tan m$) values, and comparison with theory.

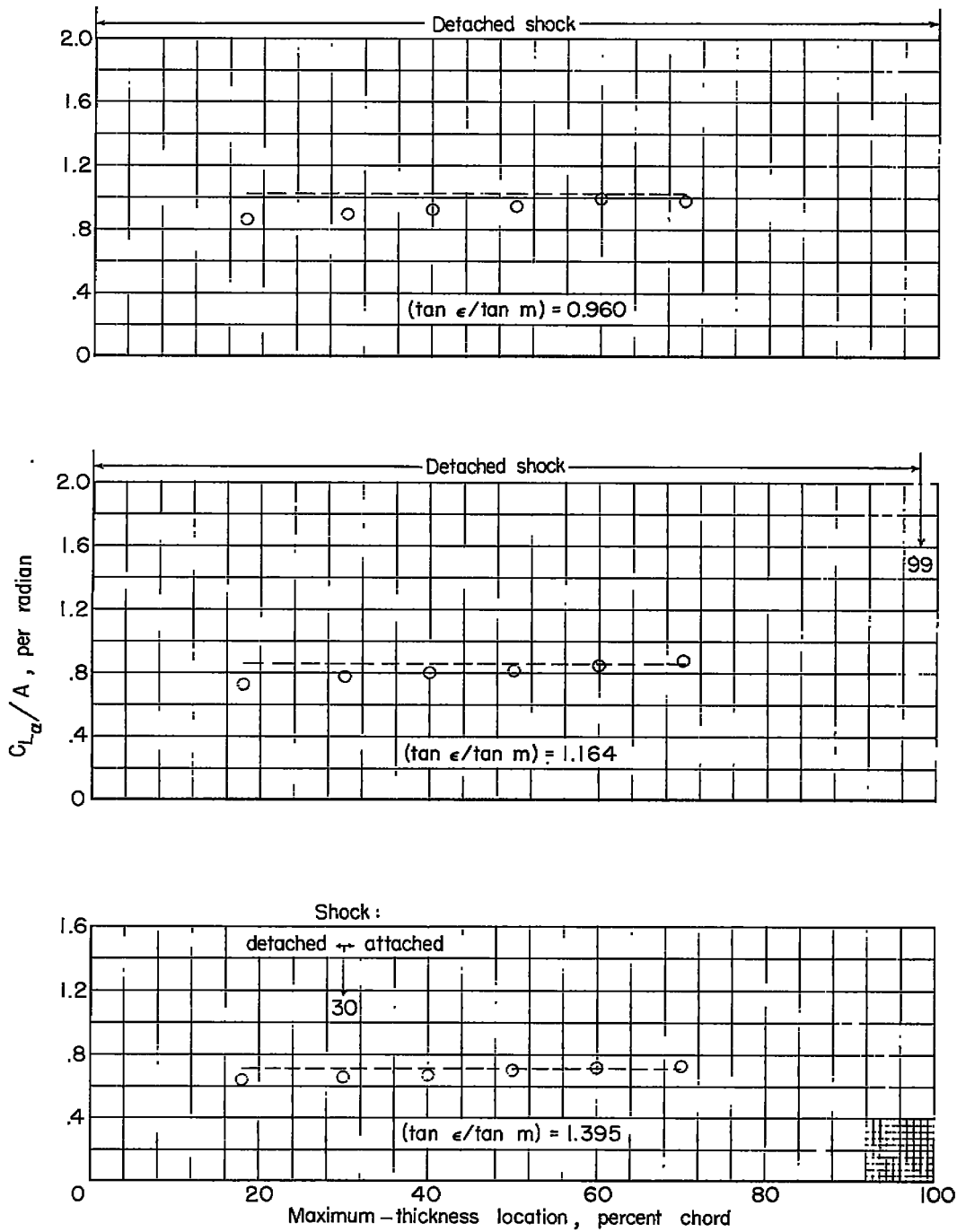
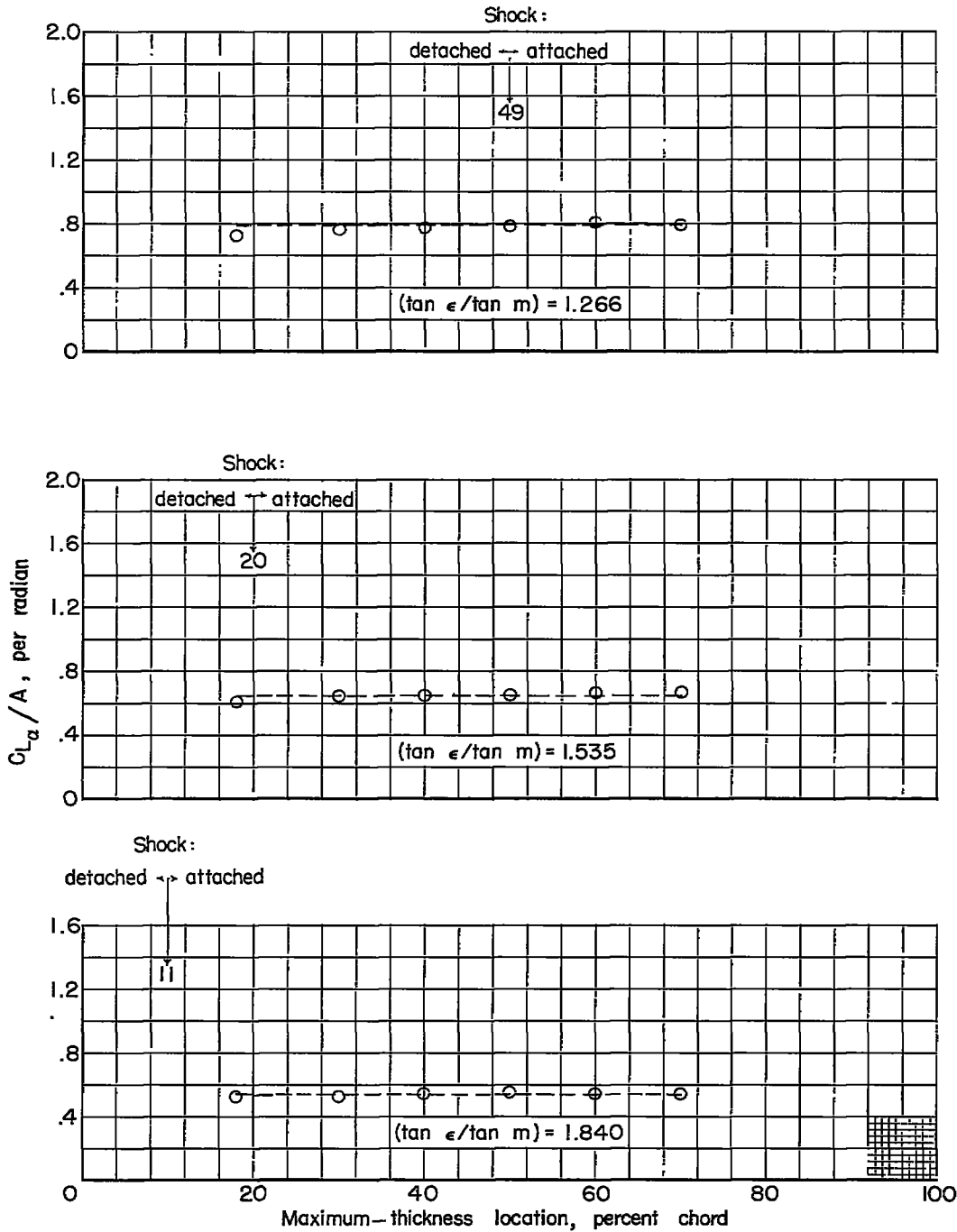
(b) $M = 1.94$.

Figure 16.- Continued.



(c) $M = 2.41$.

Figure 16.- Concluded.

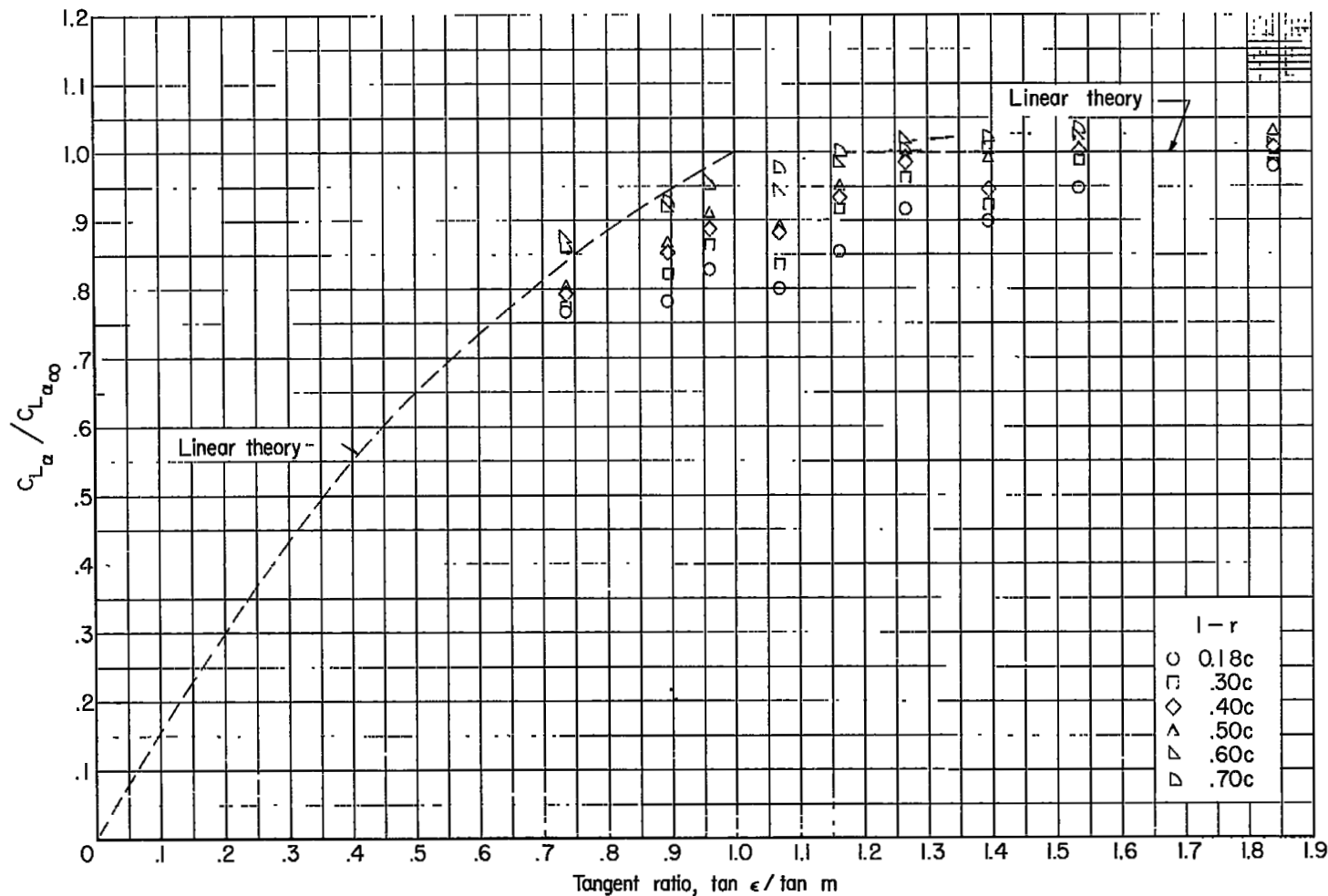
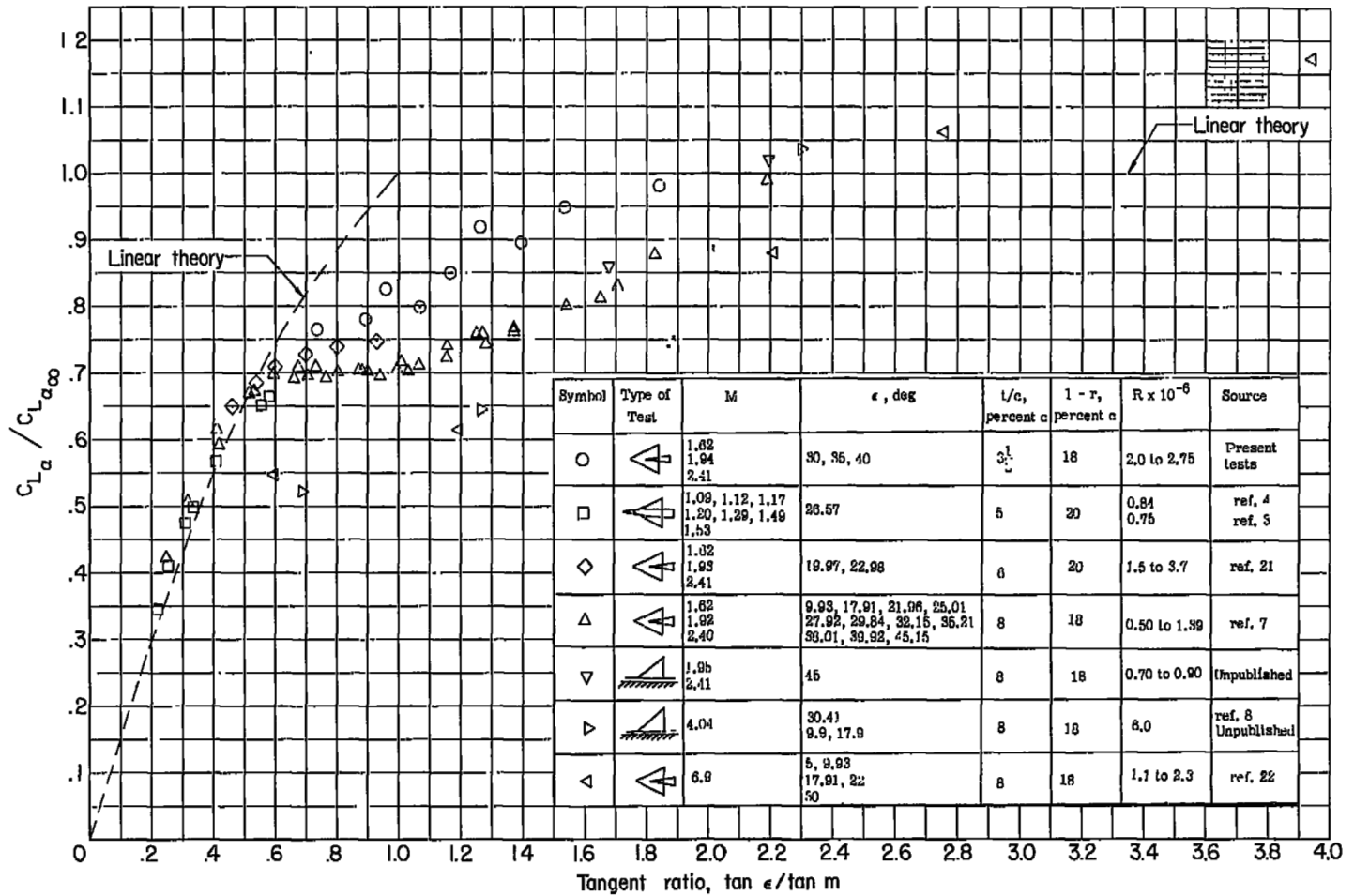
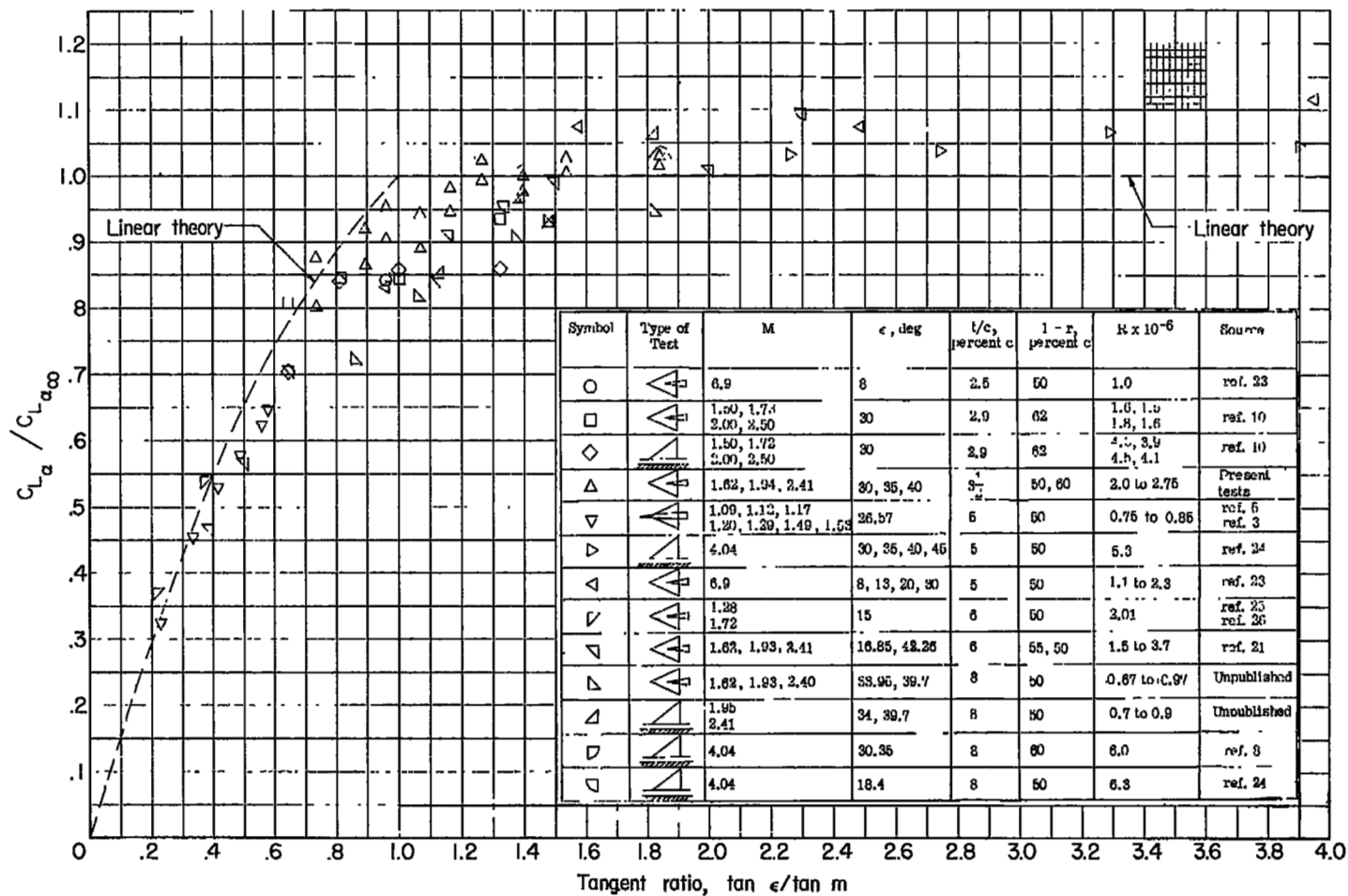


Figure 17.- Effect of chordwise maximum-thickness position on the ratio of the experimental lift-curve slope to the theoretical two-dimensional lift-curve slope against tangent ratio $\tan \epsilon / \tan m$.



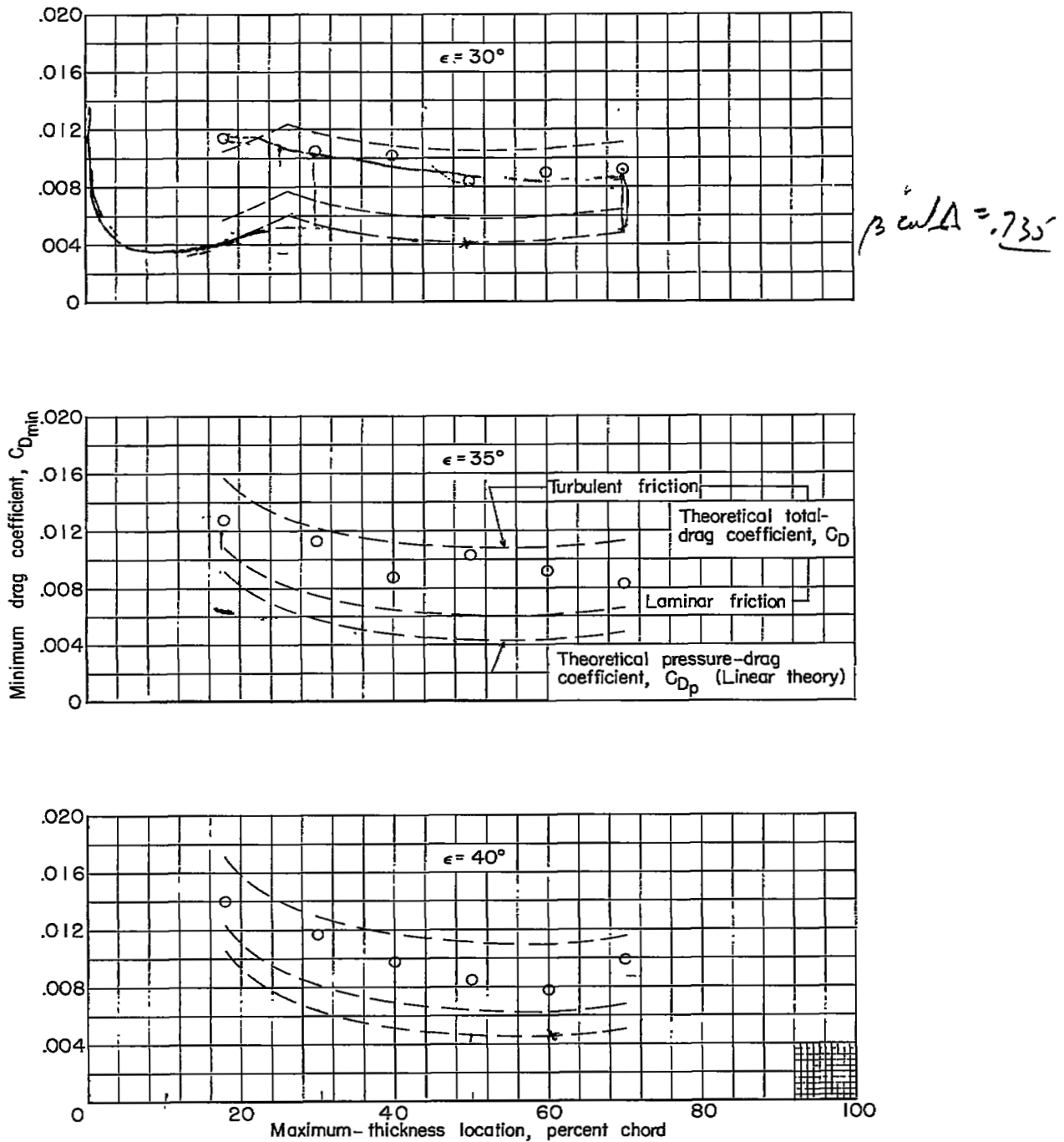
(a) $0.18c \leq 1 - r \leq 0.20c$.

Figure 18.- Variation of the lift-slope ratio with tangent ratio for double-wedge delta wings having their maximum-thickness positions well forward and near midchord.



(b) $0.50c \leq 1 - r \leq 0.62c$.

Figure 18.- Concluded.



(a) $M = 1.62$.

Figure 19.- Variation of the minimum drag coefficient with maximum-thickness location.

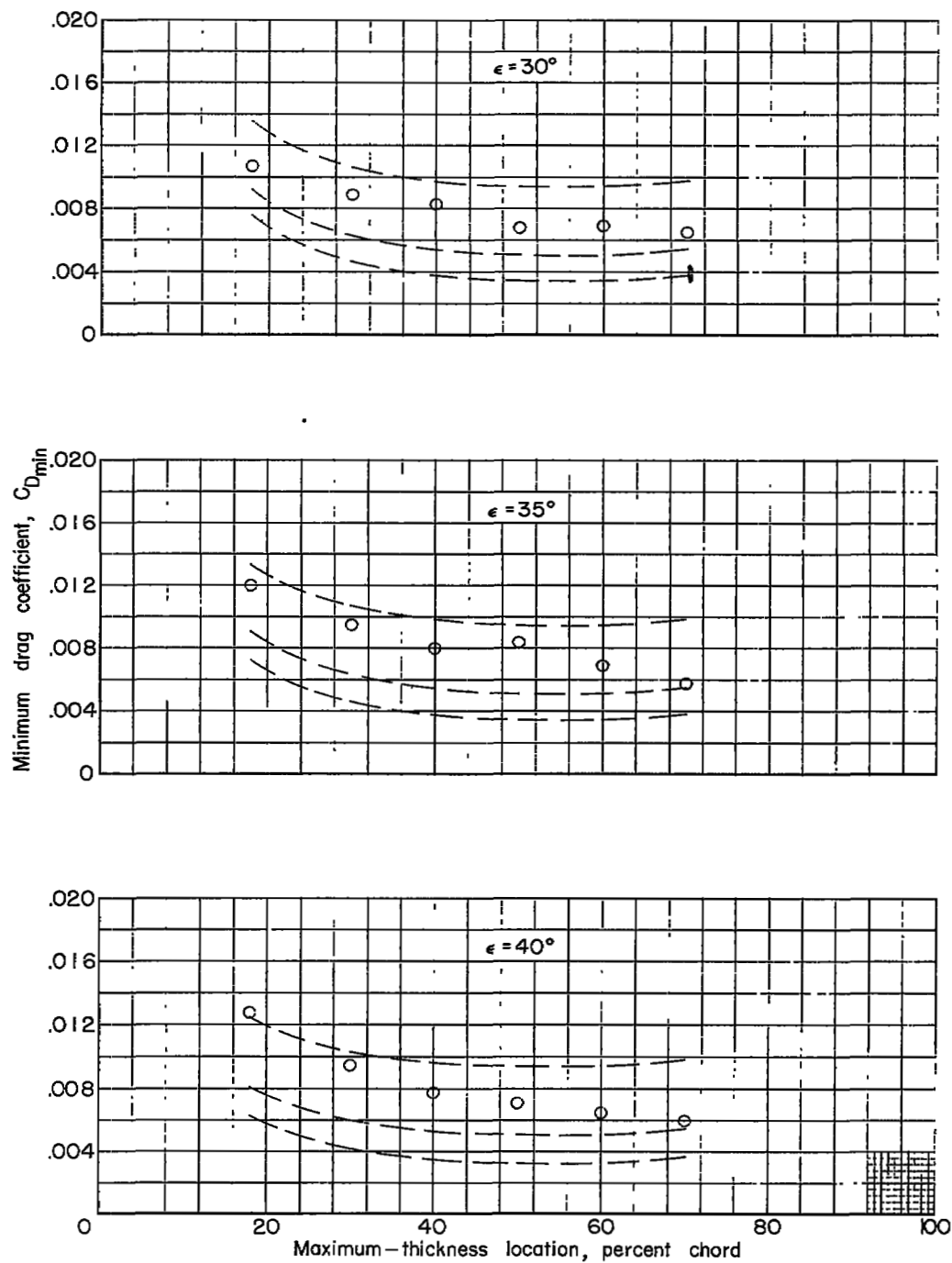
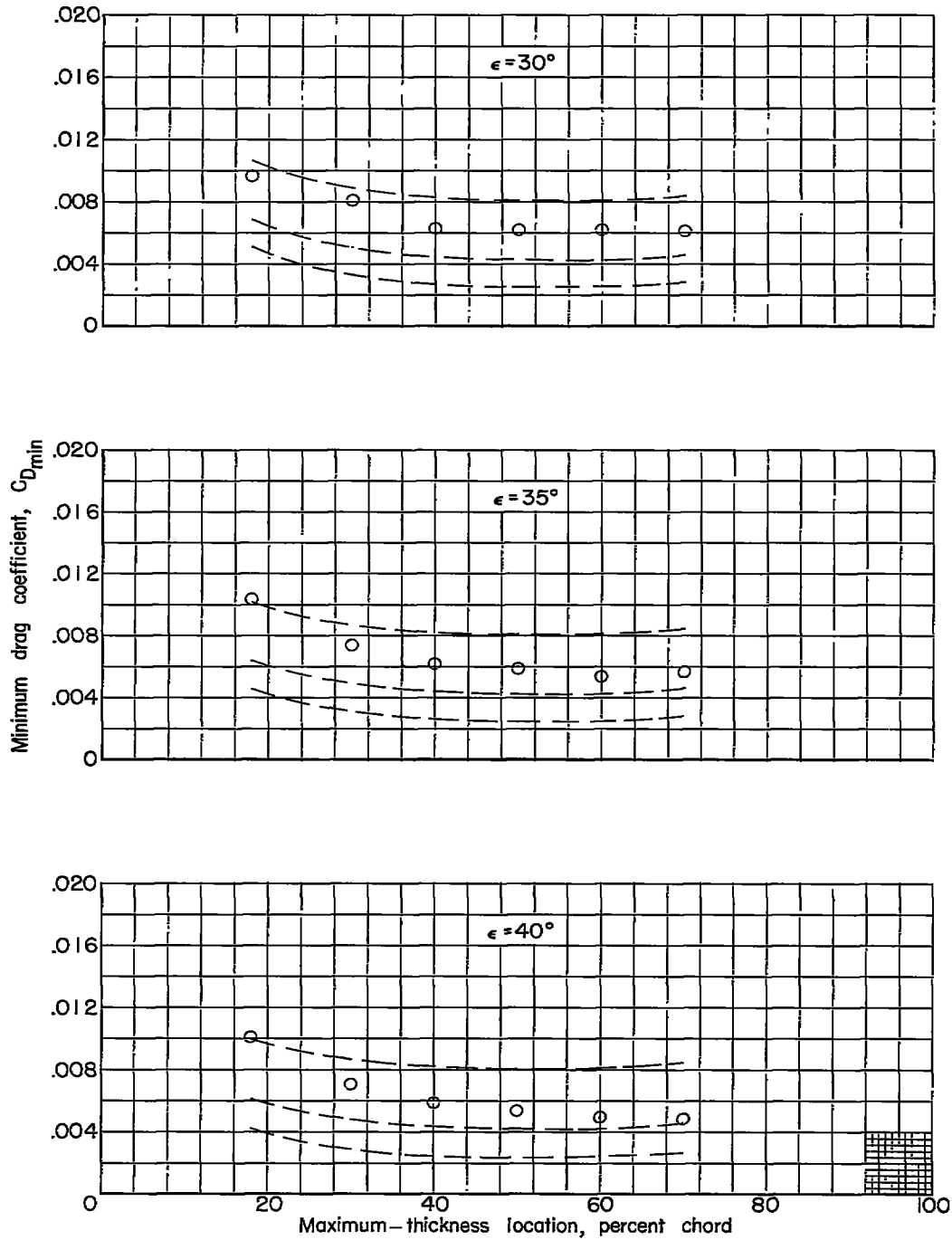
(b) $M = 1.94$.

Figure 19.- Continued.



(c) $M = 2.41$.

Figure 19.- Concluded.

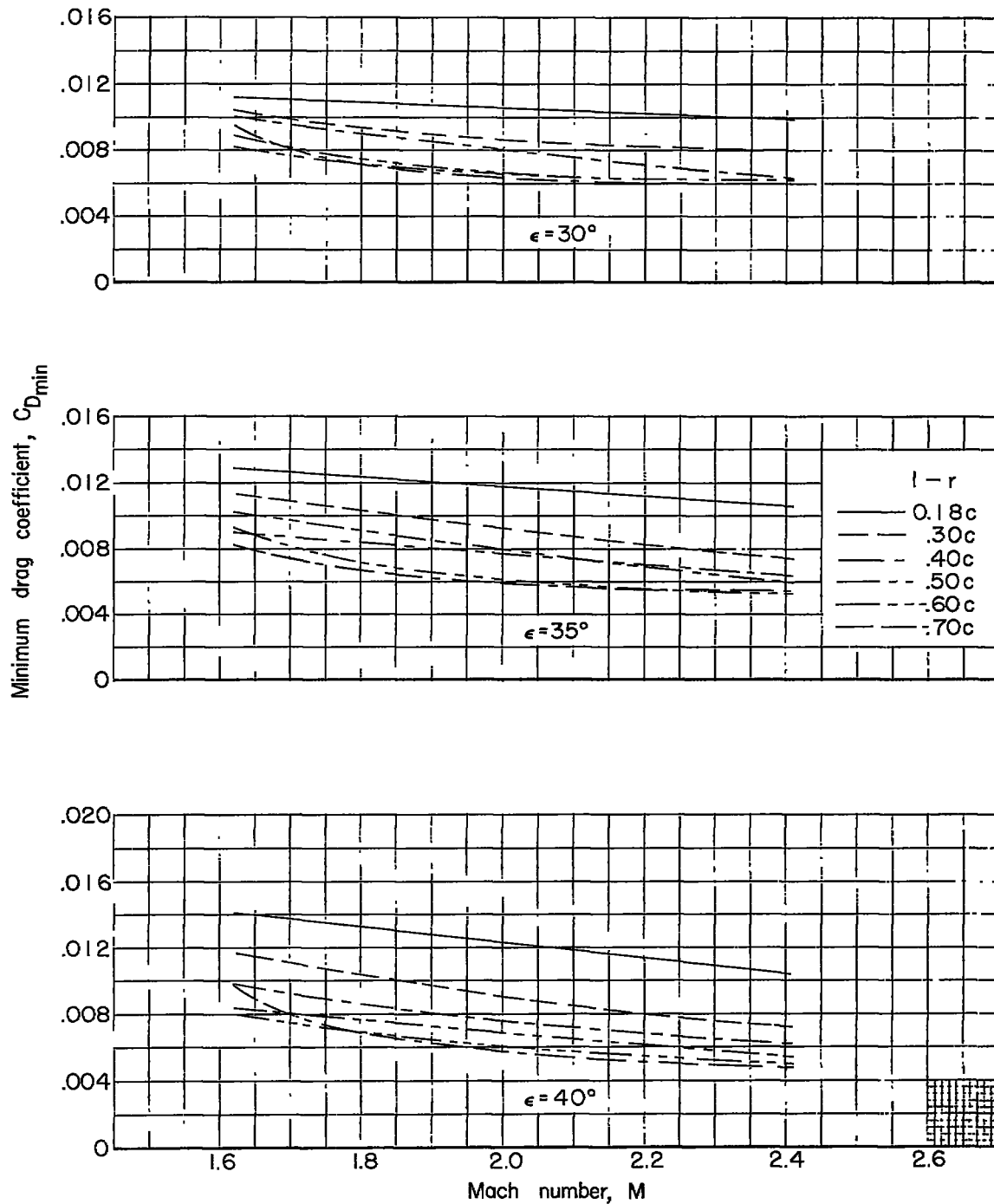


Figure 20.- Consolidated plot of minimum drag coefficients as a function of Mach number for all maximum-thickness positions and semiapex angles of the investigation.

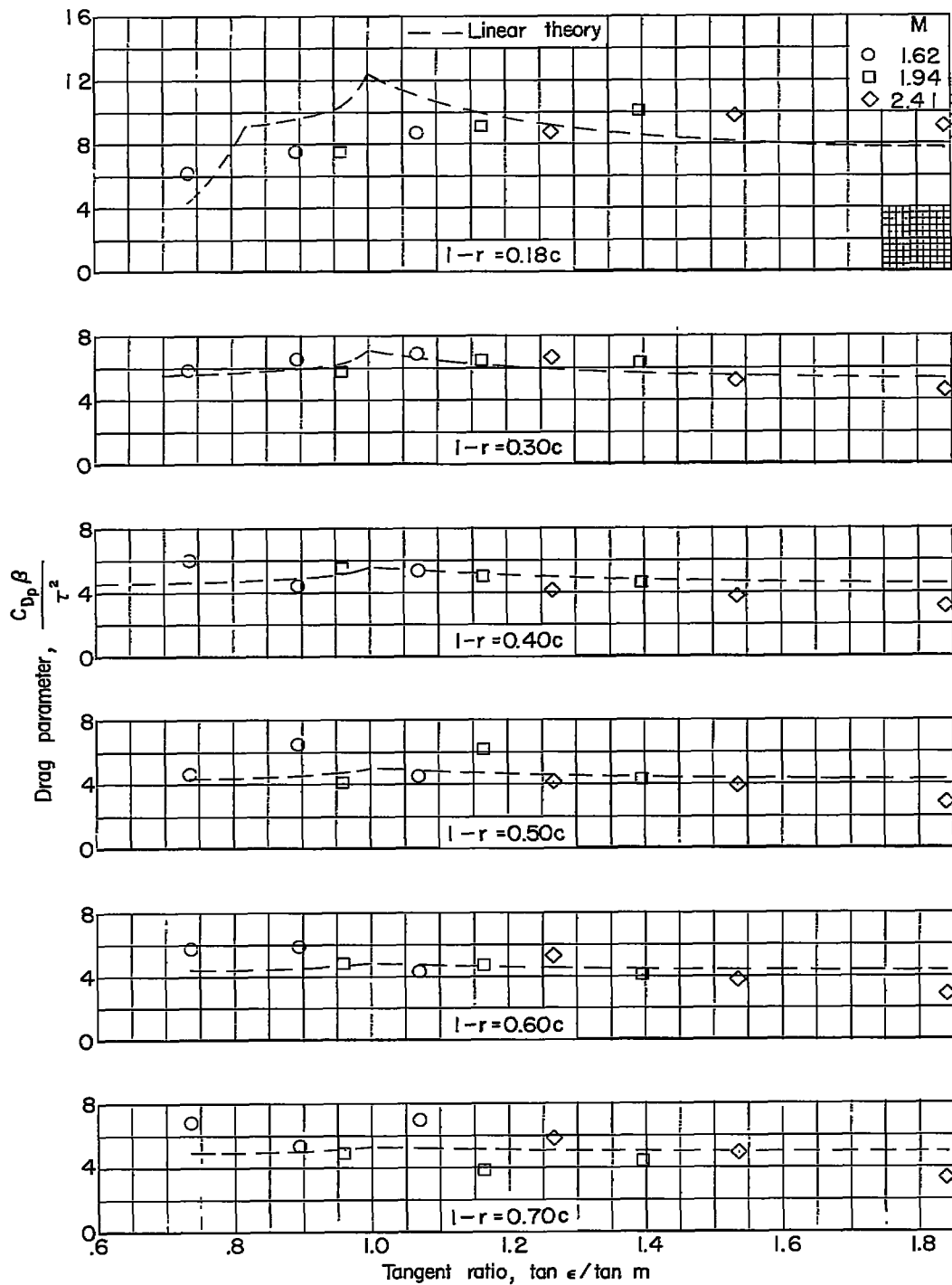
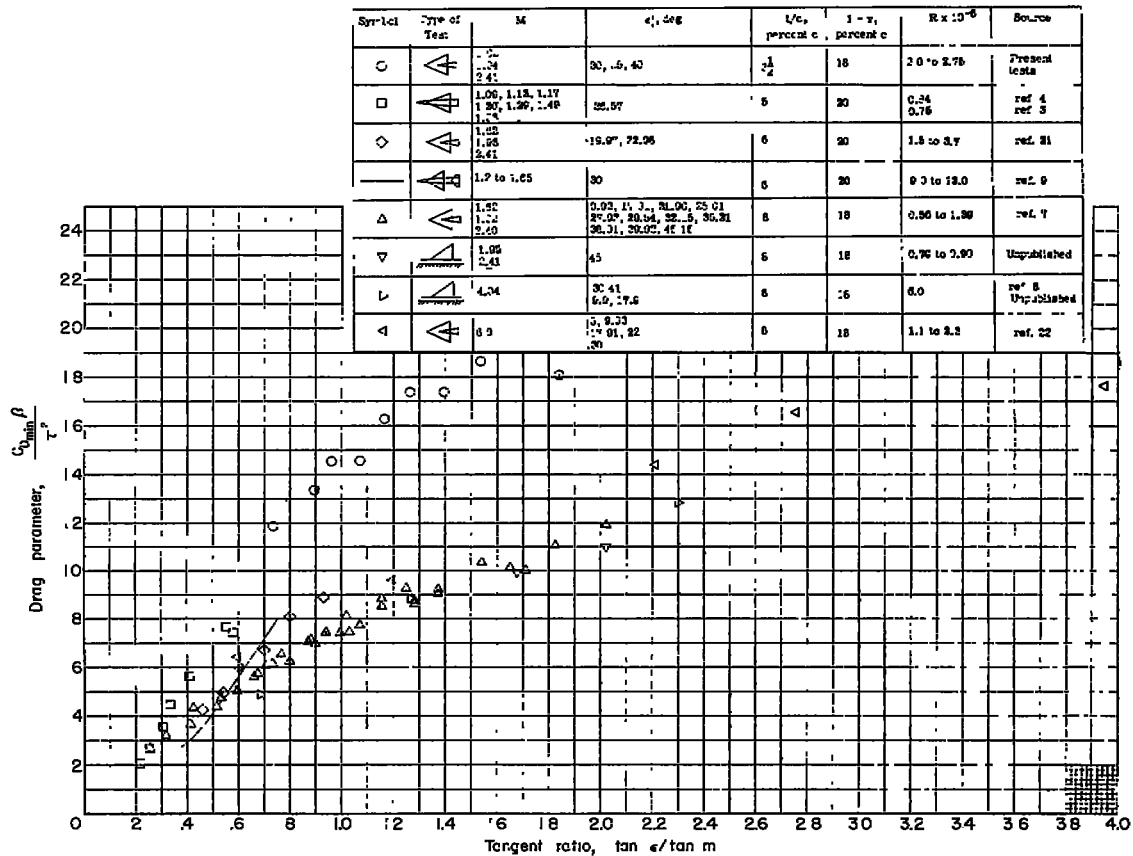
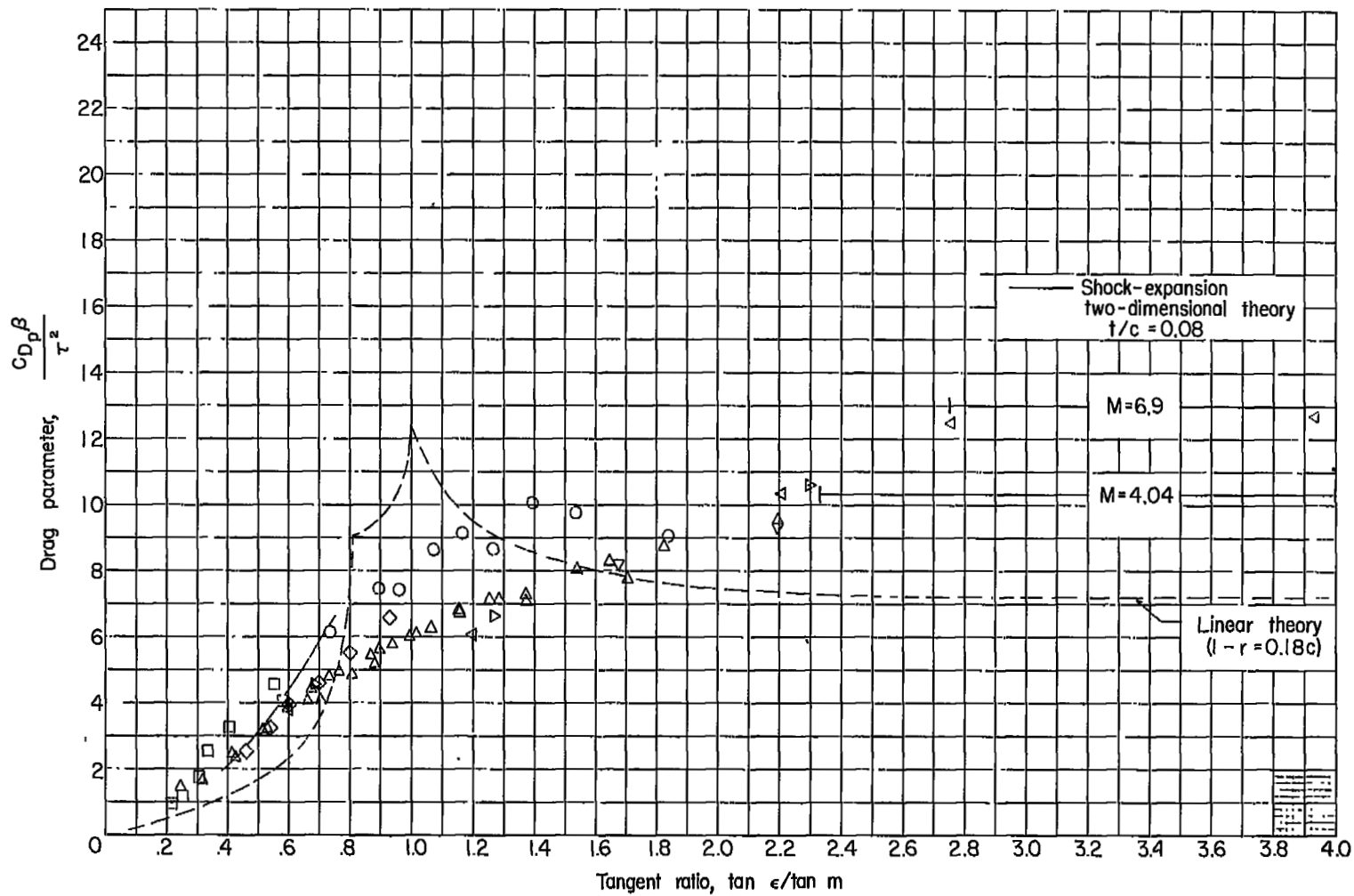


Figure 21.- Variation of the pressure-drag parameter with tangent ratio and comparison with theory.



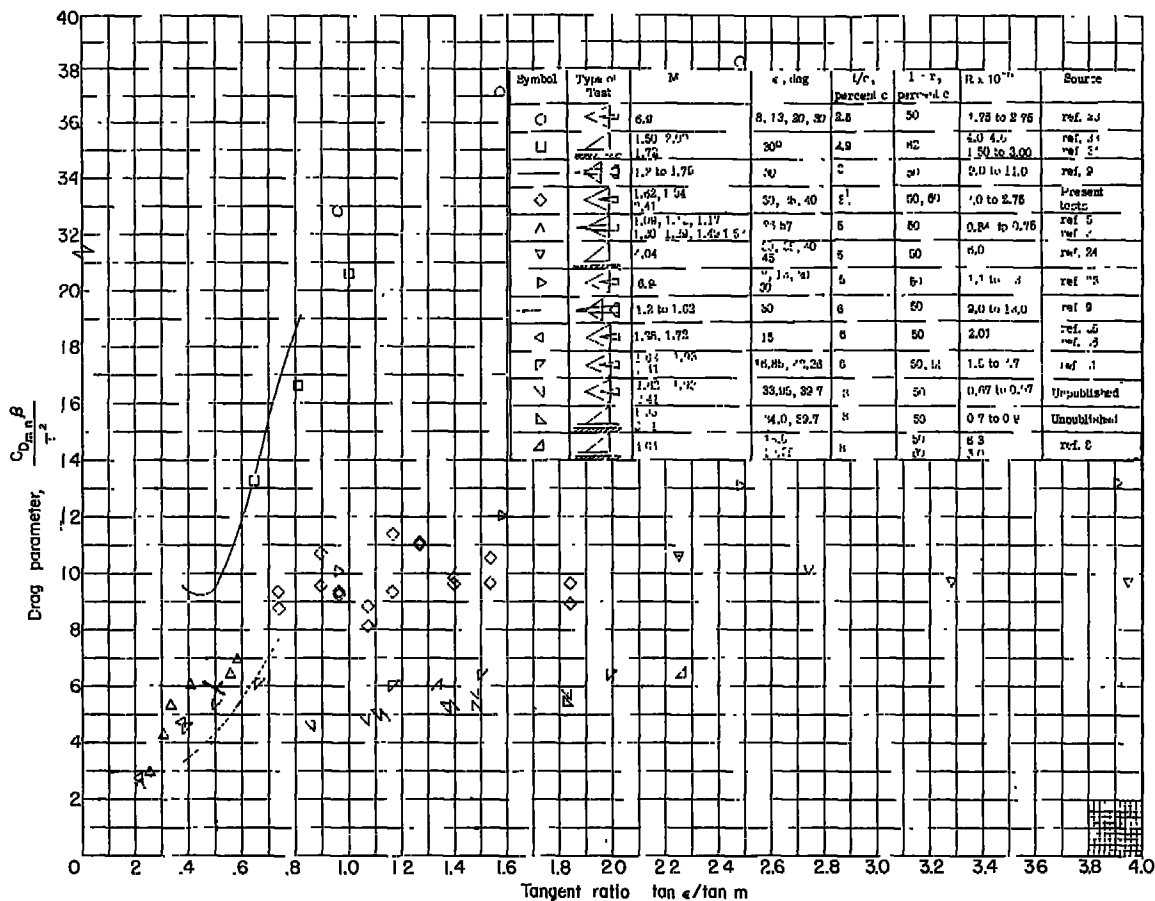
(a) $C_{D_{\min}}\beta/\tau^2$ against $\tan \epsilon/\tan m$.

Figure 22.- Variation of the drag parameters $C_{D_{\min}}\beta/\tau^2$ and $C_{D_p}\beta/\tau^2$ with $\tan \epsilon/\tan m$ for double-wedge delta wings of various thickness ratios. $0.18c \leq 1-r \leq 0.20c$.



(b) $C_{D_p} \beta / \tau^2$ against $\tan \epsilon / \tan m$.

Figure 22.- Concluded.



(a) $C_{D_{\min}} \beta / \tau^2$ against $\tan \epsilon / \tan m$.

Figure 23.- Variation of the drag parameters $C_{D_{\min}} \beta / \tau^2$ and $C_{D_p} \beta / \tau^2$ with $\tan \epsilon / \tan m$ for double-wedge delta wings of various thickness ratios. $0.50c \leq 1 - r \leq 0.62c$.

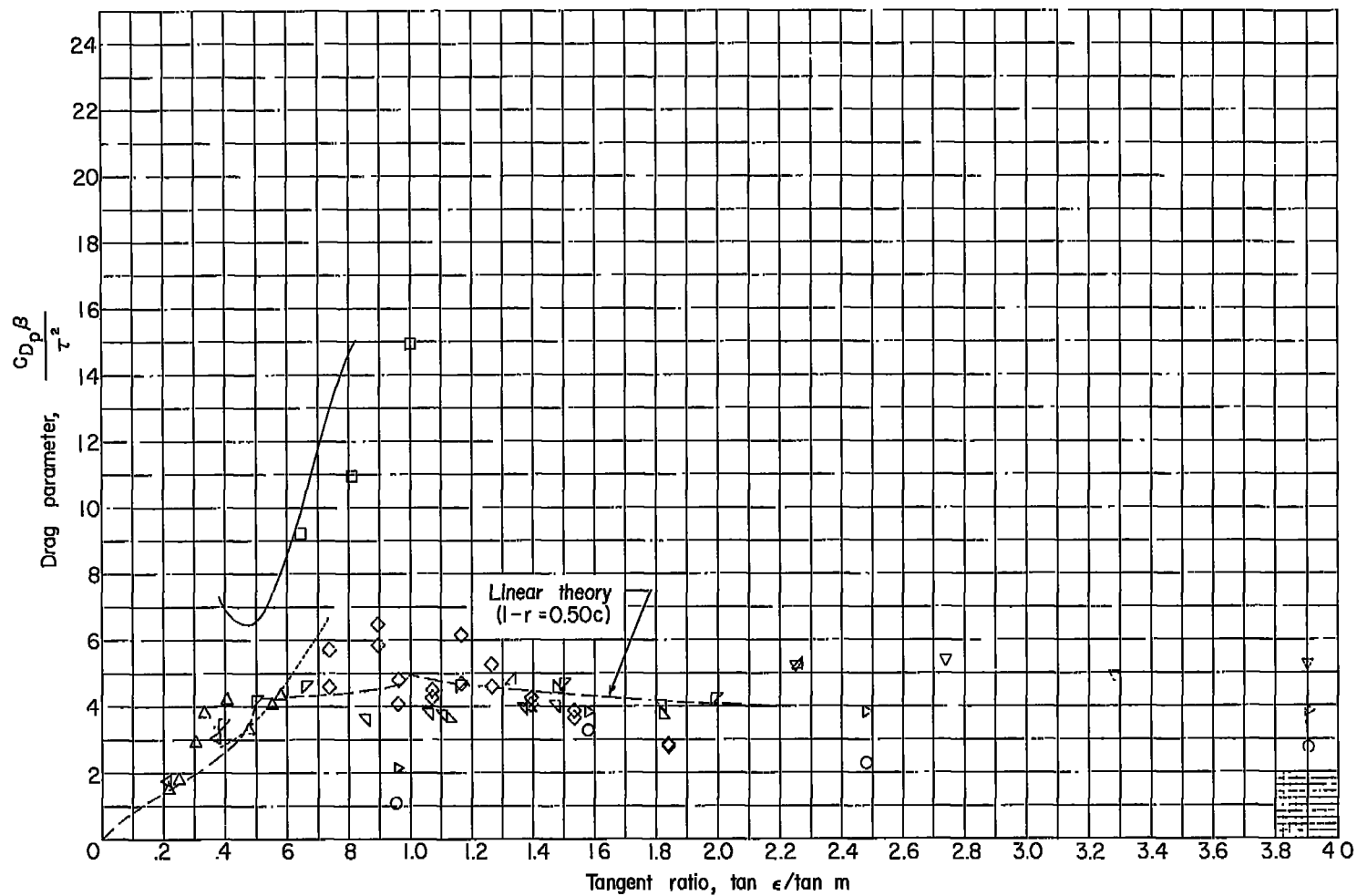
(b) $C_{D_p} \beta / \tau^2$ against $\tan \epsilon / \tan m$.

Figure 23.- Concluded.

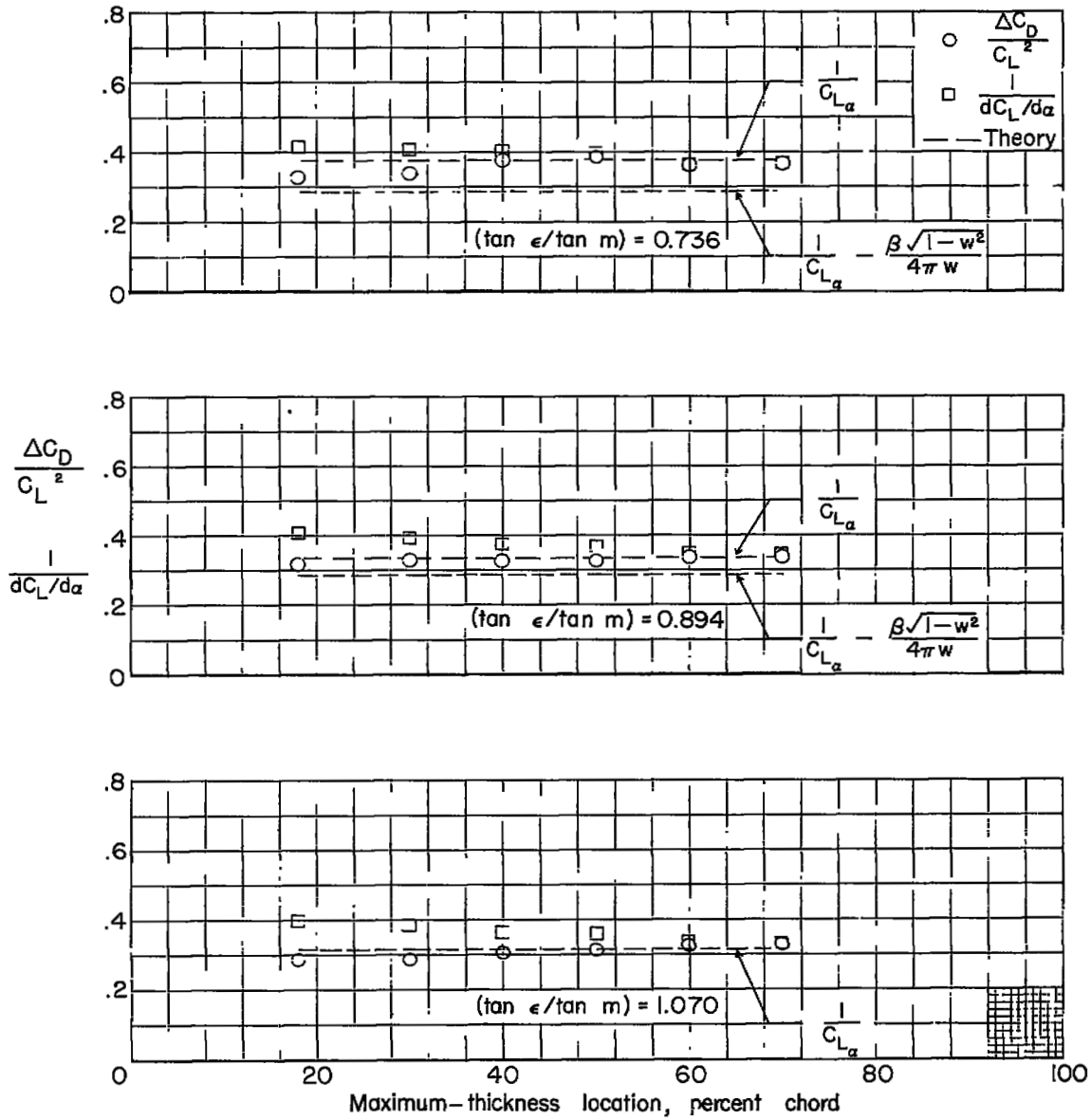
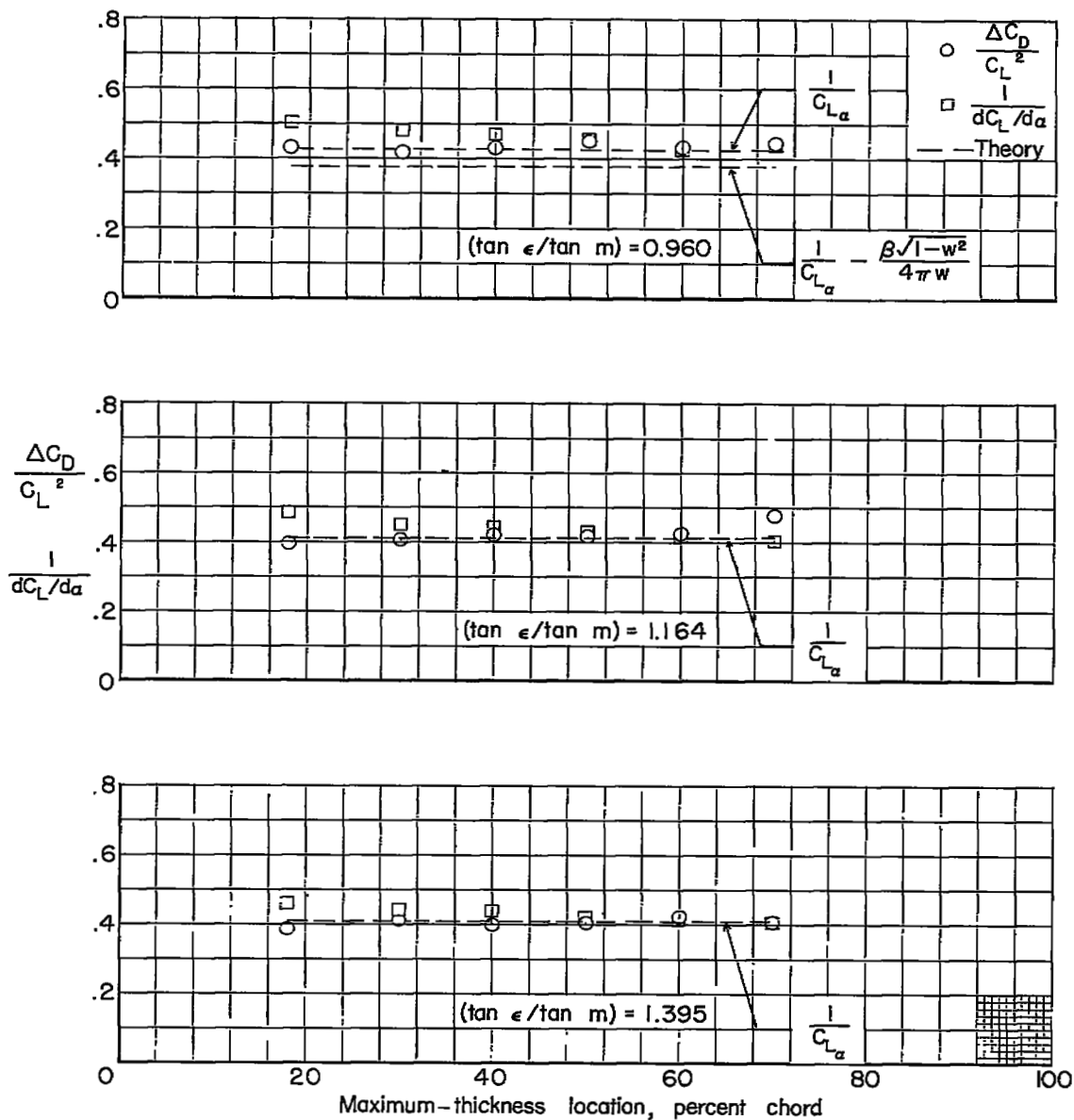
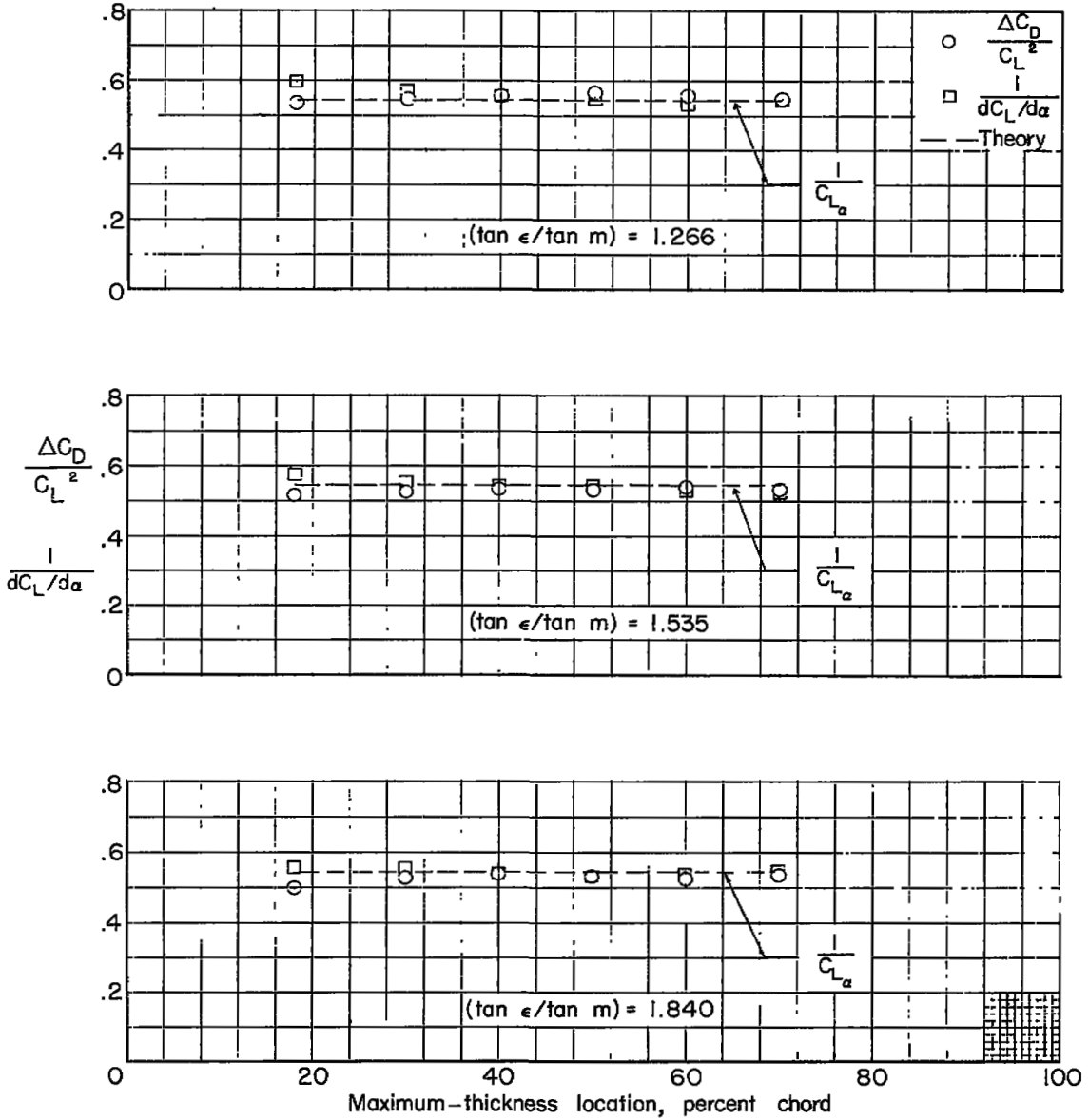
(a) $M = 1.62$.

Figure 24.- Variation of the drag-due-to-lift factor $\Delta C_D/C_L^2$ with maximum-thickness location and comparison with theory.



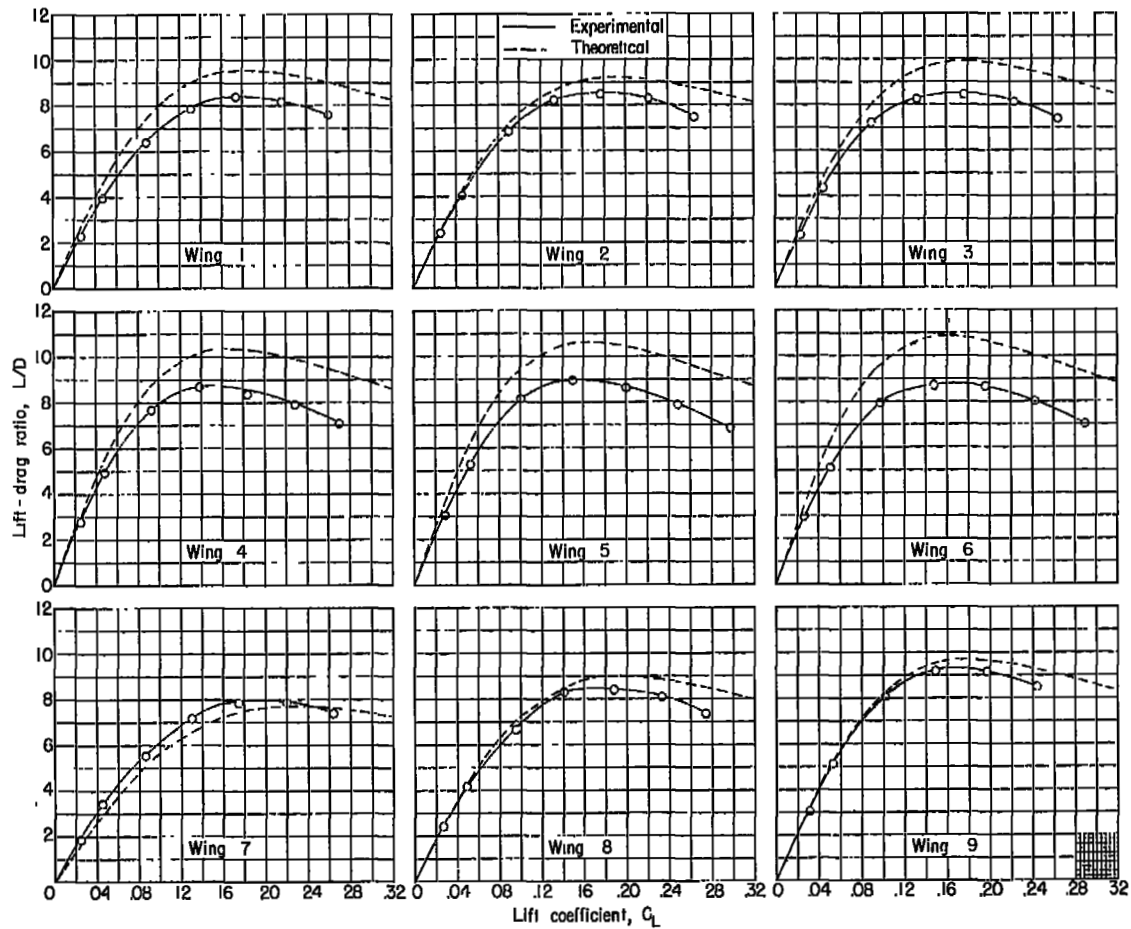
(b) $M = 1.94$.

Figure 24.- Continued.



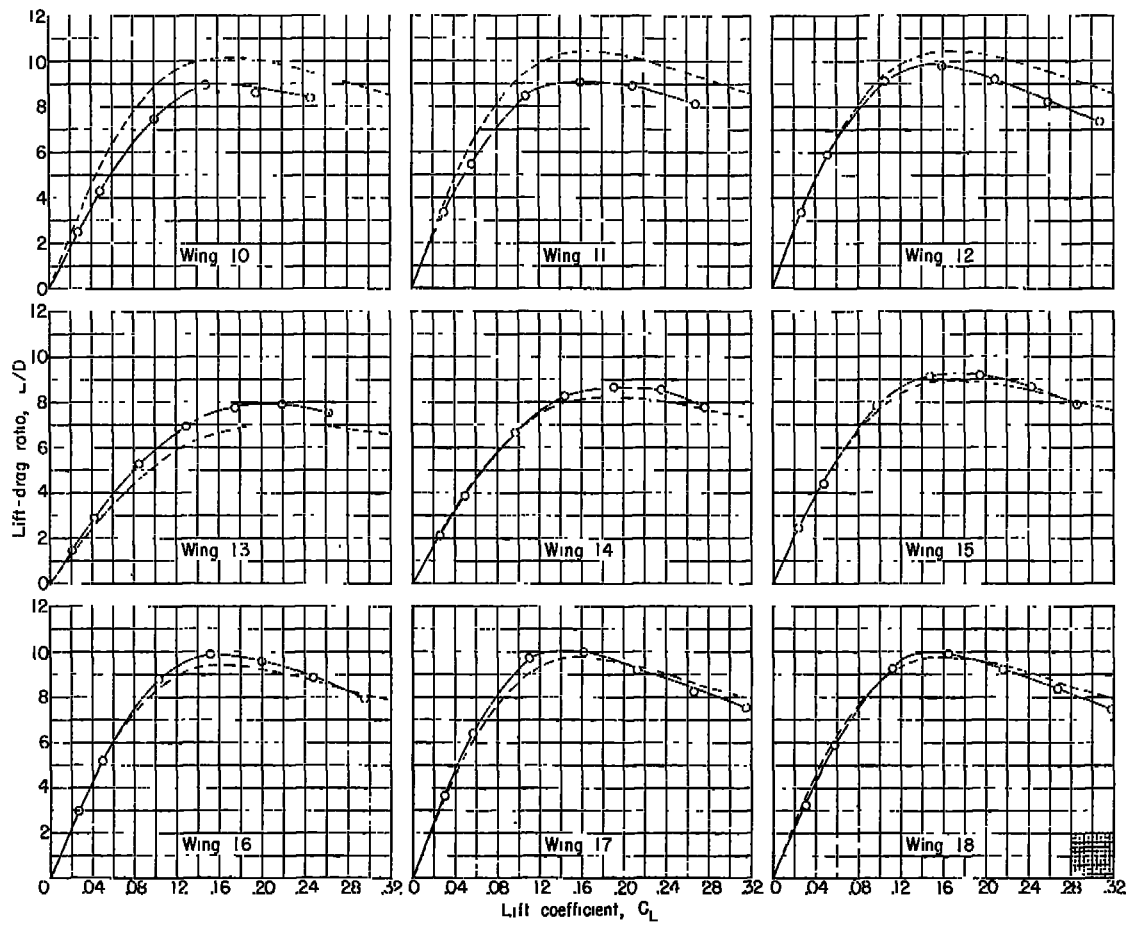
(c) $M = 2.41$.

Figure 24.- Concluded.



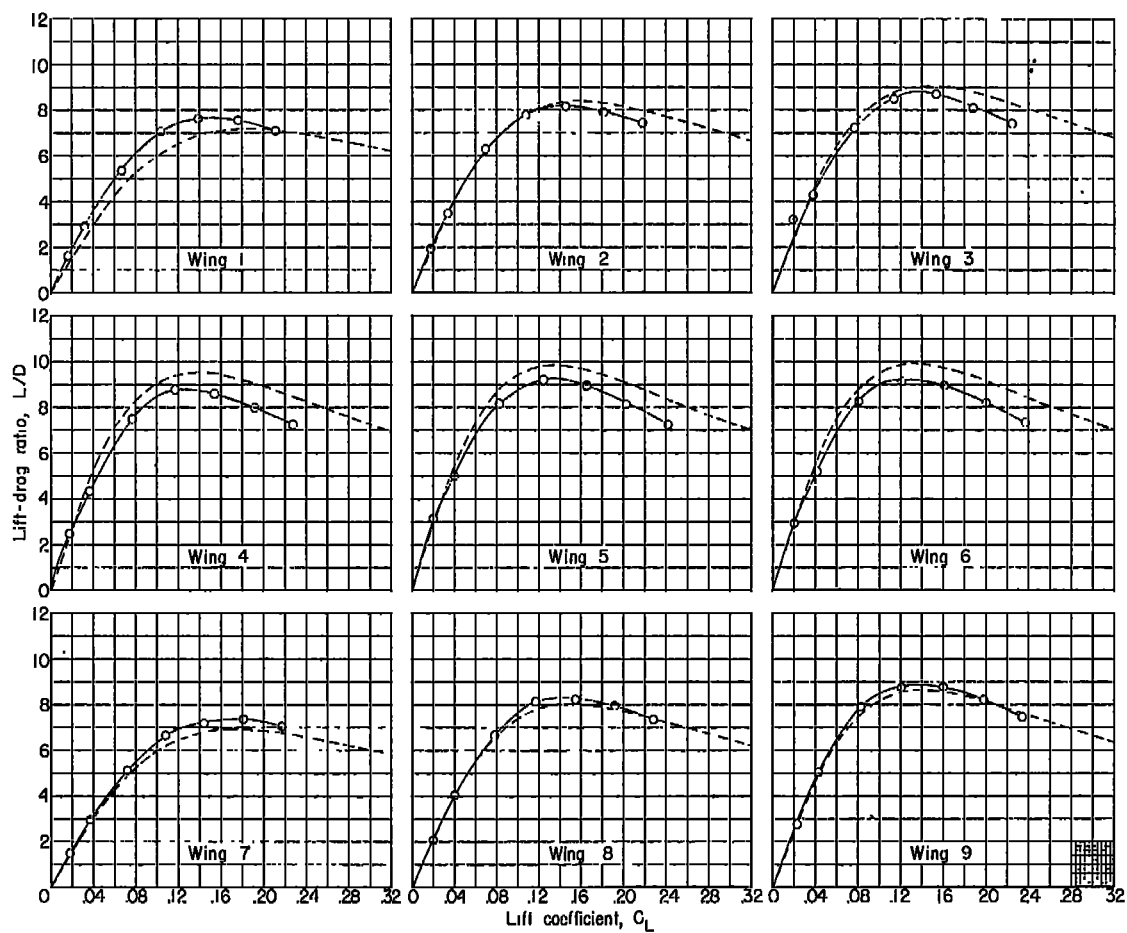
(a) $M = 1.62$.

Figure 25.- Variation of lift-drag ratio with lift coefficient at all test Mach numbers.



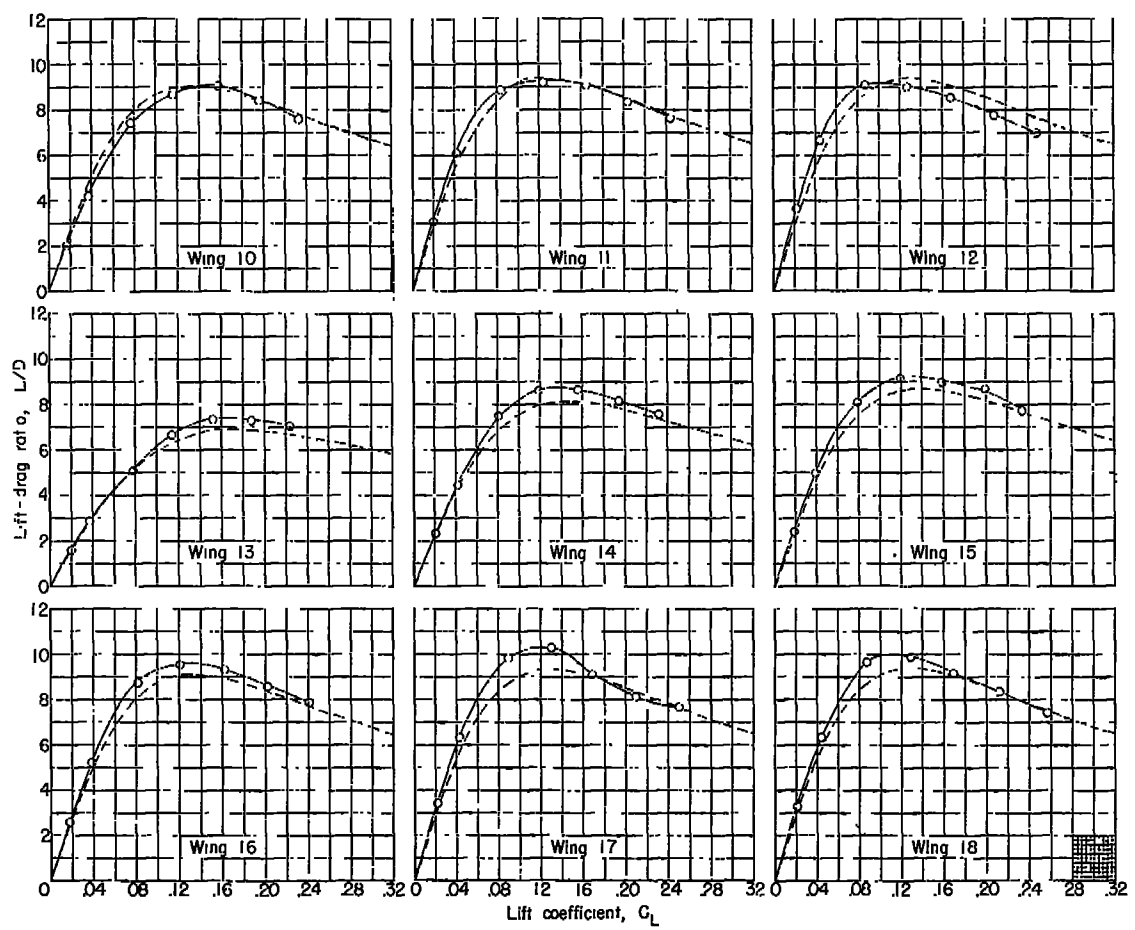
(a) Concluded.

Figure 25.- Continued.



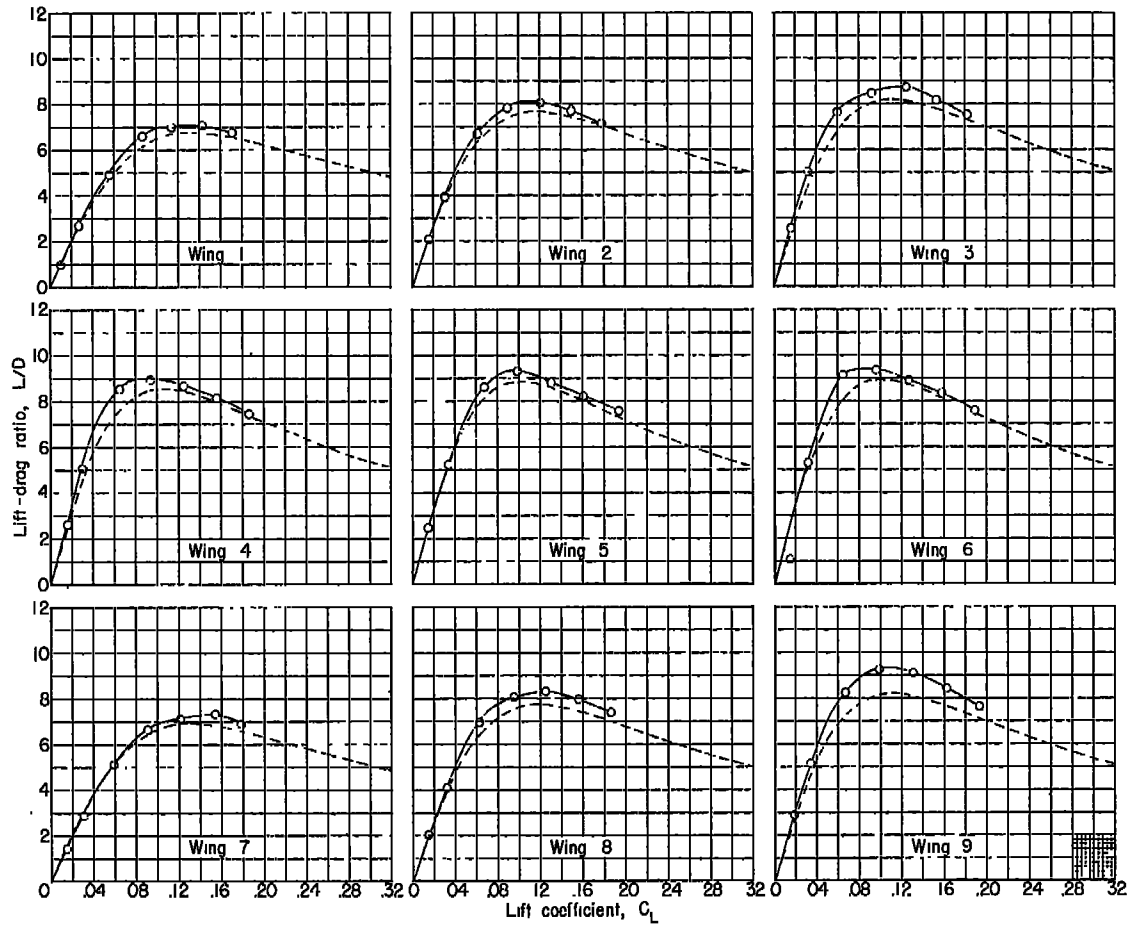
(b) $M = 1.94$.

Figure 25.- Continued.



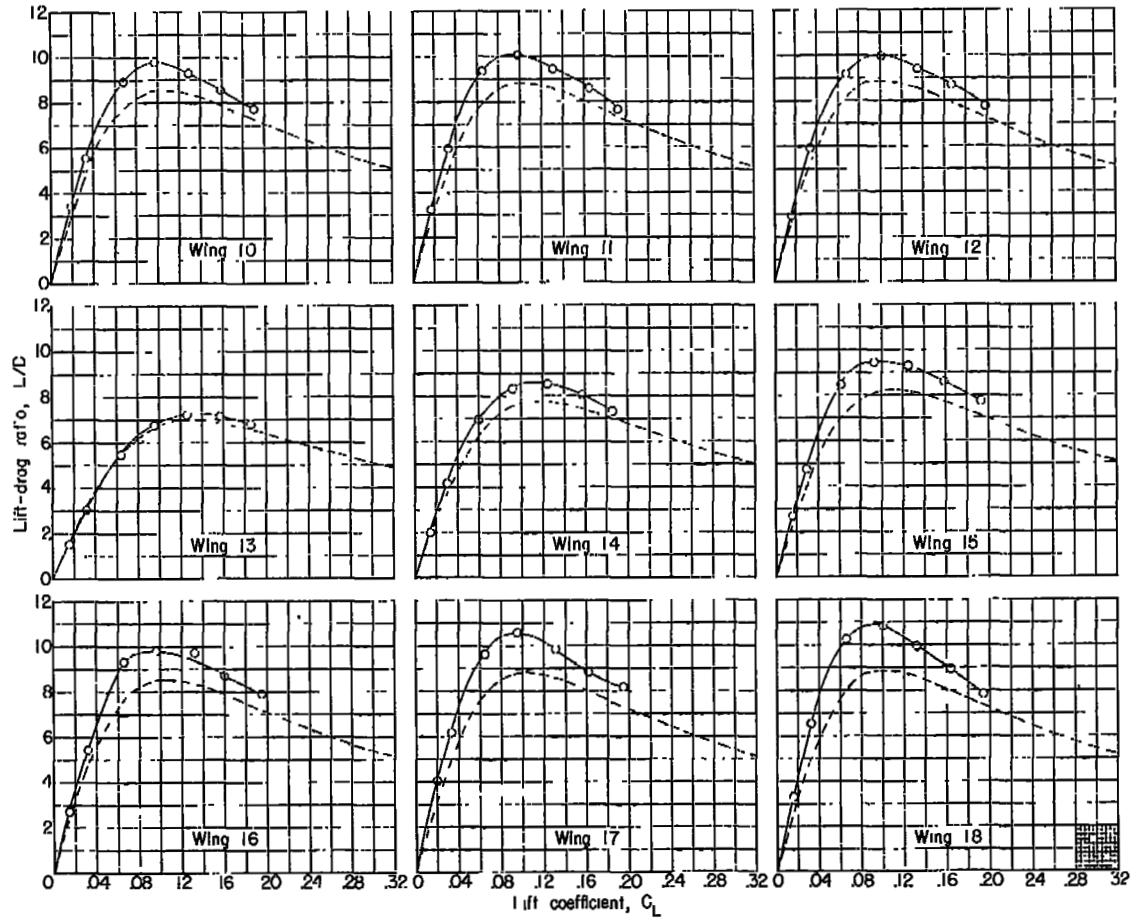
(b) Concluded.

Figure 25.- Continued.



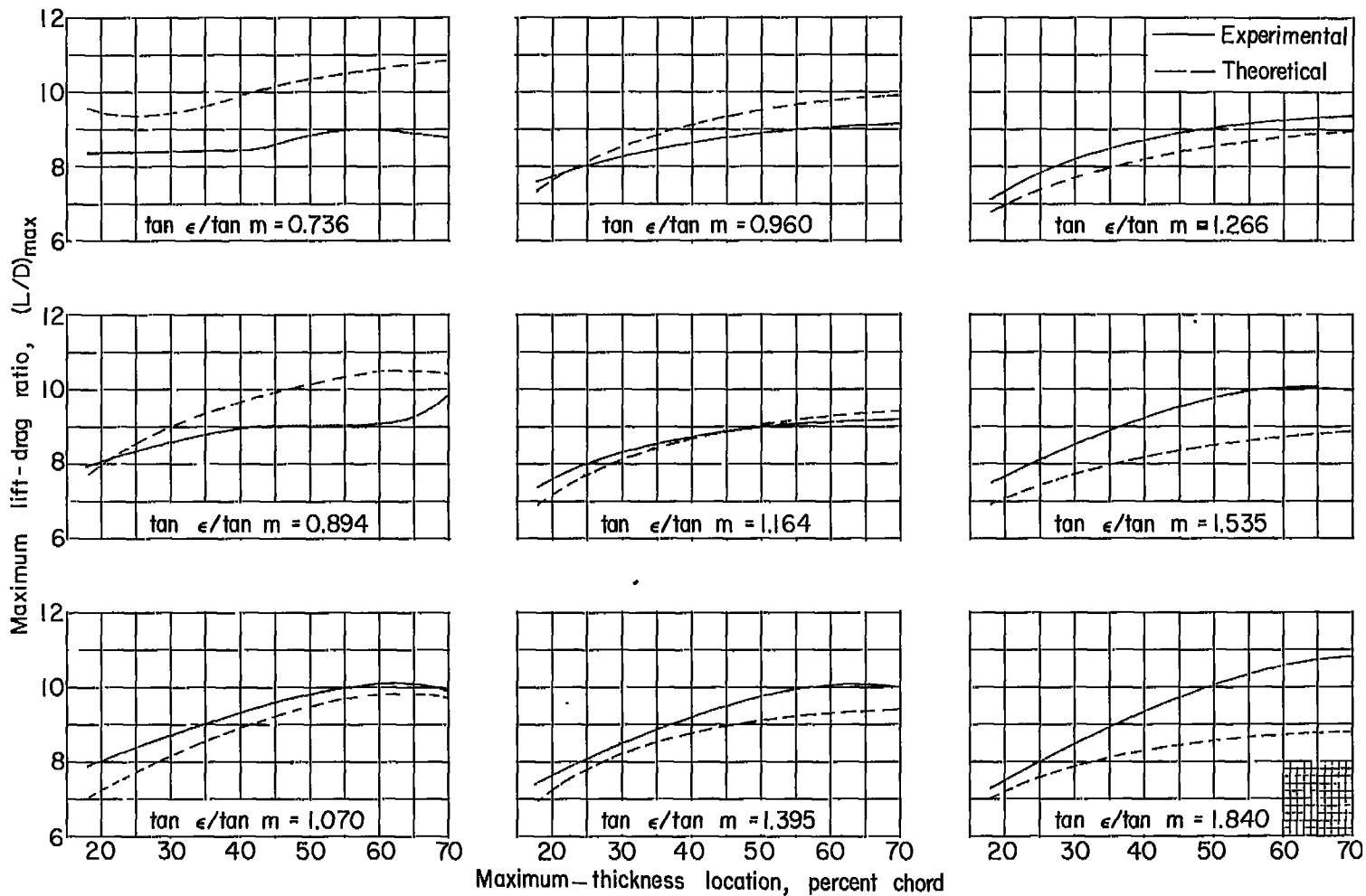
(c) $M = 2.41$.

Figure 25.- Continued.



(c) Concluded.

Figure 25.- Concluded.



(a) $M = 1.62$.

(b) $M = 1.94$.

(c) $M = 2.11$.

Figure 26.- Variation of the maximum lift-drag ratio with maximum-thickness location at several Mach numbers.

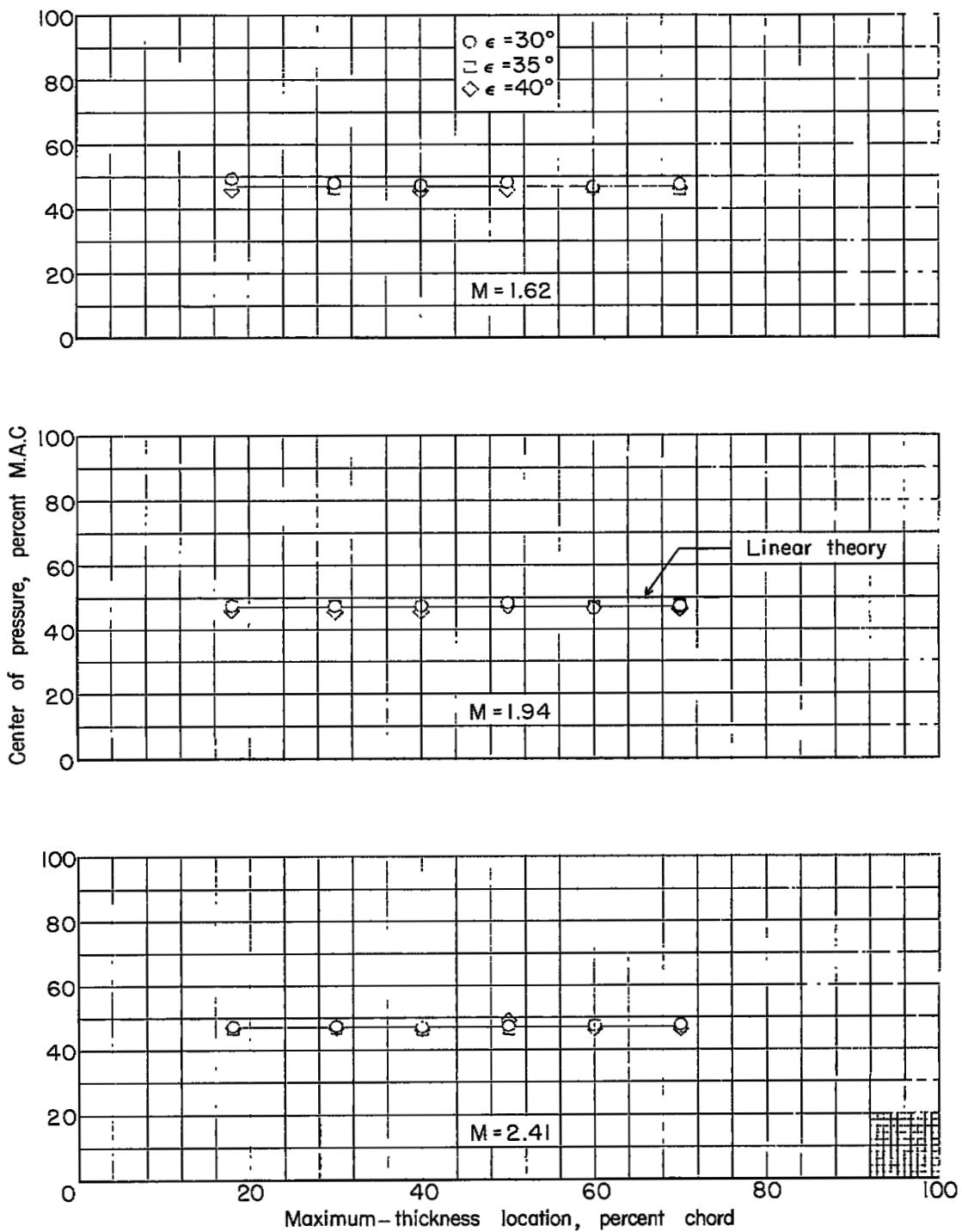
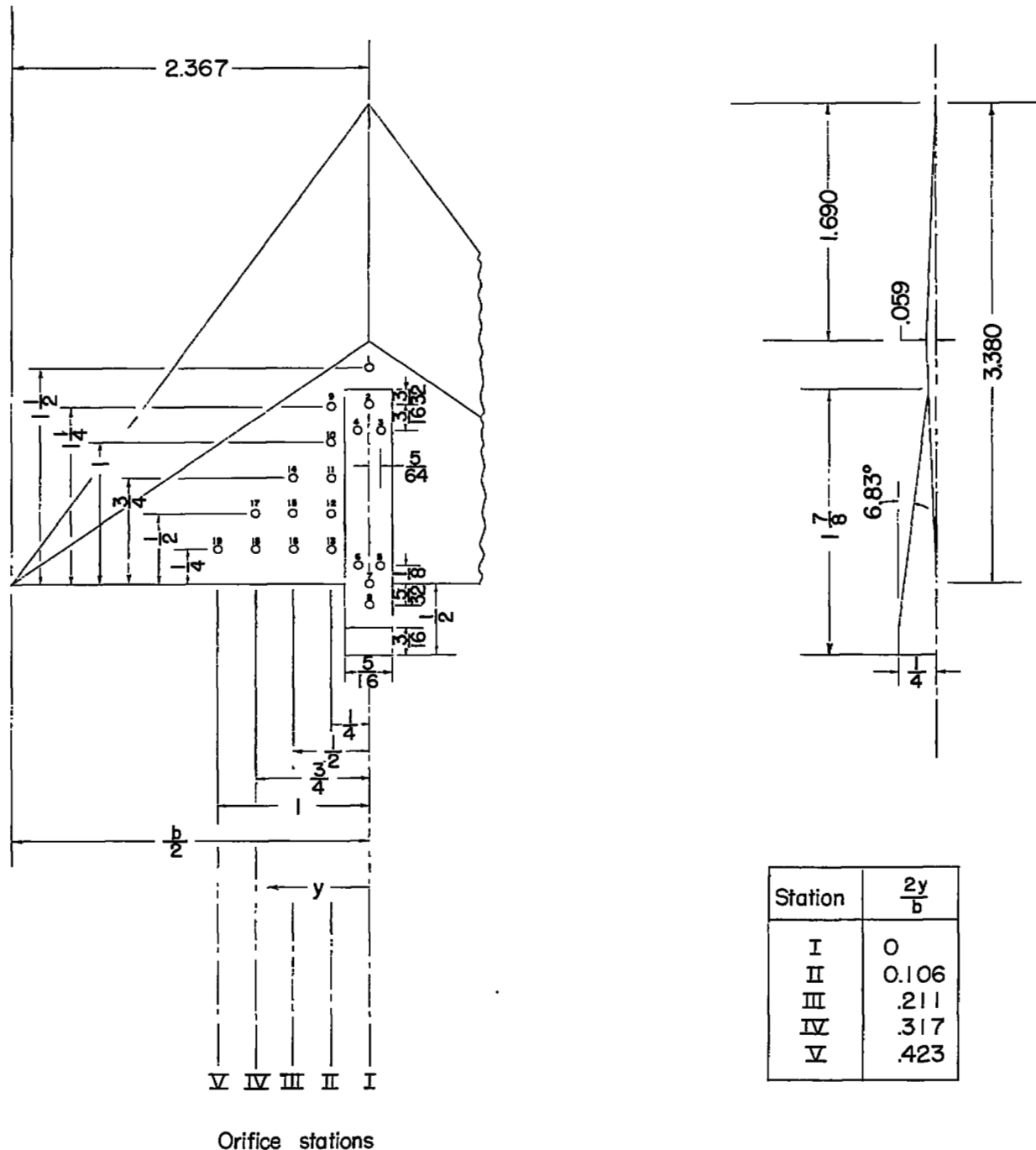
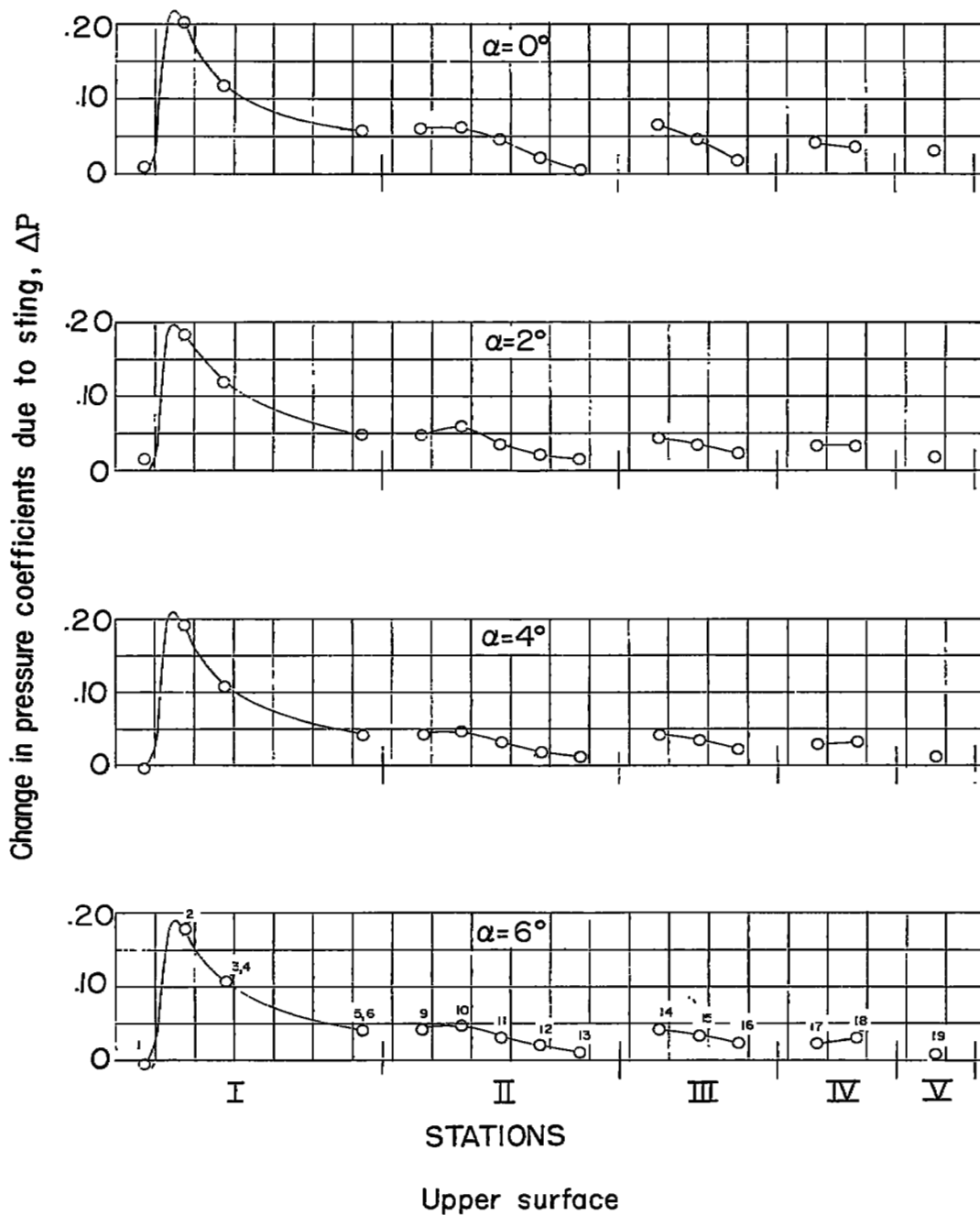


Figure 27.- Variation of the center-of-pressure location with maximum-thickness location at several Mach numbers.



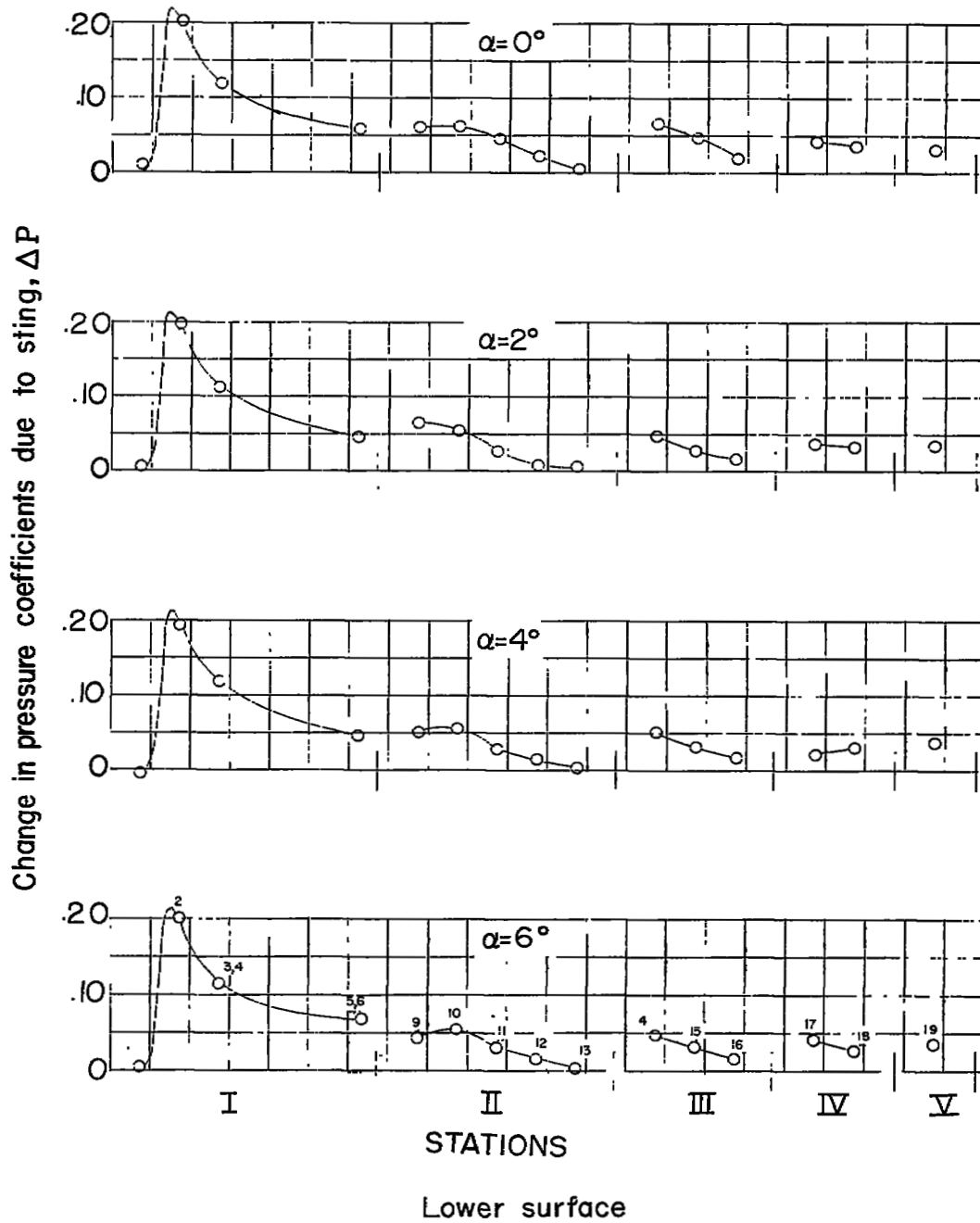
(a) Sting A on wing 10.

Figure 28.- Location of orifices in pressure-distribution models. All dimensions are in inches.



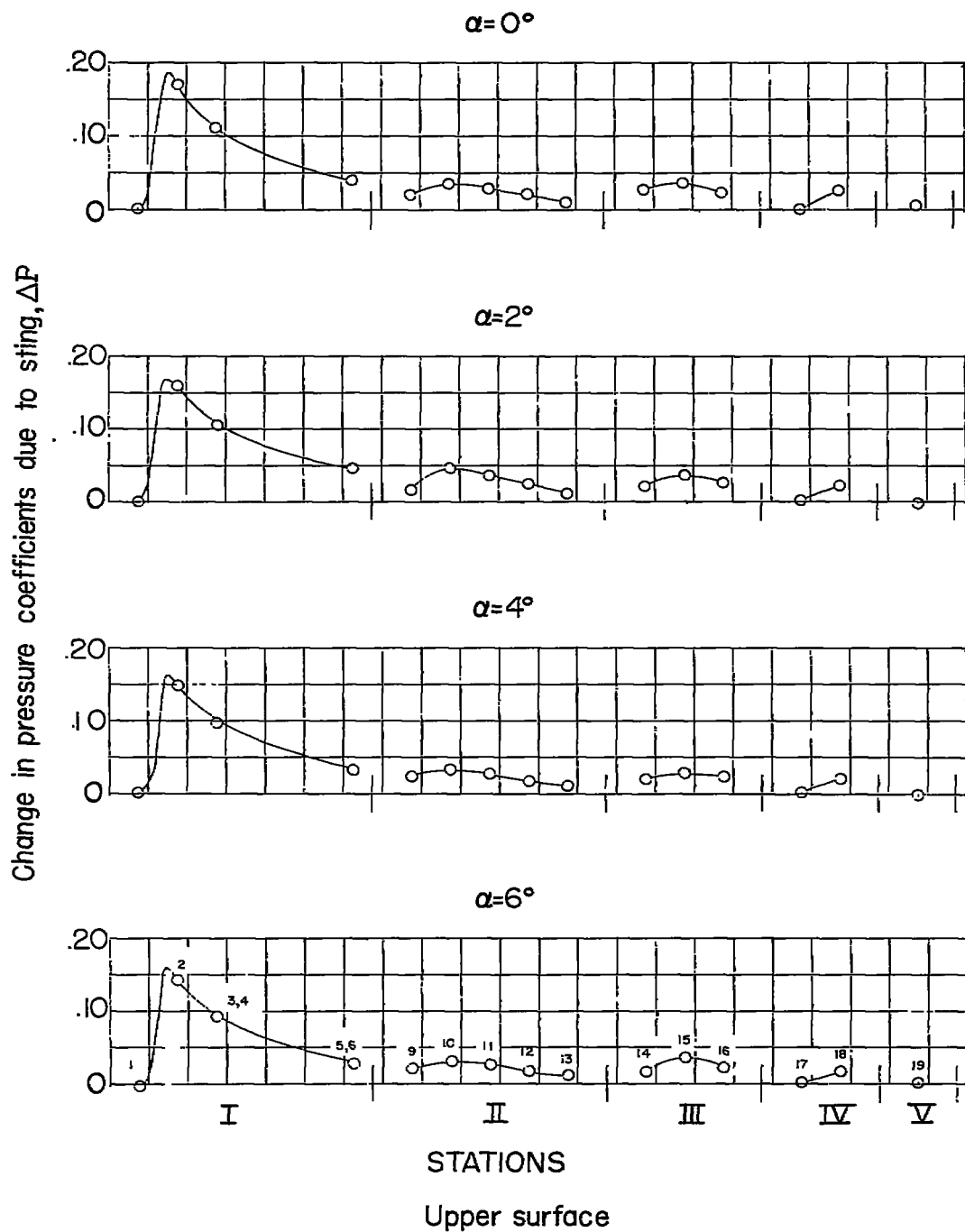
(a) $M = 1.62$.

Figure 29.- Change in pressure coefficients due to presence of sting A.



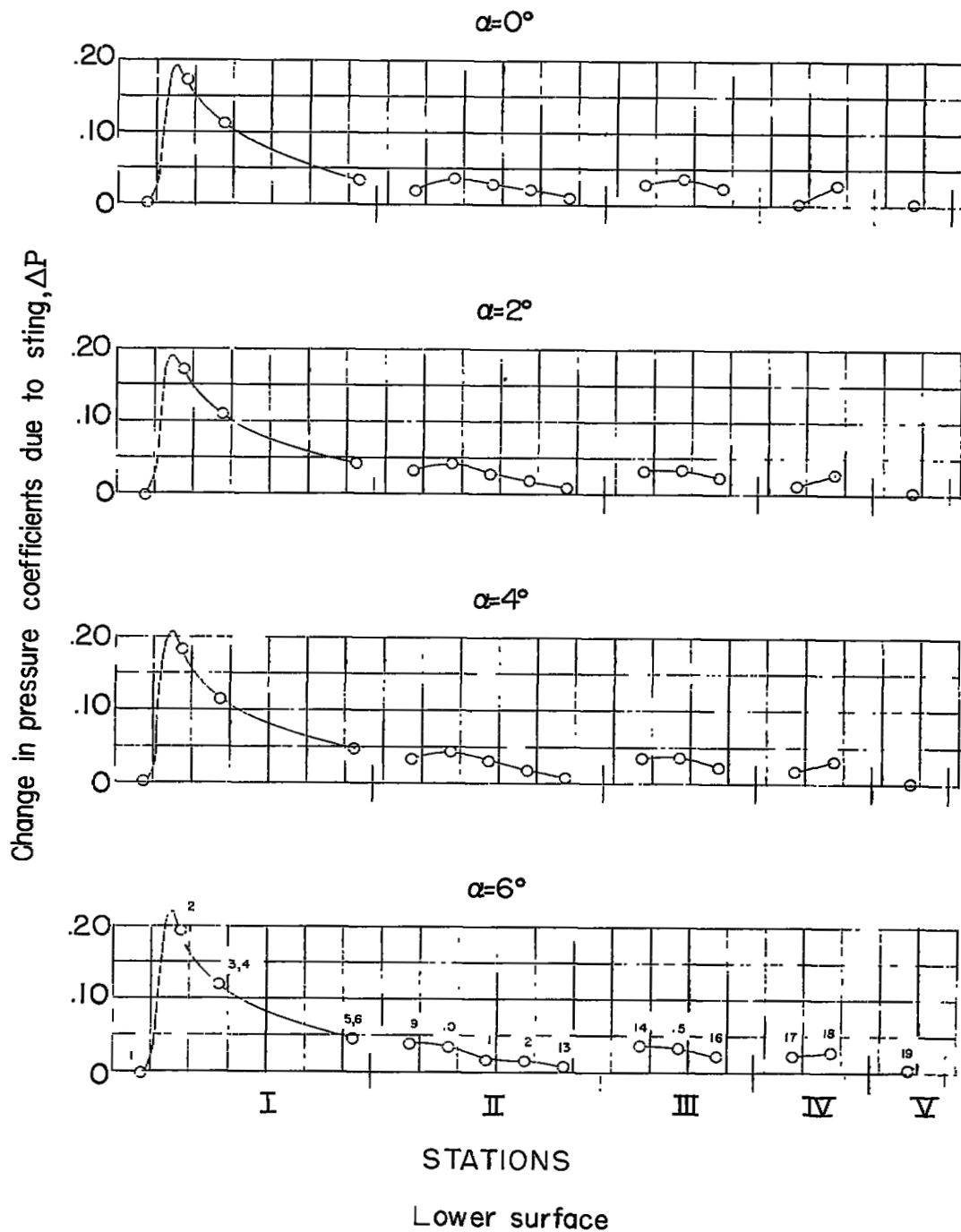
(a) Concluded.

Figure 29.- Continued.



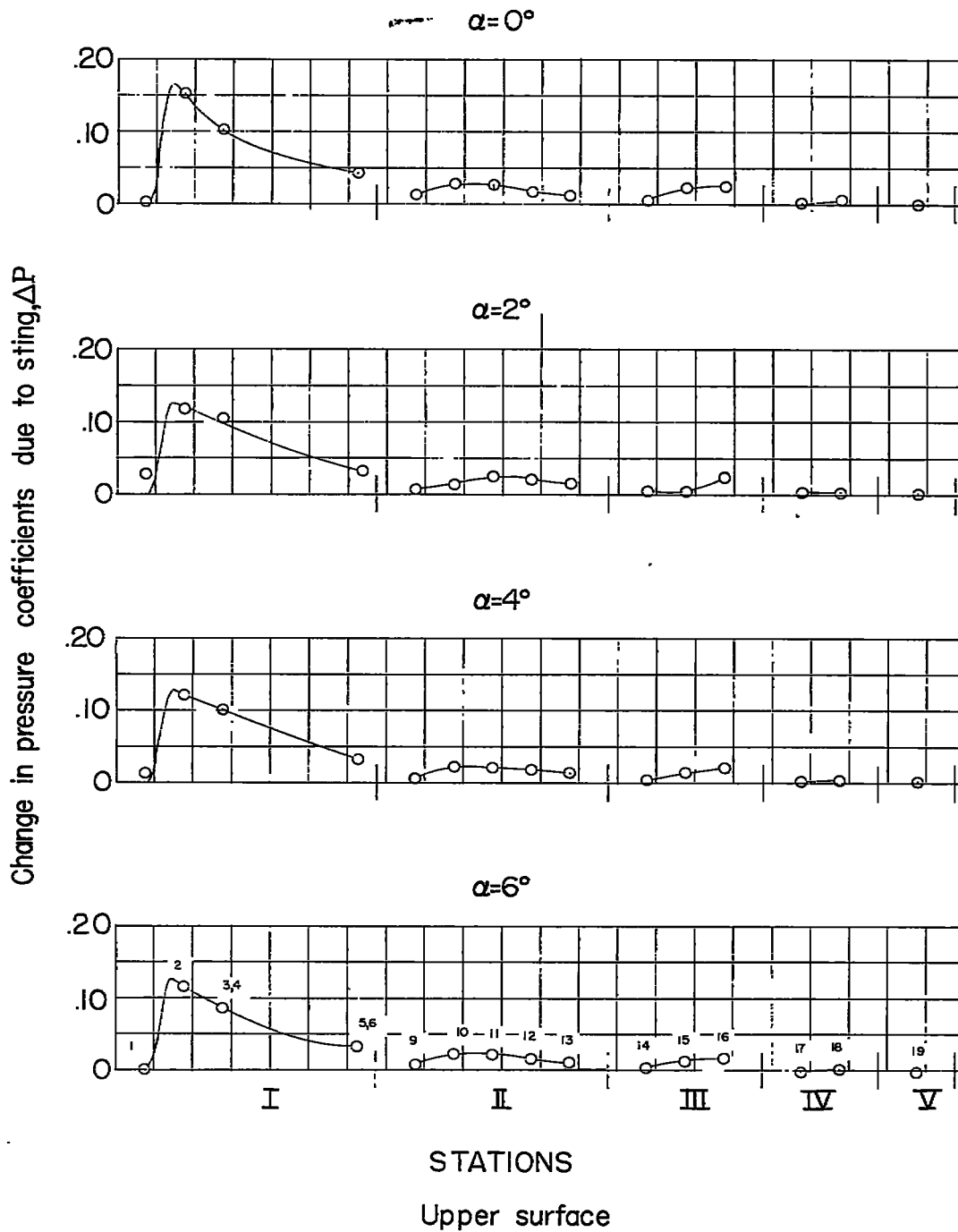
(b) M = 1.94.

Figure 29.- Continued.



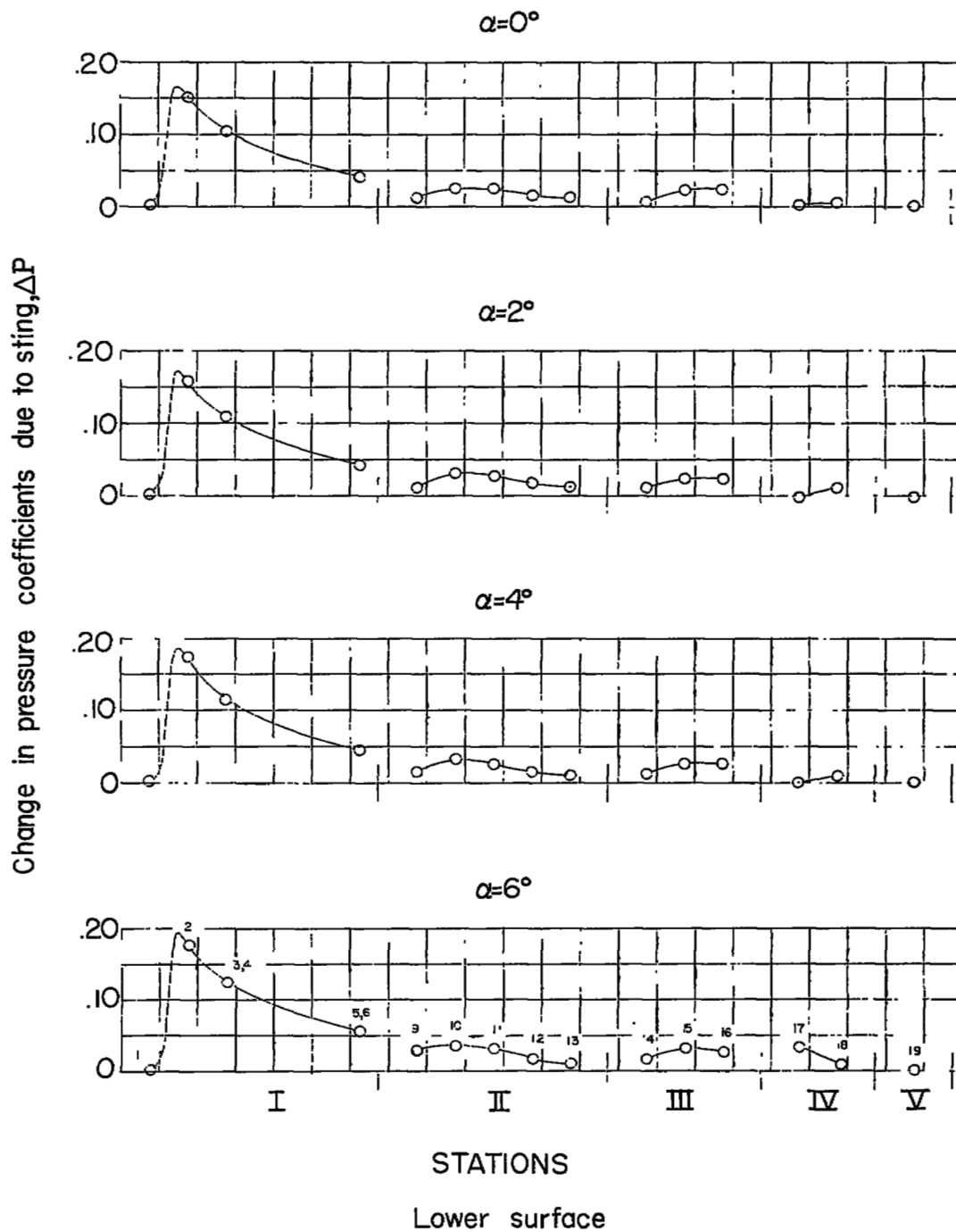
(b) Concluded.

Figure 29.- Continued.



(c) $M = 2.41$.

Figure 29.- Continued.



(c) Concluded.

Figure 29.- Concluded.

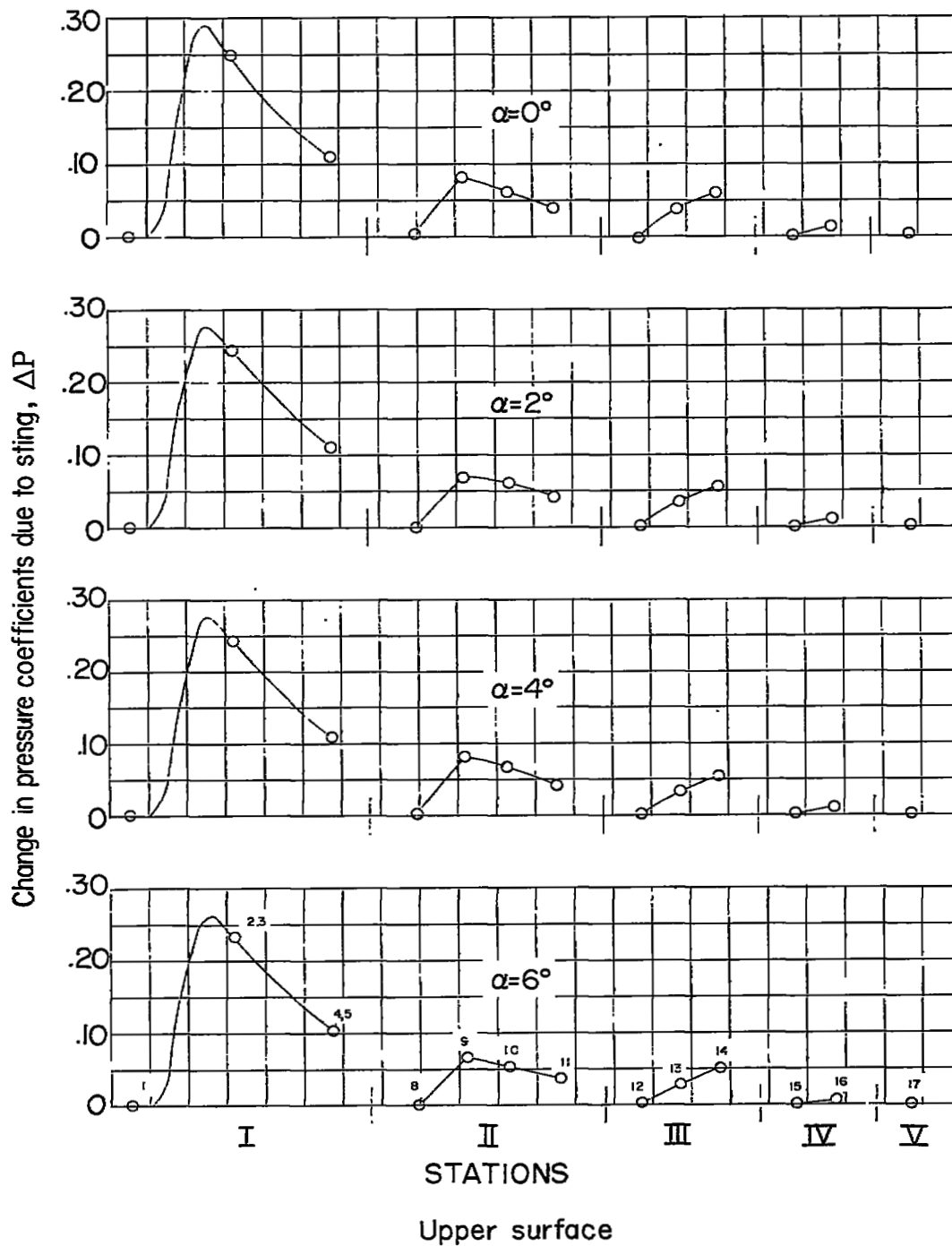
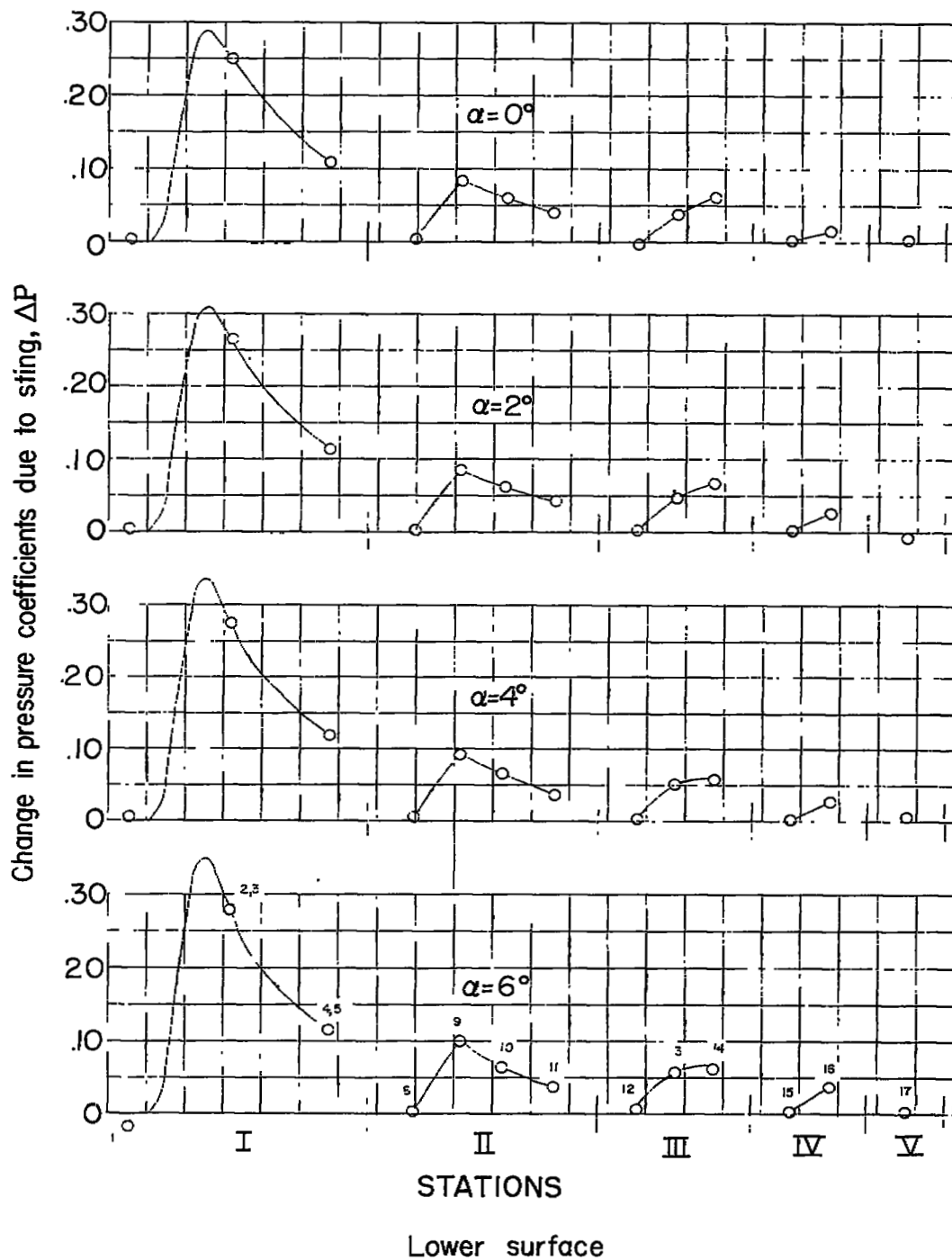


Figure 30.- Change in pressure coefficients due to presence of sting B.



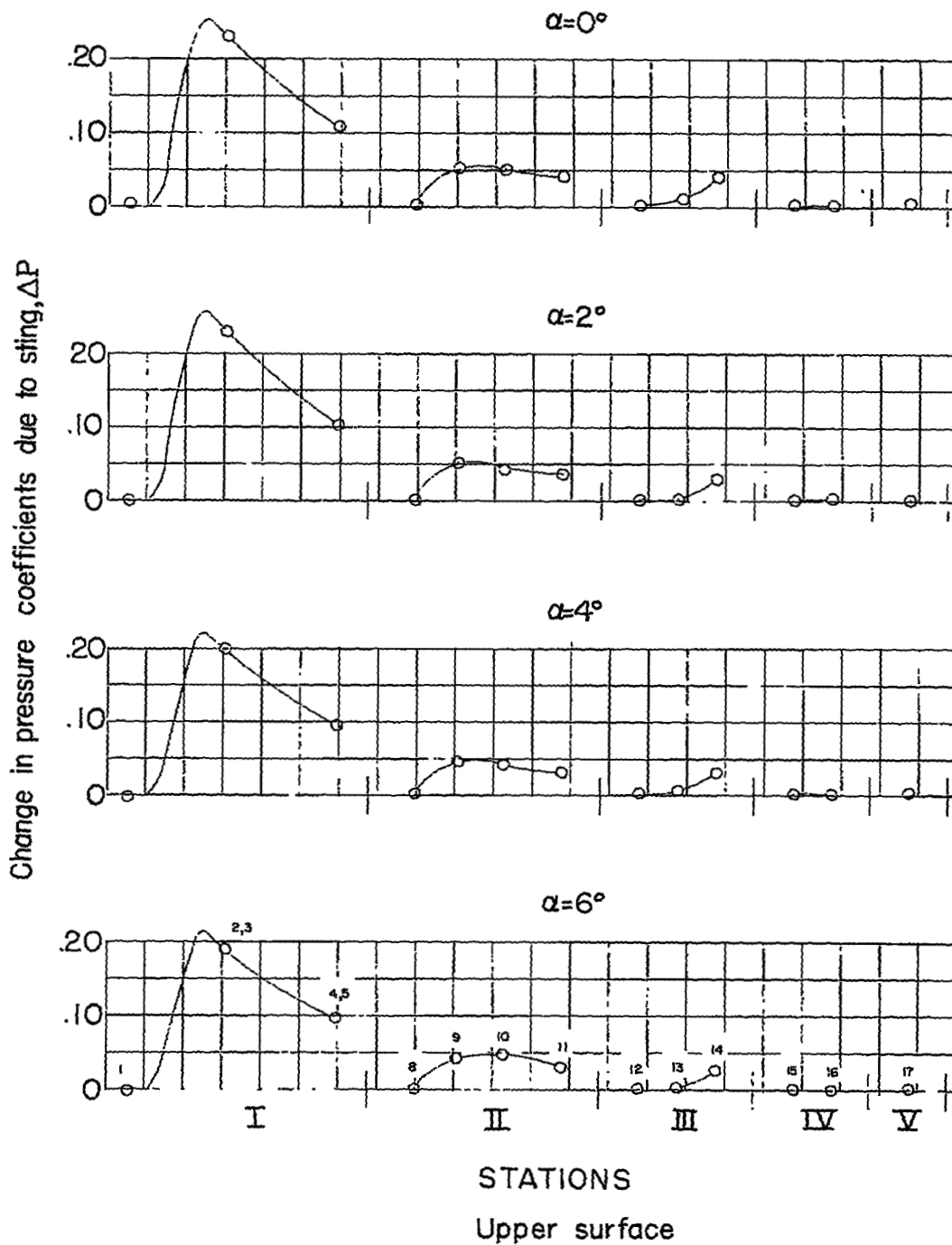
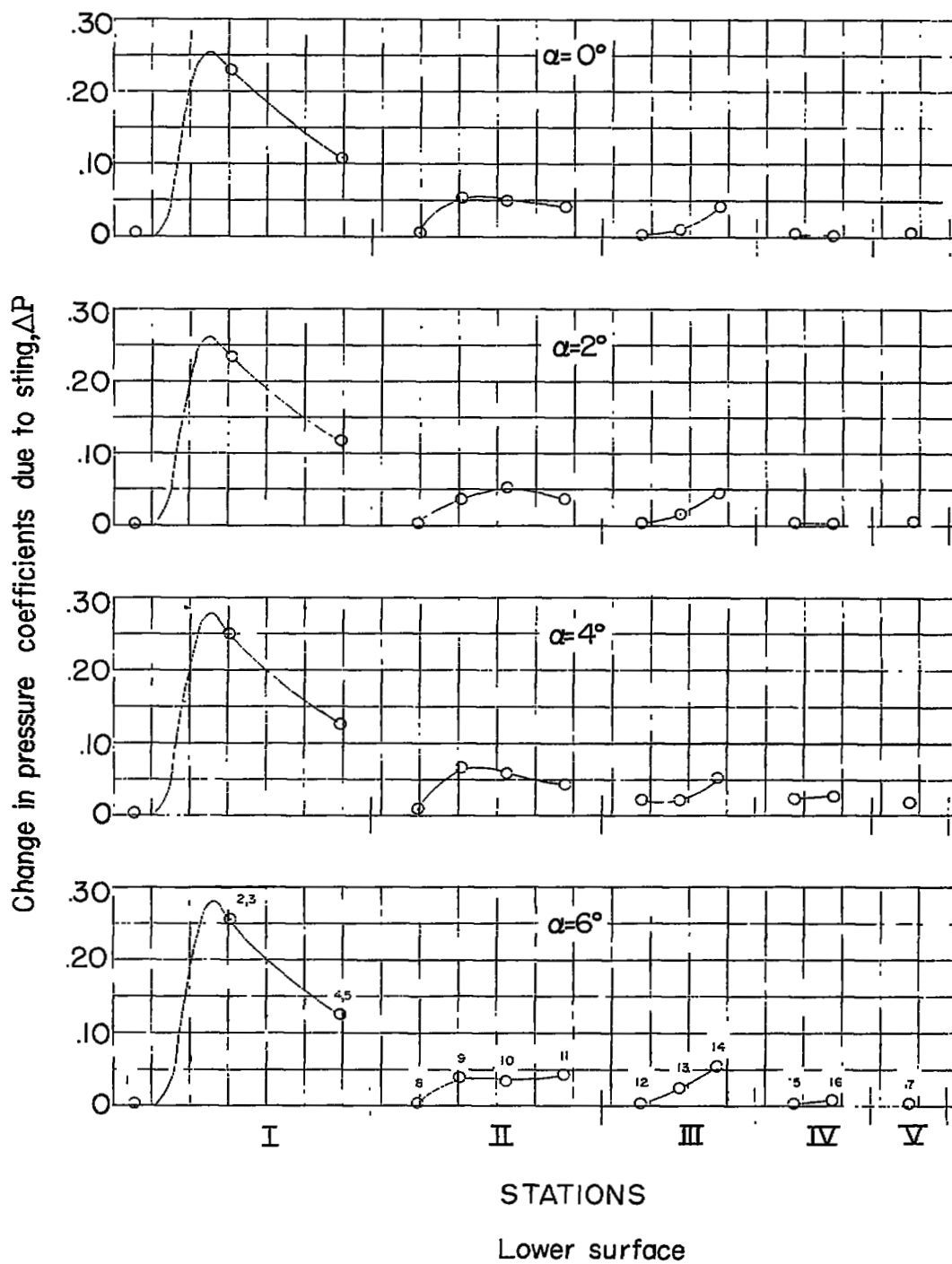
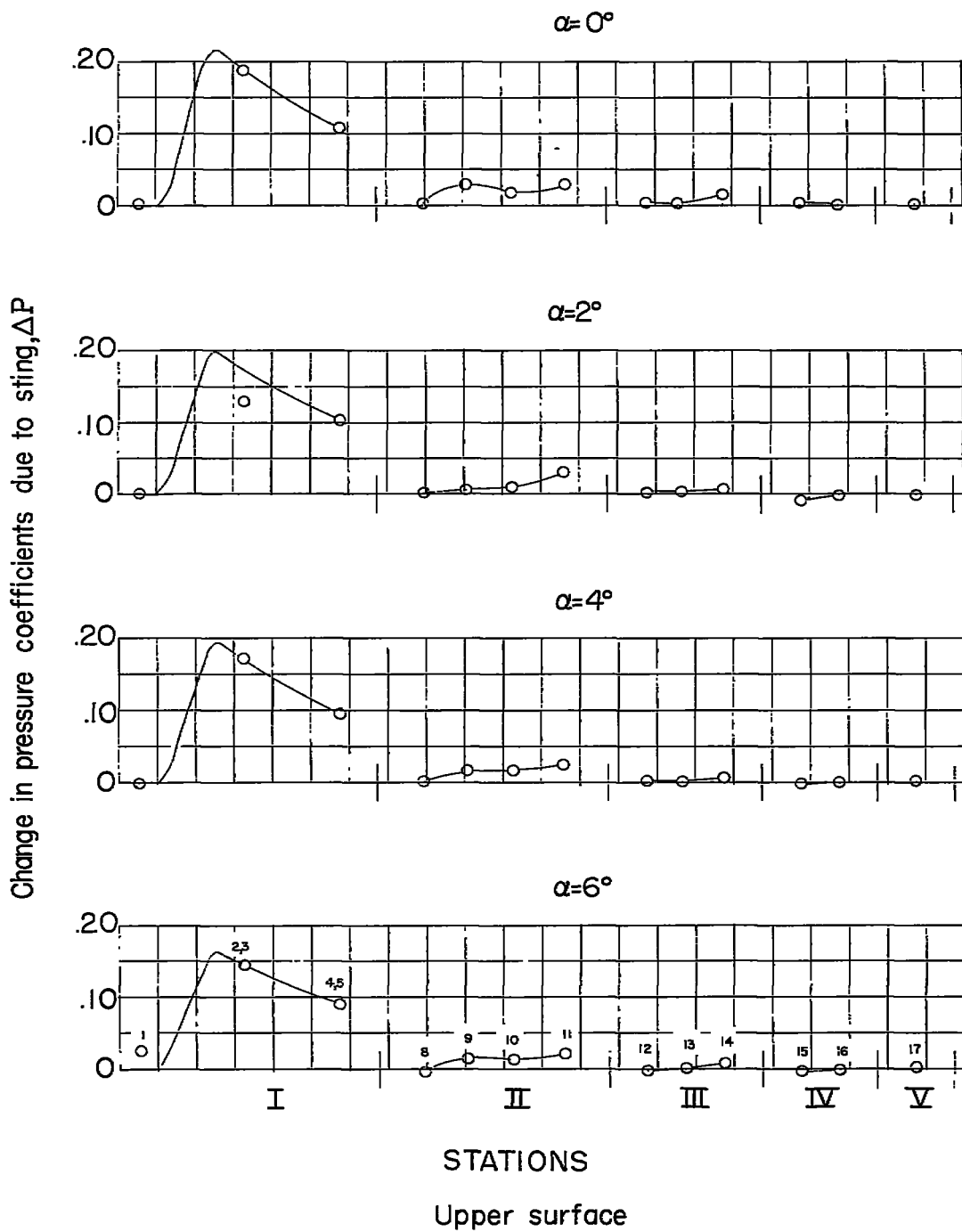
(b) $M = 1.94$.

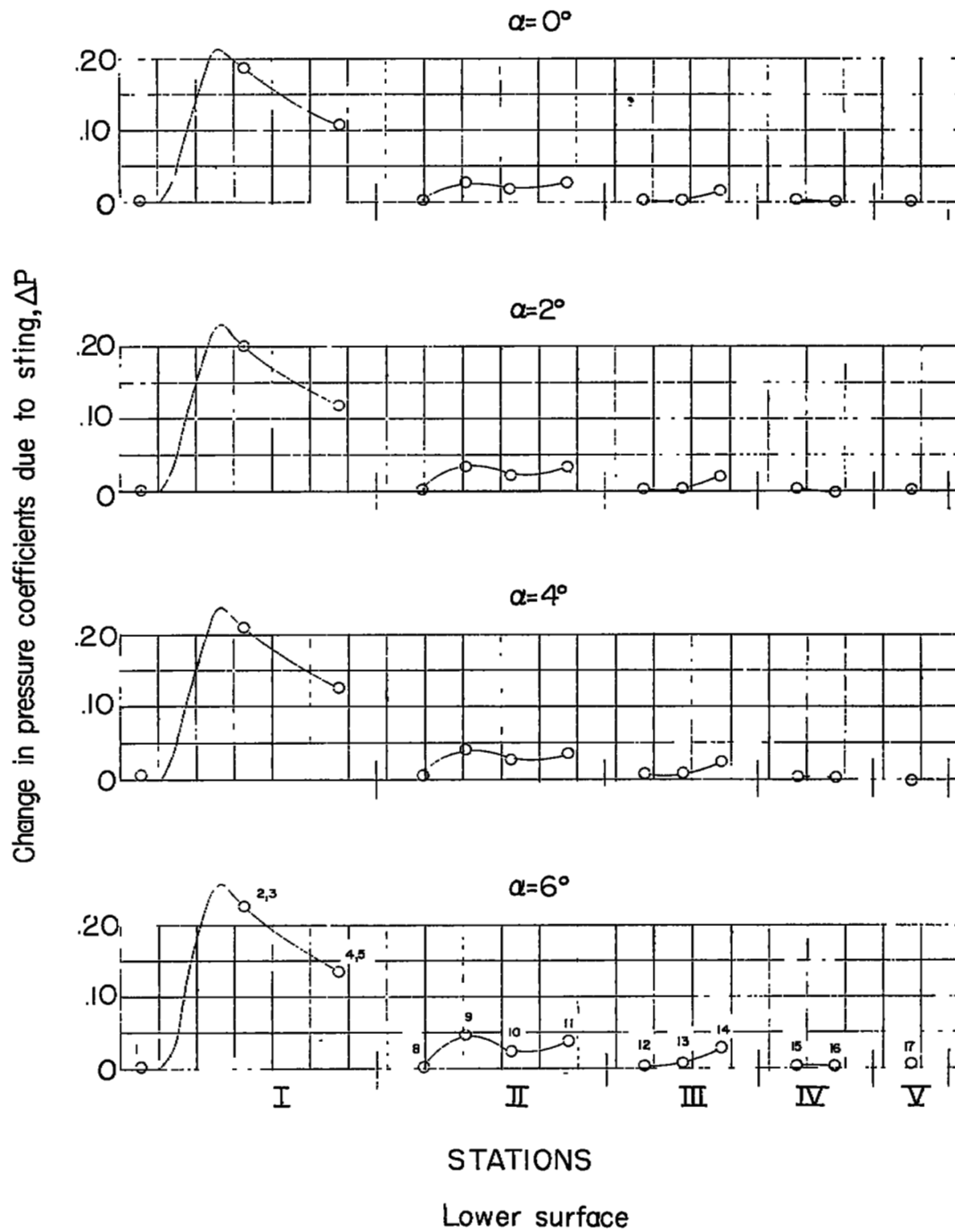
Figure 30.- Continued.





(c) $M = 2.41$.

Figure 30.- Continued.



(c) Concluded.

Figure 30.- Concluded.